Experimental Investigation and Analysis of Pure Fluid and Mixture Pulsating Heat Pipes with Varying Condenser Temperatures, Heat Loads and Fill Ratios

By

Uzoma C. Mmeje

A dissertation submitted in partial fulfillment of the requirements for the degree of

Doctor of Philosophy

(Mechanical Engineering)

at the

UNIVERSITY OF WISCONSIN – MADISON

2021

Date of final oral examination: 12/21/2021

The dissertation is approved by the following members of the Final Oral Committee:

Franklin K. Miller, Professor, Mechanical Engineering

John M. Pfotenhauer, Professor, Mechanical Engineering

Gregory F. Nellis, Professor, Mechanical Engineering

Jennifer Franck, Assistant Professor, Engineering Physics

Thompson Dakotah, Assistant Professor, Mechanical Engineering

Abstract

Pulsating heat pipes (PHPs) have been studied since the 1990s and are potential replacements for copper thermal buses or standard heat pipes. Currently there is not a well-defined process for PHP design for a particular heat load or application. This is partially because of the number of variables that affect the performance of a PHP. PHP's that operate using cryogenic fluids have been studied even less than those that operate at near room temperature and higher. In this work we endeavor to expand the understanding of the performance and behavior of cryogenic PHPs including conductance and maximum heat load capacity (load at dry out) with respect to operating temperature, fill ratio and working fluid properties. This study focuses on exploring the operating regions not previously explored in cryogenic pulsating heat pipes at UW Madison. An experimental device (pulsating heat pipe) has been built, consisting of a single evaporator and a single condenser separated by an adiabatic length. The main purpose of this study is to characterize the effective conductivity of the device for a range of condenser temperatures and increase the heat load until dry-out is achieved. This test procedure was conducted for a range of fill ratios. The data were analyzed to obtain optimal parameters that can be used in the design of a pulsating heat pipe using Nitrogen as a working fluid. The second purpose of this experimental study was to explore dry-out phenomena. Because the PHP is a cryogenic device it is non-optical, so the flow pattern cannot be visually observed, but some information about near dry-out behavior can be obtained from the temperature fluctuations observed in the condenser, evaporator, and adiabatic sections. Additional experiments with Argon and a mixture (Air) as the working fluid were run. The results of these studies and the Nitrogen results are compared with respect to conductance and dry-out behavior.

Acknowledgements

I would like to thank my academic Advisor, Prof. Franklin Miller for guiding me through my doctorate program and for introducing me to the world of experimental research. You provided me much insight into my project and guided me through the little steps I needed in order to take to make this giant leap. I would also like to thank my co-advisor, Prof. John Pfotenhauer for his contribution to this project.

Another thanks I would like to give is to Prof. Gregory Nellis. You laid the foundation for me in my doctoral journey, taught me what it meant to be a researcher and provided me with exceptional knowledge of thermodynamics and heat transfer. You were always able to provide whatever equipment I needed for my project. I would not have achieved this milestone without your support.

My gratitude goes to my family, who supported me in my plans to advance my studies in the United States. My father has always provided words of wisdom all through my lifetime. I can still hear some of the words, carried by the ocean, echoed through time. My Mother has also been so dear to me, caring for me. She always provided anything she could and with love, I dedicate this thesis to her. To my sister and brothers, where would I be without you? I still remember the day we all sat together in our living room, all of you giving me your blessings to pursue a higher degree. Don't think I forgot you, my dear brother Chinazom Wisdom Israel. I would like to thank other family members for their support at various stages of my life: my cousins, the Emelisi Family and Obinwanne Family. Thank you all!

I want to thank the department of Mechanical Engineering for supporting me with a Teaching Assistant position throughout my doctorate program. From this, I hope to give back to society by being an ethical and principled engineer, following the standards that this department has set.

To my friend, John Ikon, you gave me someone to look up to. You are humble, caring, and I consider you one of my best friends. Payam Vatani, my first roommate and guide on this foreign journey. I remember the first time we drove around Madison listening to "Long Way Home" by Gareth Emery. I can never forget your impact on my life. Thank you for being there for me all the way.

I would like to thank Brianna Van Matre, who has provided me with emotional support. She has shown me the interconnectedness of our planet, which has caused me to cherish nature more greatly. You have kept me sane during this time of insanity. Jennifer Detlor, for all the heat transfer arguments and discussion and time spent working on various project, thank you. My thanks also go to Chloe Gunderson, once my undergraduate assistants, now a researcher of her own, for her support on aspects of this project.

I would love to thank all current and former lab mates: Ian Jentz, Zhiyi Jiang, Nathan Colgate, Chen Xu, Diego Fonseca, Rodrigo Barraza, Anna Dreyson, Amy Van Asselt, Mason Mok and Logan Kossel. I would finally like to extend my gratitude to Seth Potratz for his care and support during my internship at Praxair Inc. To all I may have forgotten:

"Should auld acquaintance be forgot and never brought to mind? Should auld acquaintance be forgot and days of auld lang syne?"

Table of Contents

List of Figures

Nomenclature

PHP	pulsating heat pipe
CHF	critical heat flux
ID	inner diameter
OD	outer diameter
RTD	resistance temperature detector
PRT	platinum resistance thermometer
HTC	heat transfer coefficient
D	diameter
V	volume or voltage
x	mass quality
k	thermal conductivity
T	temperature
M	molar mass
h	specific enthalpy or heat transfer coefficient
U_∞	average/freestream velocity
$\dot{q}$	heat load
$\dot{q}^{"}$	heat flux
ΔT	temperature difference
ΔP	pressure difference
ρ	density
σ	surface tension
μ	dynamic viscosity
δ_t	thermal film thickness
γ	specific heat ratio
$\bar{\alpha}$	accommodation coefficient
g	gravitational constant (9.8 ms^{-1})

R	universal gas constant (8.3145 J $mol^{-1}\ K^{-1}$)
Subscripts	
crit	critical
sat	saturated
avg	average
eff	effective
w	wall
c	condenser or cold
e	evaporator
h	hot
f	fluid
l	liquid
g	gas
v	vapor

1 Introduction

1.1 Motivation

Since the discovery of pulsating heat pipes (PHPs), there has been a focus to extend operation to cryogenic temperatures. Some of the earliest work done on a cryogenic PHP was by G. R. Chandratilleke et al [1,2]. The PHP's self-sustaining two-phase heat transport capability means that a relatively small device can transport thermal energy without an external driving device such as a pump. PHPs have a range of potential applications. PHPS are of interest to NASA because they could potentially enable lightweight space missions while simultaneously reducing space flight thermal control system cost [3]. Closed looped PHPs have been tested as an alternative for cooling superconducting magnets in magnetic resonance imaging devices (MRIs) [4]. A study by Lu Qianyi & Jia Li was done to determine the effectiveness of PHPs for cooling a server rack. [5].

The advantages of a pulsating heat pipe compared to metal bus bars are lighter weight. Additionally, PHPs are easier to construct than standard heat pipes because they do not require a wick structure.

A large body of work has been published on the performance of room temperature pulsating heat pipes, however, the data for cryogenic pulsating heat pipes is much more limited. Optical observation of the physical behavior of room temperature PHPs is much easier than for cryogenic PHPs because optical access can be installed without the worry of heat leak. Cryogenic PHPs are not easily observed or controlled because of the large heat leaks that are inherently driven by large temperature differences between the low saturation temperatures of cryogens and the environment. Although optical observation is impractical for cryogenic PHPs, these cryogenic PHPs show more dynamic phenomena due to the discrete or measurable pressure or temperature changes even with

a relatively small heat load, as a result of the low latent heat and heat capacity of some of the cryogenic working fluids. This allows the observation of temperature and pressure in the PHP on relatively short time scales. This information can be used to give some information about the flow inside the PHP.

1.2 Objective

The objective of this research is to experimentally investigate and quantify the conductance of the Nitrogen, Argon and Air Pulsating Heat Pipes and analyze the effect of condensing temperatures and varying heat loads on the performance of the PHPs. In effect, a 3-D map of the performance can be analyzed so that optimal performance regions can be identified. The 3-D map can be useful for off-design analysis as well, when the system operates outside the original design parameters. The adjustable parameters of interest in this experiment are fill ratio, condenser temperature and heat load. The performance is characterized using the effective conductivity or conductance. In addition to conductance, the maximum heat transport capacity of the PHP, the evaporator dry-out power or critical heat flux (CHF), as a function of operating parameters was also investigated. In general, due to the unstable or uncertain nature of CHF, PHPs are typically designed to operate far from the CHF. However, understanding what goes on at the approach to CHF may shed light on the performance of PHPs when operating near the CHF zone or give indications of the onset of CHF behavior.

2 Background

2.1 Introduction to the concept of Pulsating Heat Pipes

Pulsating heat pipes are passive two-phase heat transfer devices that transport energy via the oscillation or movement of alternating liquid slugs and vapor plugs. It was first proposed by Akachi H. in the 1990s [6] as an alternative to traditional heat pipes. Its construction differs from the traditional heat pipe because there is not a porous wick structure. Instead, the pipe is sized small enough that surface tension becomes a dominant force in the system without the need for a porous wick. Rather than using capillary pumping action to move liquid from the condenser to the evaporator section as in a tradition heat pipe, the PHP works by the induced oscillatory motion of the alternating vapor bubble and liquid slugs. PHPs can have one or more condensers and one or more evaporators separated by an adiabatic length. The length is the effective distance that heat is moved from the evaporator to the condenser. The device is typically filled with a working fluid so that a saturated two-phase liquid-vapor mixture fills the tubes. PHPs are constructed to have a diameter small enough that the capillary forces are significant in the tubes. The capillary tube ensures somewhat even distribution of vapor plugs and liquid slugs during a filling process; however, such distribution is stochastic, and cannot be exactly replicated. In a perfectly constructed PHP, the initial state (no heat load) typically has negligible temperature gradient between the evaporator and condenser and the flow is assumed to be static. As heat load is applied to the evaporator plate, the temperature of the fluid at the evaporator rises until it reaches the saturation temperature of the working pressure at the evaporator. At this point nucleate boiling begins at local sites and the formation of bubbles may combine to form new vapor plugs. The imbalanced temperatures (between neighboring slugs) and capillary shape of the tubes form liquid contact angles. The temperature effect on contact angle comes the direct relationship between

contact angle and surface tension (which is a temperature dependent property). Pressure differences in the tubes induce fluid movement. As vapor reaches the condenser, its vapor pressure can drop to the saturation temperature of the condenser, causing vapor regression or liquid condensation and releasing energy into the cold sink.

There are primarily two main forms of energy transport in the PHP. The first is the latent energy transport, due to evaporation and condensation at saturation temperatures. Second, the sensible heat transport which occurs as a liquid slug rises in temperature until the saturation temperature associated with the heat load or as a vapor plug fall in temperature until the saturation temperature of condensation is achieved. This mode of heat transfer occurs by wall convection to either the liquid slug or conduction through the thin liquid fluid left behind at the wall when a vapor plug tails a liquid slug and vice versa. The thin liquid then contributes to convection at the liquid-vapor interface as well as any phase change energy that may occur.

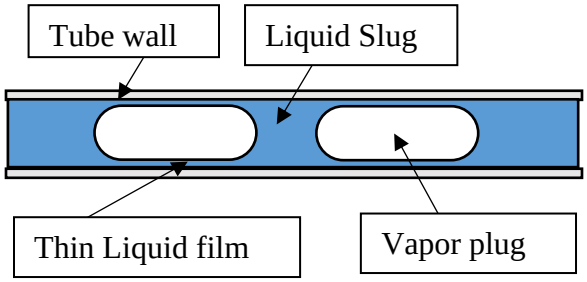

Fig 2-I. Schematic of Slug-Plug Formation

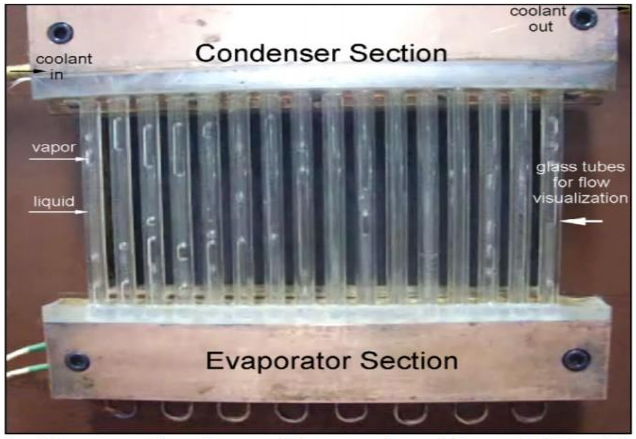

Fig 2-II . Schematic of an Ethanol PHP [7]

2.2 Critical diameter of a PHP

As was stated earlier PHPs are constructed to have a maximum diameter to enhance capillary effect. This maximum diameter is known as critical diameter of a PHP and its value is determined from an analysis on a free-floating bubble up a vertical static liquid column. The common way to determine the critical diameter in the PHP community is by the experimental relationship between three chosen non-dimensional numbers that govern a Taylor bubble's rise in a vertical stagnant liquid column as reported by White and Beardmore (1962). The non-dimensional numbers are the Froude number (Fr) which relates flow inertia force to gravitational force, E*ö*tv*ö*s number (E*ö*) also called the Bond number (Bo) which relates gravitational force to surface tension force and the Poiseuille number (Ps) which relates viscous force to gravitational force:

$$Fr = \frac{\rho_l U_\infty^2}{gD(\rho_l - \rho_v)} \tag{2.1}$$

$$E\ddot{o} = \frac{gD^2(\rho_l - \rho_v)}{\sigma} \tag{2.2}$$

$$Ps = \frac{U_\infty \mu_l}{gD^2(\rho_l - \rho_v)} \tag{2.3}$$

where ρ_l and ρ_v are the liquid density and vapor density respectively, D is the inner diameter of the tube, σ is the surface tension, g is the gravitational constant, μ_l is the viscosity of the liquid and U_∞ is the free stream velocity.

The three non-dimensional numbers above can be further correlated to produce a fourth number called the property number (Y):

$$Y = \frac{Ps^4 E\ddot{o}^3}{Fr^2} \tag{2.4}$$

The graph below shows the experimental results by White and Beardmore (1962). The root of the Froude number is plotted versus the E*ötvös* number for different fluid or property numbers:

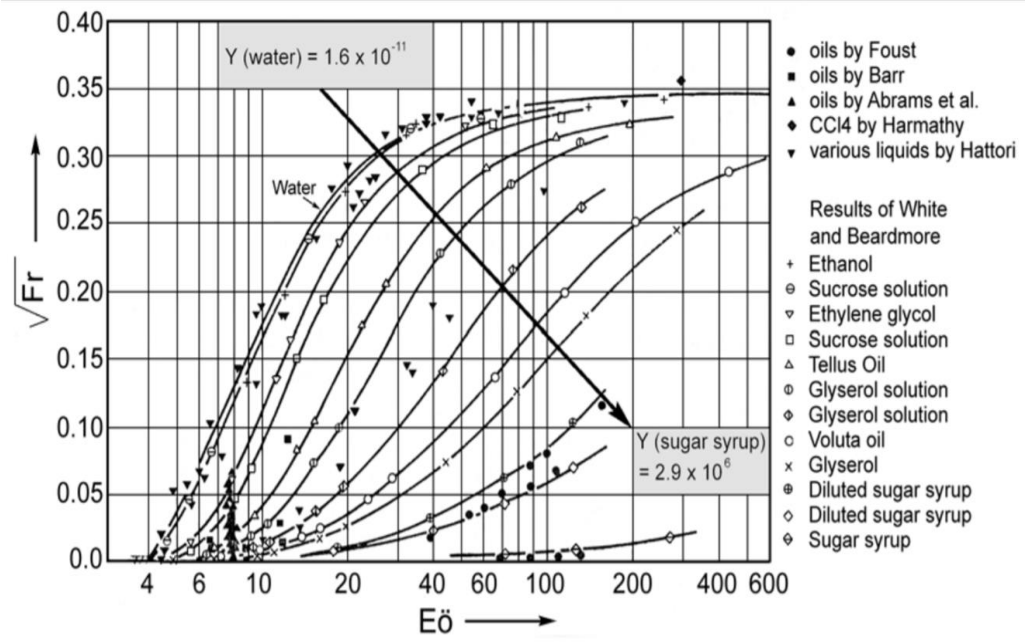

Fig 2-III. Experimental result showing the root of Fr versus E*ö* for different fluids [8]

As the capillary tube diameter is reduced, bringing the terminal velocity to zero and hence the Froude number to zero, the surface tension force becomes more dominant and the E*ötvös* number is observed to collapse to a critical value (of 4) for all the fluids tested. The E*ötvös* number can then be used to calculate a critical tube diameter:

$$E\ddot{o}_{crit} = \frac{gD_{crit}^2(\rho_l - \rho_v)}{\sigma} \leq 4 \tag{2.5}$$

Fig 2-IV shows the critical diameter of a nitrogen PHP as a function of temperature. Since PHPs can often operate at temperatures far above its sink temperature (sometimes close to the critical temperature of the working fluid), it is better to use the lower limit (higher temperatures) in choosing the critical diameter.

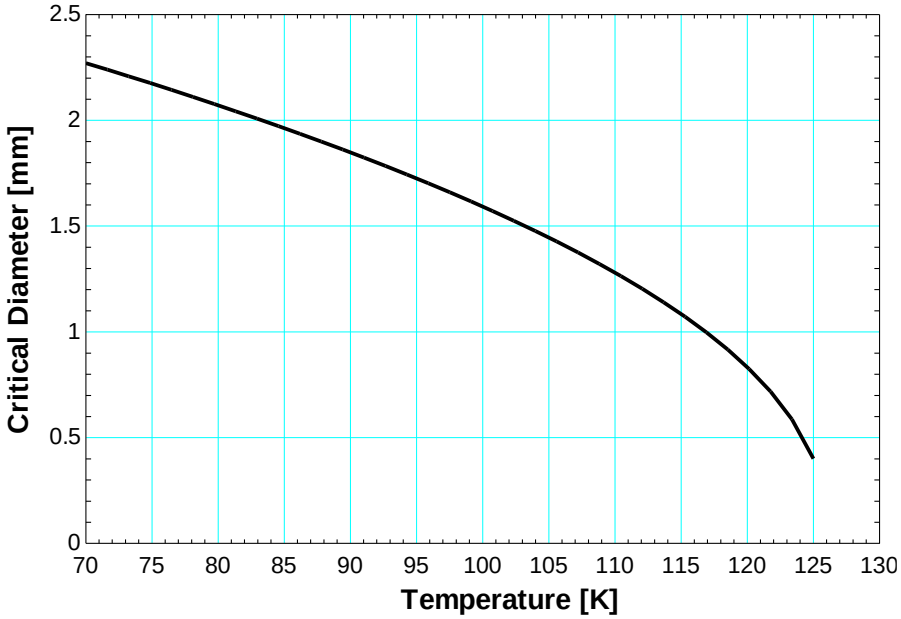

Fig 2-IV. Critical diameter as a function of temperature for a Nitrogen PHP

2.3 Design parameters of a PHP

The following list are some of the important parameters to consider when designing a PHP:

Inner diameter: The inner diameter plays a key role in the performance of a PHP. The diameter should be chosen such that surface tension is adequate to overcome unfavorable gravitational pull but not strong enough to subdue pressure inertia or cause high frictional forces. Results such as those of Fabliha Islam et al [9] suggests that the optimum diameter is closer to the critical diameter and further reducing the diameter, drops the performance of the PHP. This may be because surface tension or viscous forces begin to damp oscillations, limiting the bubble velocities. In that work the critical diameter was reported to be 3.32[mm]. Fig 2-V shows that those diameters larger than the critical diameter have the worst performance. This is apparently due to a lack of distinct liquid plugs and vapor slugs.

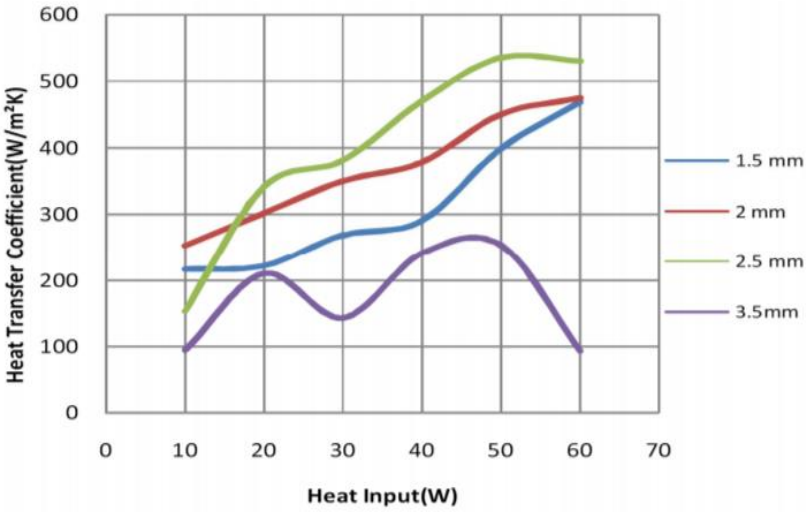

Fig 2-V. Effect of tube diameter of PHP on heat transfer coefficient [9]

Number of turns: The number of capillary-turns also influences the performance of a PHP. Khandikar showed that in his experiment [10], the higher the number of turns, the better the performance of the PHP. There have been other studies that show that there may be an optimum number of turns. In a study by Niti Kammuang-Lue et al [11], an optimum number of tubes was identified for the three fluids tested as shown in Fig 2-VI.

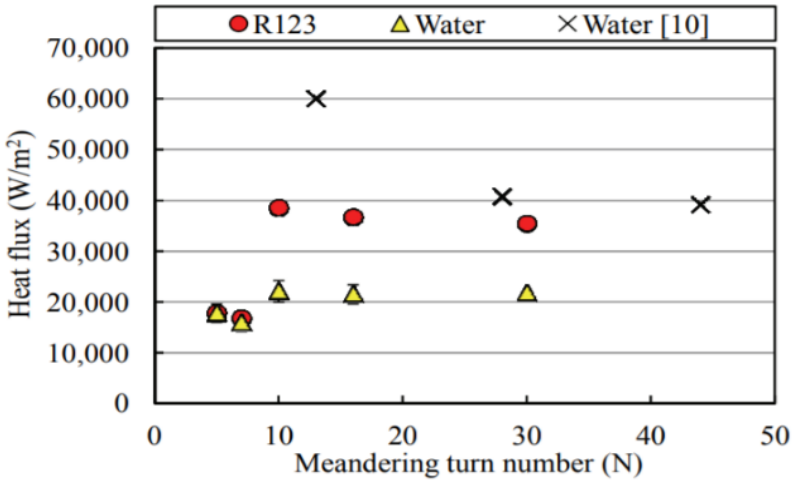

Fig 2-VI. Effect of number of turns on heat flux [11]

Orientation of the PHP: The angle of the PHP with relation to the gravity also affects performance. Not only does it affect the gravitational force involved but also affects the contact angle of the fluid, which in turn alters the pressure force necessary to sustain motion.

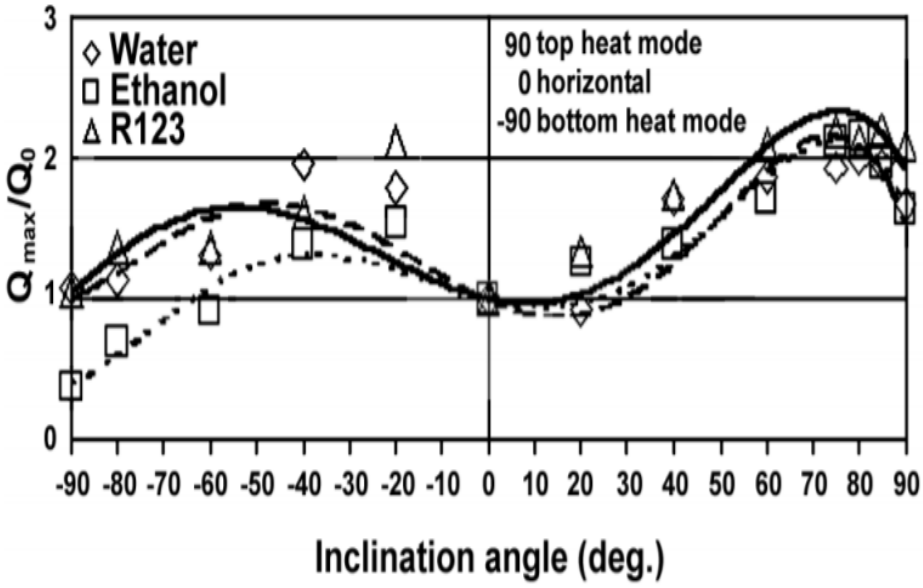

Fig 2-VII. Maximum heat flux versus inclination angle [10]

Fill Ratio: At low fill ratios there is liquid mass inventory which results in lower latent capacity and hence a lower performance and at high fill ratios there is less vapor plugs and hence lower circulation capacity leading to lower performance. It has been shown in multiple experiments that there tends to be an optimum fill ratio for a given set of conditions. Fig 2-VIII shows the effective conductivity for a Helium PHP in an experiment carried out by Fonseca at the University of Wisconsin - Madison [12]. The effective conductivity is a performance property analogous to the conductivity of a metal. It relates the amount of heat removed by the device to some temperature difference and a length scale that separates this difference as defined in chapter 5.3

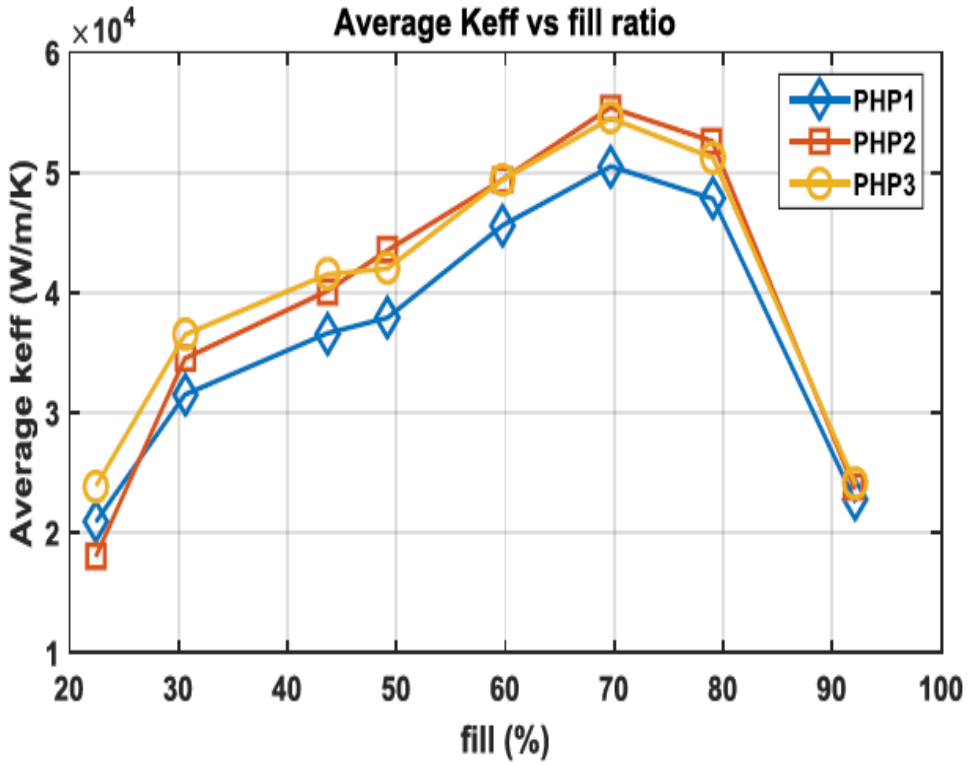

Fig 2-VIII. Effective conductivity of a He PHP as a function of fill ratio [12]

Working fluid: There have also been experiments carried out on different types of fluids to see how fluid properties affect the performance of a PHP. PHPs have been shown to operate with a wide range of fluids, from room temperature water to ethanol, down to cryogenic fluids such as Nitrogen, Neon and Helium. Fig 2-IX shows results of some room temperature experiments using a variety of working fluids.

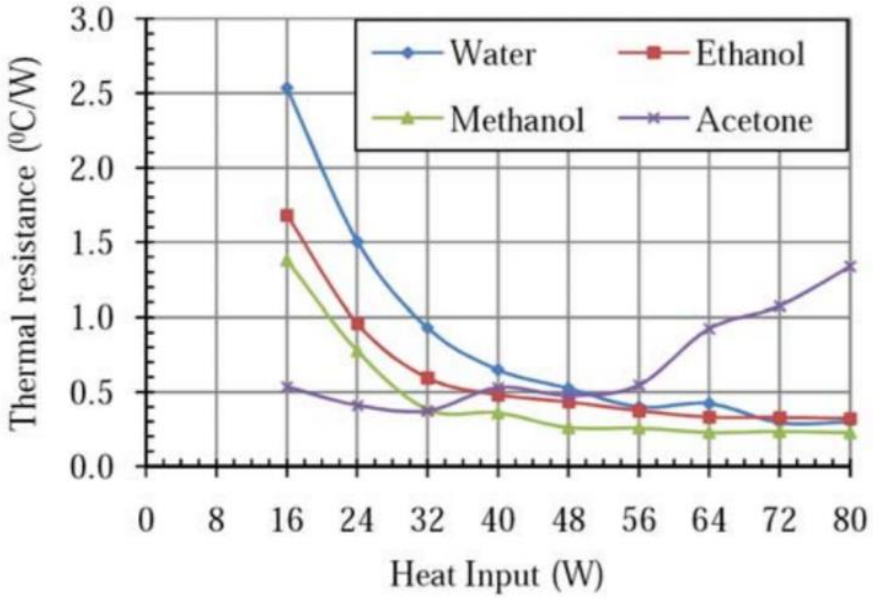

Fig 2-IX. Effect of working fluid on thermal resistance of a PHP [13]

There are other parameters that can influence a PHP's performance, although they have not been studied or reported in the literature. Some other parameters include condenser temperature, structure or geometry of the capillary tubes, orientation (horizontal/vertical or mixed sections), length of condenser, evaporator and adiabatic sections and capillary tube material. Some of these parameters are difficult to change because they require that a new PHP be built to change the physical configuration.

3 Literature Review

3.1 Nitrogen PHPs

There have been a few studies of cryogenic PHPs and most of these studies used Nitrogen as a working fluid. The literature includes studies that have explored the effect of variables including the number of turns, working fluid, and fill ratios on the performance of the PHP. Four of the studies have been found to have significance to the present work.

One of such study done by Romain Bruce et al [14] in 2018 was on a meter-long horizontal nitrogen PHP with 36 capillary tubes or 18 turns. The condenser, evaporator and adiabatic sections were 330[mm] long. The ID of the tubes was 1.5[mm] with a calculated critical diameter of 1.7[mm]. The evaporator and condenser were 400[mm] wide and made of copper. The experiment was done at a 50[%] initial liquid fill ratio and the heat load was varied from 5[W] to 30[W], with dry-out occurring at 30[W]. The results are shown in Fig 3-I. The maximum effective conductivity calculated was 85$\left[\frac{kW}{m-K}\right]$at a heat load of 15[W]. Bruce et al also reported that all pressure sensors in the PHP (two located at the adiabatic section close to the condenser and two at the adiabatic section close to the evaporator) gave similar readings and hence concluded that this is the saturation pressure of the PHP. Fonseca [12] had also noticed this negligible pressure drop in his helium pulsating heat pipe at a vertical orientation. Bruce et al also reported stability issues (rapid and relatively extreme rise in temperature and a sudden fall to a new steady state) when a high flux was immediately imposed on the evaporator section. While Bruce et al, noted the performance and stability issue of a horizontally oriented PHP, this work will evaluate the performance of a PHP that is oriented vertically including stability issues might be present in the vertical orientation. This work also explores the performance of the PHP at different fill ratios, not just 50[%].

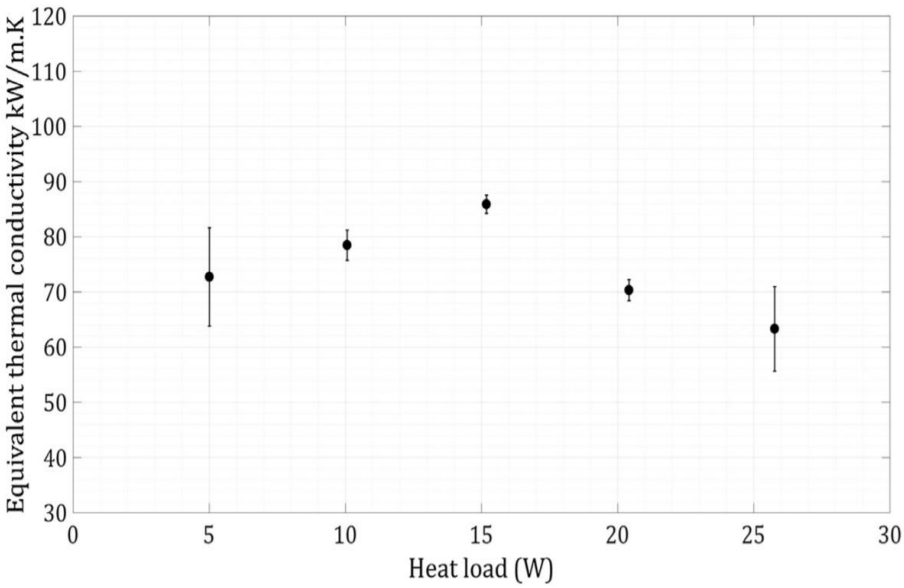

Fig 3-I. Effective conductivity versus Heat load [14]

Another study by Yi Li et al [15] investigated the dry-out phenomena in a horizontally oriented nitrogen PHP with 5 turns operating at 50[%] initial liquid fill ratio. The capillary tubes were 0.9[mm] in inner diameter. The evaporator, condenser and adiabatic lengths were 35[mm],35[mm] and 100[mm] respectively. The evaporator and condenser blocks were 100[mm] wide and made of copper. They reported a sharp rise in temperature at the evaporator during dry-out accompanied by a sharp drop in pressure, which they attribute to the non-oscillation of the PHP. Yi Li et al also reported a maximum effective conductivity of $16\left[\frac{kW}{m-K}\right]$ when tested vertically with bottom heating mode (evaporator under the condenser). Even though Yi Li et al ran loads until dry-out, the dry-out phenomenal was not investigated in detail. This work investigates the characterization of dry-out behavior as it relates to fill ratios, which was not investigated by Yi Li, as well as pressure and temperature behaviors at dry-out in a vertical orientation.

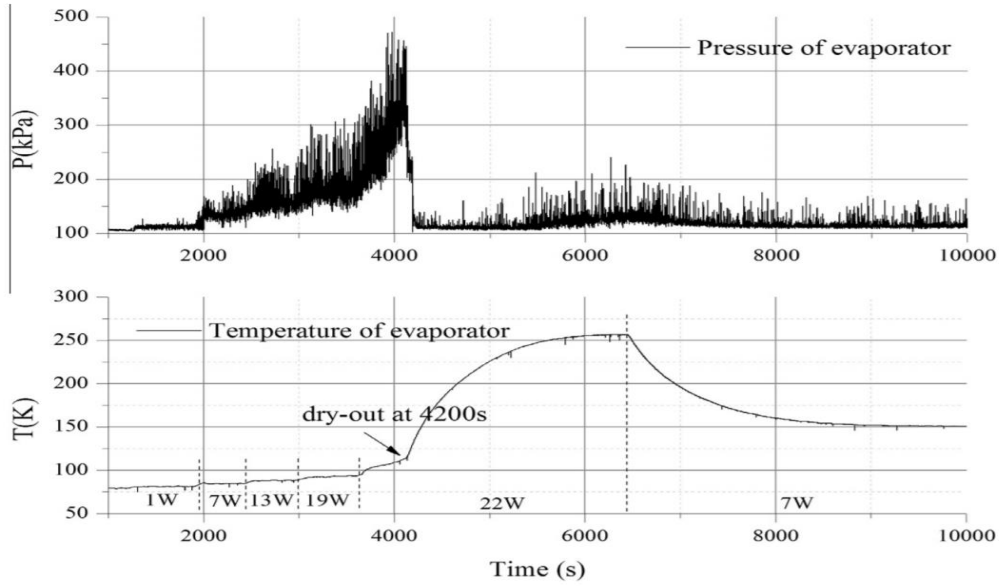

Fig 3-II. Dry-out behavior in a Nitrogen PHP [15]

Fonseca [16], at the University of Wisconsin-Madison, did a study on the effect of filling ratio on a vertically oriented Nitrogen PHP with a cylindrical evaporator having an ID of 50[mm] and a cylindrical condenser section with ID of 25.4[mm]. Both sections had an OD of 65[mm], height of 70[mm] and made from copper 110. The adiabatic length was 80[mm]. The capillary tubes where stainless steel 304 with 1D of 0.5[mm] and 20 turns. The PHP ran at a horizontal orientation had an effective thermal conductivity that ranged from $5\left[\frac{kW}{m-K}\right]$ at 46[%] liquid fill ratio to $35\left[\frac{kW}{m-K}\right]$ at 27[%] liquid fill ratio. There are some improvements made to the result by Fonseca that have been carried out in this study. First, the Nitrogen fill valve in Diego's study was left open during heat load changes and as such the mass varied during the heatload changes. This study investigates the effect of a closed/constant mass and varying heat load on the PHP performance. Second, the actual condenser temperature in Diego's study drifted from the desired sink (cold source or condenser) temperature because of thermal response on the fluid. In this study the condenser temperature, which is effectively used in calculating the effective thermal conductivity of the PHP,

is held constant and so the effect of the load is not influenced by a drifting sink temperature. Because the heat load and condenser temperature could be controlled independently in this work, the effects of the condenser temperature can be separated from the effects of heat load.

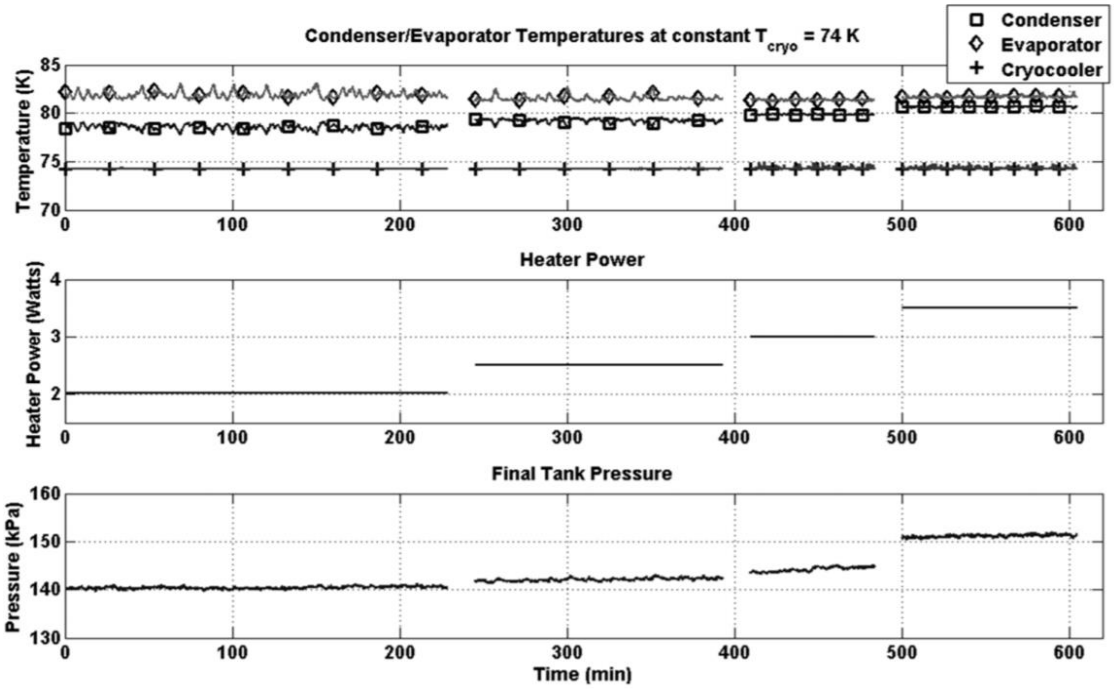

Fig 3-III. Nitrogen PHP steady state operation [16]

Finally, Kyohei Natsume et al [17] investigated the possible use of PHPs for cooling superconducting magnets. Natsume et al tested the effect of working fluids, He, H_2 and N_2 on the performance of the PHP. Also tested, was the effect of fill ratio and heat load in each case. The PHP had 10 turns of stainless tubes with ID of 0.78[mm]. The copper evaporator and condenser blocks had lengths of 30[mm] separated by a 100[mm] length adiabatic section. Table 1 shows the result of their experiment with N_2 having the highest effective conductive over the range of fill ratio tested. The study in this paper investigates one more parameter, the condenser temperature, to quantify the effect it has on the behavior of the effective thermal conductivity.

Summary of experimental results for cryogenic OHPs in pipe diameter of 1/16 in.

Working fluid	Liquid filling ratio (%)	Heat input (W)	Cooling part temperature (K)	Heating part temperature (K)	Effective thermal conductivity (W/m K)
H_2	31–80	0–1.2	17–18	19–27	500–3500
Ne	16–95	0–1.5	26–27	28–34	1000–8000
N_2	17–71	0–7.0	67–69	67–91	5000–18,000

Table 1. Summary of the experiment results by Natsume et al [17]

In addition to the small-scale test carried out on a PHP, a large-scale Nitrogen PHP has been tested by the Commission for Atomic Energy and Alternative Energies (CEA) in France. The PHP had a lateral length of 3.6[m] and comprised of 36 tubes, with an inside diameter of 1.5[mm]. Though the PHP did have a short quasi-steady state time of 33[mins] with the temperature run-off afterwards, they reported an effective conductivity of $100\left[\frac{kW}{m-K}\right]$. Quasi-steady performance, before temperature run-off, for a period of about 10 mins at dry-out power has sometimes been observed in current work and may be investigated in future work.

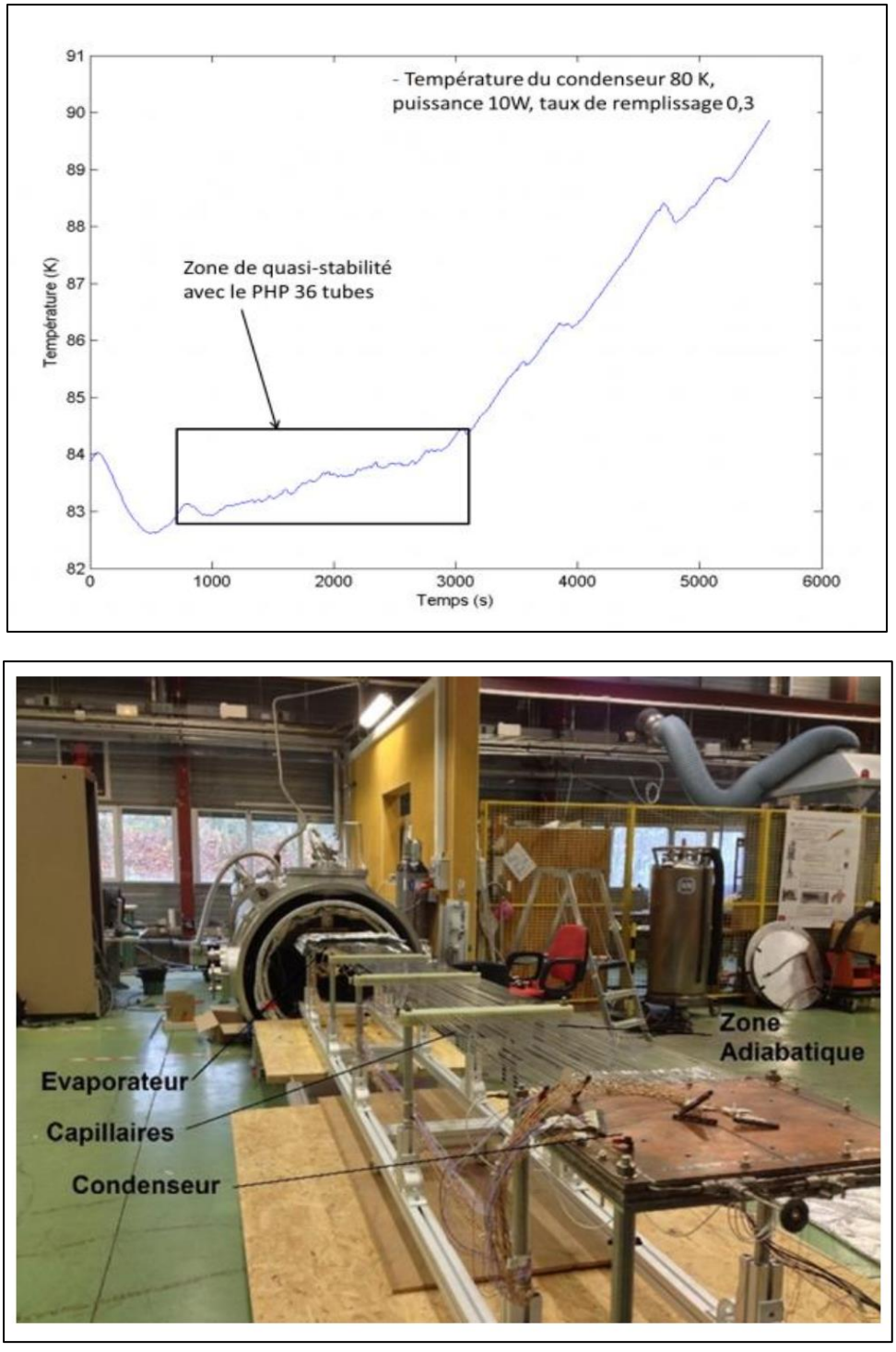

Fig 3-IV. Temperature plot (Top) and test section (Bottom) of a 10W Nitrogen PHP at CEA [18]

3.2 Some other Cryogenic PHPs

There has been one reported case where the condenser temperature was used as a performance criterion. Qing Liang et al [19] investigated the effects of condenser temperature in a Neon PHP, vertically oriented with 10 parallel tubes or 5 turns. The tubes had an ID of 1[mm]. The evaporator and condenser copper blocks had a length of 100[mm] each while the adiabatic length was 280[mm]. The figure below shows the effect of condenser temperature at an initial fill ratio of 35.9[%]. This research aims to see the effect of changing condenser temperature and the magnitude of such effect on the performance of a Nitrogen PHP. Also, while Liang et al focused on the effect of fill ratio on Neon PHPs with a few condenser temperatures, this work focuses on more intervals of condenser temperature in addition to a number of fill ratios to create a complete 3D map of the effect of condenser temperature and fill ratio on the effective conductivity of a Nitrogen PHP.

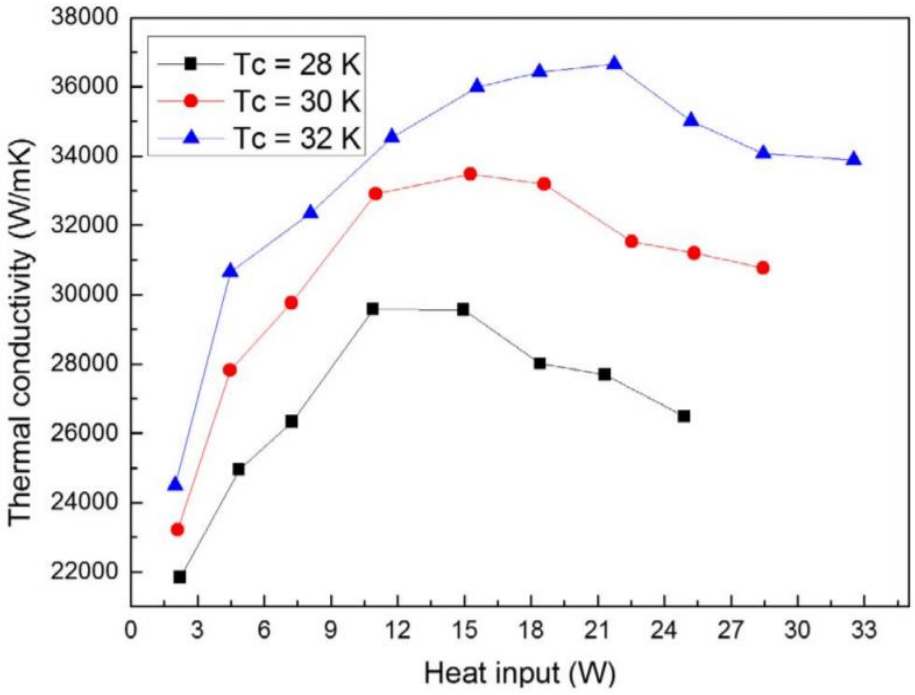

Fig 3-V. Effect of condenser temperature on Thermal Conductivity of a neon PHP [19]

Monan Li et al [20] carried out an experiment on a helium PHP to capture the effect of number of capillary tube-turns on the performance of the PHP. The initial liquid fill ratio was approximately 70.5[%] in both cases. The length of the evaporator and condenser were 50[mm] each, while the adiabatic section was 100[mm]. The experiment was used to test 8-turns and 24 turns of same size and dimensioned stainless tubes. The results showed that the 8-turn performed better (in terms of effective thermal conductivity) at lower heat loads reaching a maximum at a heat load of 271[mW]. As heat load was increased, the performance depreciated and the 24-turn performed better, reaching a maximum at a heat load of 1100[mW]. The maximum effective conductivity at the fill ratio operated was 15652$\left[\frac{W}{m-K}\right]$ for 8-turn and 12328$\left[\frac{W}{m-K}\right]$ for 24-turn leading to the presumption that a parallel configuration of the three 8-turn PHPs to make 24-turns would be more efficient that a single 24-turn loop, at least in a vertical orientation. While not directly related to current research, future work on a new PHP with fewer turns may build on such information.

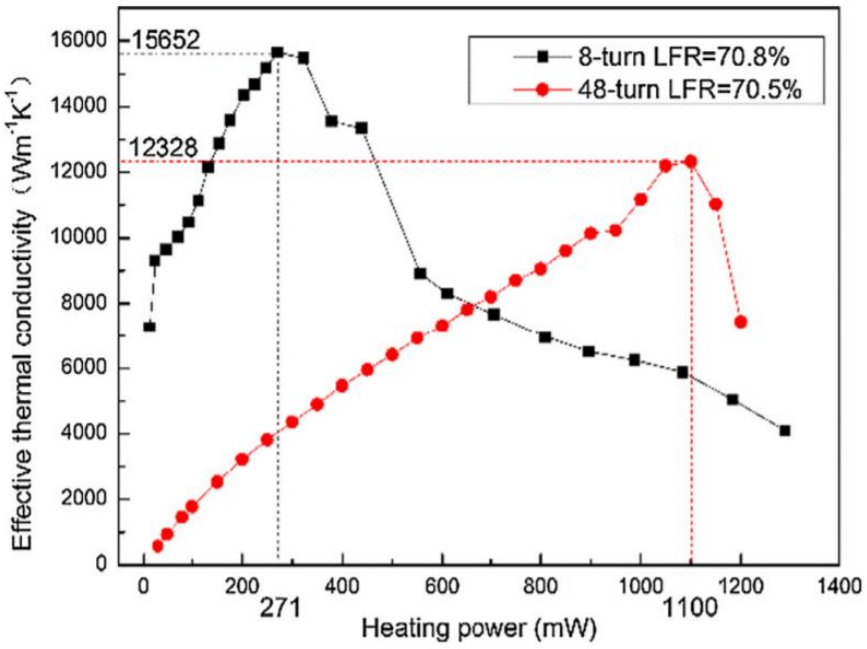

Fig 3-VI. Effective thermal conductivity versus heat load [20]

This research paper aims to address some areas of cryogenic PHPs that have not been investigated. Such areas are summarized below:

a. The effects of condenser temperature on effective thermal conductivity of both pure fluids and mixture PHPs in a vertical orientation. This is done while simultaneously looking at effects of heat load and fill ratio in order to create a 3D performance map.
b. Analyzing dry-out behaviors in those PHPs with respect to condenser temperature and fill ratio.

4 Experimental Setup and Calculations

4.1 Main Equipment Construction/Setup

4.1.1 Cryocooler

The PHP is cooled by a Cryomech AL-25 GM Air-cooled Cryocooler with a CP820 Cryomech Compressor. It is a single stage cryocooler providing a cooling load of 22[W] at 70[K]. The Cryocooler is attached to a circular aluminum block, to which the PHP is attached.

4.1.2 Dewar

The dewar is a stainless-steel cylindrical container with OD of 9.5[in] and a height of 24.5[in]. The top plate of the dewar is made from aluminum with a diameter of 12.5[in] and 1.16[in] thick. The top plate has three active 19 pins Amphenol connectors, one carrying current to the temperature sensors (2 pins for each temperature sensor), one returning the voltages to the controlling instruments (2 pins for each temperature sensor), and one designated for heat loads and control (4 pins for each heater). The top plate also serves as the entry point of the cryocooler into the dewar as well as that of the gas supply line. The dewar is pumped to high vacuum ($\leq 10^{-5}$torr) to eliminate convective heat transfer.

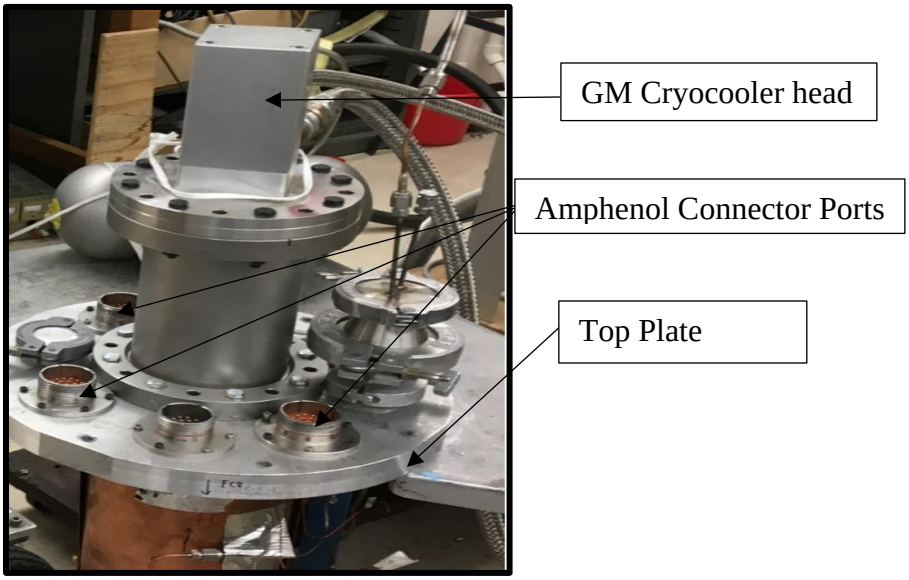

Fig 4-I. Top plate of dewar with mounted cryo-head

4.1.3 Pulsating Heat Pipe

The pulsating heat pipe, shown in Fig 4-II and Fig 4-III, is made up of 40 stainless steel capillary tubes or 20 serpentine turns. The tubes have an ID of 0.5[mm] which is about half the critical diameter at 115[K]. This diameter was chosen based on available laboratory material and with the intent of running helium as the working fluid. The evaporator and condenser are identical copper circular hollow blocks with one closed end. The ID, OD, and height of 55[mm], 63.8[mm] and 50[mm] respectively. The length of the adiabatic section is 265[mm]. The condenser and evaporator have forty 0.25[mm] deep grooves that run the height of the copper block to which the capillary tubes are soldered on for good thermal contact. The capillary pipe was bent with a pitch size of about 5[mm]. Each pair of tubes is connected at the top and the bottom with bent copper extensions soldered to the tubes. These extensions are originally designed to make it possible to alter the number of working turns. However, this area of research was abandoned because of the difficulty in creating a leak tight seal in multiple solder joints. The PHP fill line is connected to two of the capillary lines from the evaporator via a copper tee-block. The PHP assembly is connected to the circular aluminum block via the condenser block, which in turn is fixed to the cryocooler head. A copper thermal jacket is attached with screws to circular supports around the PHP and this provides good thermal contact between the PHP condenser and the cryocooler. Around this thermal jacket are layers of multilayer insulation, MLI, to reduce the radiation parasitic heat leak.

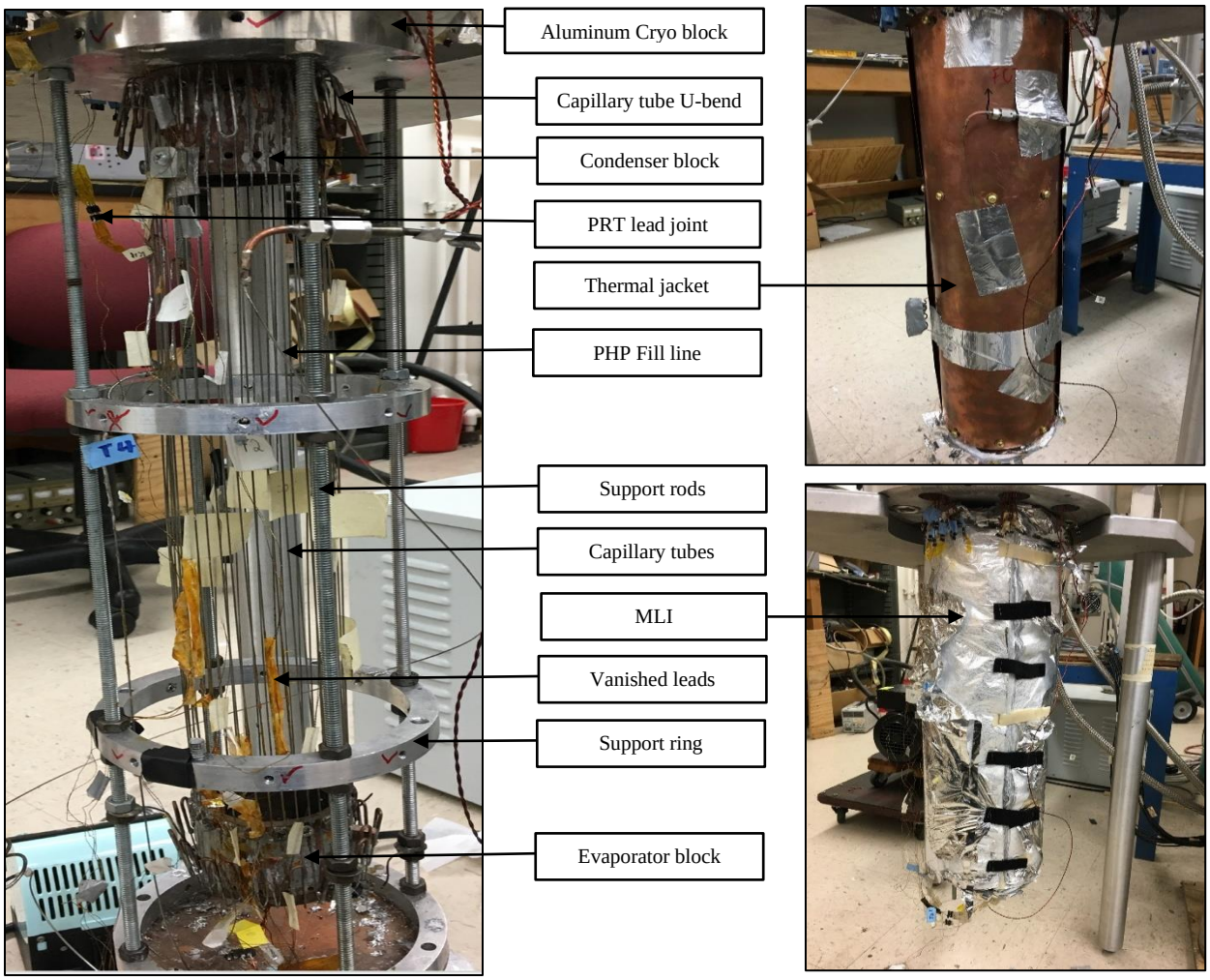

Fig 4-II. PHP Core Assembly

4.2 Auxiliaries

There are two auxiliary DC current/voltage producing boxes connected to the experiment. One is a Lakeshore 120 Current Source box providing 1[mA] DC current to the lakeshore PT100 temperature sensors. The other is a BK Precision 1698 Power supply box providing the voltage to power the chassis resistor connected to the evaporator and hence provide a known heat load. This power supply has a variable voltage setting and hence the heat load to the evaporator can be controlled.

4.3 Measurement Devices

4.3.1 Temperature sensors

There are five (5) PT100 Lakeshore temperature sensors used in the experiment. One placed on the condenser block, one on the evaporator block and three on the stainless capillary tubes in the adiabatic section. One of the adiabatic section sensors (T2) is located 7.9[cm] above the evaporator sensor (T6). The next adiabatic section sensor (T4) is 1[cm] above T2 and finally the last adiabatic section sensor (T5) is 2[cm] above T4. All three (3) adiabatic section sensors are relatively closer to the evaporator than to the condenser. All the sensors are attached at their individual locations with VGE-7031 varnish [22] and their leads also varnished to ensure parasitic heat to the sensors are grounded to the measuring temperature. The sensors were connected using the 4-wire technique with a pair of wires carrying the current to and from the sensor and the second pair acting as the voltage leads. The PRTs are sensitive to resistance changes especially at low temperature, therefore a small change in resistance could correspond to a sensible change in temperature. Since wire leads are significantly long, their resistances begin to have meaningful impact on actual measurements. This technique eliminates any voltage drop due to the resistance of the wire leads and the voltage drop measured is only because of the resistance of the sensors, ensuring higher accuracy.

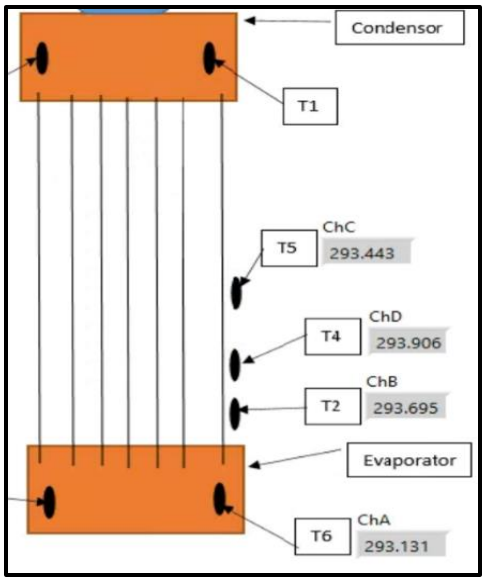

(a)

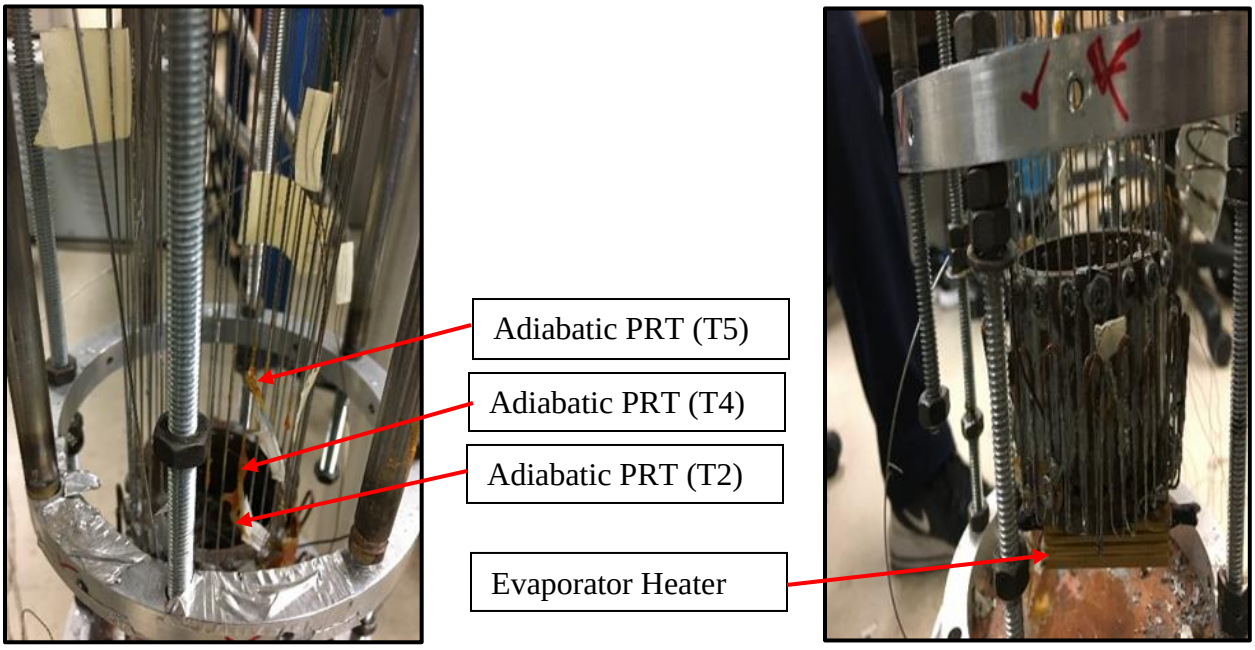

(b) (c)

Fig 4-III. (a) Schematic location of PRTs (b) mounted adiabatic section PRTs (c) location of evaporator heater

4.3.2 Pressure sensors

There are two Endevco 8530B pressure sensors used in the experiment. One (0-500psig) is placed at the end of the Buffer Tank, used in the calculation of the initial fill ratio in the PHP device. The other (0-500psia) is located on the gas line just before the safety valve and is connected to the adiabatic section of the PHP. That sensor is used to measure the working or saturation pressure of the PHP. The pressure sensors were excited with 10[V] from a DC power supply. The sensors have sensitivity of $0.6 \pm 0.2 \left[\frac{mV}{psi}\right]$ with a full-scale output of 300 ± 100[mV]. The sensors were calibrated with a Endress+Hauser (EH) pressure gauge (absolute) having a 0.05% accuracy. The voltage readings from the sensor were recorded in LabVIEW via the DAQmx (Refer to 4.6.2 Pressure DAQs).

4.4 Heaters

Two chassis resistors, each 50 Ω, are used with the PHP setup. One is located under the evaporator block and is used to provide the heat load to the device. The other is located on the aluminum block attached to the condenser. That is used, along with the temperature controller, to maintain a desired condenser temperature. Both heaters are wired using the 4-wire measurement technique. The relationship between voltage and a given resistance produces the necessary current to achieve a given power according to Ohm's law:

$$I = \frac{V}{R} \tag{4.1}$$

$$P = IV \tag{4.2}$$

The voltage, V for both the evaporator heater and condenser heater can be varied via the BK Precision 1698 Power Supply and Lakeshore 332 Temperature controller, respectively. The BK is a 1-60[V], 0-3.3[A] Power Supply capable of delivering a maximum of 200[W]. It has a $\pm 1\%$

relative error for both its current and voltage measurements plus 2 counts or 0.02 for voltages above 5[V] and currents above 0.5[A].

4.5 Vacuum System

The vacuum in the dewar is provided by an oil free Pfeiffer vacuum station consisting of a diaphragm pump and a turbo unit. The vacuum pressure registered with the device after leak checks was $\cong 10^{-5}$torr. The current device used to monitor the vacuum pressure is a Kurt J. Lesker convective gauge with a minimum read out of 10^{-4}torr. This gauge was zeroed at vacuum with a turbo pump. Throughout the experiment, the vacuum pump remained on to ensure that vacuum pressure is maintained.

4.6 Data Acquisition Systems (DAQs)

4.6.1 Temperature Controllers

A Lakeshore 332 Temperature Controller is used to control and maintain a preset setpoint temperature of the condenser. The condenser (T1) PT100 sensor is wired directly to the Lakeshore controller. The Lakeshore controller is designed to supply 1μA at low temperatures to the sensor to reduce parasitic heat load due to ohmic generation in sensor leads, although for positive temperature coefficient RTDs, it supplies 1mA. The default read rate is 10 samples per second. The standard temperature curves for platinum RTDs were used with all the sensors. The temperature control is via the internal variable DC current source to the condenser heater, which is controlled by a PID (Proportional-Integral-Derivative) controller integral to the Lakeshore box. It is designed to produce 1A at 50W, which translates to 100% full power at High setting for a 50Ω resistor. The controller, via feedback loop, then varies the percentage of full-scale current and hence full-scale power necessary to maintain a setpoint temperature. The PID coefficients were picked based on trial-and-error method as described by [23]. Throughout the course of the experiment, these coefficients had to be constantly optimized because of their sensitivity to the

set-point temperature chosen. Initially a large P-Gain of 22 and I-Reset of 4 were chosen. It was later discovered that two-phase instabilities could cause a ripple effect in control instability and lead to large temperature swings that took a long time to stabilize. Also, during changes in setpoint, the entire PID history is reset, and the system starts from scratch to build its stability at steady state. For this reason, in later experimental runs, a high baseline manual output coefficient of 15 was set. A small variable P-Gain of 2 and I-Reset of 0.2 were chosen. This ensured that the system always keep this baseline memory and could adjust slowly around this baseline for more stable operation. This produced the best results in terms of temperature stability in the condenser.

The second temperature controller is a Cryocon 24C Temperature controller. The evaporator (T6) PT100 temperature sensor, as well as the three adiabatic section temperature sensors T2, T4 and T5 are connected to this controller. The controller is used as a reading device rather than a controlling device. It supplies a current of 1mA to the sensors and directly converts the resulting voltage to a temperature read out. The sample rate on each of the inputs to the Cryocon is 15Hz.

4.6.2 Pressure DAQs

The voltage leads of the two pressure sensors are connected to an NI 9201 Module that is plugged into a cDAQ instrument. The 8 channel NI Module is rated at $\pm$10V with a sample rate of 500kS/s and a resolution of 12bits. As mentioned before, the two pressure sensors were calibrated using an Endress+Hauser pressure gauge and a linear fit between pressure (from the EH gauge) and voltage (from the sensors) was used in the LabVIEW program. The EH gauge readings were also compared to pressure readings from an attached compound gauge. To keep up with the CPU processing, 10 samples at a rate of 10Hz was chosen. This is adequate, since we are most interested in steady state performance and pressure data at intervals shorter than 1 sec is identical to data sampled at 1 sec. The RMS (Root Mean Squared) error from the Fill Tank pressure sensor and the PHP pressure

sensor were 0.999 and 1 respectively. Though the uncertainty of the sensors is low, the accuracy is not very low. The calibration curves in *section 12.4* (12.4 Pressure calibration curves.) shows the linear fit of two different calibration done on the PHP sensors, spaced 9 months apart. The accuracy of the sensor at zero voltage was calculated to be 18%. This might be due to the inevitable drift of pressure sensors over time.

4.6.3 Data Acquisition Software Interface and Control (LabVIEW)

The functionality of the experiment is mostly controlled and read by the LabVIEW program. This includes condenser temperature control (PID settings), evaporator heat load adjustments, temperature value readouts and storage, pressure value readouts and storage, condenser, and evaporator heater power calculations. Each LabVIEW run is automated and can be controlled remotely. The BK Precision 1698 (Power Supply), Cryocon 24C (Temperature Controller) and Lakeshore 332 (Temperature Controller) have LabVIEW VIs associated with their hardware. Some of these VIs' were used to setup the main LabVIEW program that runs the PHP real time data collection and control. National Instrument's internal VIs were used to set up logging for pressure data.

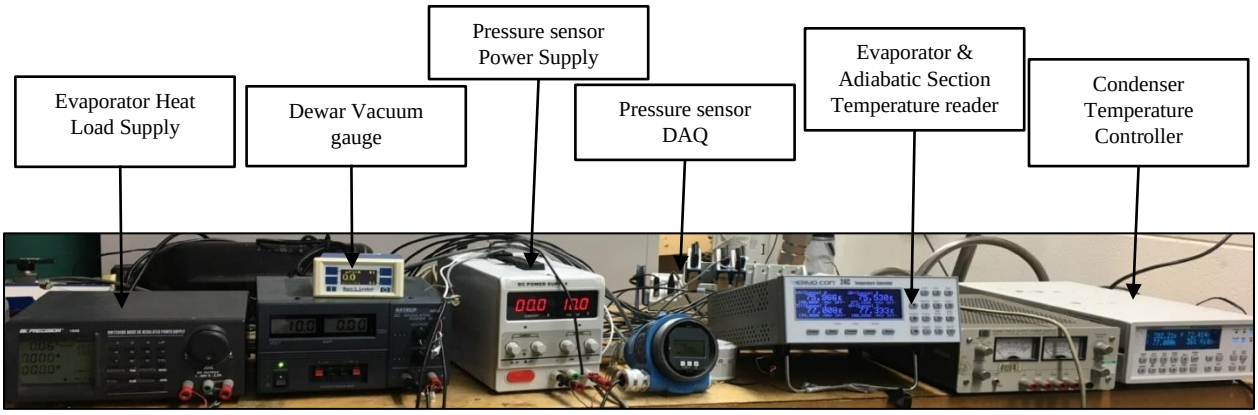

Fig 4-IV. Auxiliary Devices and Controllers

4.7 Heat Leaks/Parasitic loads

4.7.1 Heat Generations & Solid conduction

In the PRT and heater wire leads, heat generation is calculated to be larger than conduction through the leads because of the long length as well as the small cross-sectional area. Therefore, the heat leaks due to the presence of the PRT, and heater wires is based on the ohmic heating:

$$\dot{Q}_{leads} = I_c^2 R_e \tag{4.3}$$

$$R_e = \frac{\rho(T)L}{A_c} \tag{4.4}$$

where $\rho(T)$ is the temperature dependent electrical resistivity of the wire, L is the total length of each wire, A_c is the cross-sectional area of the wire and I_c is the current sent by the controllers, which for the PRT wires is 1mA standard and for the heater wires is a maximum of 1A. The result is a maximum heat load through the leads, $\dot{Q}_{leads}$, of 0.75W with the generation in the heater leads, the dominant source. The PID limits the maximum current to less than 50% or a $\dot{Q}_{leads}$ of 0.19W

4.7.2 Molecular Gas Conduction

A good vacuum is desired to ensure that residual gas conduction is minimized. The residual gas conduction can be calculated by Corruccini equation [24]:

$$\dot{Q}_{res} = \bar{\alpha}\frac{(\gamma+1)}{(\gamma-1)}\left(\frac{2R}{\pi M\bar{T}}\right)^{\frac{1}{2}} PA_{s,s}(T_h - T_c) \tag{4.5}$$

where P is the vacuum pressure, $\bar{T}$is the inner temperature of dewar wall, γ is the ratio of specific heat and $A_{s,s}$ is the surface area of the copper shield. This leads to a $\dot{Q}_{res}$ approximately equal to 0.3W.

4.7.3 Radiation Shield/MLI Parasitic

Radiation is an important mode of heat transfer in cryogenics. Since vacuum pressures are typically kept low, radiation becomes a dominant source of heat transfer and steps must be made to reduce it. Two common methods of doing this are: including a thermal shield between the dewar surrounding and the test device and wrapping the thermal shield with a non-conductive reflective material, the most common being multilayer insulation (MLI). MLI is typically made up of alternating layers of Mylar or Kapton and Aluminum or Silver. The former acts as an insulating material between the highly conductive metal and the later acts as a reflective material with low emissivity to reduce irradiation. During MLI construction the following factors are worth noting:

i. The heat flux scales as $(N+1)^{-1}$
ii. The axial heat transfer down the length of the MLI is much greater than the heat transfer through the layers of the MLI
iii. Exposed areas of MLI can lead to significant radiation leaks
iv. Contaminants such as oil, even from human hands, can adversely affect the performance of the MLI

The plot in Fig 4-V is used as a reference for MLI radiation calculation. This includes the radiation and well as conduction effect through the MLI.

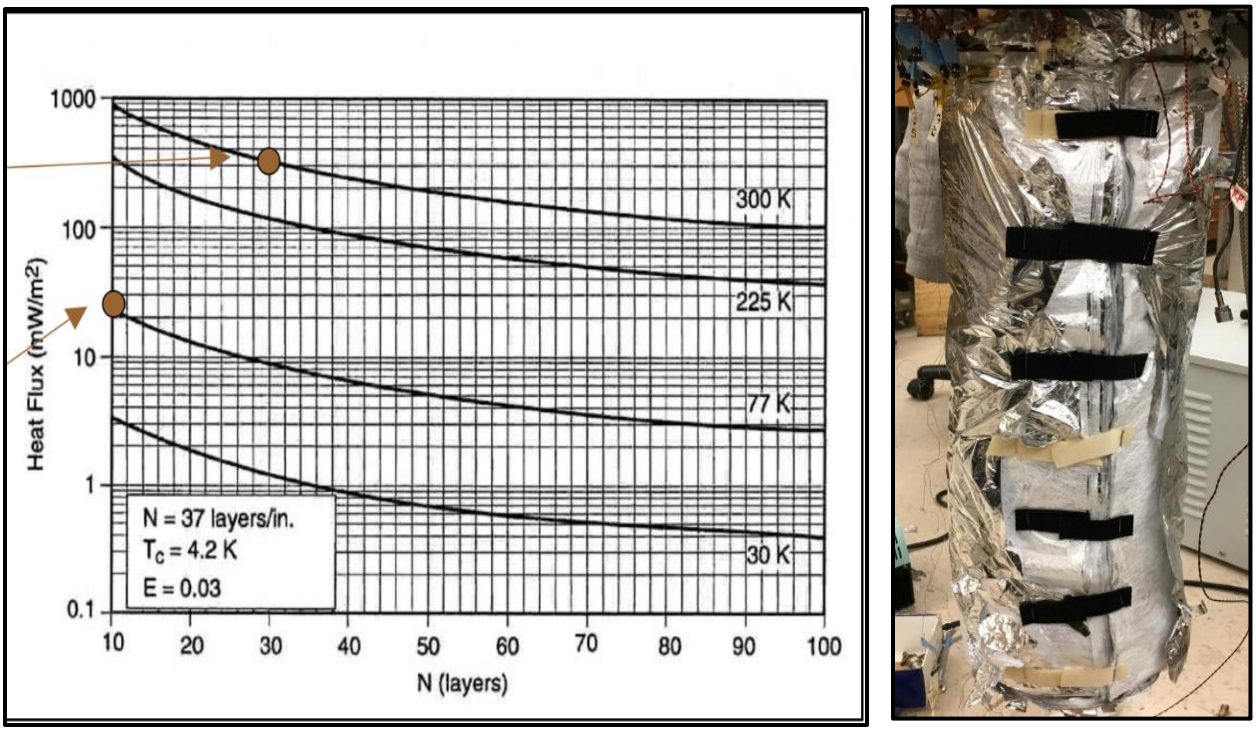

Fig 4-V. (Left) Heat flux as a function of number of MLI layers [25], (Right) Velcroed edges of MLI

The current PHP experiment uses 30 layers of MLI and so from the plot above a heat flux of $300\frac{mW}{m^2}$ is assumed to be incident on the copper thermal shield. This results in $\dot{Q}_{rad}$ of 0.07[W].

4.7.4 Modified Residual leaks through MLI

The heat transfer rate has been found experimentally to be a function of the vacuum pressure showing that both molecular gas conduction, radiation heat transfer and conduction through the MLI are happening at the same time. One such empirical equation to predict the heat flux is by the "Lockheed equation" [26] & [27]:

$$q'' = \frac{C_s \bar{N}^{2.63}(T_h^2 - T_c^2)}{2(N+1)} + \frac{C_R \varepsilon (T_h^{4.67} - T_c^{4.67})}{N} + \frac{C_G P (T_h^{0.52} - T_c^{0.52})}{N} \qquad (4.6)$$

The first term accounts for solid conduction heat transfer (The temperature squared term falls from a fit for the temperature dependent conductivity incorporated to ΔT), the second for the radiative

heat transfer and the last for the gaseous conduction heat transfer. The above equation was later modified by McIntosh [28] and given as:

$$q'' = \frac{C_2 f K (T_h - T_c)}{\Delta x} + \frac{\sigma (T_h^4 - T_c^4)}{\frac{1}{\varepsilon_h} + \frac{1}{\varepsilon_c} - 1} + C_1 P \alpha (T_h - T_c) \tag{4.7}$$

where C_1 is 1.1666 for air and C_2 is an empirical coefficient. The above equation is not easily computed because of unknowns such as C_2 and so experimental data by Jeffrey Robert Feller et al [29] helps in the calculation of heat transfer through MLI. The equation provided by [29] is given below:

$$\dot{q}'' = k_{app} \left(\frac{C}{1 + k_{app}} \right) \frac{d}{t} P (T_h - T_c) + \dot{q}_0'' \tag{4.8}$$

$$\frac{d}{t} \cong \frac{1}{N - 1} \tag{4.9}$$

$$C = \bar{\alpha} \frac{(\gamma + 1)}{(\gamma - 1)} \sqrt{\frac{R}{8 \pi M T_h}} \tag{4.10}$$

$$d = \frac{1}{\overline{N}} \tag{4.11}$$

$$k_{app} = a (Pd)^{\beta} \tag{4.12}$$

where a and β are fit coefficients, $\overline{N}$ is the layer density, $\dot{q}_0''$ is the experimental residual heat at zero pressure, $\bar{\alpha}$ is the accommodation coefficient and γ is the ratio of specific heat. Using the above expressions, and an $\bar{\alpha}$ of 0.8, the heat transfer through the MLI, $\dot{Q}_{MLI}$ was calculated to be 0.14W.

In conclusion the two major parasitic heat loads are summarized as $\dot{Q}_{leads}$ = 0.19W and $\dot{Q}_{MLI}$ = 0.14W

4.8 Experiment Assembly and Methodology

(Refer to Fig 4-VII for the schematics that accompanies this section). The PHP fill line is connected via a gas line to the buffer tank as well as the high-pressure tank. There are three needle valves and one safety valve on the gas line train. The safety valve was tested to 80psig which is its setpoint. The first valve (valve 1) is a vent valve and is used to empty the system before any fill gas from the buffer tank is released into the assembly. The second valve (valve 2) is in front of the buffer tank and third valve (valve 3) is located before the safety valve. This is the valve that would be used to isolate the PHP system from the room temperature gas line. Before each fill, the buffer tank may be filled from the high-pressure tank to a sufficient pressure (must be below 80psig to prevent safety valve from opening) by opening the main valve on the High-pressure tank with valve 1 and 3 closed and valve 2 open. When the desired high pressure-tank regulator pressure equals that of the buffer tank, the main valve and valve 2 is closed. The end of valve 1 houses a KF fitting that is connected to a vent pumping station (Roughing & Turbo pumps). Valves 1 and 3 are then opened and entire system is vented to produce a vacuum after which the valves are closed. Now valve 2 is opened (with valves 1 and 3 closed) and the buffer tank steady state pressure at this point is being read and recorded on the LabVIEW program. This is known as the start pressure P_{start}. Valve 3 is then slowly opened until the pressure required to achieve a preset fill ratio is achieved and then the valve is closed. A few minutes is allowed for equilibrium of the buffer tank gas content with the surrounding. The new pressure of the buffer tank is read and recorded from LabVIEW. This pressure is known as P_{end}. These pressures are then used in an EES (Engineering Equation Solver) script to calculate the initial fill ratio of the run.

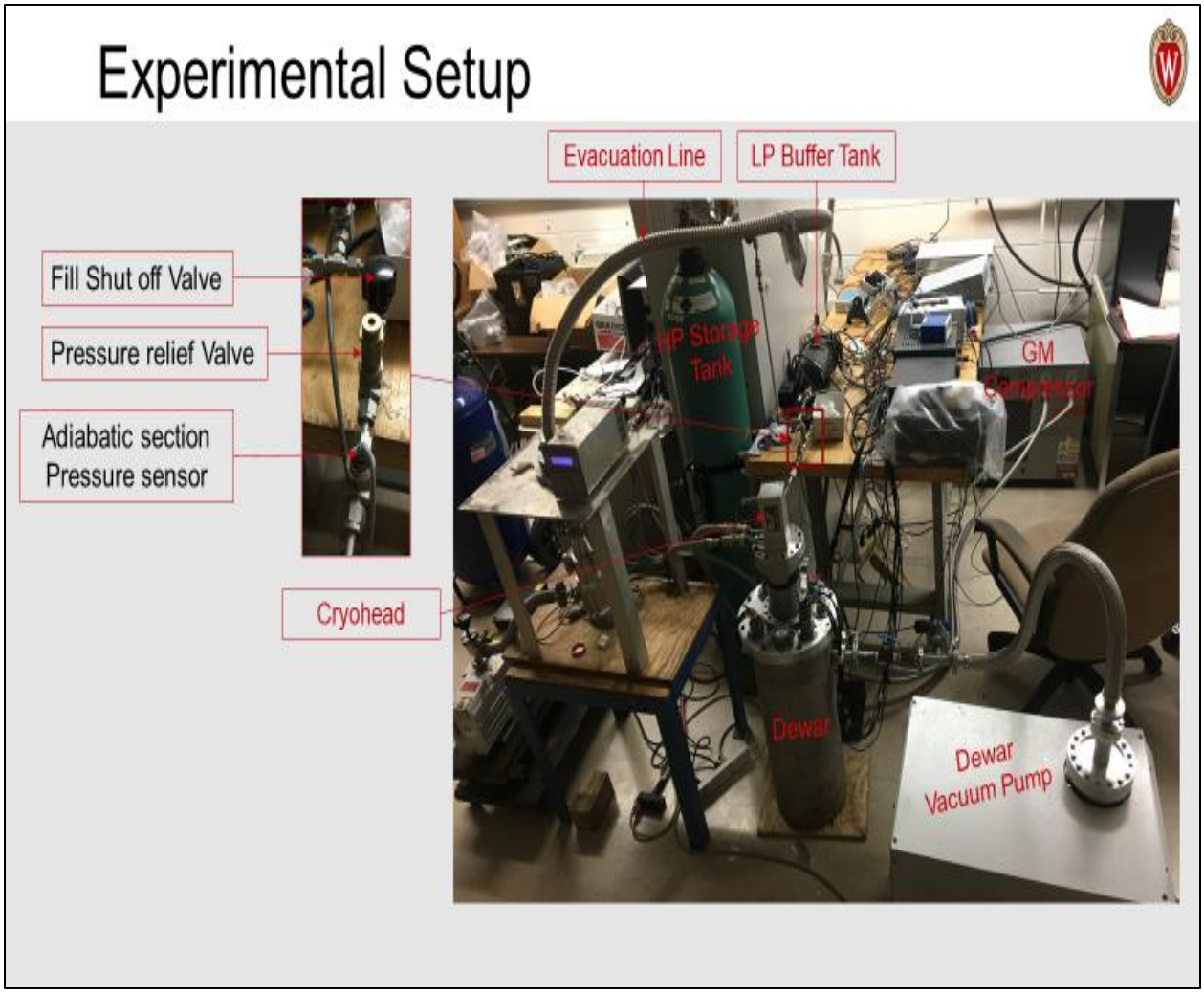

Fig 4-VI. Complete Experimental Setup

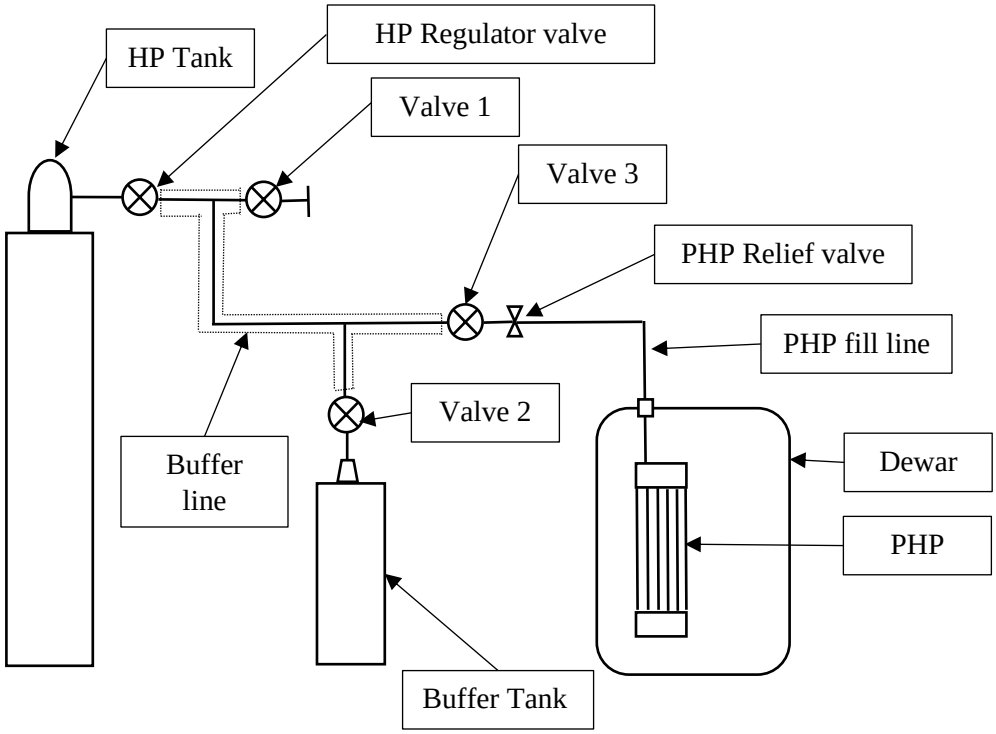

Fig 4-VII. Schematic of gas train showing valve locations

5 Methods and Results

5.1 Condenser Temperature intervals & Heat Loads

The condenser temperature was varied from 71K to 83K in intervals of 2K. The Lakeshore 332 temperature controller was used to maintain the set condenser temperature to within $\leq 0.3K$ of the setpoint. The heat load is normally varied from 0W to the onset of dry-out in interval of 1W and then increased by 0.2W after the onset of dry-out (onset of dry-out is taken to be when there is a largest temperature gradient with the next 1W increment). The duration of each applied input depends on various factor such as how long until the evaporator reaches steady state (steady state is defined by temperature oscillations about a mean value, with amplitudes typically $\leq$ 1K), how long from an instability point to a new steady state or unattended period. However, the typical length of each heat input run is $\geq$ 30mins.

5.2 Data Averaging and Processing Software (MATLAB & Excel)

Real time data of the pressure and temperatures in the system is taken at least once every second, therefore these large sets of data need to be averaged at steady state condition. The temperatures and pressure data are stored by LabVIEW measurement file (.lvm), which is a text-based file. This was found to be the most compressed form for such a large data and one that resulted in little to no output problems. A MATLAB script was written, which uses an external function created by M. A. Hopcroft [30] to read the file, and then graphically process and average the data. The averaged data for each heat load at a given condenser temperature was then exported to an Excel sheet that computed the effective thermal conductivity and registered the critical heat load for that condensing temperature.

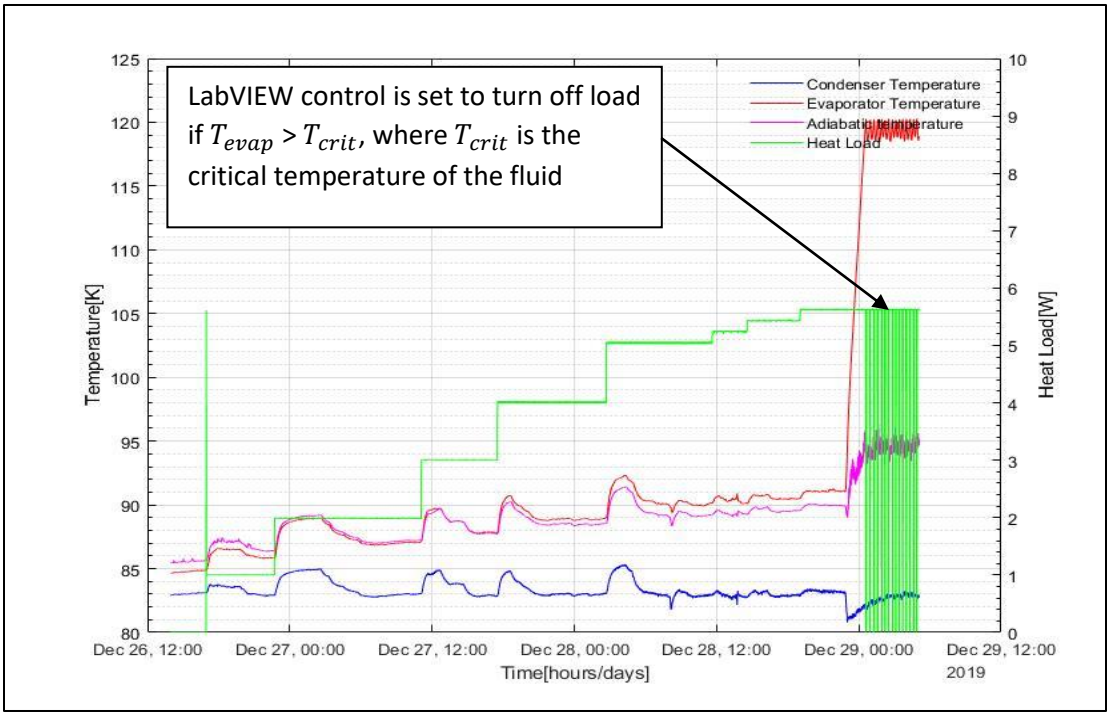

	A	B	C	D	E	F	G	H	I	J	K	L
1			77K									
2	Power	Avg_cond	Avg_evap	Avg_DT	P_avg	DP_t	DT_t	DP/DT	Avg_adiat	Dta_t	DP/Dta	k_eff
3	0	76.95	79.03	2.08	14.28	0	0	0	81.66	0	0	0
4	0.5	77.08	80.11	3.03	14.52	0.24	1.08	0.222222	81.54	-0.12	-2	6791.226
5	1	77.04	80.82	3.78	14.55	0.03	0.71	0.042254	80.65	-0.89	-0.03371	10887.52
6	1.5	77.03	81.32	4.29	14.75	0.2	0.5	0.4	80.98	0.33	0.606061	14389.8
7	2	77.14	82.13	4.99	15.18	0.43	0.81	0.530864	81.55	0.57	0.754386	16494.92
8	2.5	77.03	83.33	6.3	15.42	0.24	1.2	0.2	82.75	1.2	0.2	16331.28
9	3	77.07	83.52	6.45	16.06	0.64	0.19	3.368421	83.8	1.05	0.609524	19141.78
10	3.5	77.04	84.61	7.57	16.48	0.42	1.09	0.385321	84.76	0.96	0.4375	19027.99
11	4	77.09	85.21	8.12	17.19	0.71	0.6	1.183333	85.31	0.55	1.290909	20273.32
12	4.5	77.1	85.4	8.3	17.77	0.58	0.19	3.052632	85.35	0.04	14.5	22312.86
13	5	77.2	86.41	9.21	19.14	1.37	1.01	1.356436	86.19	0.84	1.630952	22342.47
14	5.5	77.08	86.66	9.58	19.07	-0.07	0.25	-0.28	86.41	0.22	-0.31818	23627.51
15	6	76.99	88.68	11.69	22.7	3.63	2.02	1.79703	87.69	1.28	2.835938	21123.09
16	6.5	76.97	89	12.03	22.61	-0.09	0.32	-0.28125	87.65	-0.04	2.25	22236.61
17	6.75	77.05	89.49	12.44	23.16	0.55	0.49	1.122449	87.9	0.25	2.2	22330.8
18	6.9	77.02	89.78	12.76	23.63	0.47	0.29	1.62069	88.09	0.19	2.473684	22254.57
19	7	77.03	89.94	12.91	23.87	0.24	0.16	1.5	88.27	0.18	1.333333	22314.78
20	7.2											AD
21												

Fig 5-I. (Top) An example of a post-processed graphical result in the MATLAB script file, (Bottom) Excel Macro calculating the effective thermal conductivity for a given condenser temperature

5.3 Thermo-analysis of the condenser and evaporator states

The tools available in this project for measuring the states in the PHP are the temperature and pressure sensors. Since the PHP must be in a cold controlled environment with reduced heat leaks, no optical observation techniques were used in this experiment. Fig 5-II shows the states of the condenser, evaporator, and adiabatic sections, as well as a hypothetical equilibrium state based on the temperature and pressure measurements. The pressure sensor is attached to the gas line connected to the fill line of the adiabatic section.

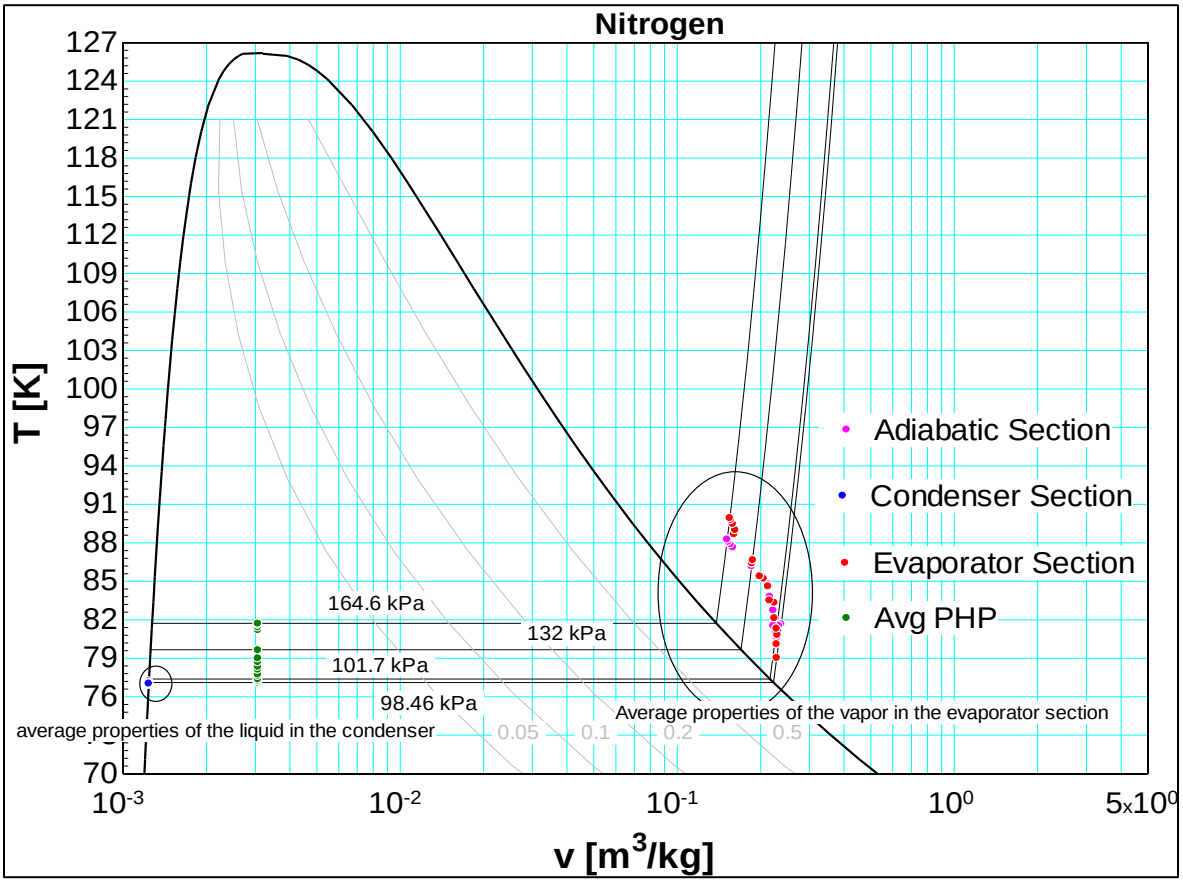

Fig 5-II. Thermodynamic states of the PHP at an initial liquid FR of 40% and T_{cond} = 77K

The condenser is maintained at a constant temperature with respect to time, using a Lakeshore 332 controller. The blue dot represents the condenser, which is predominantly in the liquid state, though as observed in room temperature PHP's [7], some vapor plugs can temporarily move into

the condenser from the evaporator. The red dot represents the evaporator, which is in a superheated state, suggesting that it is mostly occupied by vapor though cold liquid can move into the region being transported from the condenser. The temperatures measured are those of the copper block which would represent wall superheat. The adiabatic section follows the evaporator section closely which is reflective of the fact that the PRTs in the adiabatic section are much closer to the evaporator. The green dot represents a two-phase equilibrium situation where the entire content is at a conserved initial specific volume and the steady state pressure for each load input. The steady state pressure for a given load is assumed to the uniform throughout the PHP. Experiments like the one carried out by M. Barba et al [31], where the mean temperature difference of all the pressure sensors in the PHP was $\leq$ 0.05bar, suggests that this is a reasonable assumption. The fact that the PHP in this current work shows the thermal behavior in the T-v diagram in Fig 5-II is consistent with the experimental result obtained by P. Gully et al [32] shown in Fig 5-III. The mean temperature of the evaporator wall being an average of the bulk temperature of the vapor inside the evaporator region of the PHP.

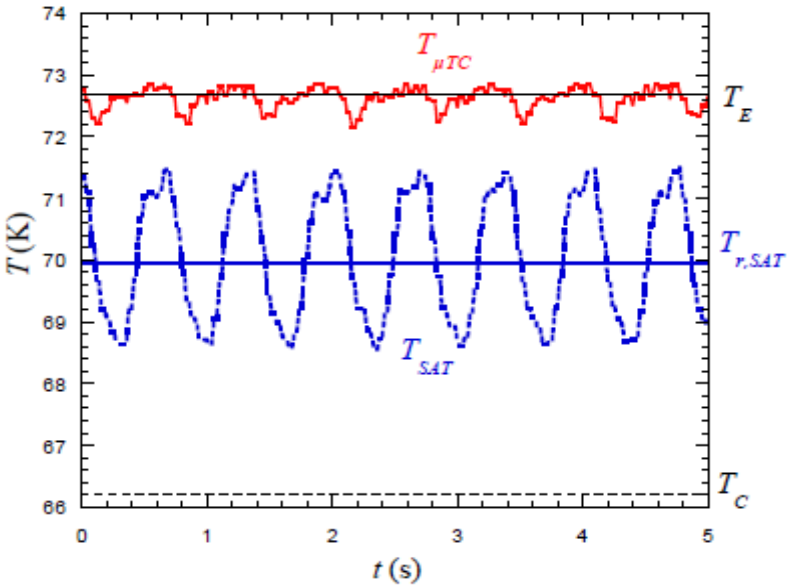

Fig 5-III. Pseudo-steady state temperature in the evaporator, reservoir, and condenser [32]

5.4 Initial Liquid Fill Ratio

In the Experimental Assembly section at the end of the last chapter, some steps, and variables are defined that help in determining the initial fill ratio of each run. This section aims to expand on that and use the First Law of Thermodynamics to analyze the theoretical liquid fill ratio in the PHP based on properties of the gas in the buffer tank. The ideal gas law, $Pv = mRT$ is used to determine the initial and final gas inventory in the low-pressure buffer tank. While all valves except valve 2 are closed, the start pressure, P_{start}, of the buffer tank is measured. The inlet valve (valve 3) to the PHP section is then opened and when the pressure reaches a valve equal to a pre-determined mass necessary to give a required initial fill ratio in the PHP section, the inlet valve is closed and after a few minutes, the pressure of the buffer tank is measured again as P_{end}. It is assumed that there is good heat transfer between the buffer tank wall and that the temperature at the beginning is the small as the temperature at the end and thus:

$$m_{out} = \frac{(P_{start} - P_{end})V_{tank+buffer-line}}{RT_{amb}} \tag{5.1}$$

The unknowns right now are m_{out} and P_{end} and as such one more equation is needed. The second equation comes from a two-phase mass balance on the PHP section at an assumed liquid fill ratio. The PHP section is divided into two zones: Zone 1 is the section enclosed in the thermal shield and MLI and Zone 2 is from that point up until the PHP inlet valve (Valve 3). The ideal gas law is used to determine the mass in Zone 2 with the assumption that this mass is to the right of the vapor dome i.e., gaseous state and thus does not contribute to the fill ratio calculation:

$$m_{z,2} = \frac{P\{T_{sat}\}V_{z,2}}{RT_{avg}} \tag{5.2}$$

where T_{sat} is assumed to be the condenser temperature which is known (ΔT in the PHP at 0W is typically $\leq 2K$), T_{avg} is the mean temperature between the saturation temperature and room temperature, R is the specific gas constant of Nitrogen and $V_{z,2}$ is the volume of Zone 2 of the PHP.

Zone 1 is assumed to be in two phase equilibrium and for a known liquid fill ratio, the mass in Zone1 can be calculated according to:

$$Fill_{ratio} = \frac{\left(1 - x_{php}\left\{T_{sat}, \frac{V_{z,1}}{m_{z,1}}\right\}\right).\, v_{sat}\{T_{sat}, x = 0\}.\, m_{z,1}}{V_{z,1}} \tag{5.3}$$

where x is quality. From the above equation, the only unknown is $m_{z,1}$. The total mass leaving the buffer tank can then be computed by:

$$m_{out} = m_{z,1} + m_{z,2} \tag{5.4}$$

Revisiting equation 5.1, P_{end} can thus be calculated.

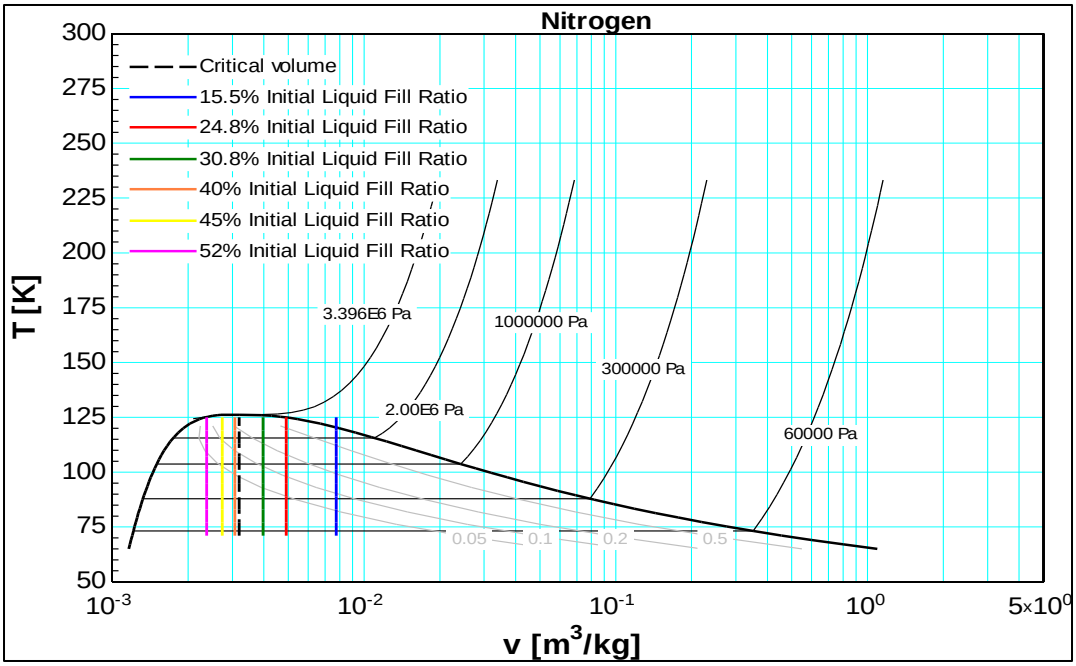

Fig 5-IV. T-v diagram for Nitrogen

5.5 Effective conductivities versus condenser temperature at select fill ratios

One of the goals of this project is to estimate the effective thermal conductivity of the PHP device so that the performance can be compared to conventional passive devices such as a copper bar or heat pipes. For a given load at the evaporator, during steady state condition, the condenser and evaporator temperatures are recorded and averaged as $\bar{T}_c$ and $\bar{T}_h$ respectively. The heat transfer is theoretically modelled as conduction through the liquid-vapor content of the capillary tubes such that:

$$k_{eff} = \frac{\dot{q} L_{eff}}{N A_c \Delta T} \tag{5.5}$$

where $\dot{q}$ is the applied heat load at the evaporator, N is the total number of capillary turns, L_{eff} is the normal distance between the condenser sensor and evaporator sensor (middle of condenser to middle of evaporator), A_c is the inside cross-sectional area of the capillary tube (i.e., using the

inner diameter) and ΔT is the steady state temperature difference between the evaporator and condenser.

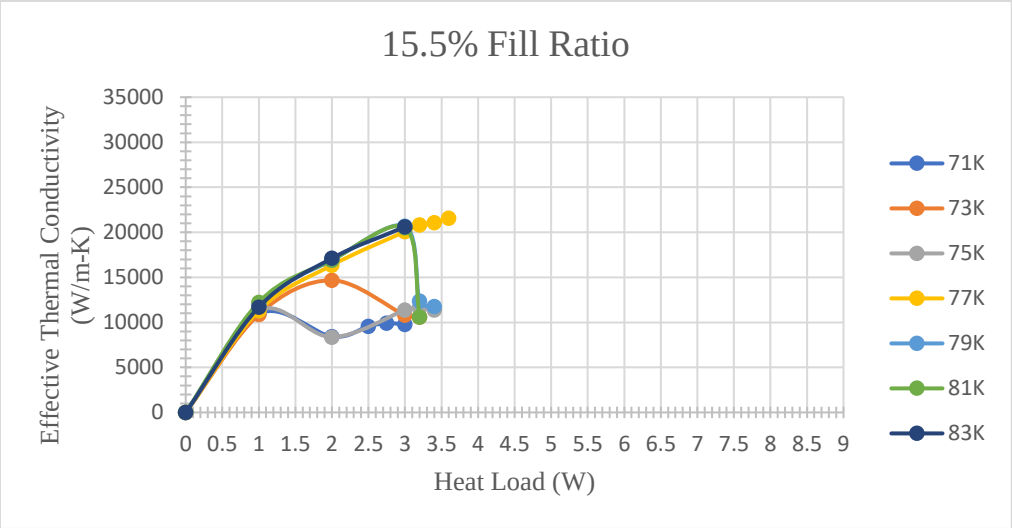

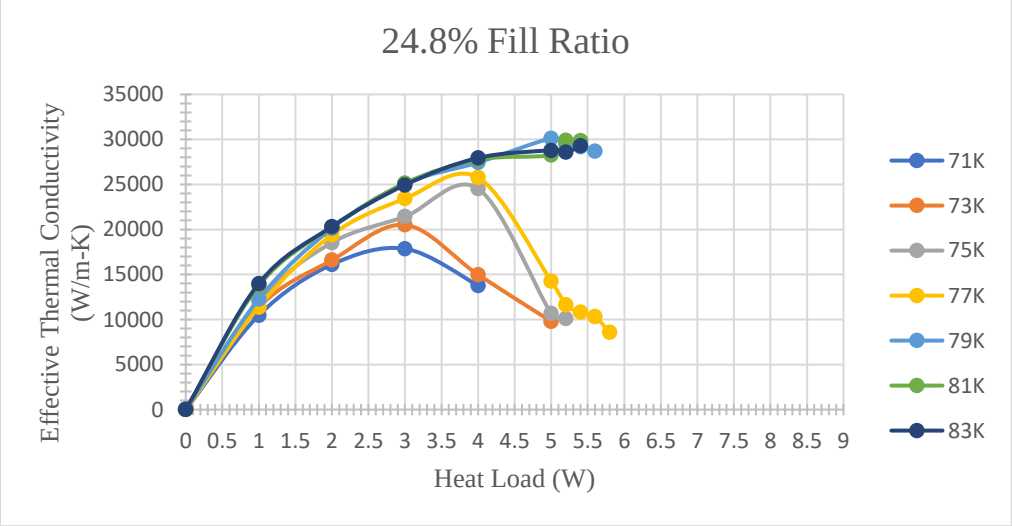

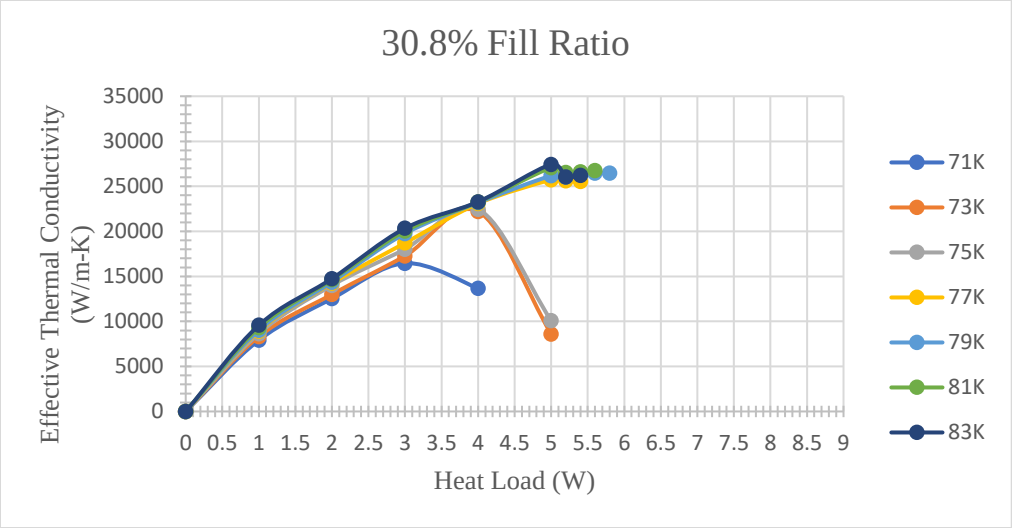
30.8% Fill Ratio
Effective Thermal Conductivity (W/m-K)
35000
30000
25000
20000
15000
10000
5000
0
0 0.5 1 1.5 2 2.5 3 3.5 4 4.5 5 5.5 6 6.5 7 7.5 8 8.5 9
Heat Load (W)
71K
73K
75K
77K
79K
81K
83K

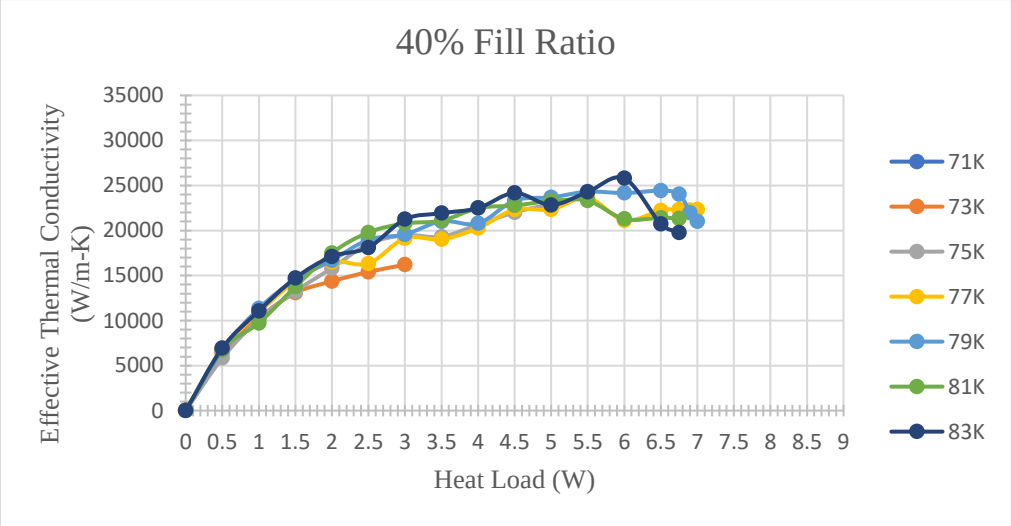
40% Fill Ratio
Effective Thermal Conductivity (W/m-K)
35000
30000
25000
20000
15000
10000
5000
0
0 0.5 1 1.5 2 2.5 3 3.5 4 4.5 5 5.5 6 6.5 7 7.5 8 8.5 9
Heat Load (W)
71K
73K
75K
77K
79K
81K
83K

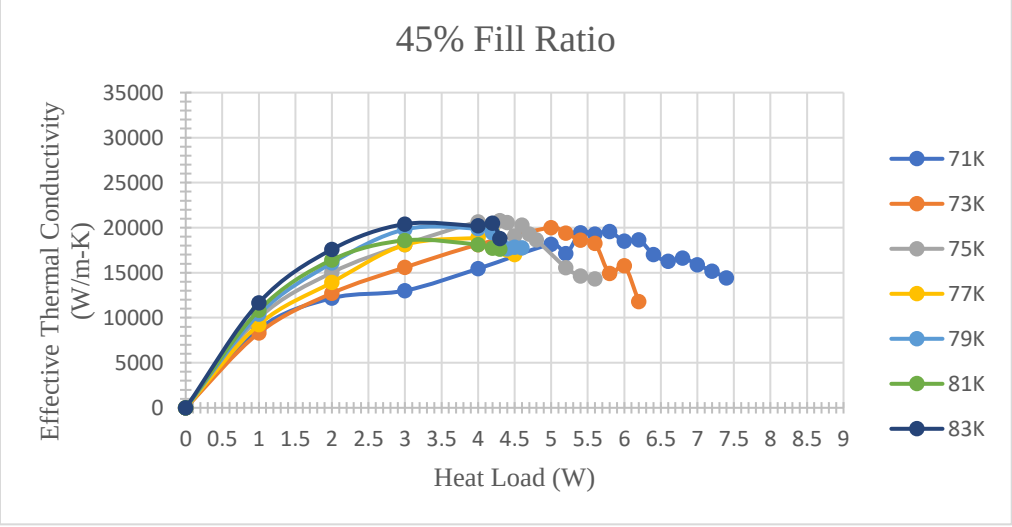
45% Fill Ratio
Effective Thermal Conductivity (W/m-K)
35000
30000
25000
20000
15000
10000
5000
0
0 0.5 1 1.5 2 2.5 3 3.5 4 4.5 5 5.5 6 6.5 7 7.5 8 8.5 9
Heat Load (W)
71K
73K
75K
77K
79K
81K
83K

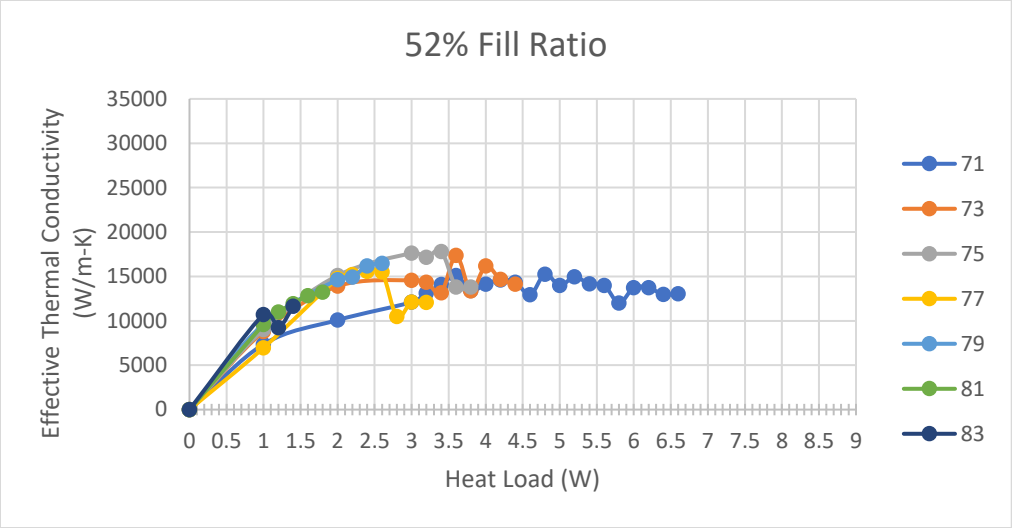

Fig 5-V. Effective thermal conductivity versus heat load for at different condenser temperatures

The effective conductivity is the parameter of interest used to compare a PHP to other heat transfer devices of similar category such as a copper bar or a heat pipe. From the experiment, the effective conductivity of this PHP can be quantified as well as some behavior documented. Fig 5-V show the effective conductivity of the PHP as a function of the evaporator heat load for different condenser temperature and initial liquid fill ratios.

One feature to note is the behavior of the effective conductivity with increase in heat load. Initially, the effective conductivity goes up with an increase in load at the evaporator. This behavior can be linked to an increase in nucleate boiling, which transfers energy from the inner surface of the capillary tube to the center to form vapor plugs. The amount of nucleation reduces as the velocity increases and the heat transfer is dominated by the boundary layer heat transfer. Vapor plugs are surrounded or coated with a thin layer of liquid film. As the heat flux on the surface of the tube increases, this liquid film becomes smaller or thinner.

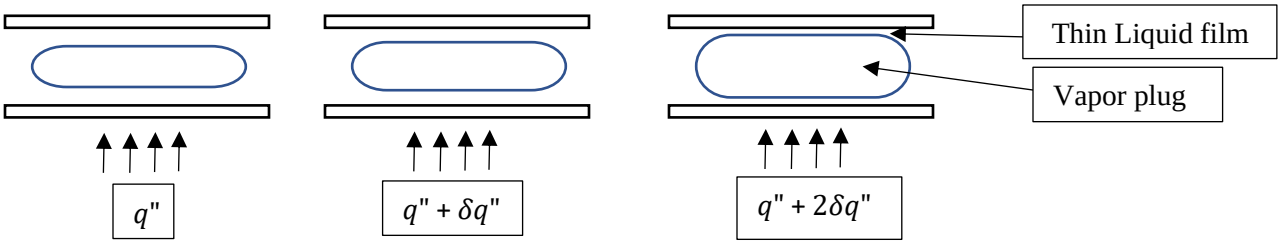

Fig 29. Reduction of thin liquid film layer with the increased heat flux

The growth of the thin film layer δ_t, can be inferred from the simulation done by Mauro et al [33], which shows the liquid film thickness reducing as the vapor quality goes up. This behavior of liquid film thickness with increasing heat flux was also experimentally verified by P Srikrishna et al [34].

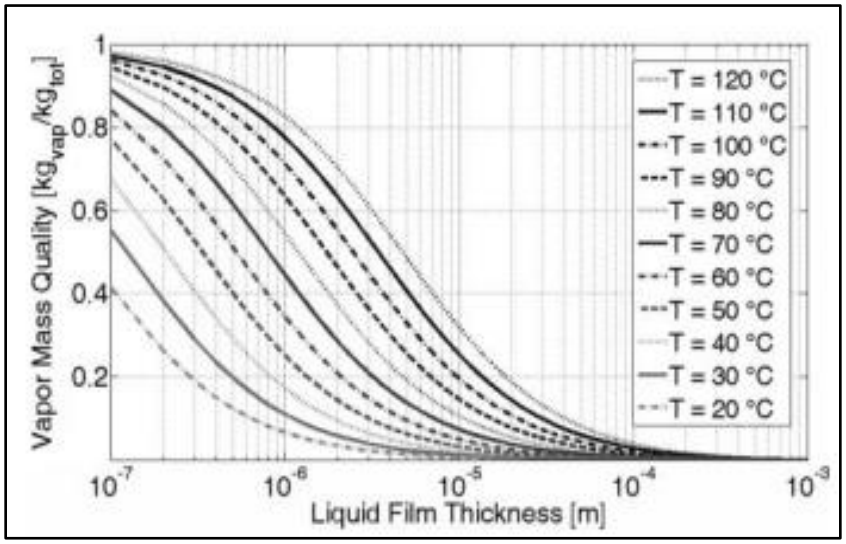

Fig 5-VI. Vapor mass quality vs liquid film thickness for different fluid temperature [33]

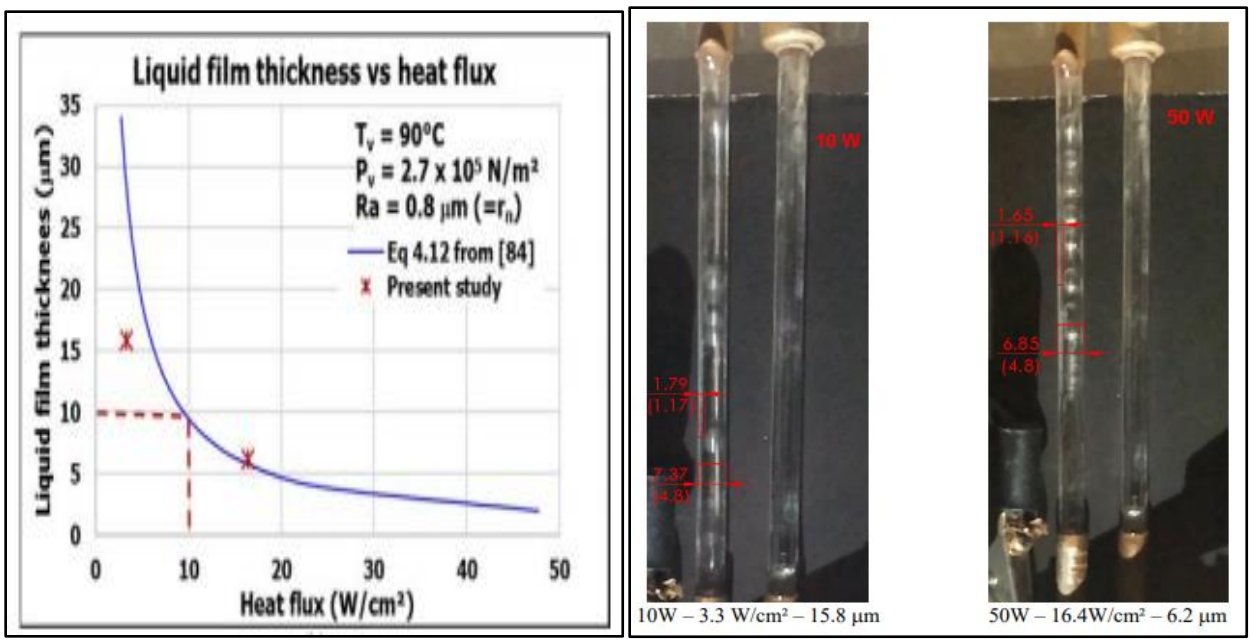

Fig 5-VII. Liquid film thickness experiment of a methanol PHP [34]

Consider conduction heat transfer through the thermal boundary layer is given by:

$$q" = \frac{k\Delta T_s}{\delta_t} \tag{5.6}$$

and the convective heat transfer can be represented by:

$$q" = h\Delta T_s \tag{5.7}$$

the heat transfer coefficient h, can then be related to the thermal conductivity of the fluid k, and the boundary layer thickness, δ_t as:

$$h \approx \frac{k}{\delta_t} \tag{5.8}$$

and so, for a finite value of δ_t, the heat transfer coefficient becomes bigger as the boundary layer thickness becomes smaller and hence the effective thermal conductivity behaves just like the heat

transfer coefficient. Fig 5-VIII shows that as evaporator temperature goes up (due to a higher heat load), the velocities or oscillation of the liquid slugs sensible and latent heat also increases.

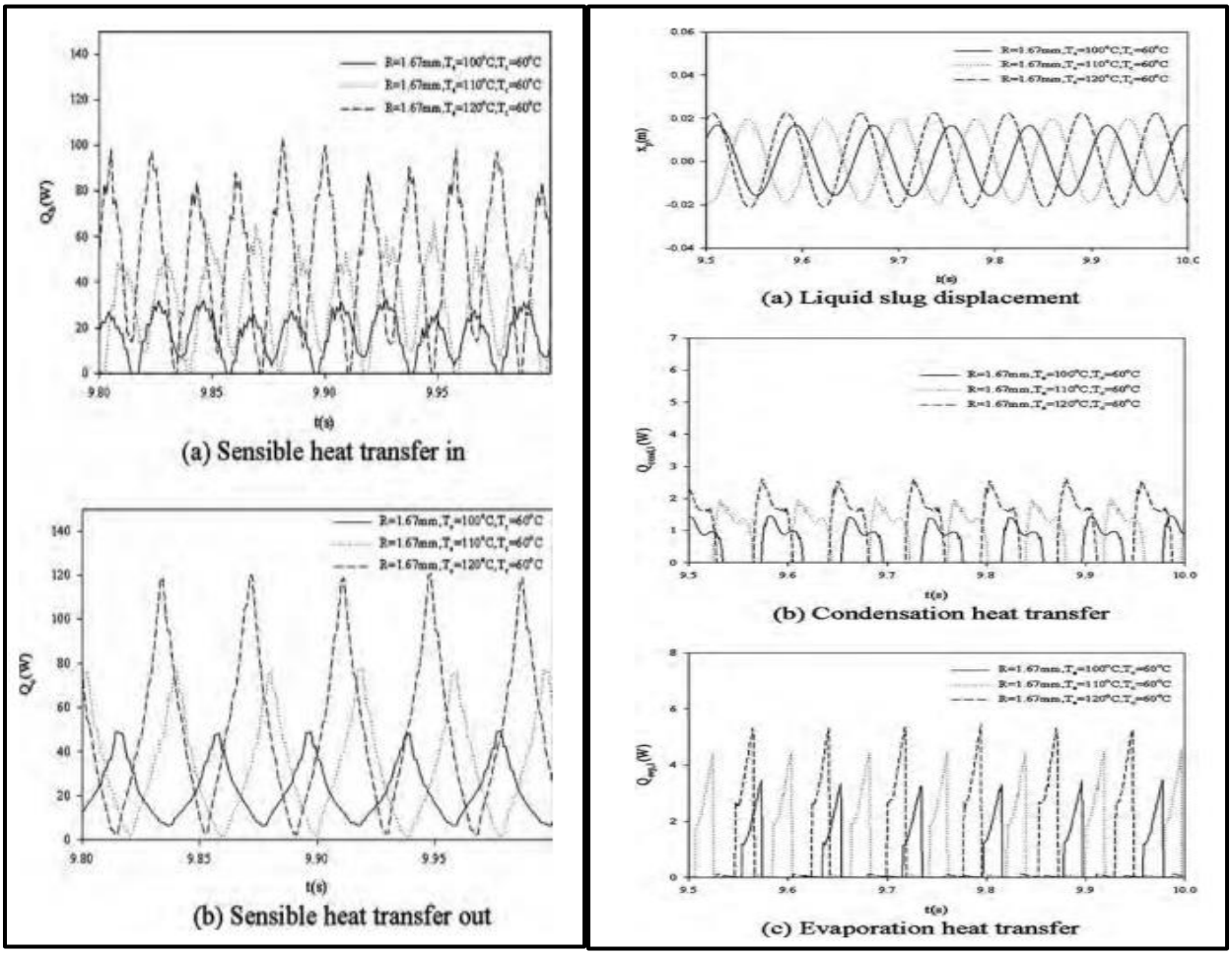

Fig 5-VIII. Influence of evaporator temperature on oscillatory flow and heat transfer [35]

At the interface between the vapor and liquid, the wall heat flux must balance the heat flux of vaporization. The thinner the boundary layer, the less mass available for vaporization. Further increasing the heat flux can result in the onset of dry-out, where the liquid film is completely evaporated and there is a jump in the wall temperature (Fig 5-IX) because of a dip in heat transfer coefficient (HTC) from a two-phase HTC to a single vapor phase HTC (Fig 5-X). Fig 5-XI supports this hypothesis. After this, there are two possible scenarios. One, a recovery from dry-

out, where there is intermittent rewetting of the wall to with a large reduction in heat transfer coefficient due to the large jump in wall temperature. This results in the maxima, displayed by most of the effective conductivity plots in Fig 5-V . In a few cases recovery is not possible and there is immediate dry-out. This is the case where the maximum effective conductivity occurs at the maximum heat input. The rewetting phenomena is a complex two-phase behavior that would require optical access at cryogenic temperatures and for experimental investigation is therefore outside the scope of this project. However, in room temperature PHPs (Fig 5-XII & Fig 5-XIII) the progression from nucleation to slug flow through annular flow has been observed. Mist flow occurs at the on-set of dry-out or at dry-out itself depending on the rewetting condition.

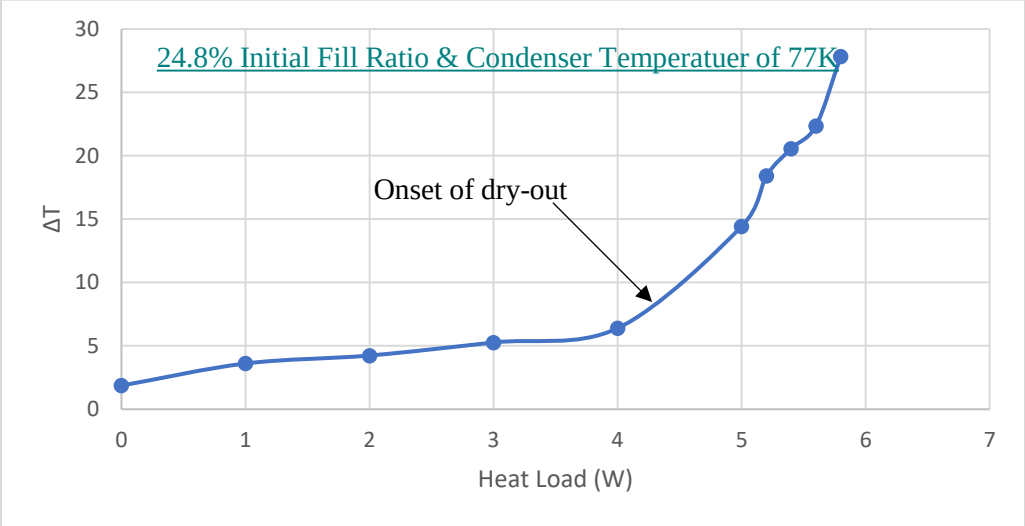

Fig 5-IX. Temperature difference between condenser and evaporator vs heat load (present study)

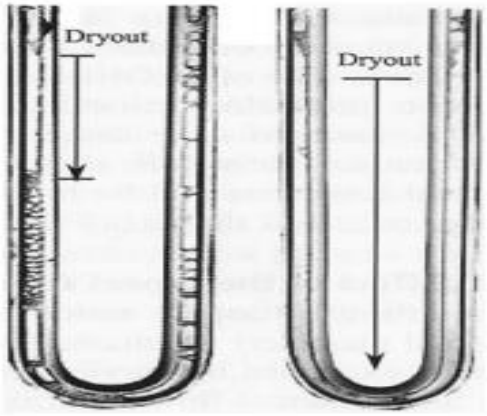

Fig 5-X. Dry-out seen at the oscillating heat pipe heating section [36]

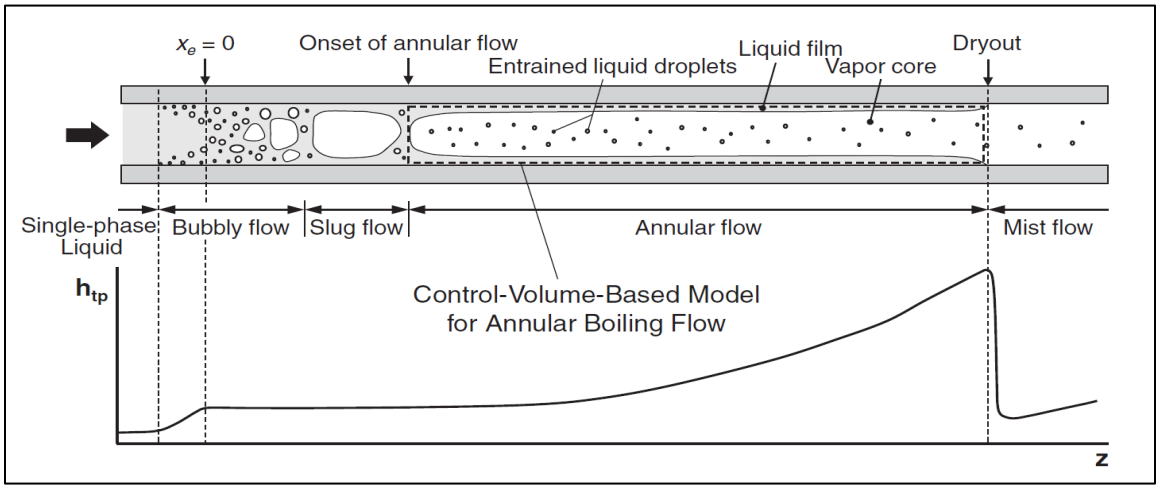

Fig 5-XI. Flow regime and convective heat transfer coefficient as a function of position in a microchannel [37]

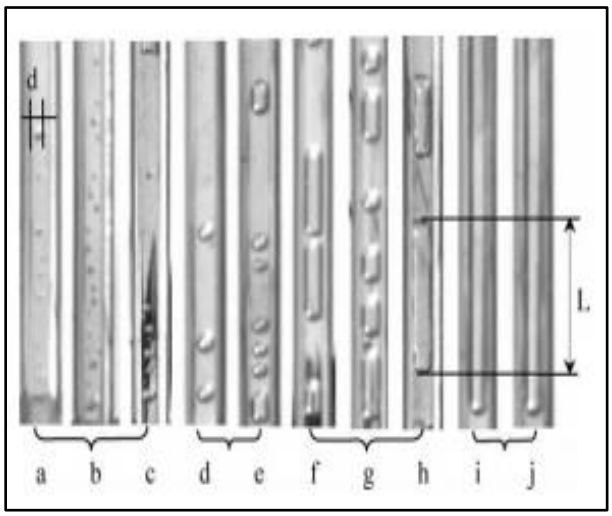

Fig 5-XII. Flow pattern in methanol PHP [38]

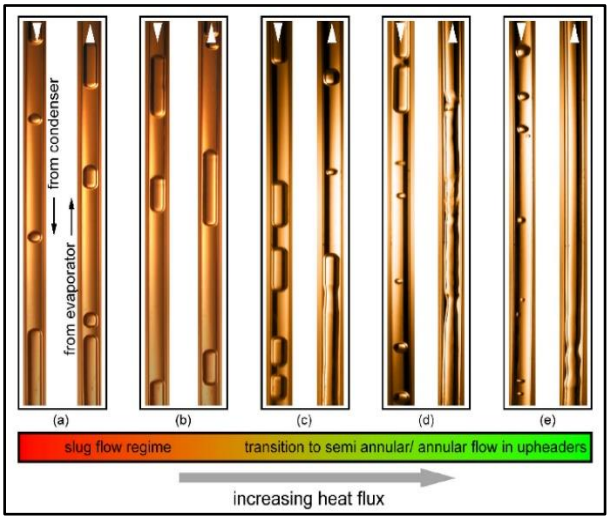

Fig 5-XIII. Flow pattern single-loop ethanol PHP [39]

Another feature to note is that, as the condenser temperature is increased, at a given load, the effective thermal conductivity increases (Note that in some cases, especially at high fill ratios, the onset of dry-out can cause slight variation to this behavior). Consider the simple analysis below where the heat flux $q"$ is constant and known and the wall temperature T_w is also constant and known:

$$q" = h(T_w - T_v) \tag{5.13}$$

As the vapor temperature, T_v increases, the temperature difference goes down. If the heat flux is to remain constant, the heat transfer coefficient h, must go up. This explains why there is higher performance at higher condenser temperature as seen in Fig 5-XV. The gain in effective thermal conductivity because of higher condenser temperature becomes more prominent with higher condenser temperature gap. For example, the benefit of running the condenser at 77K instead of 71K is much greater than running at 79K versus 77K. However, the experiments show that as we go to higher condenser temperature, the effective conductivity lines start to collapse on one another.

One more feature to note is the behavior of the effective conductivity as a function of the fill ratio. Below is a plot of the maximum effective conductivity at a condenser temperature of 77K as a function of fill ratio:

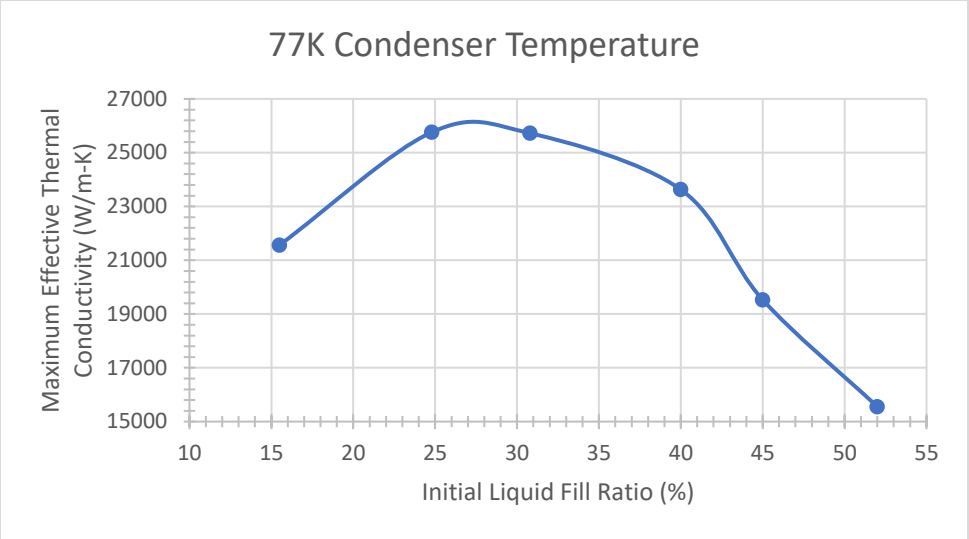

Fig 5-XIV. Maximum effective conductivity versus initial liquid fill ratio

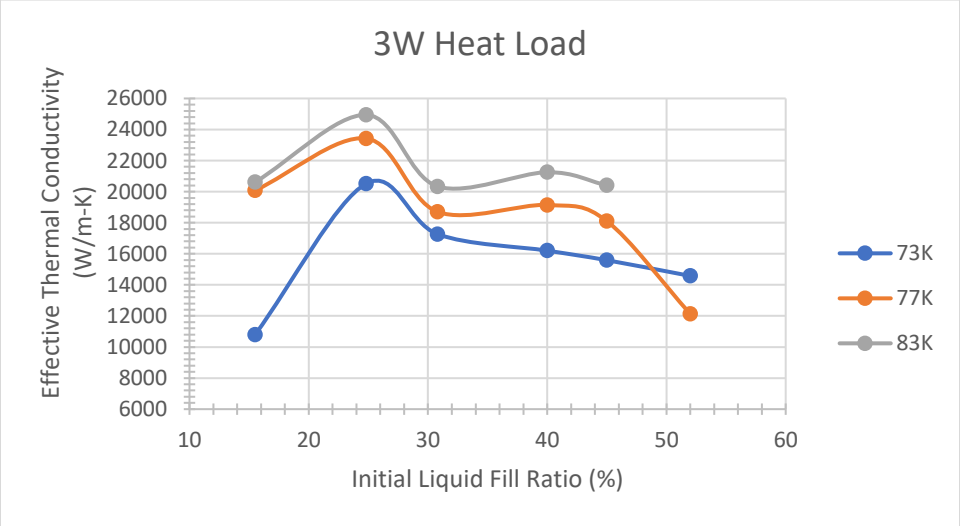

Fig 5-XV. Effective conductivity versus initial fill ratio for three different condenser temperatures

when the fill ratio is low, there is little liquid inventory or high vapor quality and so reduced heat transfer coefficient on the other hand, when the fill ratio is higher, there is less bubble formation and hence reduced total wall shear which translate to reduced heat transfer coefficient. The optimum tends to reduce these two effects.

5.6. Flow regimes

Using temperature data and knowledge of the boiling process in room temperature PHP we can attempt to decipher flow regimes in non-visual cryogenic PHPs. Fig 5-XVI shows a typical pool boiling curve, a flow boiling curve in a microchannel based on experiments by A. Kalani and S. Kandlikar [**40**] and flow regimes in a capillary tube [**41**]. Pool boiling usually starts with a single-phase liquid and progresses through nucleate boiling to annular boiling. Flow boiling does include some of the flow pattern of pool boiling such as bubbly flow, slug flow and annular flow, although the slug flow in flow boiling is confined by the wall of the tube. The flow boiling curve will be used for comparison to the current research data.

A

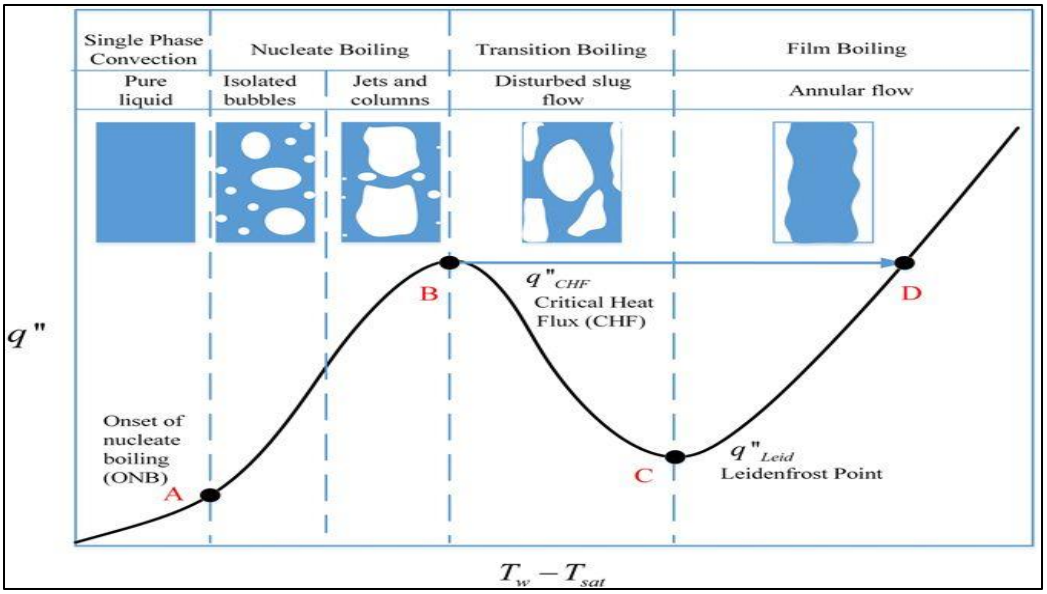

B

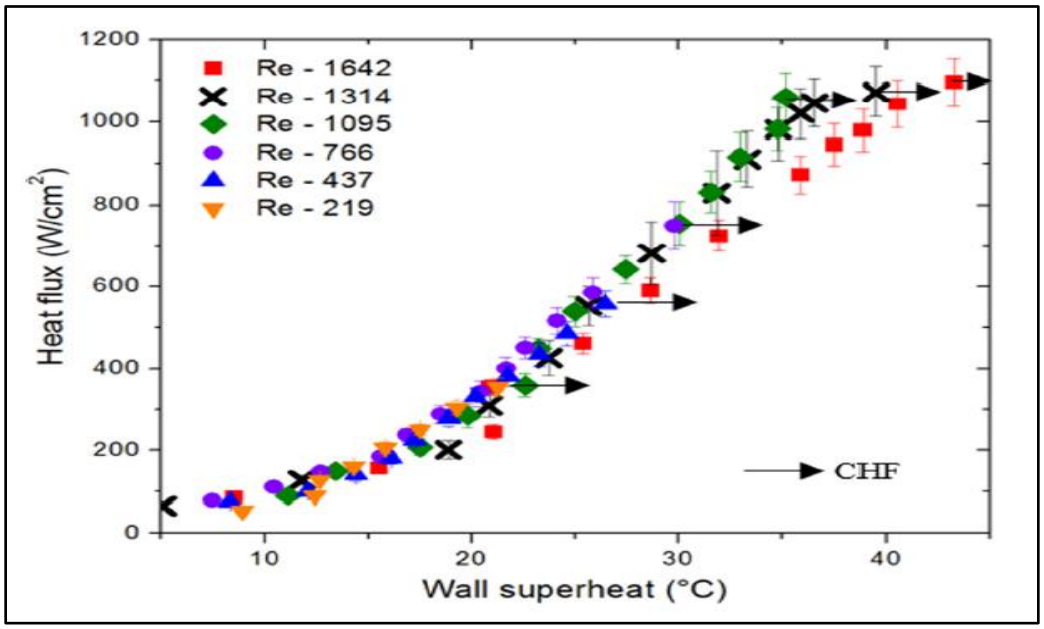

C

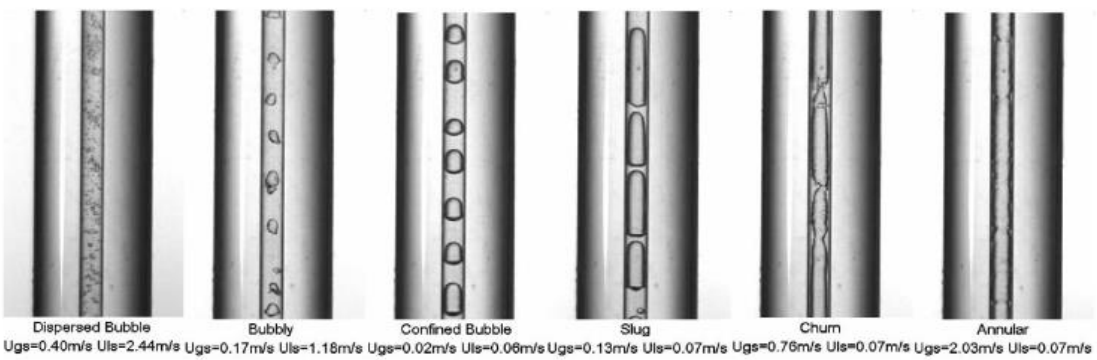

Fig 5-XVI. (A) Pool boiling curve [42], (B) Flow boiling curve [40], (C) Flow boiling flow pattern [41]

The start condition in a PHP is often a two-phase condition with some vapor plugs and often long liquid slugs owing to the surface tension effect of a properly sized PHP. As heat is added, nucleation comes into effect at the liquid sites (long liquid columns/slugs). As the heat flux is increased, larger nucleate bubbles form bubbly flow. As the heat flux is further increased, since the PHP is a microchannel, these bubbles become confined by the micro-diameter and coalesce or join to divide large slugs into smaller liquid slugs with the creation of more vapor plugs. Nucleation is also often suppressed in the vapor plug sections at these loads (though some nucleation can still occur at the liquid slugs at the evaporator). Most of the flow regimes that have been observed at room temperature fall into this flow pattern. At higher heat flux, annular flow has been observed to occur, where vapor plugs burst through a liquid slug and separates the liquid from the core. During long annular flow, thin film evaporation can occur at the wall, where a layer of vapor may separate the liquid film from the wall. This begins the onset of dry-out and dry out occurs at the critical heat flux.

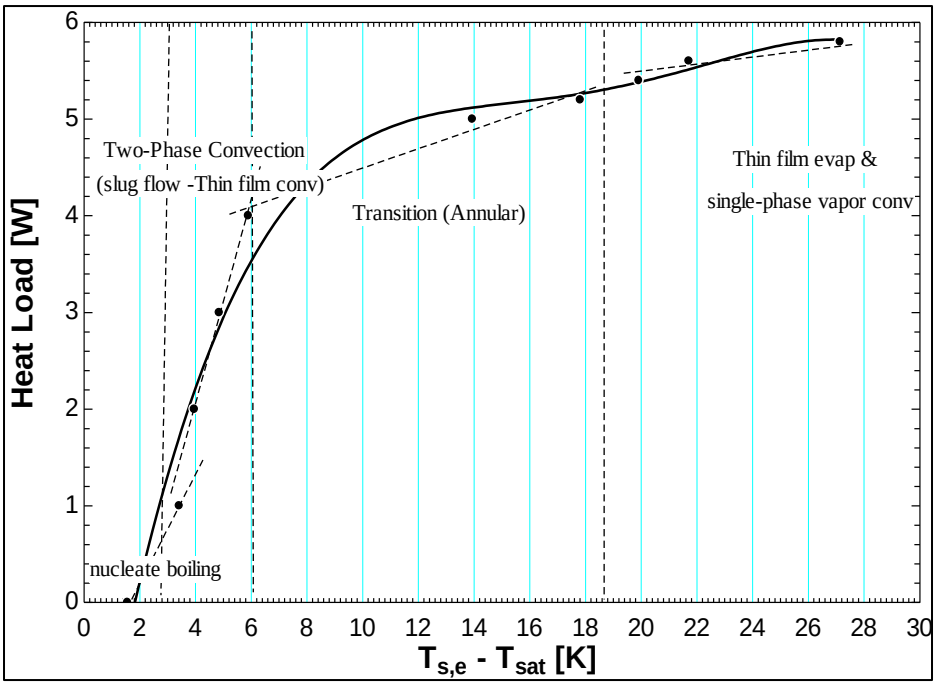

Fig 5-XVII. Flow boiling curve in the Nitrogen PHP (FR 24.8%, T_c 77K)

The heat transfer coefficient or slope in the above figure increases as nucleation starts. This slope becomes larger when bubble formation begins to create more vapor slugs because of the enhancement in HTC due to thin film conduction and the creation of more two-phase regime. There is a drop in this heat transfer coefficient as we enter annular regime due to vapor conduction at the wall. There may be variants of the curve depending on fill ratio, two-phase instabilities, and condenser temperature but distinct zones can most times be identified and the trend is fairly consistent. Since the contents of the PHP cannot be visualized, this acts as a basis to predict flow regimes in cryogenic PHPs and future detailed measurements would need to be carried out to at least predict with higher certainty these flow regimes. Fig 5-XVIII show examples of curves from other fill ratios and condenser temperatures. These curves show similar trend to Fig 5-XVI-B.

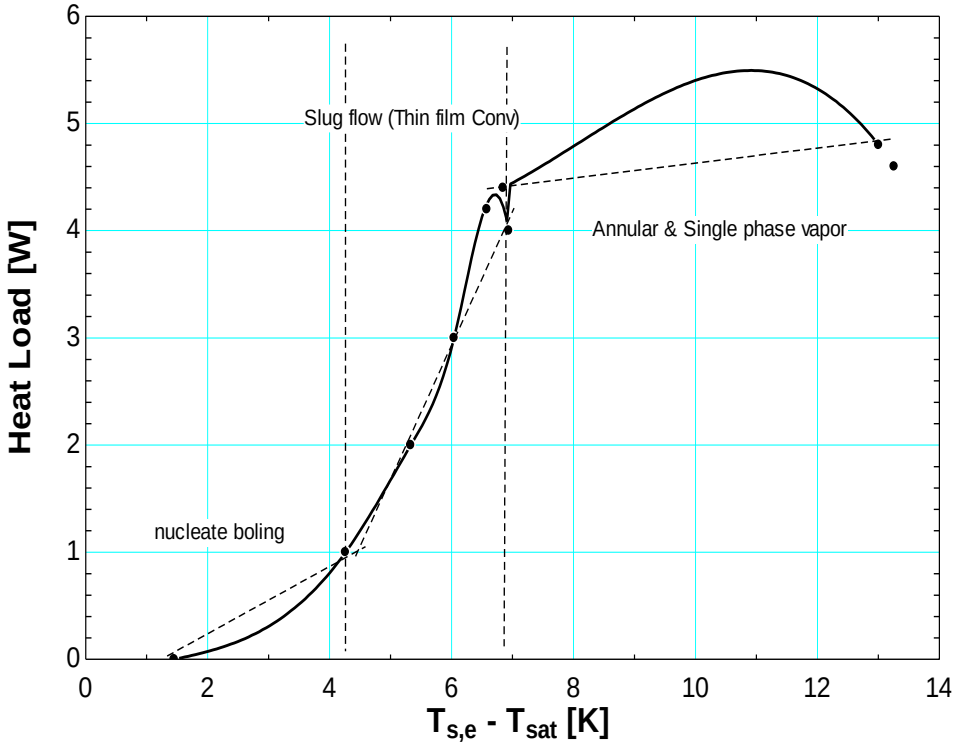

(a)

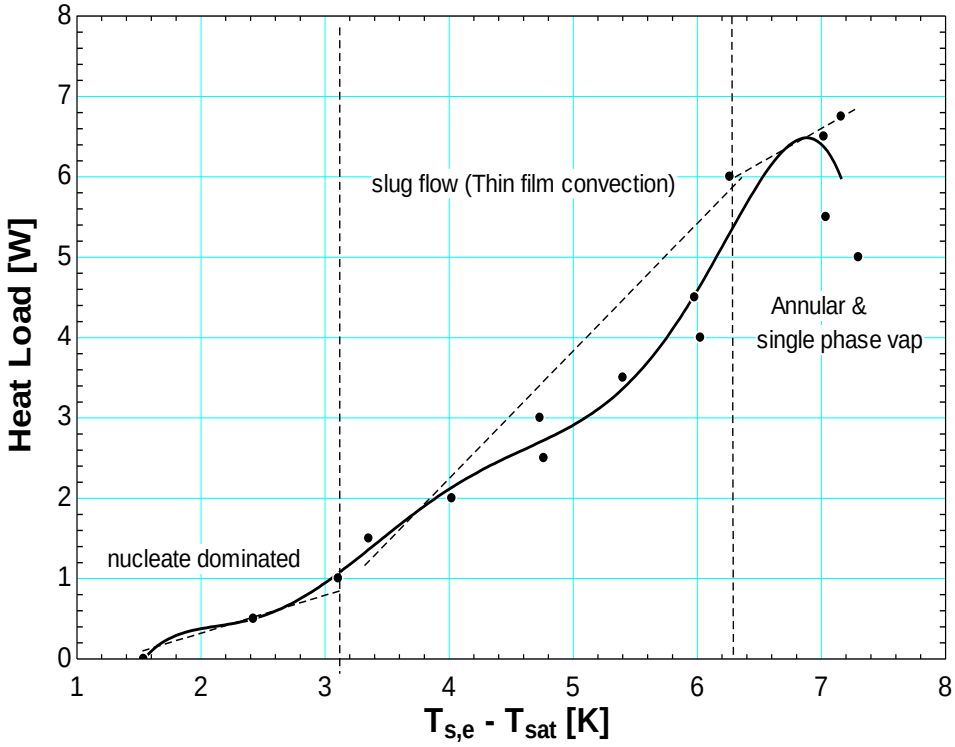

(b)

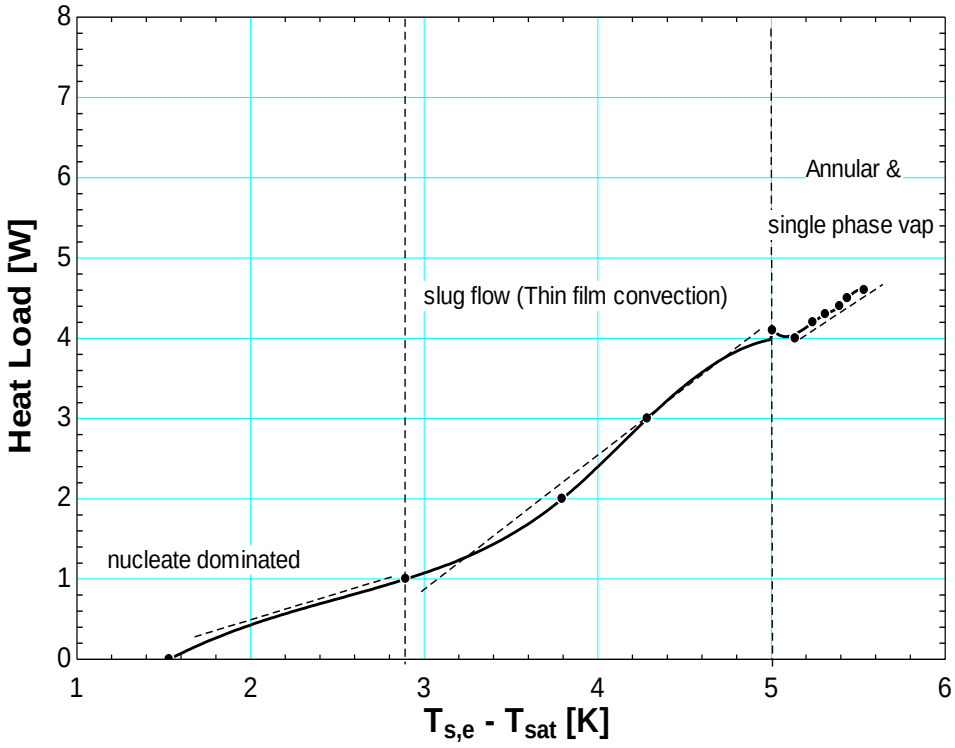

(c)

Fig 5-XVIII. Boiling curve for (a) FR 30%, T_c 75K (b) FR 40%, T_c 83K (c) FR 45%, T_c 79K

5.7 Thermodynamic Process

There are two type of thermodynamic steady state process that has been observed with the Nitrogen PHP. One is an isobaric or almost isobaric process which occurs at low fill ratios (fill ratios with specific volumes to the right of the critical volume) and the other is a baric (changing pressure) process occurring at high fill ratios (fill ratios with specific volumes to the left of the critical volume).

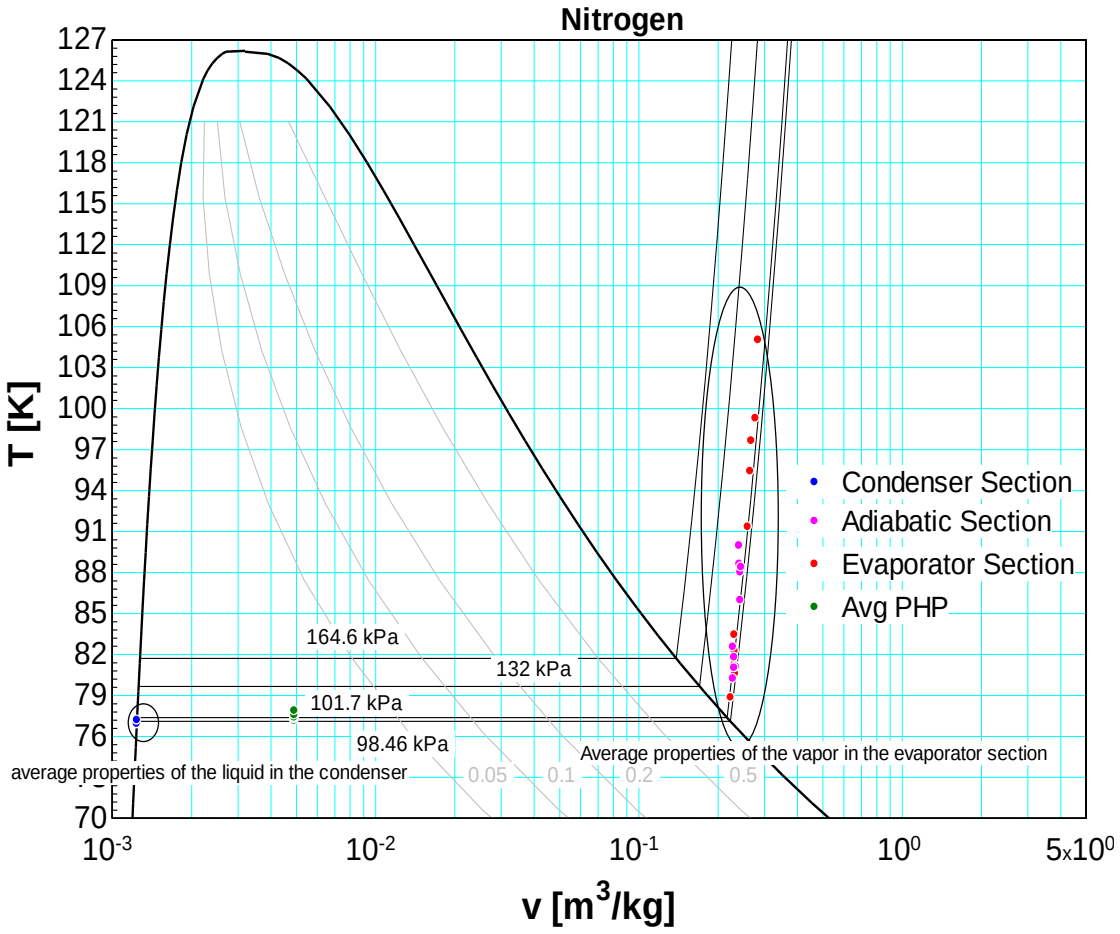

(a)

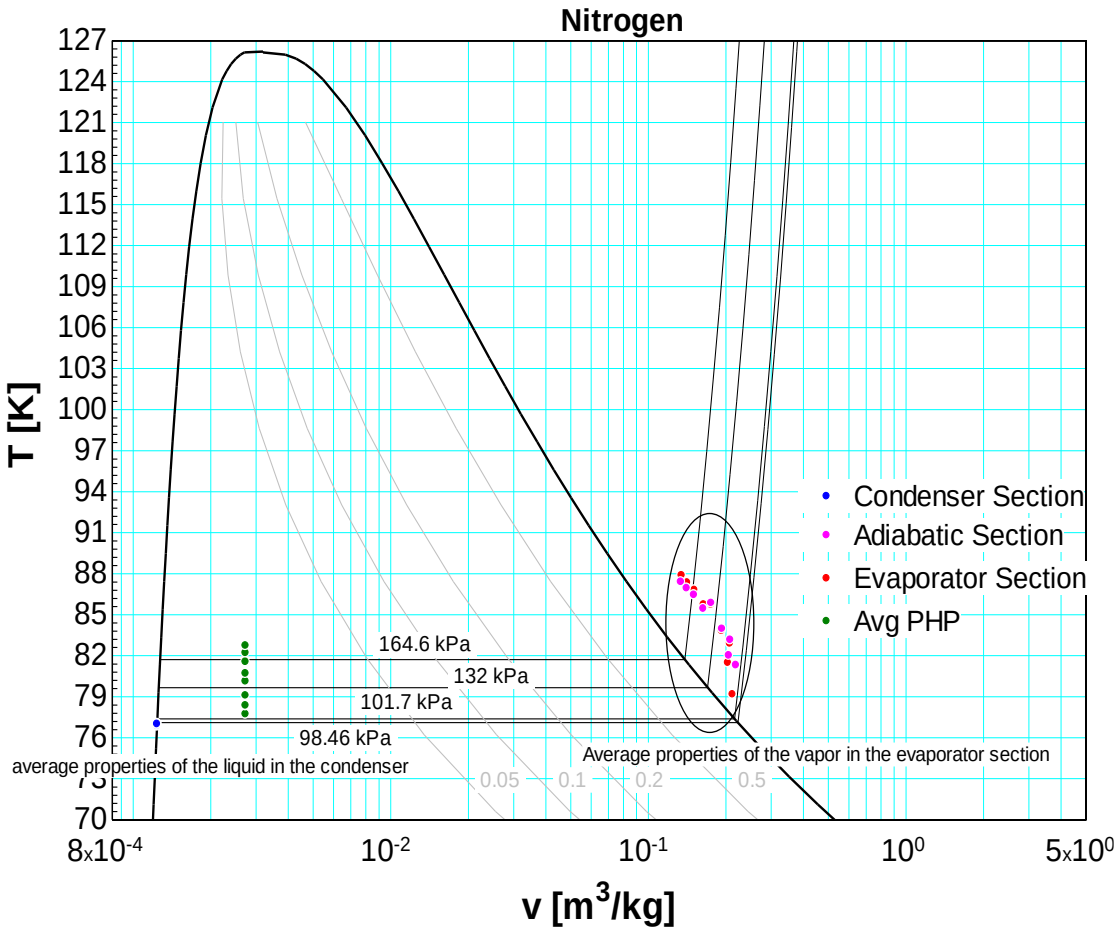

(b)

Fig 5-XIX. T-v states for (a) FR 24.8%, T_c 77K (b) FR 45%, T_c 77K

The pressure in an enclosure is typically set by the liquid-vapor interface. At low fill ratio, the bulk interface will be at a temperature closer to the condenser and since the condenser is maintained at a constant temperature, this pressure does not change much. The case is different at high fill ratio where the interface predominantly sits at the high adiabatic section or closer to the evaporator temperature and so the pressure would be significantly influenced by the high-end temperature which increases with heat load. Moreover, the hydrostatic pressure in vertical orientation, may become important at high fill ratio due to long liquid slugs. The thermodynamic equilibrium state of the low fill ratio therefore corresponds to the vapor side, where an increase in temperature drives

the state towards saturated and superheated vapor at higher temperatures. On the other hand, at high fill ratios, the equilibrium state corresponds to the liquid side so an increase in temperature drives the state towards saturated and compressed liquid at comparably lower temperatures.

5.8 Dry-out Flux

The dry-out heat flux has two set of behaviors. One occurring at low fill ratios and the other at high fill ratios. At low fill ratios the pressure in the PHP remains almost constant even at the dry-out heat load. The temperature on the other hand continues to increase and sees a sharp exponential increase towards the critical temperature at the dry-out heat load. At high fill ratios, both temperature and pressure increase significantly. At the dry-out heat load, the system experiences a sharp and continuous increase in temperature, accompanied by a sudden and sharp increase in pressure. The condenser temperature at this point is observed to drop too. This could mean that there is a stop in the motion of the working fluid and a disconnect between the cold liquid at the condenser and hot vapor at the evaporator.

5.8.1 Low Fill Ratios Dry-out Load versus condenser temperature

At low fill ratio (specific volume to the right of the critical specific volume) the critical heat load exhibits a parabolic behavior with a maximum occurring between the low and high condenser temperatures. The value of the critical heat load also increases with increasing fill ratio. This is to be expected since increasing the fill ratio increases the heat transfer capacity associated with increased liquid mass inventory in the system.

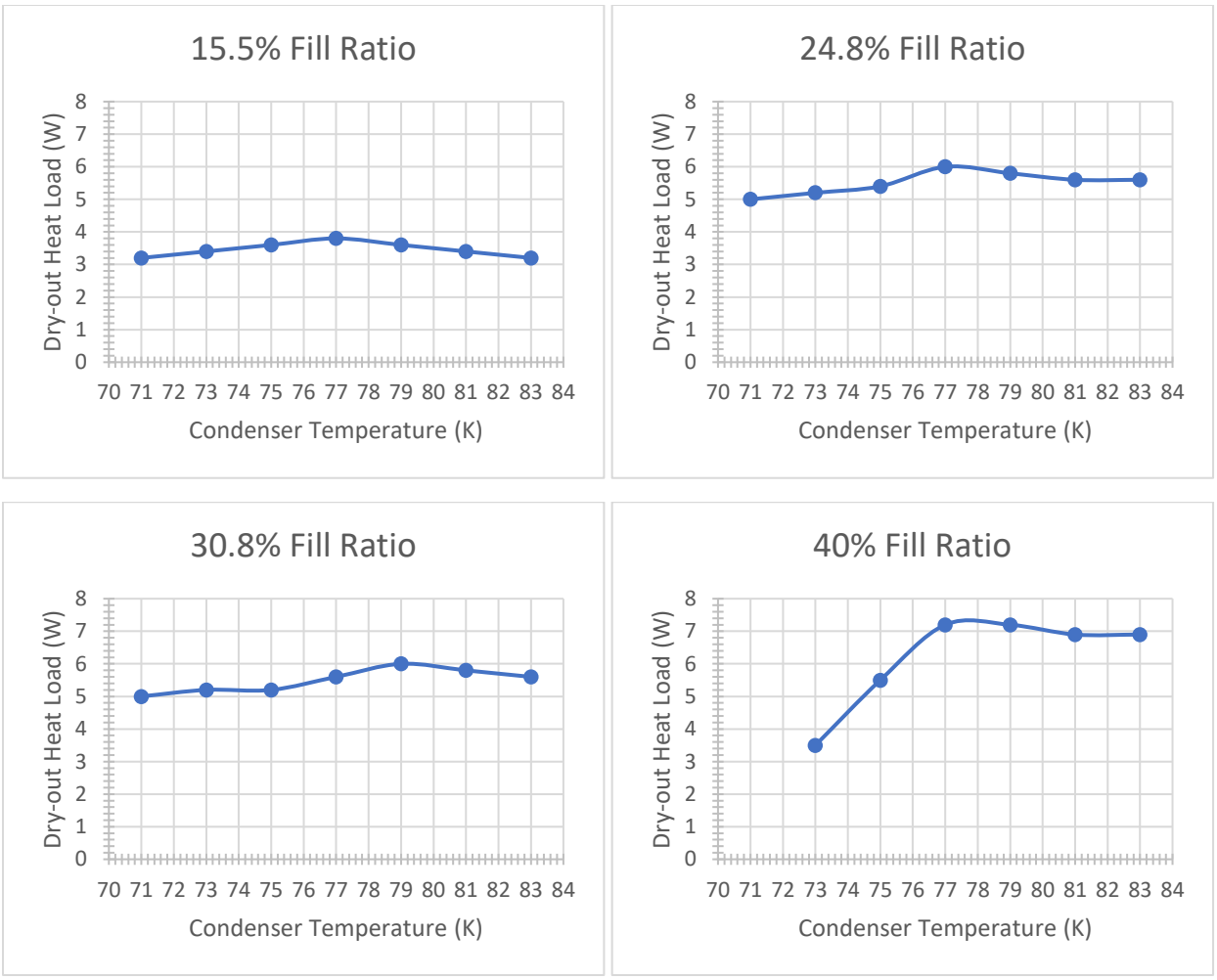

Fig 44. Dry-out load versus condenser temperature for different low fill ratios

The thermodynamic conditions that affect the behavior of the dry-out heat load are the heat of vaporization and the liquid fill ratio. As the condenser temperature is reduced, the liquid fill ratio at a constant fluid mass, also decreases and so there is less mass inventory to support high heat loads. On the other hand, as the condenser temperature is increased, the heat of vaporization of the system is reduced resulting in a lower critical heat flux. These two effects counter each other to produce a maximum.

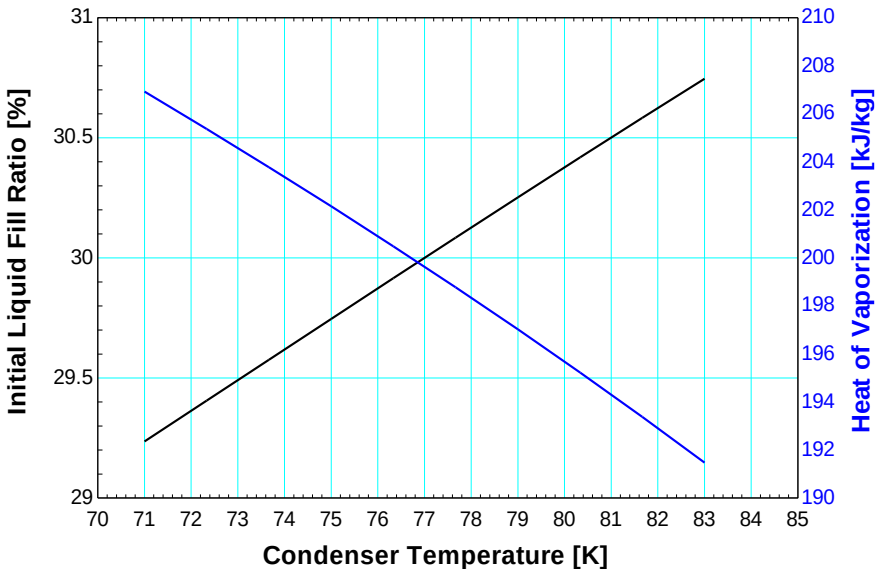

Fig 5-XX. Liquid Fill ratio and Heat of Vaporization as a function of condenser temperature

The pressure peaks in Fig 5-XXI represent a transitional pressure measurement. The system pressure returns to the average value during steady state conditions (the period when the load is held constant, and temperature of the evaporator remains constant) which remains constant as the heat load is increased. Also notice that the evaporator is thermally disconnected from the condenser, but the adiabatic section is still partially thermally connected to the condenser. The steadiness of the condenser temperature at the critical heat load and small changes in adiabatic section at that point suggest that the PHP is still operational (moving fluid) and so the cryocooler control can still maintain the temperature of the condenser at that point since thermal energy is still transferred into it, but the liquid heading toward the evaporator completely evaporates as it gets into the evaporator resulting in a highly reduced heat transfer coefficient of a hot gas and an ever increasing wall temperature.

Pressure Peaks (due to sudden load/temperature changes) returns to mean value at steady state

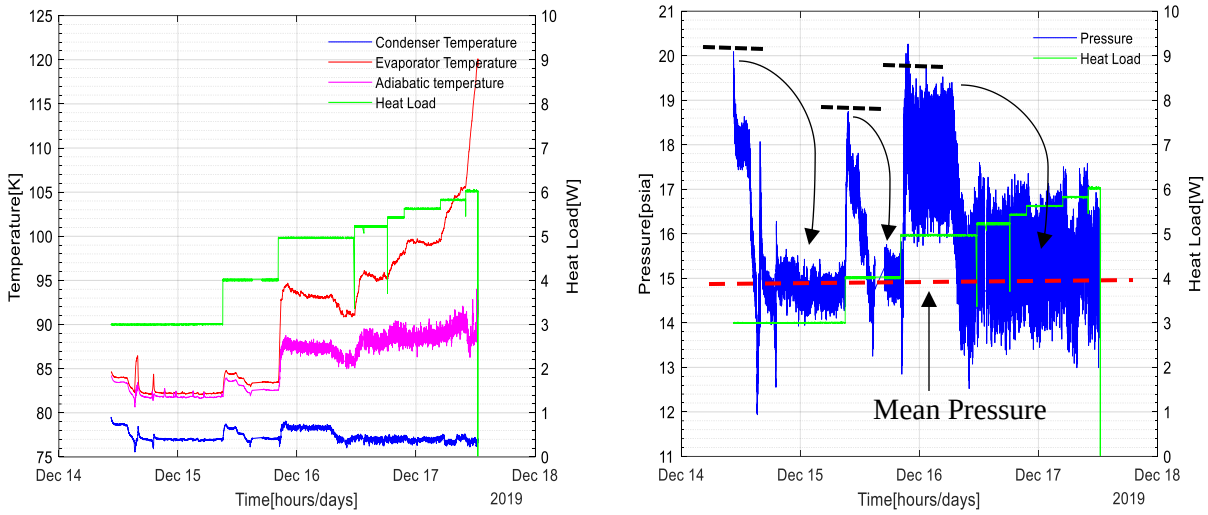

Fig 5-XXI. Temperature and Pressure measurement in PHP at Initial Fill Ratio of 24.8%

5.8.2 High Fill Ratios Dry-out Load versus condenser temperature

At high fill ratio (specific volume to the left of the critical specific volume) the critical heat load exhibits a decreasing value with increasing condenser temperature with the maximum occurring at the lowest temperature. In this case the critical heat load appears to decrease with increasing fill ratio.

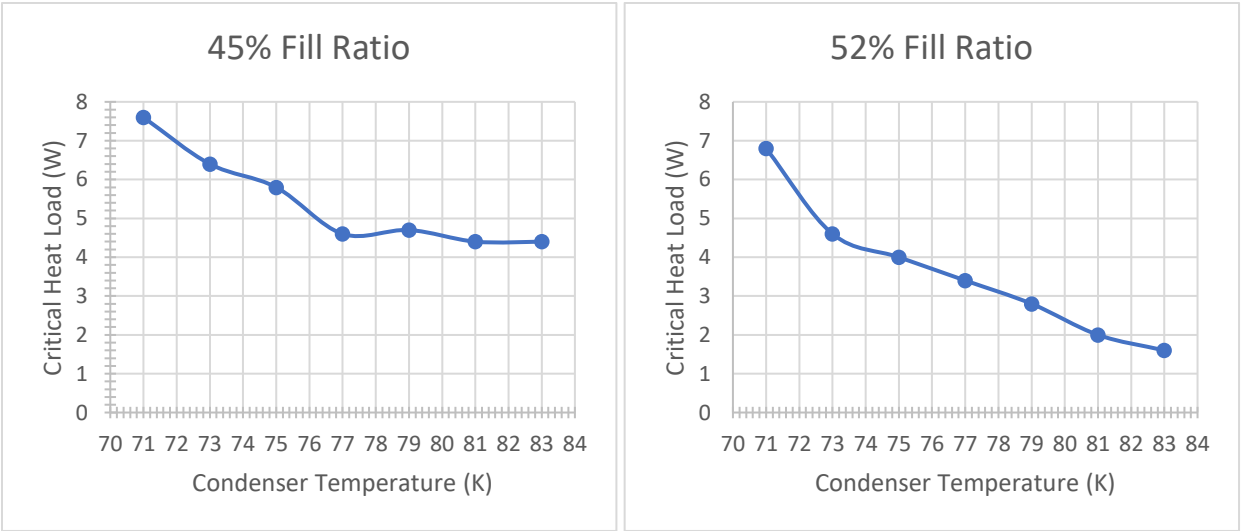

Fig 5-XXII. Critical heat load versus condenser temperature for different high fill ratios

The change in the critical heat flux behavior could be explained by the thermodynamic process during heat load addition. For low fill ratios, the pressure remains almost constant and so there is little liquid recovery at the evaporator to be used for rewetting the wall. However, at high fill ratios, there is a large pressure gradient at the onset of heat flux which will increase the two-phase liquid fill ratio and hence there will be liquid recovery that could be used for rewetting the evaporator wall. Hence while low condenser temperature would not have the benefit of more liquid production as heat is increased at the evaporator for low fill ratio, it would have this benefit at high fill ratio. (Rewetting occurs when a passing liquid slug, replaces the thin liquid film normally seen in annular flow at high heat flux, after complete evaporation of this film).

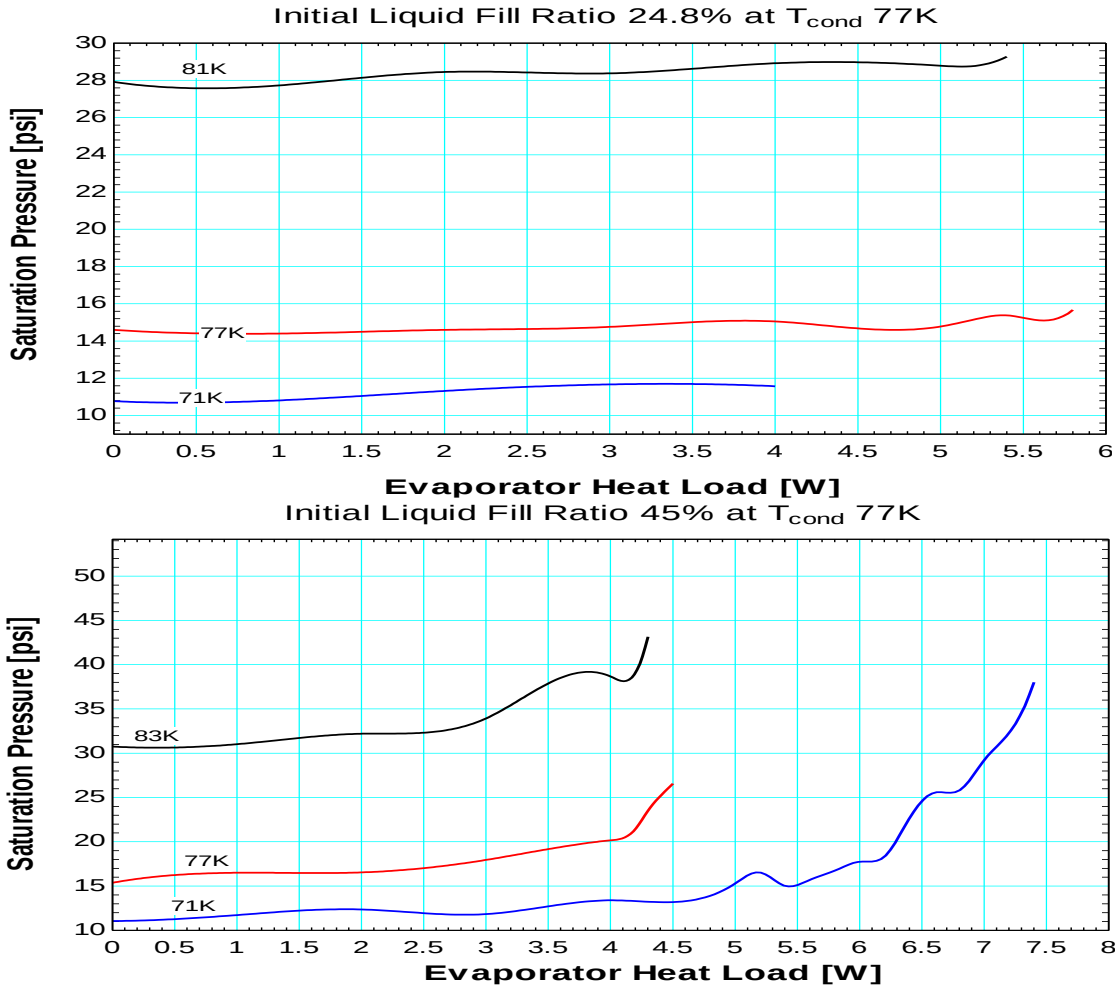

Fig 5-XXIII. Saturation pressure versus heat load for different condenser temperature

Perhaps a clearer way of understanding the transitional behavior of the critical heat flux at higher fill ratio, is that of liquid slug velocity. The rewetting process is bolstered by the ability of liquid slugs to make it to the evaporator (increased velocity). In general, as the fill ratio is increased the liquid velocity is reduced and so the advantage higher condenser temperature, gains from having more liquid fill ratio, is reduced by the reduction in pumping speed at higher fill ratios. For instance, in this experiment, the maximum velocity for an initial fill ratio of 24.8% and condenser temperature of 83[K] is double that of the case with an initial liquid fill ratio of 45% and the same condenser temperature. (Refer to

Table 12.1 Polynomial fit tables for performance maps

12.7 Velocity estimate for fluid inside PHP, for the calculation used in estimating the velocity).

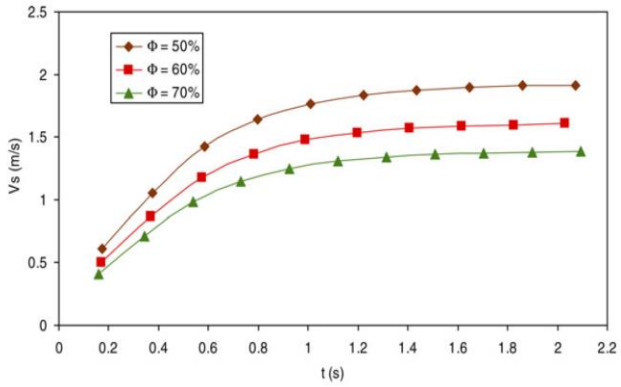

Fig 5-XXIV. Liquid velocity for different fill ratio: Experiment by K Rama Narashima et al [43]

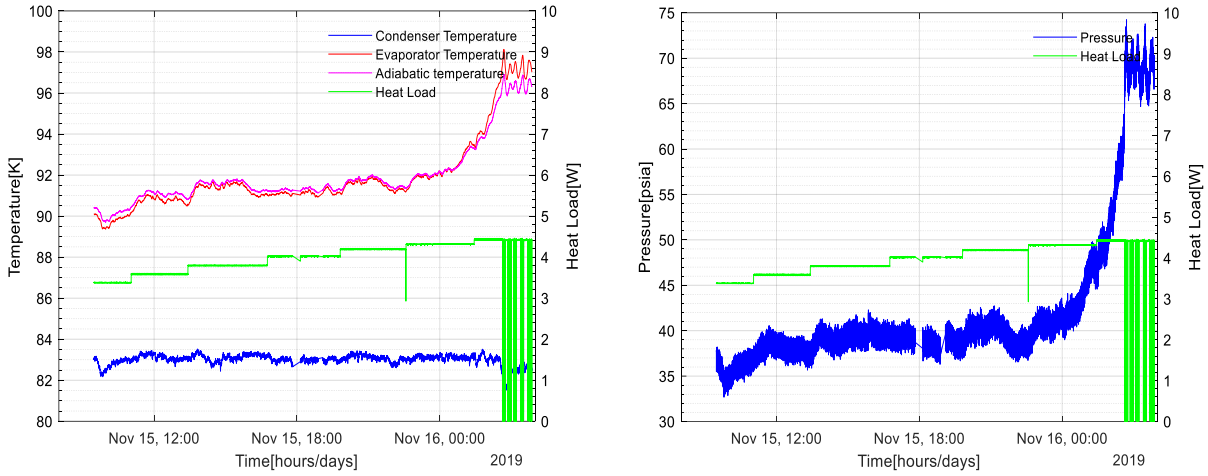

Fig 5-XXV. Temperature and Pressure measurement in PHP at Initial Fill Ratio of 45%

Fig 5-XXV shows that unlike in the case shown in Fig 5-XXI, pressure is not constant with increasing load and there is both a temperature run-off and pressure run-off at the critical heat flux. Also note that unlike in the case of low fill ratio, there is energy that goes into heating the adiabatic section as well since the fill ratio presents the possibility of long liquid slug that could act like a thermal link to the evaporator (solid conduction). The immediate and steep drop in the temperature of the condenser at the critical heat load suggest a separated flow (non-moving fluid) where cold liquid congregates at the condenser carrying no energy and so the cryocooler control at this point cannot maintain the temperature while the hot gas congregates at the evaporator increasing its wall temperature. The thermal contact of the gas with the adiabatic section also causes a rise in temperature at that location.

5.9 Summary (Performance Maps)

3D plots can be made showing how condenser temperature and heat load affects the effective conductivity for different fill ratios. The effective conductivity data is fitted with the highest order polynomial fit that does not result in unphysical behavior or does not produce multiple minimums or maximums. The effective conductivity is forced to zero at critical heat power. The z-axis (red)

legend represents the effective conductivity K_{eff} in units of $\frac{W}{m-K}$, the x-axis (blue) is the condenser temperature T_{cond} in units of K and the y-axis (green) represents the heat load, P in units of W. This performance maps will be further analyzed in future work to determine optimal operating regions and to see the relative effect of operating perturbations in condensing temperature or heat load on the performance of the PHP.

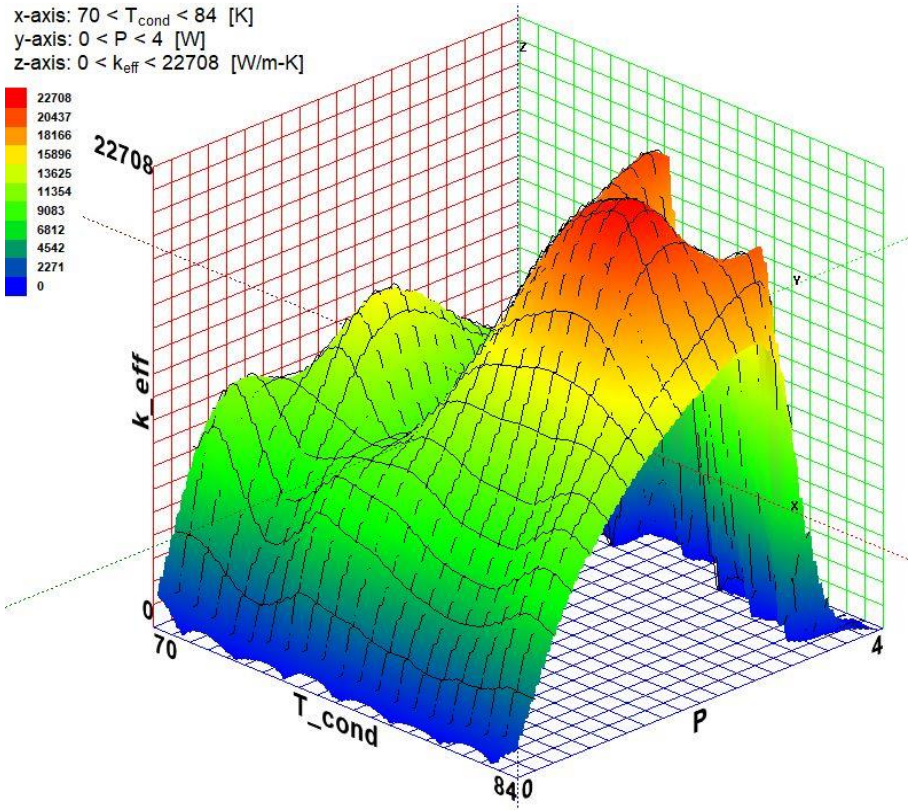

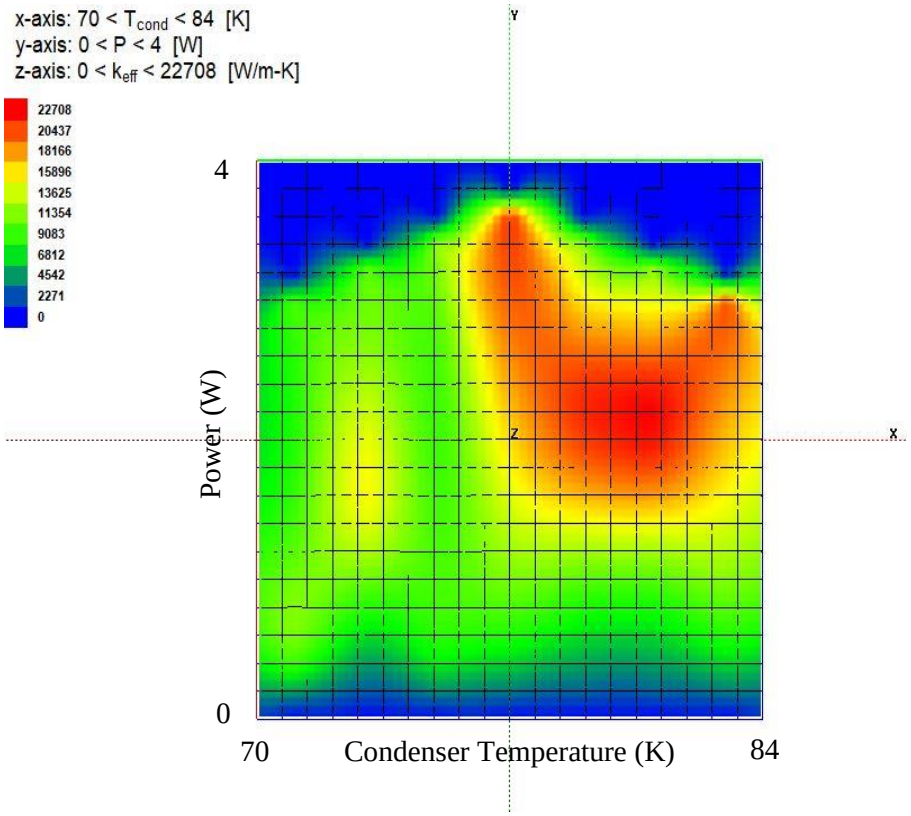
x-axis: 70 < T_cond < 84 [K]
y-axis: 0 < P < 4 [W]
z-axis: 0 < k_eff < 22708 [W/m-K]
22708
20437
18166
15896
13625
11354
9083
6812
4542
2271
0
4
Power (W)
0
70
Condenser Temperature (K)
84

(a)

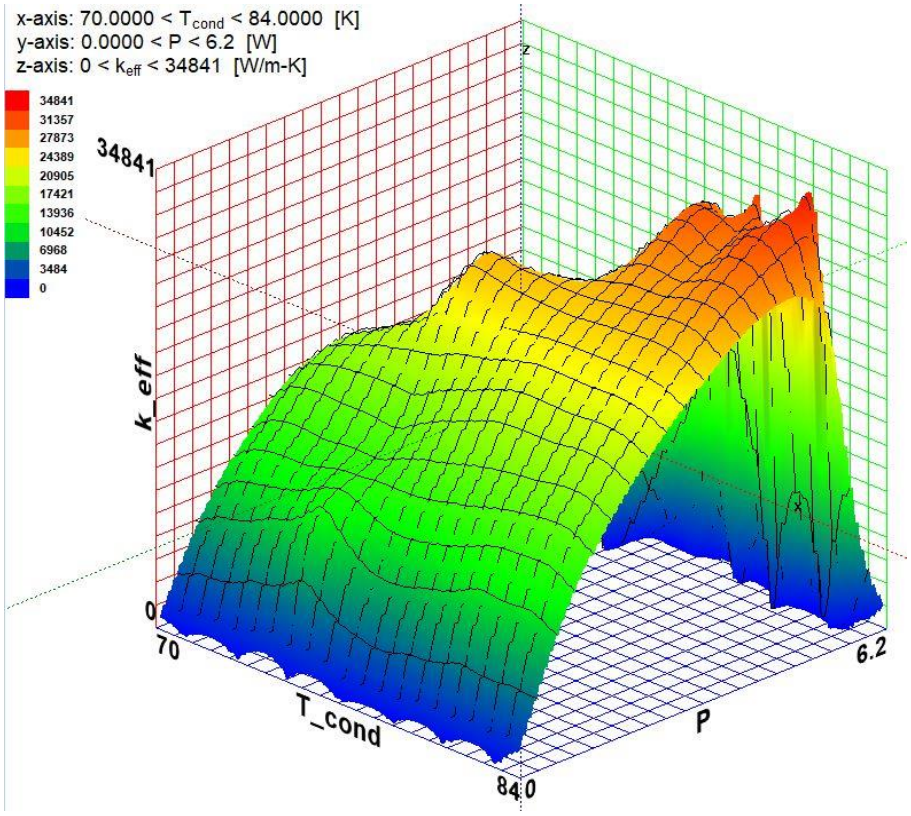
x-axis: 70.0000 < T_cond < 84.0000 [K]
y-axis: 0.0000 < P < 6.2 [W]
z-axis: 0 < k_eff < 34841 [W/m-K]
34841
31357
27873
24389
20905
17421
13936
10452
6968
3484
0
34841
k_eff
0
70
T_cond
84
0
P
6.2

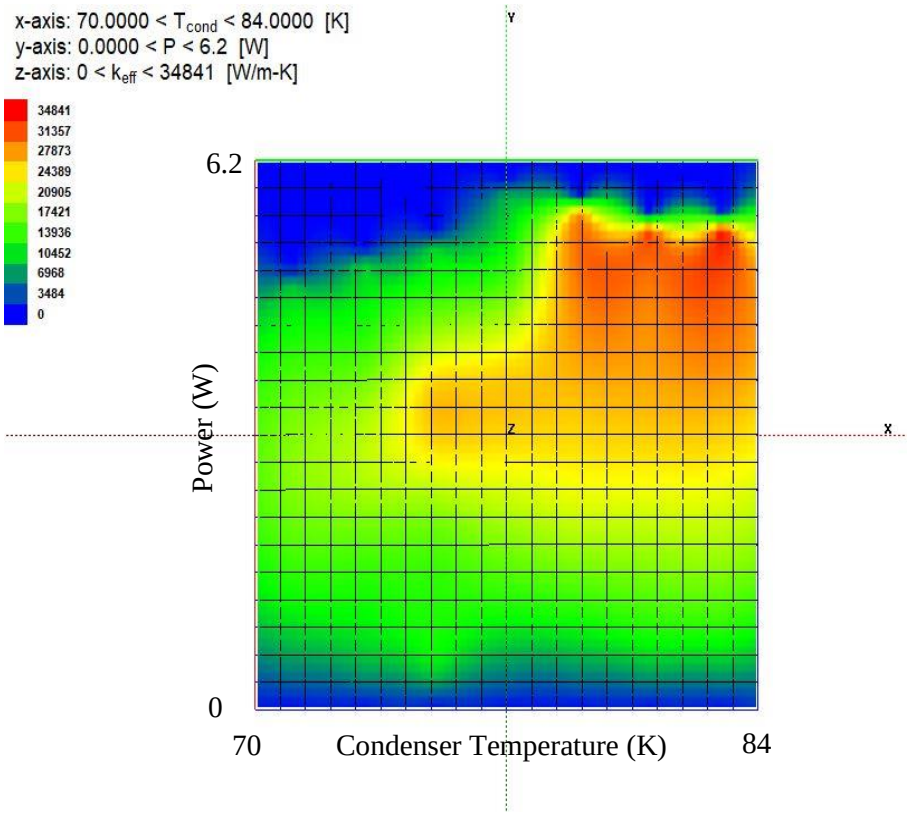
x-axis: 70.0000 < T_cond < 84.0000 [K]
y-axis: 0.0000 < P < 6.2 [W]
z-axis: 0 < k_eff < 34841 [W/m-K]
34841
31357
27873
24389
20905
17421
13936
10452
6968
3484
0
6.2
Power (W)
0
70
Condenser Temperature (K)
84
Y
X
Z

(b)

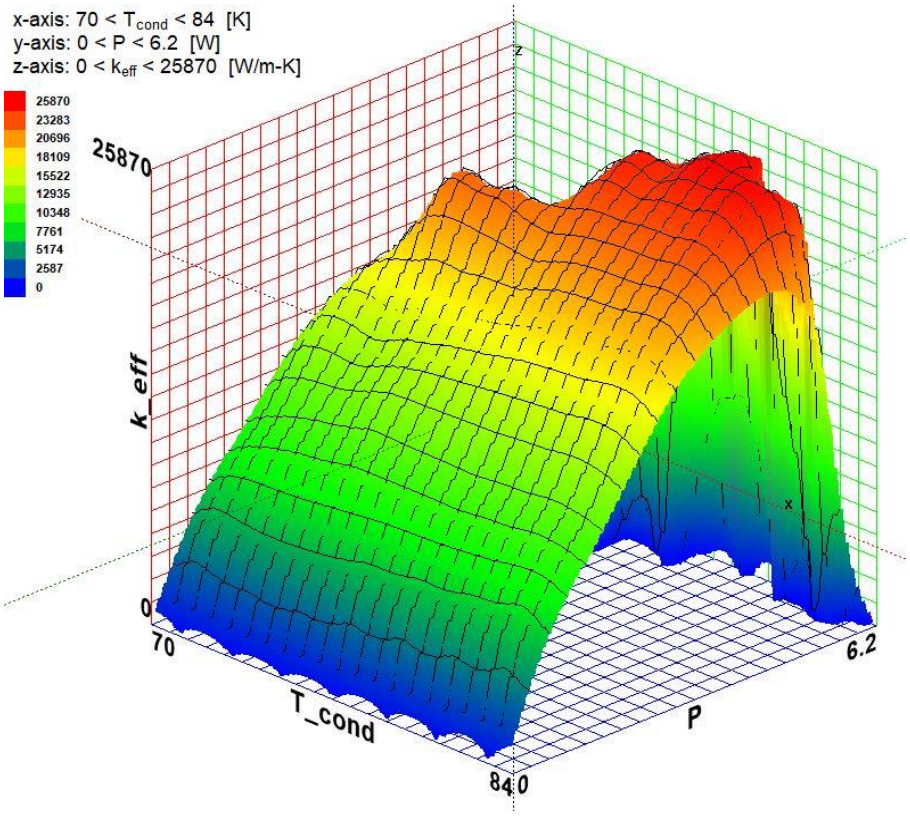
x-axis: 70 < T_cond < 84 [K]
y-axis: 0 < P < 6.2 [W]
z-axis: 0 < k_eff < 25870 [W/m-K]
25870
23283
20696
18109
15522
12935
10348
7761
5174
2587
0
25870
k_eff
0
70
T_cond
84.0
P
6.2
Z
X

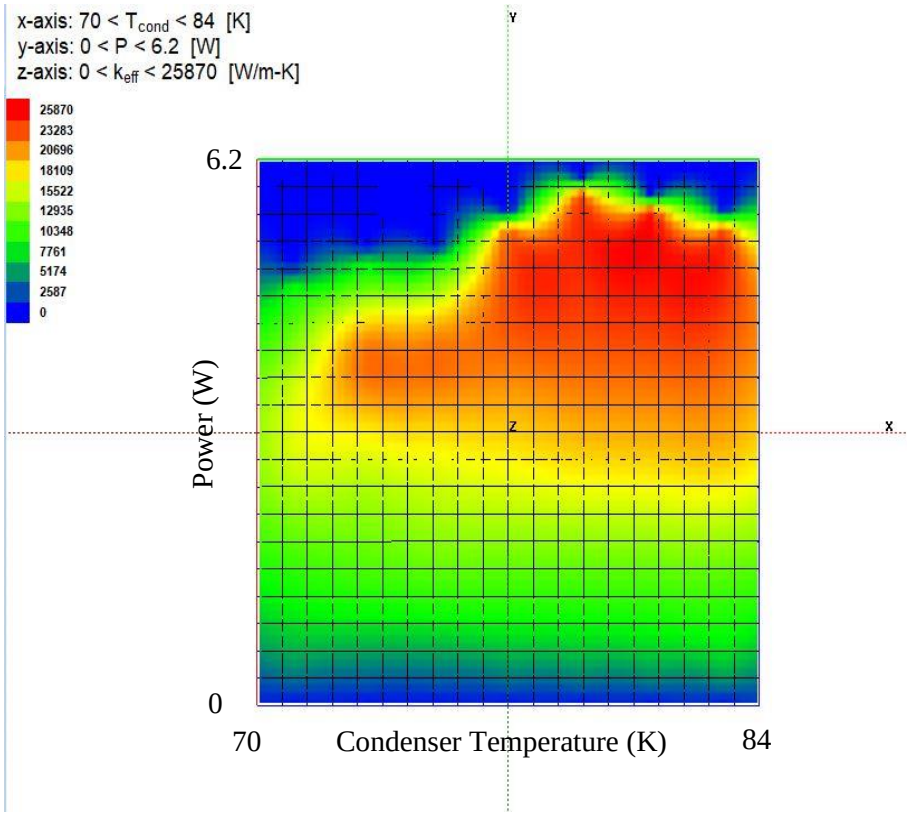
x-axis: 70 < T_cond < 84 [K]
y-axis: 0 < P < 6.2 [W]
z-axis: 0 < k_eff < 25870 [W/m-K]
25870
23283
20696
18109
15522
12935
10348
7761
5174
2587
0
6.2
Power (W)
0
70
Condenser Temperature (K)
84

(c)

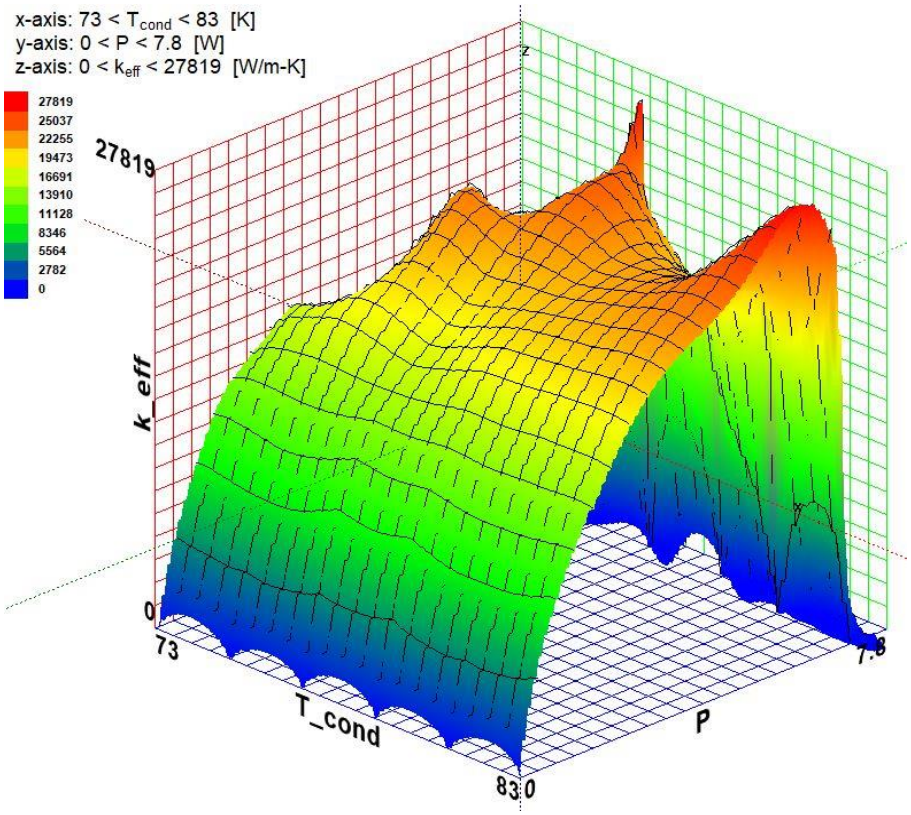
x-axis: 73 < T_cond < 83 [K]
y-axis: 0 < P < 7.8 [W]
z-axis: 0 < k_eff < 27819 [W/m-K]
27819
25037
22255
19473
16691
13910
11128
8346
5564
2782
0
27819
k_eff
0
73
T_cond
83
0
P
7.8

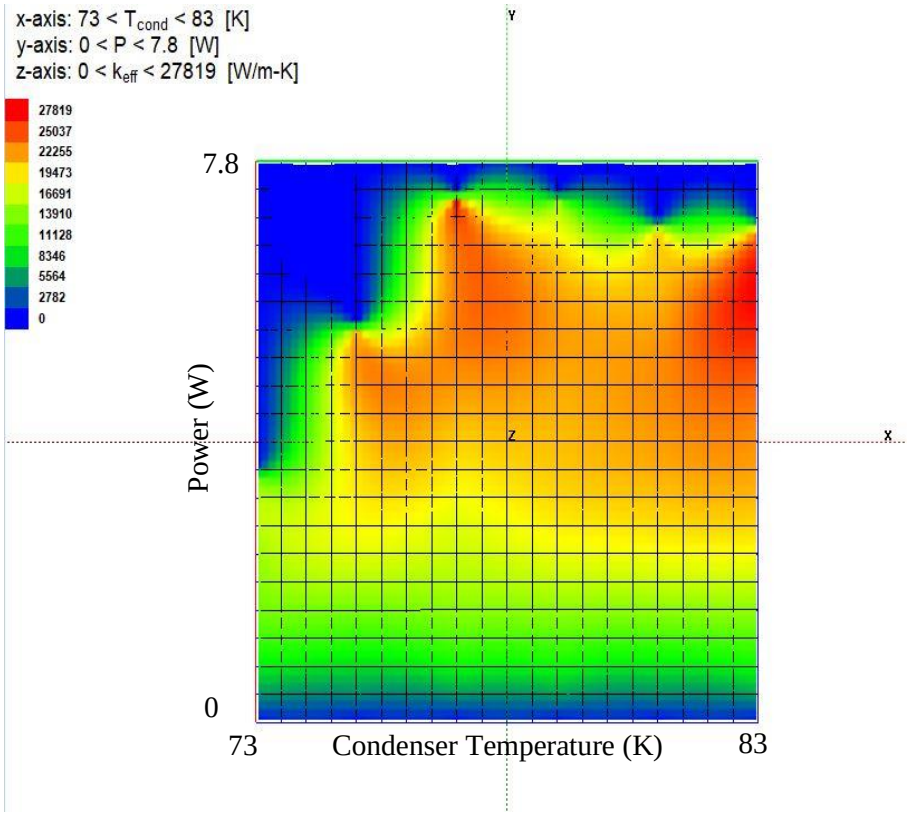
x-axis: 73 < T_cond < 83 [K]
y-axis: 0 < P < 7.8 [W]
z-axis: 0 < k_eff < 27819 [W/m-K]
27819
25037
22255
19473
16691
13910
11128
8346
5564
2782
0
7.8
Power (W)
0
73
Condenser Temperature (K)
83
Y
Z
X

(d)

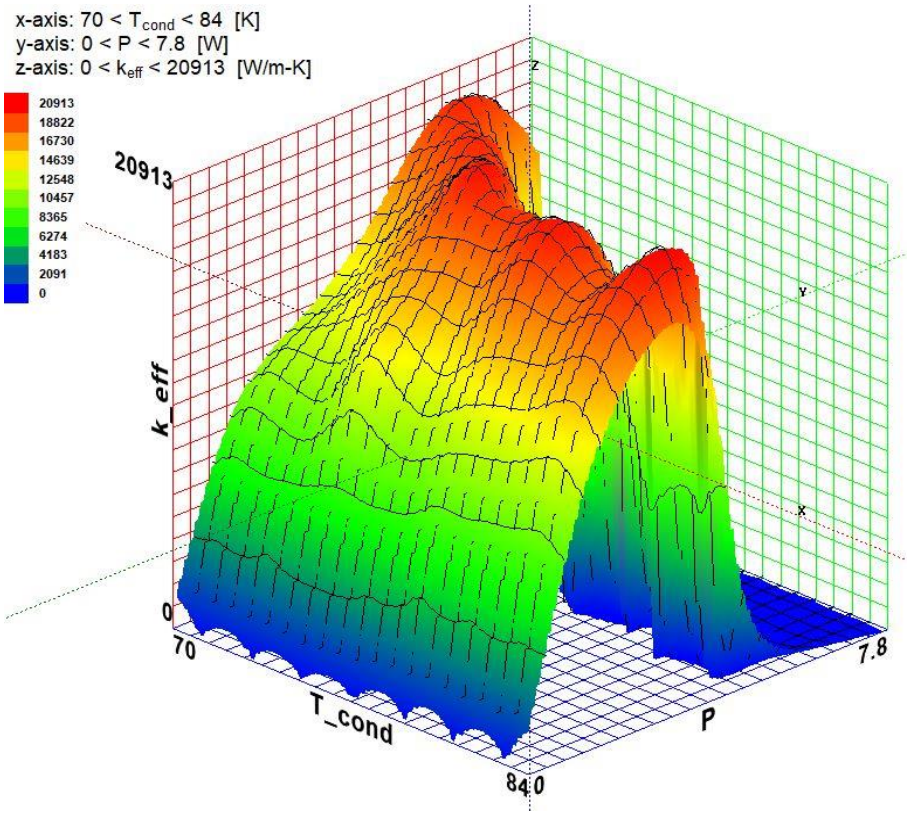
x-axis: 70 < T_cond < 84 [K]
y-axis: 0 < P < 7.8 [W]
z-axis: 0 < k_eff < 20913 [W/m-K]
20913
18822
16730
14639
12548
10457
8365
6274
4183
2091
0
20913
k_eff
0
70
T_cond
84.0
P
7.8
Z
Y
X

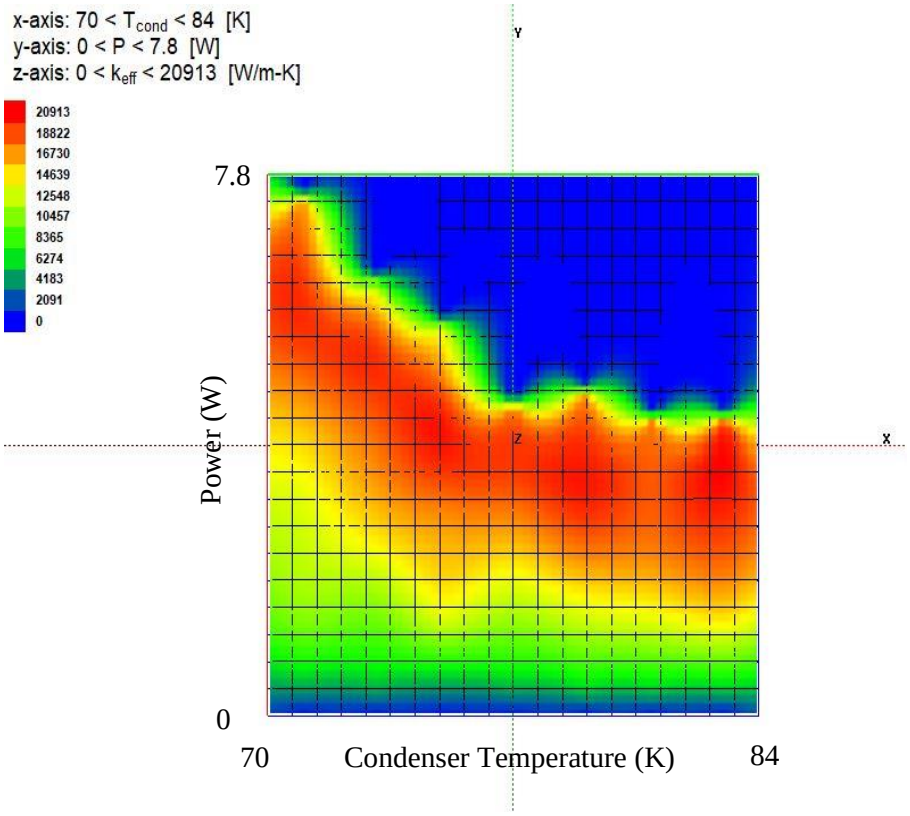
x-axis: 70 < T_cond < 84 [K]
y-axis: 0 < P < 7.8 [W]
z-axis: 0 < k_eff < 20913 [W/m-K]
20913
18822
16730
14639
12548
10457
8365
6274
4183
2091
0
7.8
Power (W)
0
70
Condenser Temperature (K)
84
Y
X
Z

(e)

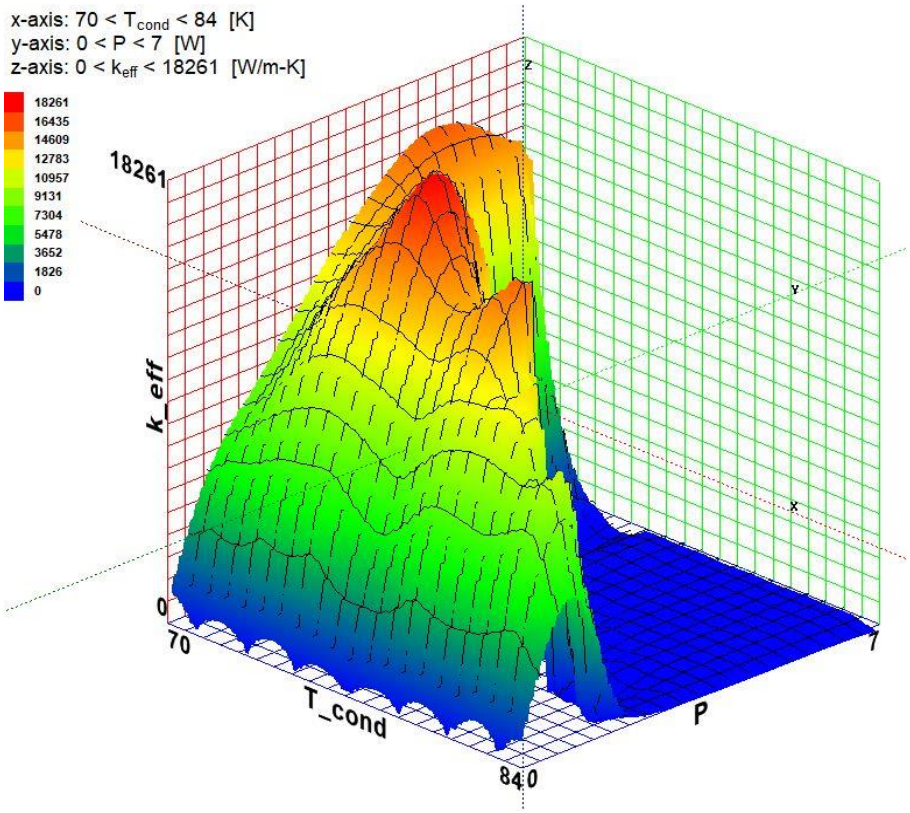
x-axis: 70 < T_cond < 84 [K]
y-axis: 0 < P < 7 [W]
z-axis: 0 < k_eff < 18261 [W/m-K]
18261
16435
14609
12783
10957
9131
7304
5478
3652
1826
0
18261
k_eff
0
70
T_cond
84
0
P
7
Z
Y
X

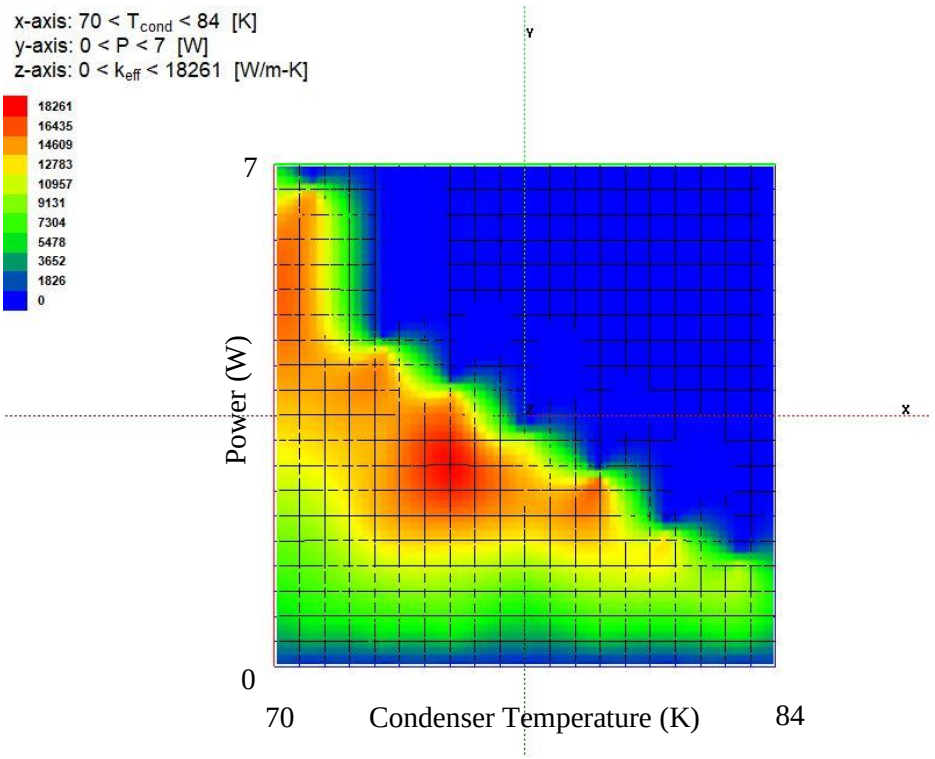

(f)

Fig 5-XXVI. (a) FR 15.5% (b) FR 24.8% (c) FR 30.8% (d) FR 40% (e) FR 45% (f) FR 52%

An optimally sized PHP should be designed to operate in regions not too close to CHF. This criterion would avoid the penalty (effective thermal conductivity either drops drastically or the system completely dries out at the heat source) in thermal performance as a result of small perturbations in operating parameters. In this case, those operating parameters are condenser (or heat sink) temperature and heat load. The performance maps help identify optimal range of operating parameters.

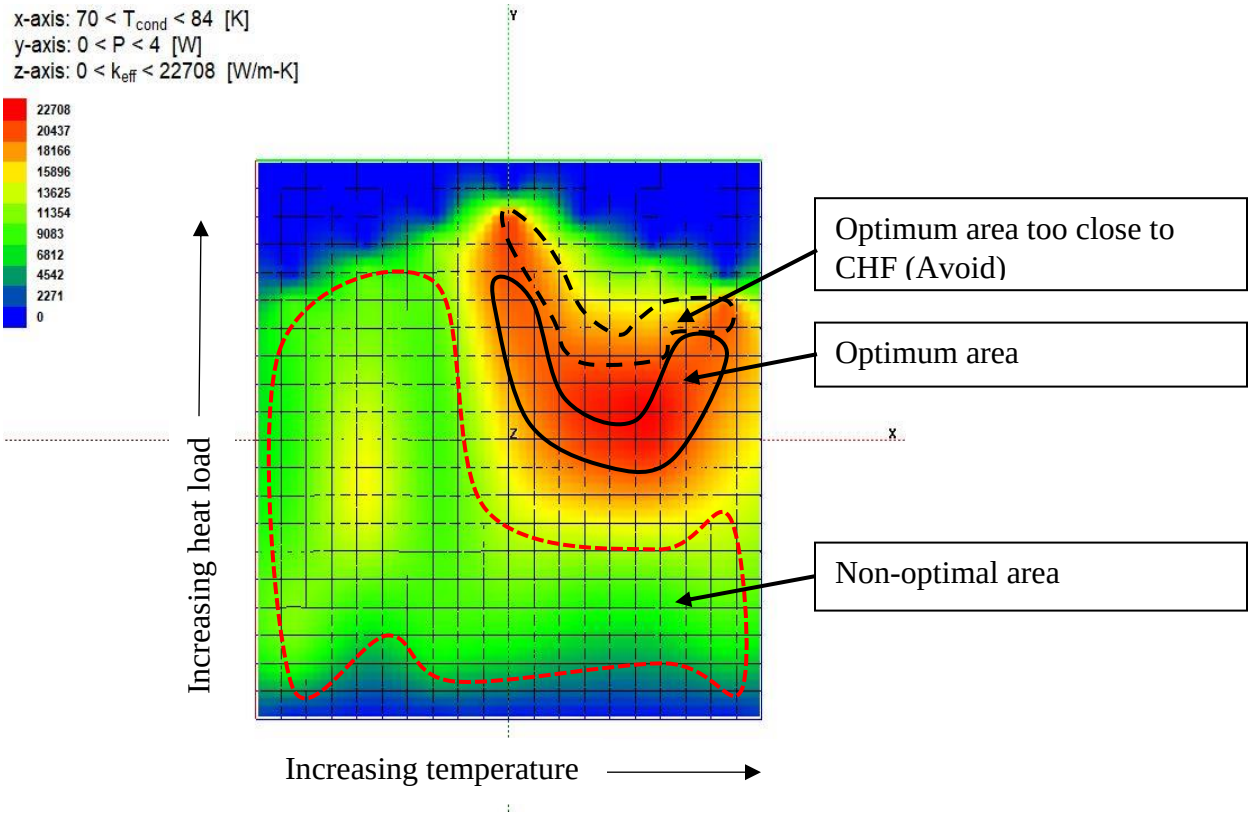
x-axis: 70 < T_cond < 84 [K]
y-axis: 0 < P < 4 [W]
z-axis: 0 < k_eff < 22708 [W/m-K]
22708
20437
18166
15896
13625
11354
9083
6812
4542
2271
0
Y
Z
X
Optimum area too close to CHF (Avoid)
Optimum area
Non-optimal area
Increasing heat load
Increasing temperature

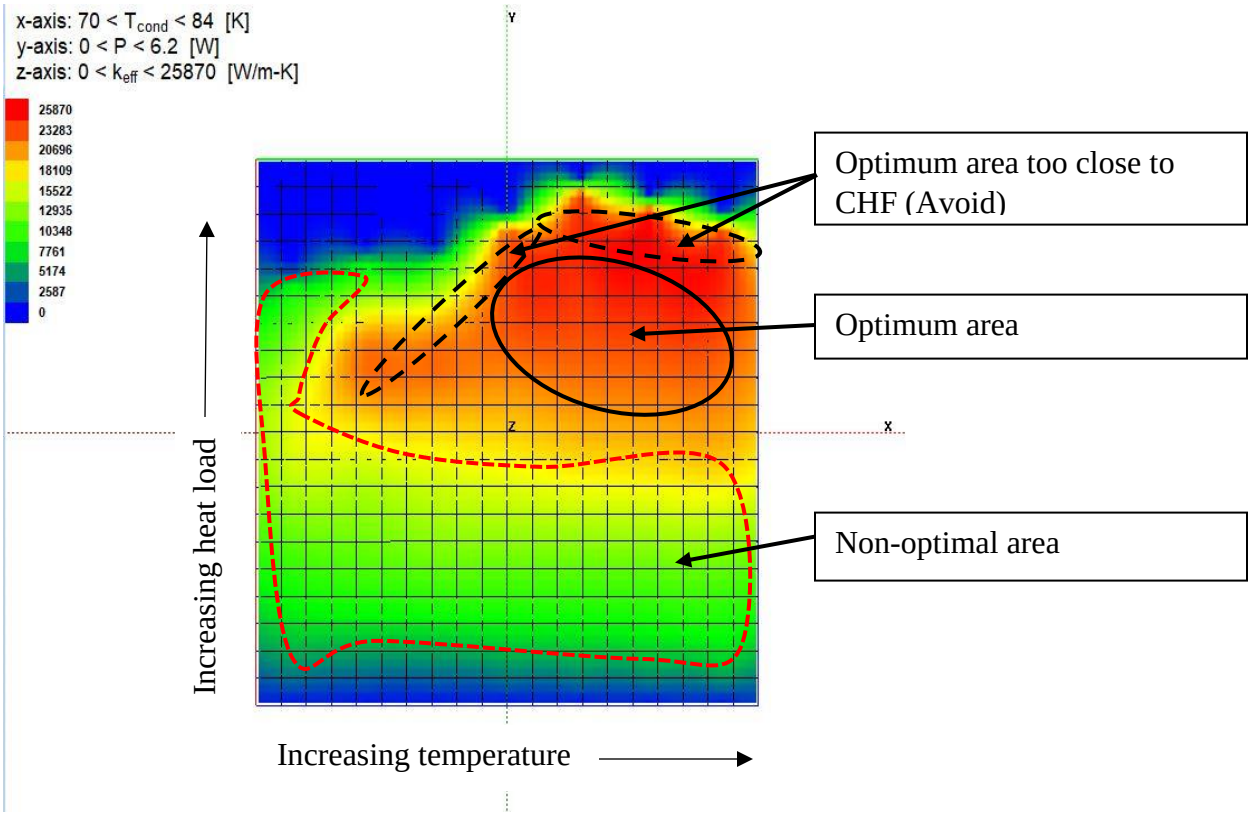

Fig 5-XXVII. Examples of performance maps showing optimal and non-optimal areas of operation

Although the PHP should be designed to work in the optimal region, it can also be designed to work in the non-optimal area that is close to the optimal region.

From the Nitrogen data, it can be observed that the optimal area increases as we get to higher fill ratios, spreading from higher temperatures as seen in Fig 5-XXVIa to lower temperatures as seen in Fig 5-XXVIb through Fig 5-XXVIf. However, at higher fill ratios (Fig 5-XXVIe &Fig 5-XXVIf), there is less range to work with, especially at higher temperatures and/or higher heat loads.

6 Other Pure Fluids in PHPs

6.1 Argon as a working fluid

There is a need for cooling Liquid Natural Gas (LNG) inside tankers during transportation. When these tankers are at rest, heat transfer into the sides results in locally elevated temperatures. After sufficient time, the resulting temperature stratification and buoyant instability results in a sudden 'roll-over' bringing the warm fluid to the top of the liquid and leading to a rapid and dramatic pressure rise. The rise in the pressure typically triggers the pressure relief valves designed to maintain the pressure within a safe range, thereby venting gas into the environment. This has both an economical and environmental impact. PHPs as heat spreaders could have a practical application in this case. Heat can be removed from the hotter bottom liquid and transported to the cooler upper liquid using a PHP operating with Argon as the working fluid.

Argon has a boiling point of 87.3[K] at standard atmosphere, a triple point of about 83[K], and a critical point of 150.7[K], giving a wide working temperature range for an argon PHP. Methane, the primary component of natural gas has a boiling point of 111.6[K] at atmospheric pressure, triple point of 90.7[K] and critical temperature of 190.55[K] so a PHP charged with Argon should work as a heat transfer device in this temperature range typical for LNG tanks.

Argon was chosen a working fluid for further PHP tests for two additional reasons. First, the similarity in working temperature (in terms of range), and property behavior like T-v (temperature-volume) relationship make Argon a good choice for a PHP working fluid that can be compared to PHPs operating with Nitrogen as the working fluid. The performance data from the Argon PHP can be compared to that from the Nitrogen PHP tests to explore potential advantages of Argon

PHPs. Secondly, there are existing data sets available for Nitrogen, Helium and even some Neon PHPs but little work has been done on Argon PHPs.

Fig 6-Ia shows the specific heat capacity of Argon compared to Nitrogen from 300[K] to 90[K]. Argon has a smaller heat capacity than Nitrogen throughout that range and should thermally respond faster. However, since the PHP comprises copper blocks that have masses much greater than the working fluid, the thermal response time would be governed by those solids. The smaller heat capacity of Argon compared to Nitrogen also means that Nitrogen should be able to pick up more sensible heat per unit mass than Argon.

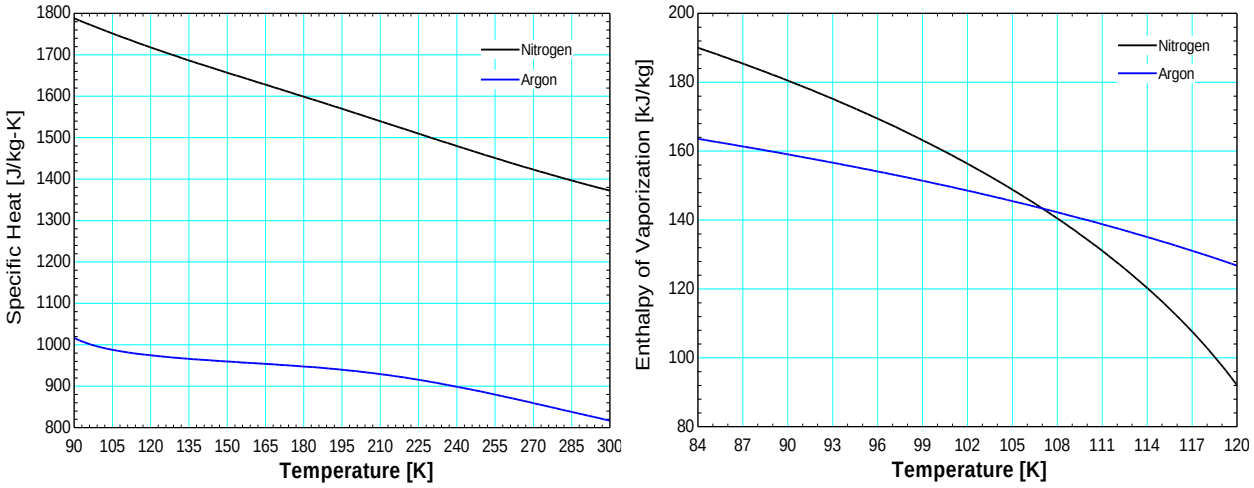

(a) (b)

Fig 6-I (a) Specific Heat versus Temperature (b) Heat of Vaporization versus Temperature

Fig 6-Ib shows the enthalpy of vaporization for both fluids over a working temperature range of 84[K] to 120[K]. At the lower temperatures, nitrogen will carry more latent heat per unit mass but as temperature rises above 107[K], argon becomes more advantageous in terms of latent heat transfer. One of the major advantages of Argon as a working fluid, especially in pressure vessels, is its lower operating pressures. Fig 6-IIa shows the working pressures of Nitrogen and Argon

across the temperature range stated earlier. Another advantage is that for the same liquid fill ratio, the mass inventory inside the PHP would be larger for Argon than for Nitrogen. That difference gets bigger as you increase fill ratio as shown in Fig 6-IIb. Such property comparison, as well as behavior of other thermodynamic properties like surface tension should be explored in future work.

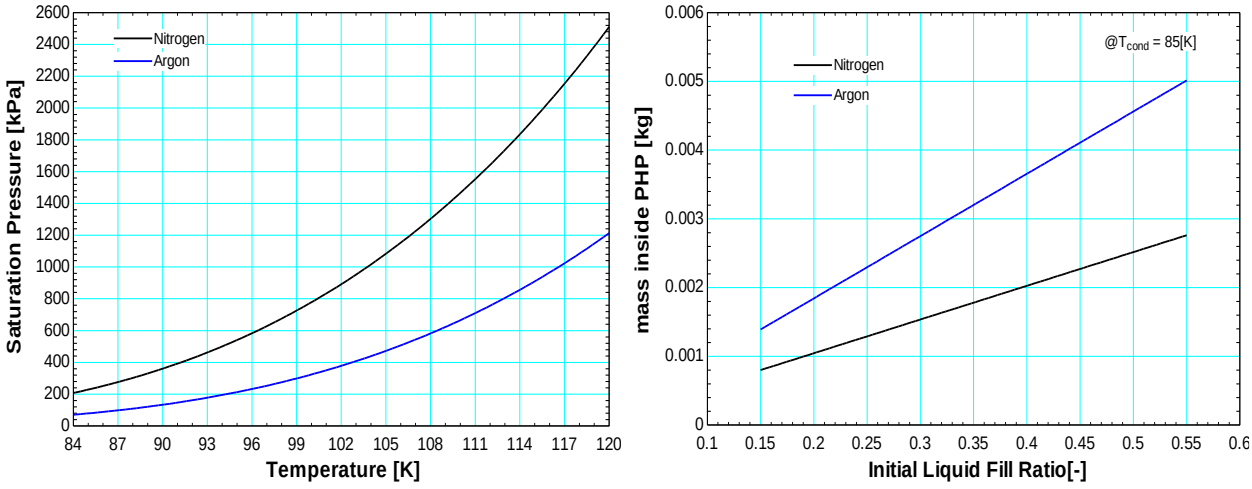

(a) (b)

Fig 6-II(a) Saturation pressure vs temperature (b) PHP fluid mass vs liquid fill ratio

6.2 Experimental results for Argon at Low Fill ratios

6.2.1 Effective conductivities versus condenser temperature for low fill ratio

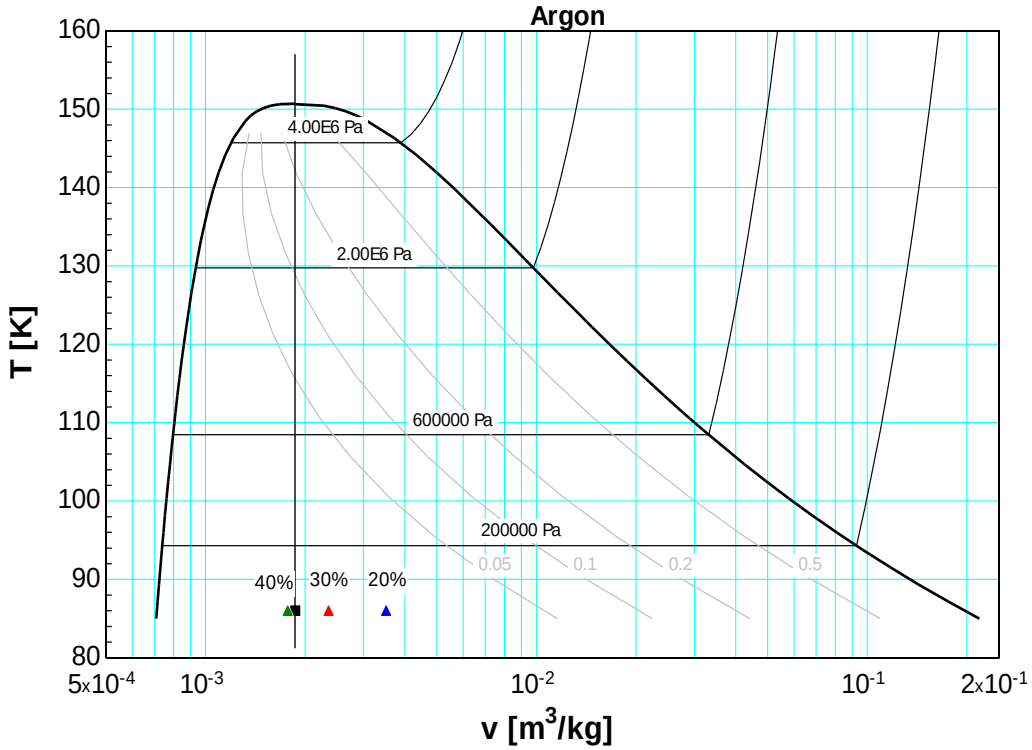

Fig 6-III. T-v diagram for Argon

Two low fill ratio runs were completed for Argon. One at 20% initial fill ratio and the other at 30% initial fill ratio at 86K. The range of condenser temperature runs for Argon was 86K to 101K with a temperature interval of 3K. The results of the effective thermal conductivity as a function of heat load for various condenser temperatures are shown in Fig 6-IV.

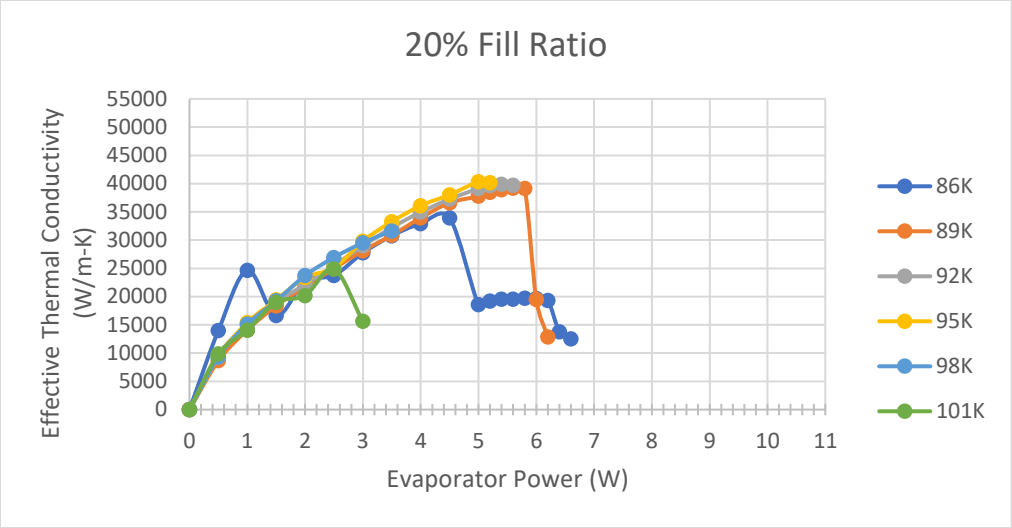

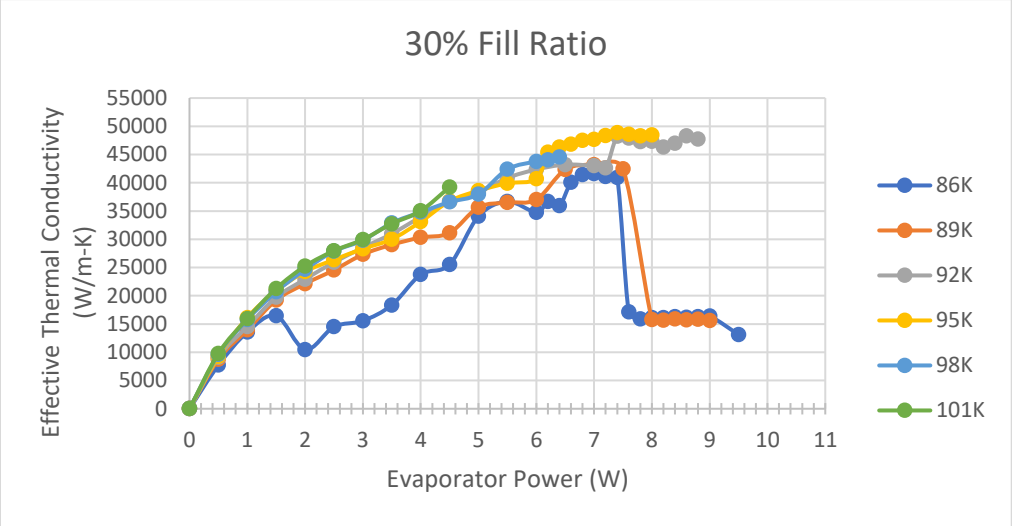

Fig 6-IV. Effective thermal conductivity versus heat load for different condenser temperatures

The effective thermal conductivity as a function of heat load is consistent with the behavior seen in Nitrogen. As heat load is increased, the effective thermal conductivity goes up, possibly due to smaller thin film layer, up until the point close to dry-out where the wall temperature goes up as the heat is convected to a single-phase gas. The behavior of effective thermal conductivity with increase in condenser temperature is also consistent with that of Nitrogen. i.e., as condenser temperature goes up, so does the value of effective thermal conductivity (except at regions where intermittent dry-out occurs i.e., regions after the maximum effective conductivity).

6.2.2 Dry-out versus condenser temperature for low fill ratio

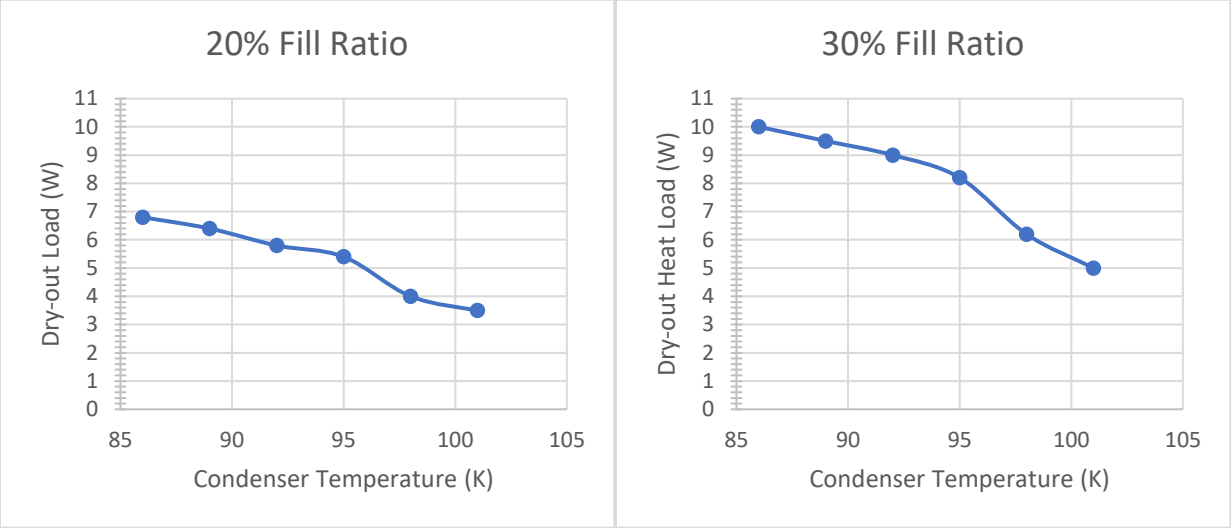

Fig 6-V. Argon Dry-out load versus condenser temperature for low fill ratios

The dry-out power as a function of condenser temperature for Argon at the fill ratio tested behaved differently than that of Nitrogen. The dry-out power was maximum at the temperature of initial fill (86K) and drops off as temperature goes up. For both 20 and 30 percent fill ratio, Argon exhibited the ability to maintain the same heat transfer coefficient after the point of maximum effective conductivity. This is clearly seen at 86K in the 20% fill ratio and 86K and 89K in the 30% fill ratio as seen in Fig 6-IV. Recall from the nitrogen chapters, there are two possible scenarios after the onset of dry-out. One of those scenarios was a rewetting ability of the flow which sustains operation for a bit. It is postulated that Argon has a higher rewetting effect since it is able to maintain operations after maximum effective conductivity (Fig 6-IV) when the performance drops. If we look at the load at the maximum effective thermal conductivity instead (Fig 6-VI), to eliminate the effect of sustained wall rewetting, then the behavior seen is like the behavior in the Nitrogen PHP.

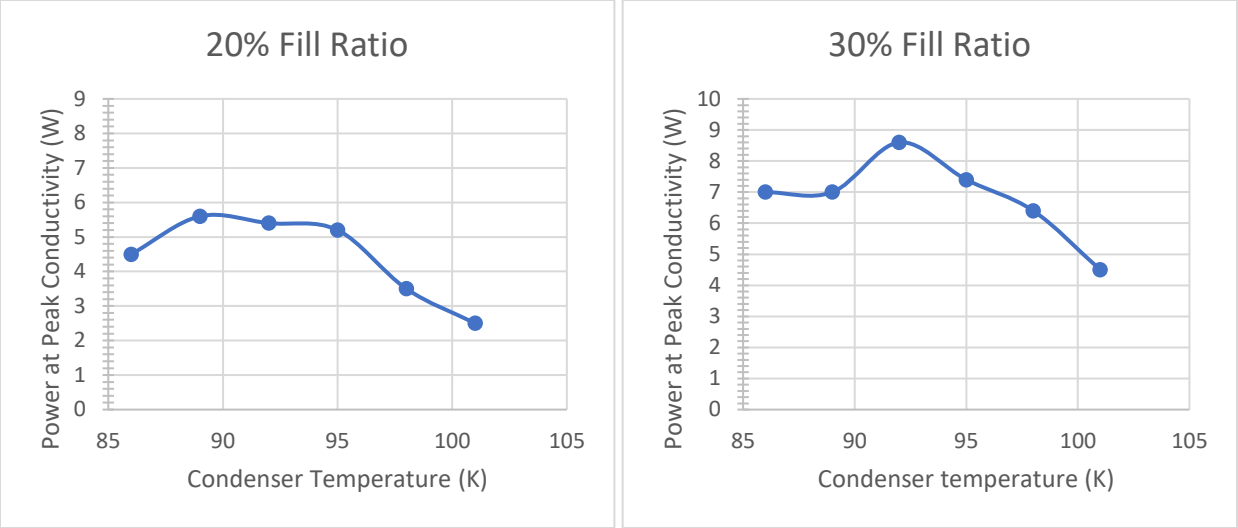

Fig 6-VI. Power at Maximum Effective Conductivity for Argon PHP

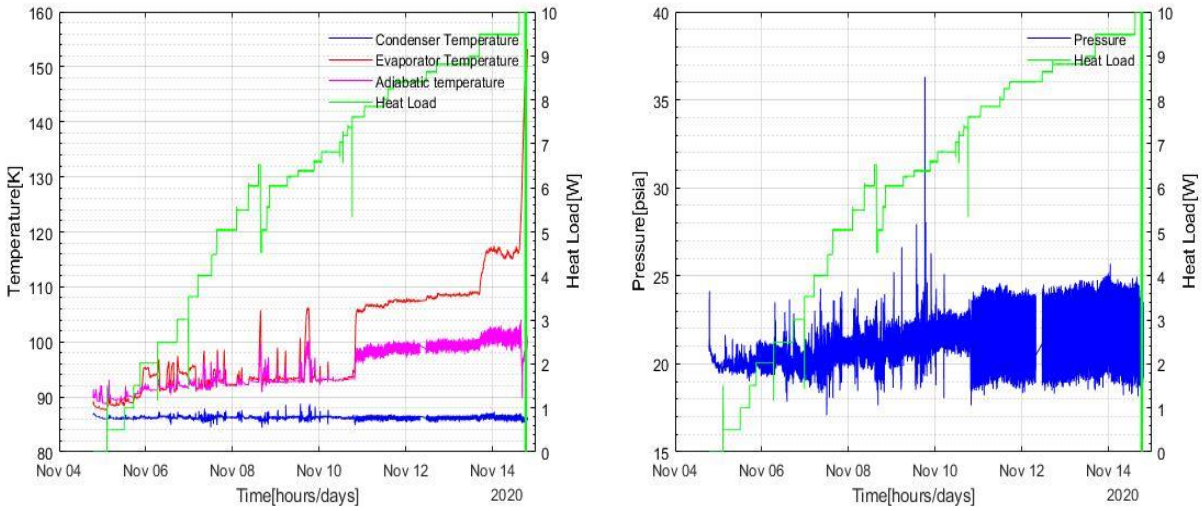

(a)

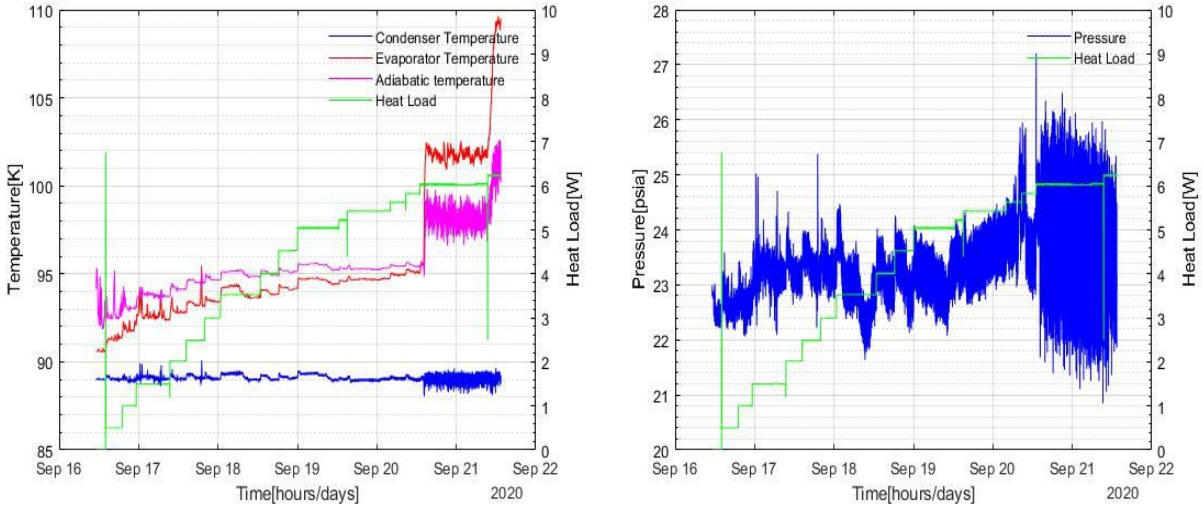

(b)

Fig 6-VII. Temperature and Pressure data for (a) FR = 30%, Tc = 86K (b) FR = 20%, T_c = 88K

Fig 6-VII shows the temperatures and pressure data for two low fill ratio cases for Argon. As with the case for the Nitrogen PHP, the pressure remains fairly constant, even at the dry-out load. At heat load approaches the dry-out load, there is thermal disconnection between the condenser and the evaporator. The constant condenser temperature and much lower adiabatic section temperature (as compared to the evaporator) suggest that the fluid is still in motion and the adiabatic section is somewhat thermally connected to the condenser, but the thin liquid film completely dries off at dry-out load and the little liquid slugs that might make it to the evaporator cannot maintain the wall temperature, leading to the temperature run-off of the evaporator observed at the end.

6.2.3 Boiling curves for Argon

It might be worthwhile to look at the slopes of the heat load versus the temperature difference between the evaporator and saturation temperature, to predict flow regimes. As with standard boiling curves, this would be an indication of the bulk heat transfer coefficient of the fluid. Any significant changes in the slope could correspond to a new flow regime.

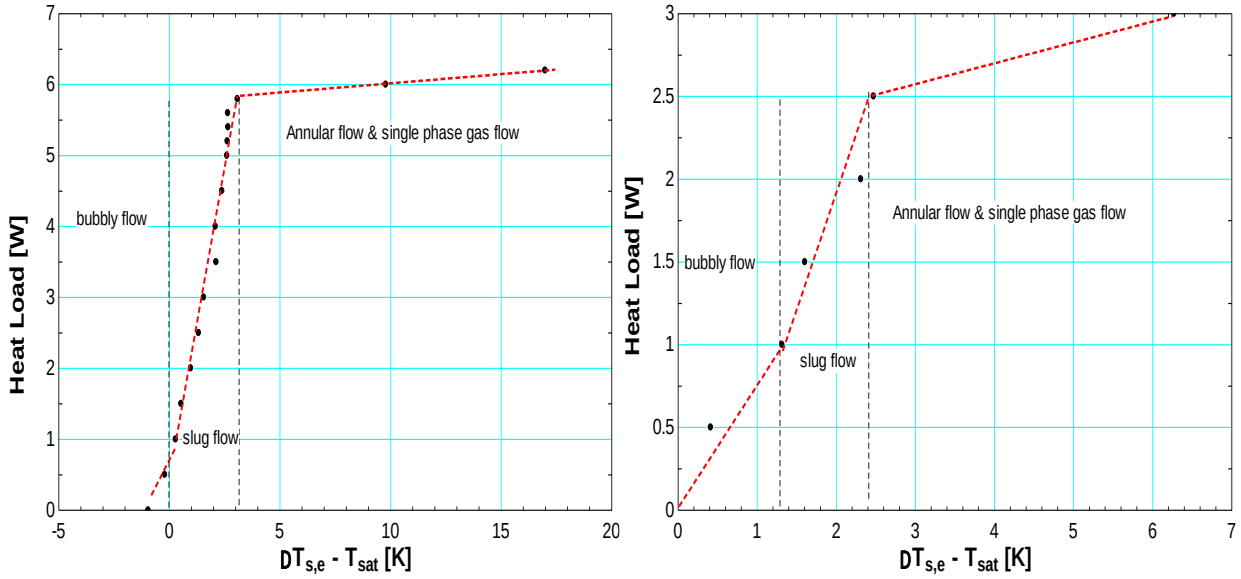

Fig 6-VIII. (L-R) Boiling curve for (a) FR 20%, T_c 89K (b) FR 20%, T_c 101K

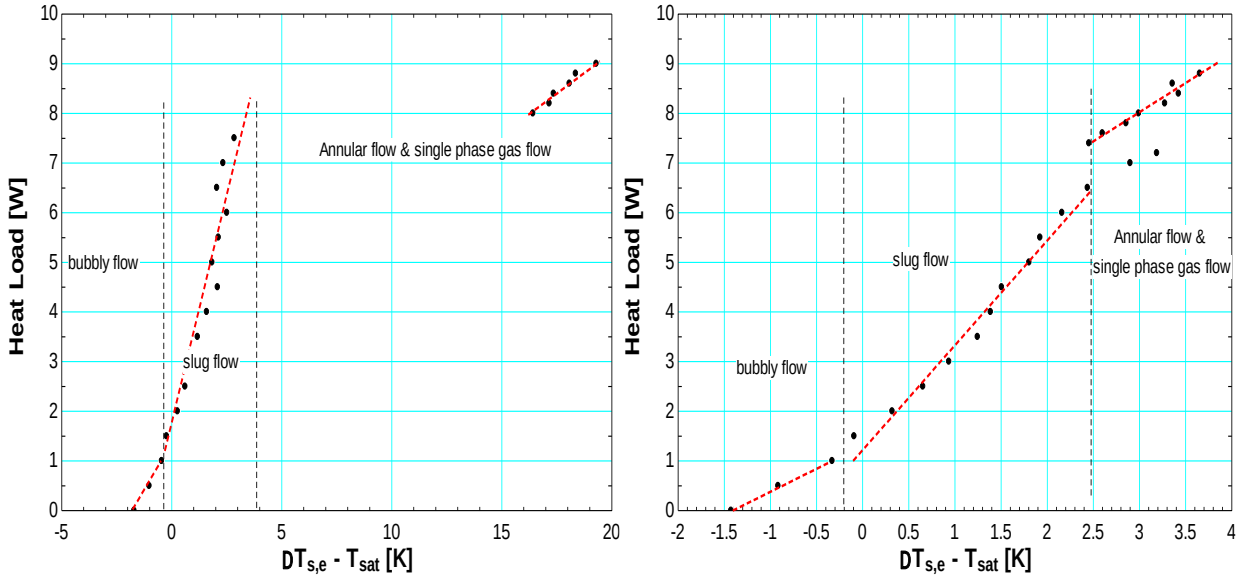

Fig 6-IX. (L-R) Boiling curve for (a) FR 30%, T_c 89K (b) FR 30%, T_c 92K

The Argon data exhibited distinct slopes along the boiling curve. This supports the hypothesis that these slopes likely suggest different flow regimes. It was also found that the first flow regime (most likely slug flow with sustained nucleation) is confined to low powers (≤ 1W). This finding is

similar to that of the nitrogen data (≤ 0.5W), suggesting that the performance of the PHP would be independent of condenser temperature or fill ratios at those low powers.

6.2.4 Thermodynamic Process: Heat Addition for Argon PHP

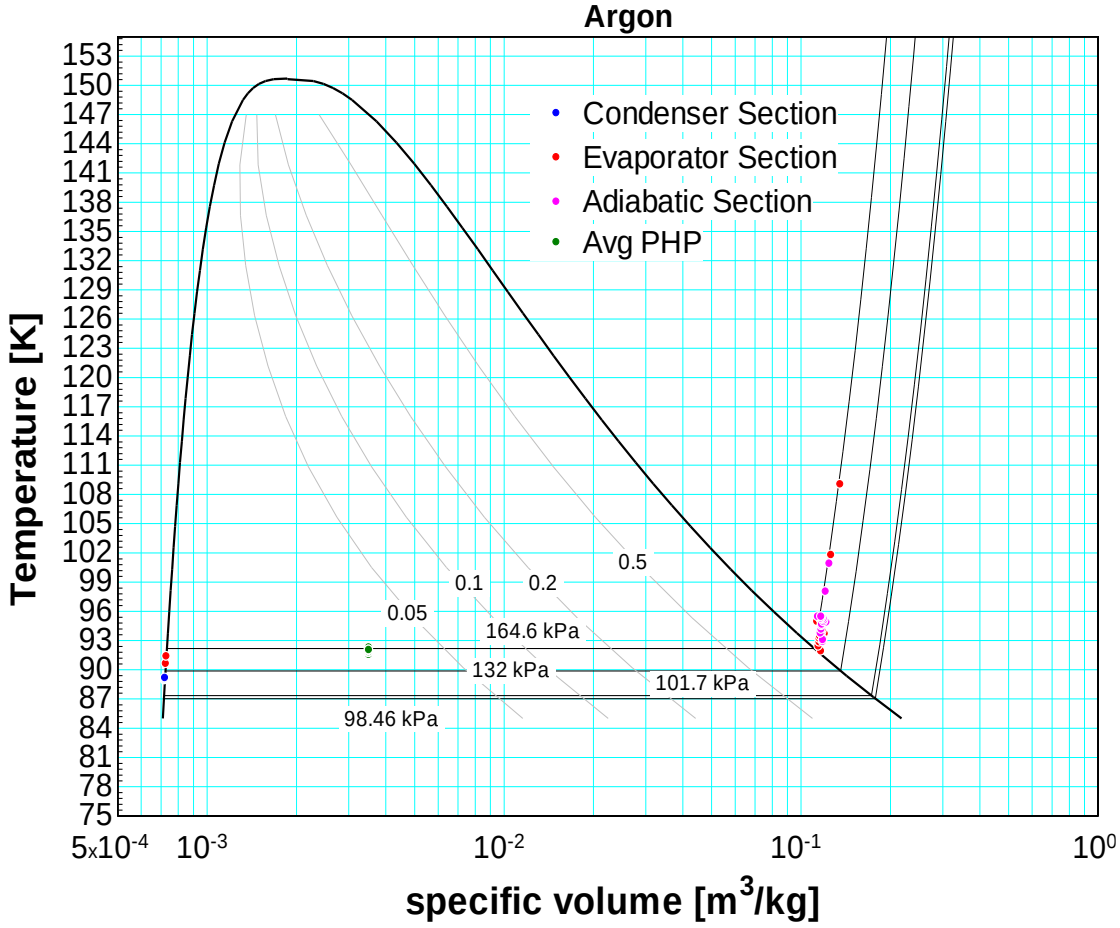

(a)

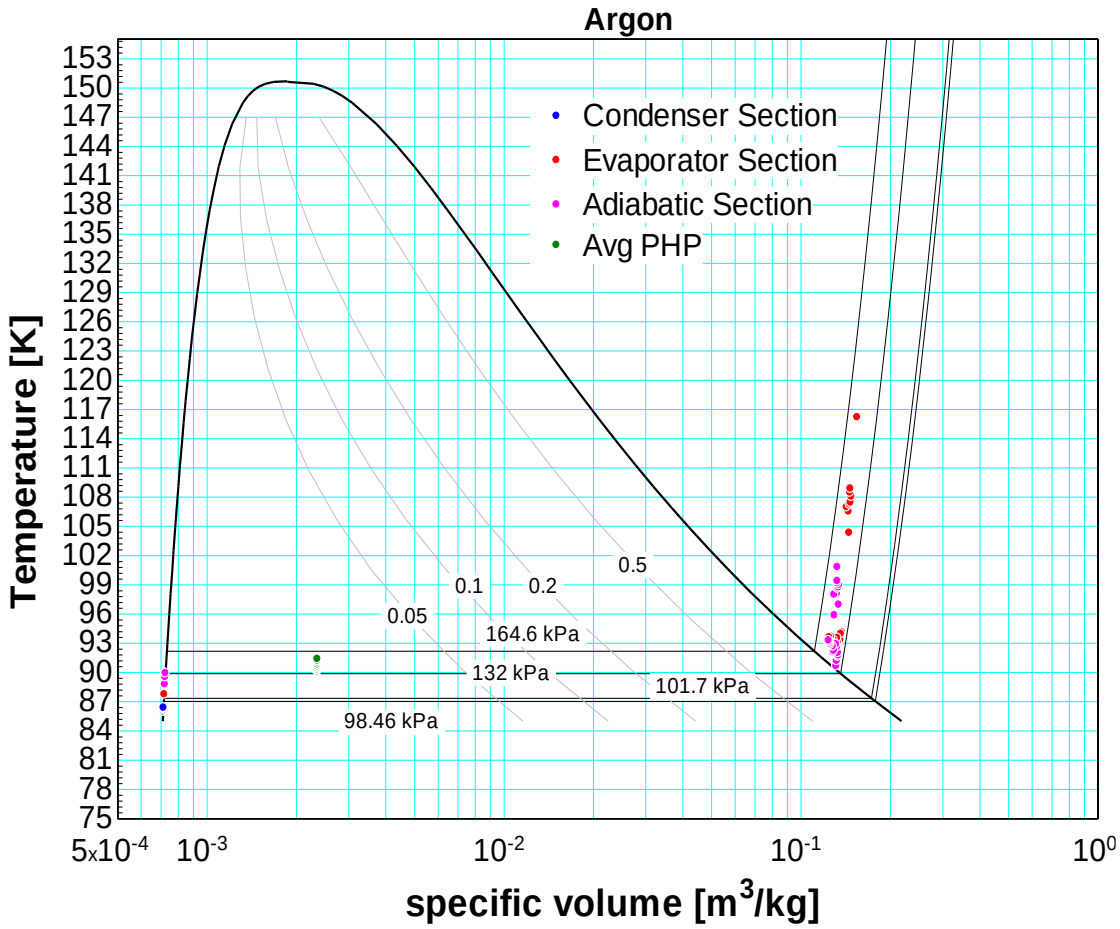

(b)

Fig 6-X. T-v states for (a) FR 20%, T_c 89K (b) FR 30%, T_c 86K

The figures above show the thermodynamic heating process for the Argon PHP for the two initial fill ratios tested. The two fill ratios tested are both low liquid fill ratios (fill ratios whose specific volume are to the right of the critical specific volume). Just like with the Nitrogen fill ratios, these fill ratios have the capacity to sustain operations at higher ΔT_{php} (temperature difference between the condenser and the evaporator) than at high fill ratios (from Nitrogen data). The boiling process also appears to be isobaric or near isobaric just as with the low fill ratios of the Nitrogen PHP. This suggests that the same conclusion as with the Nitrogen PHP can be made. That the average equilibrium interface (between the vapor and liquid) sits closer to the constant condenser

temperature. Hence, the equilibrium pressure would be largely set by this temperature. One difference between this thermodynamic process and that seen in the Nitrogen PHP is that the initial state of the fluid in the evaporator appears to be largely liquid. As heat is introduced to the evaporator, the average state of the fluid in the evaporator moves from largely being liquid to largely being superheated vapor. This is likely because Agon is much denser than Nitrogen. The density of liquid Argon at 1 standard atmosphere is $1395\frac{kg}{m^3}$ compared to $806.1\frac{kg}{m^3}$ for liquid Nitrogen. Argon also has a higher surface tension than Nitrogen ($0.01253\frac{N}{m}$ for Argon versus $0.00888\frac{N}{m}$ for Nitrogen at standard atmosphere). Therefore addition, the capillary forces that holds the liquid to the tubes are stronger for an Argon PHP than for a Nitrogen PHP.

6.2.5 Pressure responses/ Flow velocity

There is no device currently installed to measure the velocity or mass flowrate of the fluid inside the PHP, but the pressure oscillation of the fluid can provide some information about the behavior of the liquid slug in response to increased evaporator heat load. It should be noted that the pressure sensor is attached to the adiabatic section.

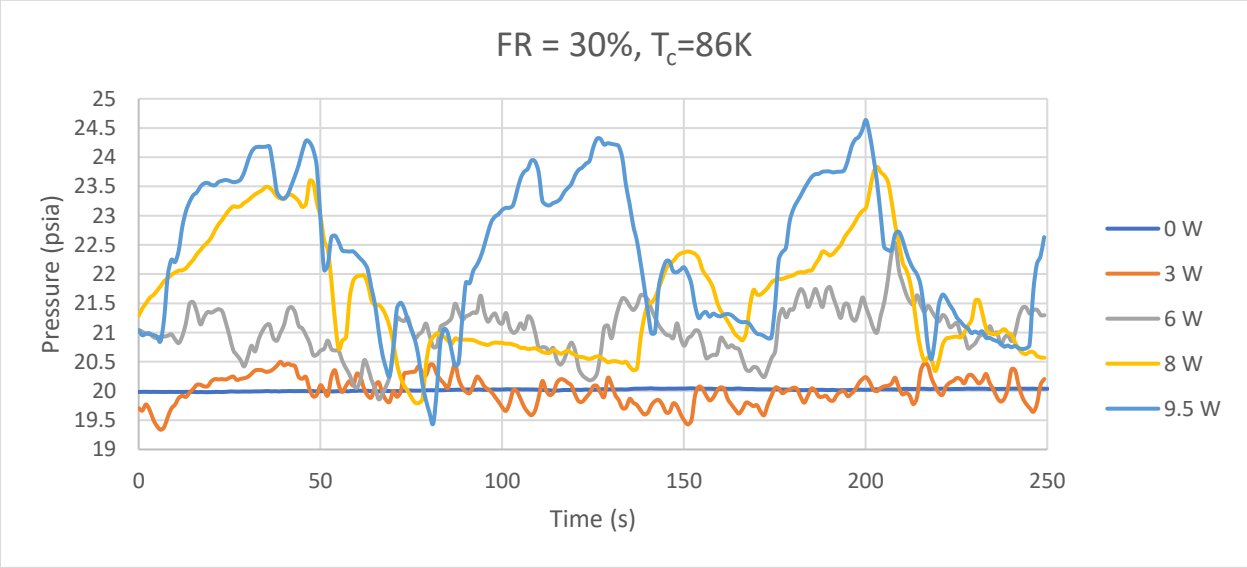

(a)

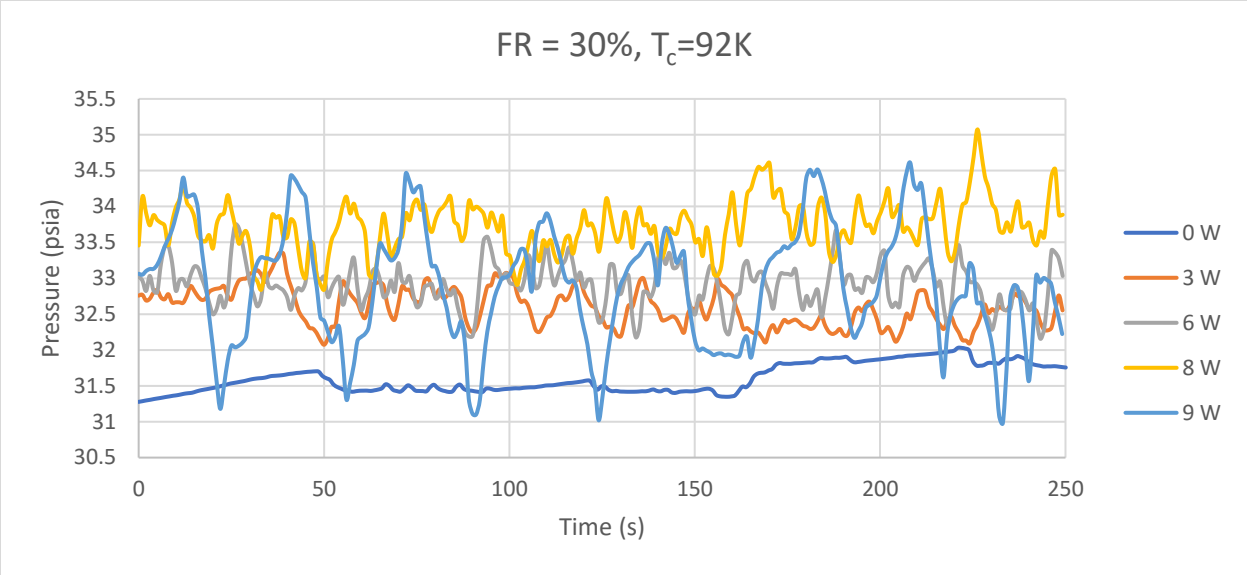

(b)

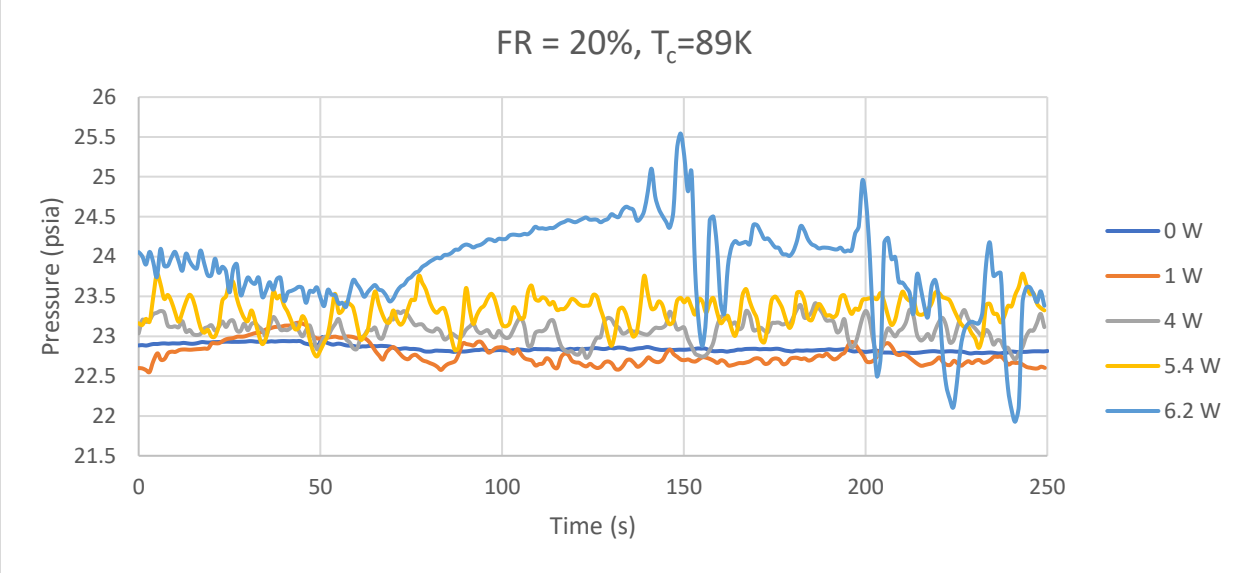

(c)

Fig 6-XI. Pressure oscillations at the adiabatic section for different Heat Loads

Fig 6-XI (a-c) shows the pressure oscillations in the PHP as a function of time for different heat loads. Initially the pressure oscillation is almost zero, when the heat load is zero. This shows that there is very little movement of the fluid. As the heat load is increase, so does frequency of oscillation, suggesting that the velocity of the fluid goes up. As the device approaches the dry-out

power, the frequency goes down again (reduced velocity), resulting in a delay between liquid slugs. Such a delay will result in the evaporation of the thin liquid film at the evaporator and is a precursor to complete dry-out.

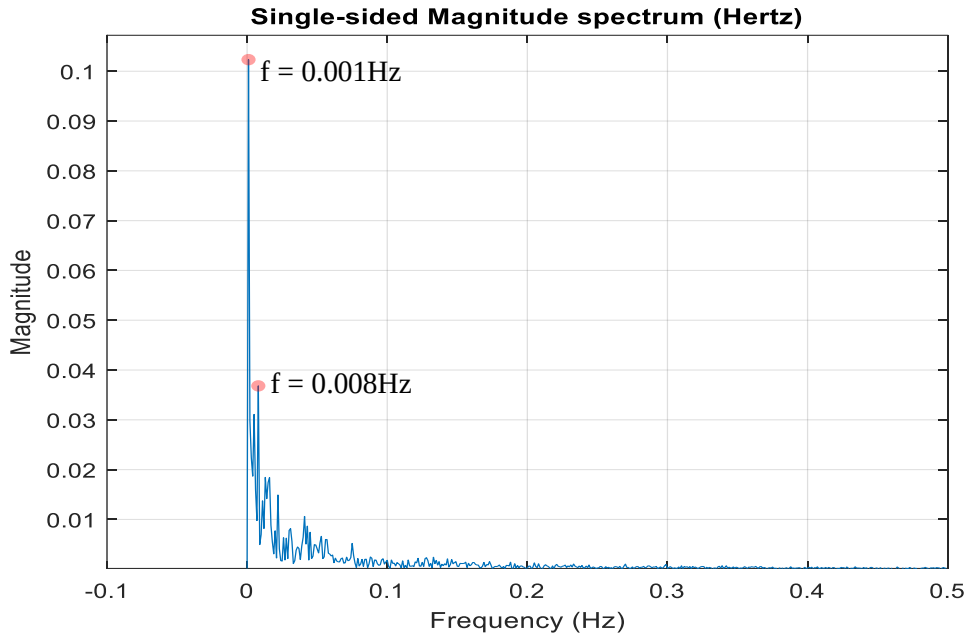

(a) 0W

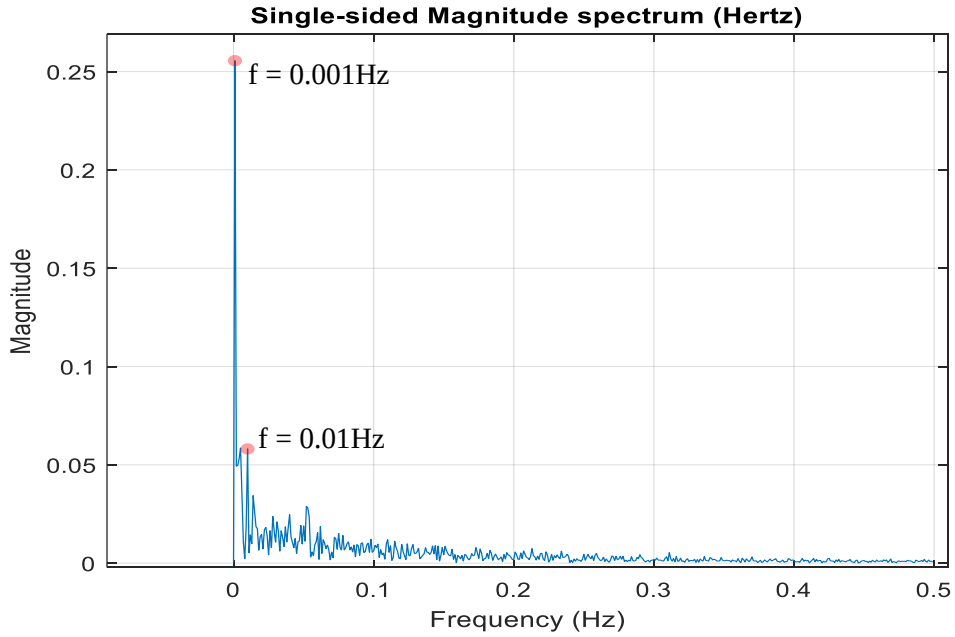

(b) 3W

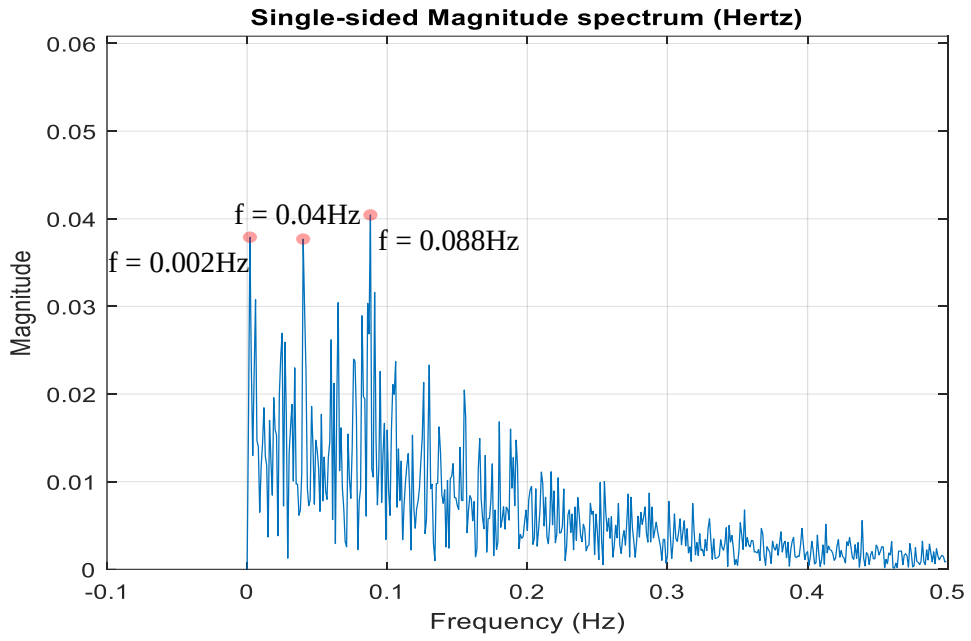
Single-sided Magnitude spectrum (Hertz)
Magnitude
Frequency (Hz)
f = 0.002Hz
f = 0.04Hz
f = 0.088Hz
0.06
0.05
0.04
0.03
0.02
0.01
0
-0.1
0
0.1
0.2
0.3
0.4
0.5

(c) 6W

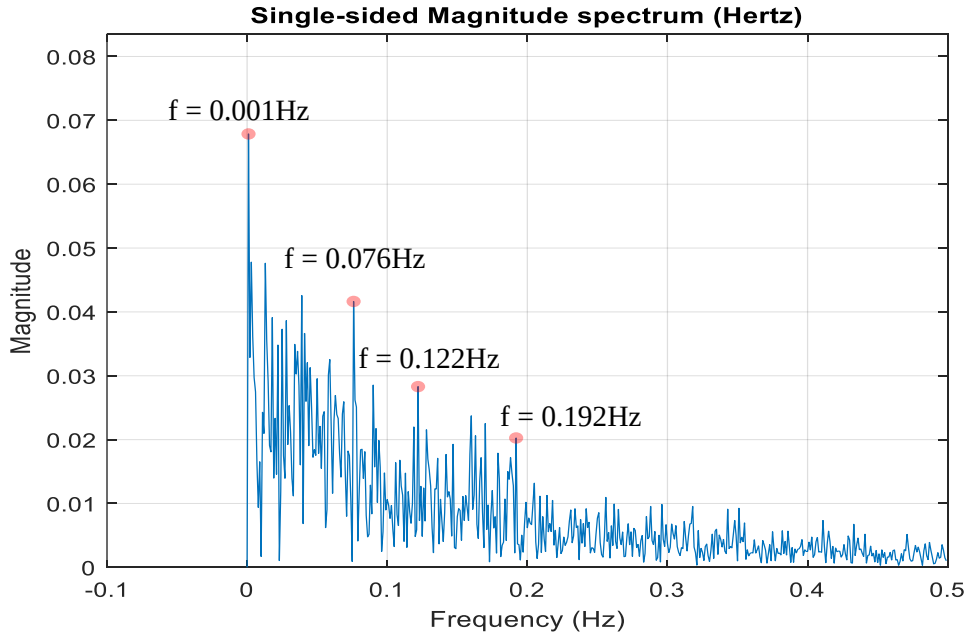
Single-sided Magnitude spectrum (Hertz)
Magnitude
Frequency (Hz)
f = 0.001Hz
f = 0.076Hz
f = 0.122Hz
f = 0.192Hz
0.08
0.07
0.06
0.05
0.04
0.03
0.02
0.01
0
-0.1
0
0.1
0.2
0.3
0.4
0.5

(d) 8W

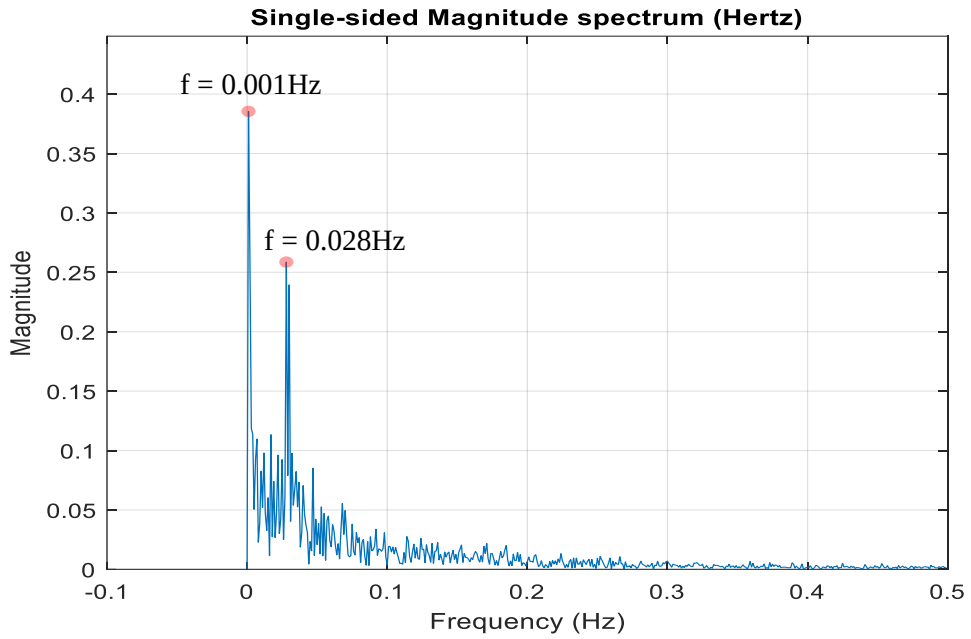

(e) 9W

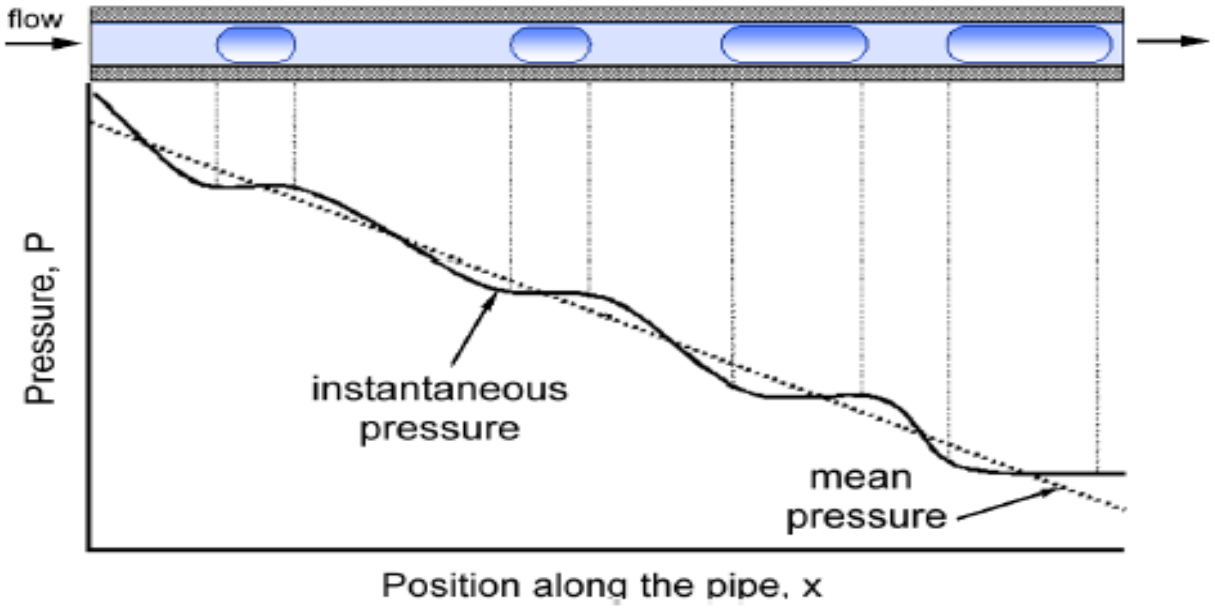

(f)

Fig 6-XII (a-e). Frequency plots of pressure oscillation at FR = 30% and T_c = 92K (f) Pressure drop profile in slug flow (Khandlikar – Thesis pg. 69)

Fig 6-XII (a-e) show the normalized frequency plot of Fig 6-XIb. At 0W, a low base frequency is established. This movement of liquid slug is induced due to non-equilibrium temperature difference between the condenser and evaporator. As heat is added, higher frequencies as well as more frequencies with similar magnitudes begin to emerge, as fluid velocity increases. At 8W, multiple frequency peaks are evident, with a low frequency of 0.001Hz and a high frequency of 0.19Hz. At 9W, which was the load before dry-out, the frequency goes back down, with dominant frequencies of 0.001Hz and 0.028Hz. It is worth noting that one of the frequencies at dry-out is higher than the base frequency at zero load. This means that the fluid, though slowed, still oscillates faster than at zero load. The magnitude of the oscillation could be an indication of the size of the liquid slug since the magnitude is a representation of the instantaneous pressure rise/fall from the mean, of that frequency. The pressure gradient occurs across a slug (Fig 6-XIIf). For this case, there are mainly smaller liquid slugs as heat is increased (i.e., magnitude goes down), up until dry-out, where annular flow is dominant, and the magnitude goes back up. The data sampled for the FFT (Fast Fourier Transform) was 1000 samples with a sampling frequency of 1Hz.

6.3 Summary (Performance Maps)

Below are 3D plots of the Argon PHP showing the relationship between effective thermal conductivity, condenser temperature and heat load. The effective conductivity data is fitted with the highest order polynomial fit that does not result in unphysical behavior or does not produce multiple minimums or maximums. The effective conductivity is forced to zero at critical heat power. The z-axis (red) legend represents the effective conductivity K_{eff} in units of $\frac{W}{m-K}$, the x-axis (blue) is the condenser temperature T_{cond} in units of K and the y-axis (green) represents the heat load, P in units of W.

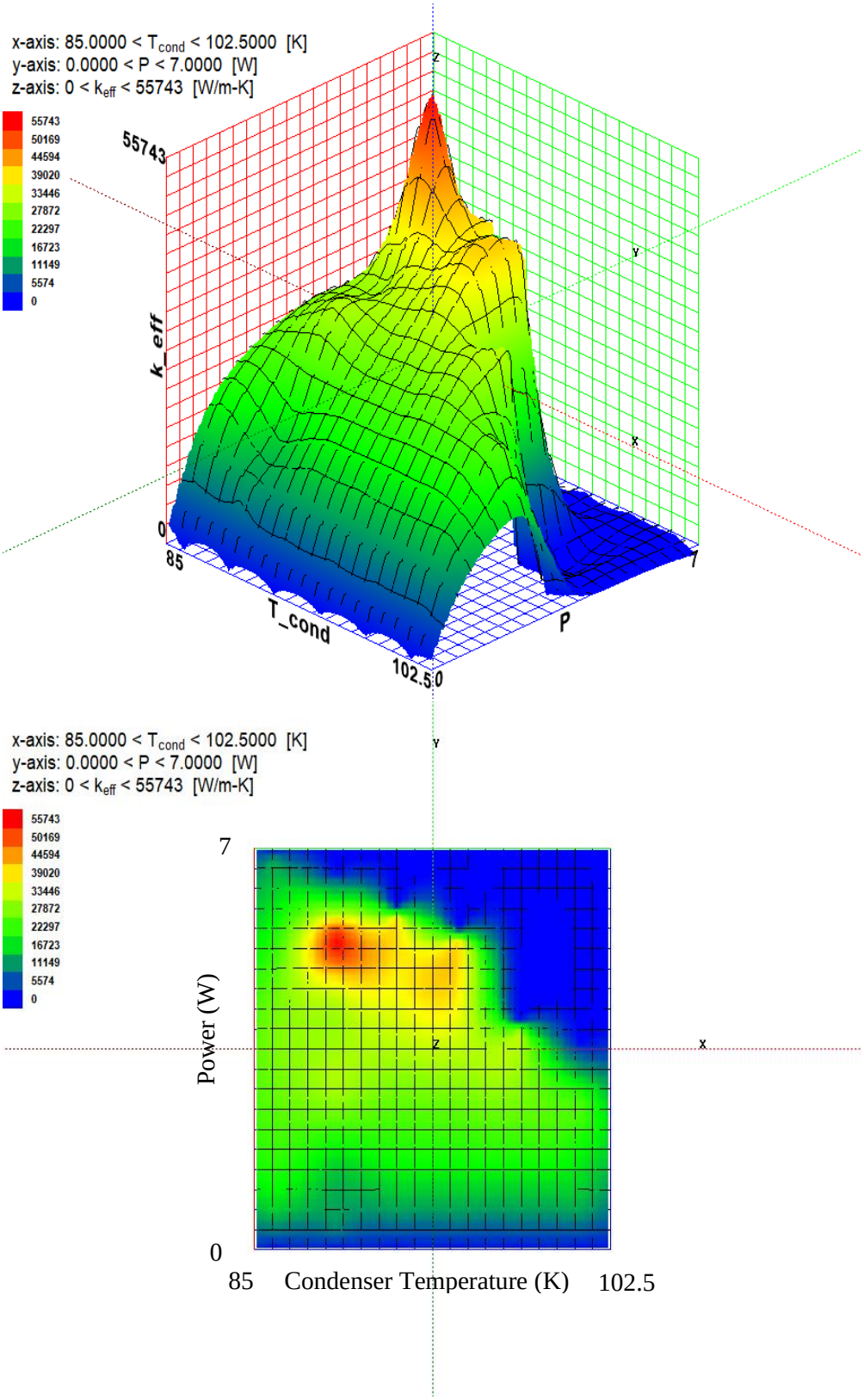
x-axis: 85.0000 < T_cond < 102.5000 [K]
y-axis: 0.0000 < P < 7.0000 [W]
z-axis: 0 < k_eff < 55743 [W/m-K]
55743
50169
44594
39020
33446
27872
22297
16723
11149
5574
0
k_eff
55743
0
85
T_cond
102.5
P
7
z
y
x
x-axis: 85.0000 < T_cond < 102.5000 [K]
y-axis: 0.0000 < P < 7.0000 [W]
z-axis: 0 < k_eff < 55743 [W/m-K]
55743
50169
44594
39020
33446
27872
22297
16723
11149
5574
0
7
Power (W)
0
85
Condenser Temperature (K)
102.5
z
x
y

(a)

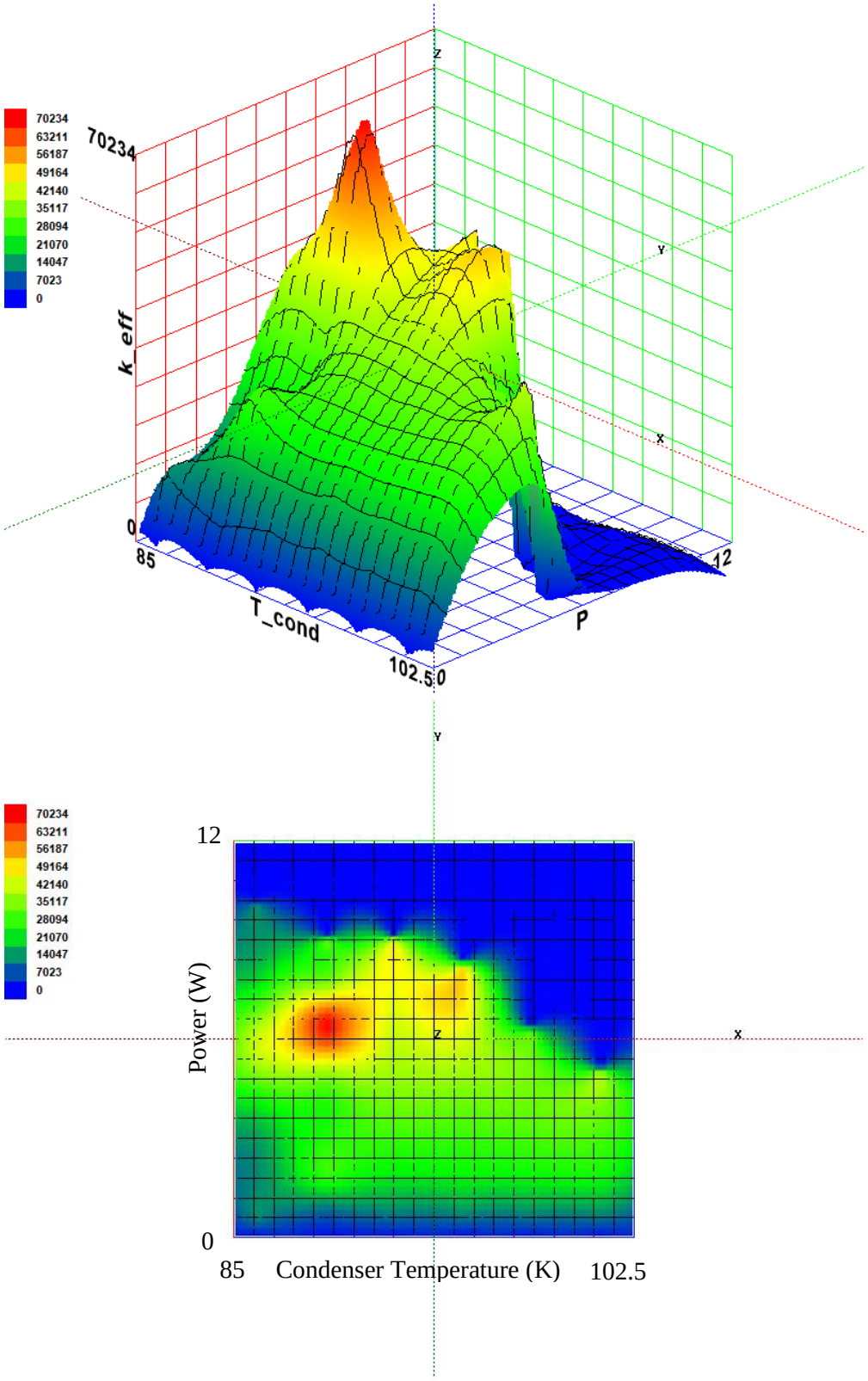

(b)

Fig 6-XIII. (a) FR 20%, (b) FR 30%

The Argon performance maps show a much smaller optimization area or region as opposed to the much wider optimization area of the Nitrogen PHPs. This means that perturbation from an optimized operating point in an Argon PHP could have more significant consequence in terms of performance drop than in the Nitrogen PHP. The Argon maps also do not show an increase in optimization area spread as fill ratio goes up unlike in the Nitrogen PHP, however the optimal area does move away from the dry-out zones (blue area). Therefore, though an optimized area may take a hit in performance, it is less likely to dry-out.

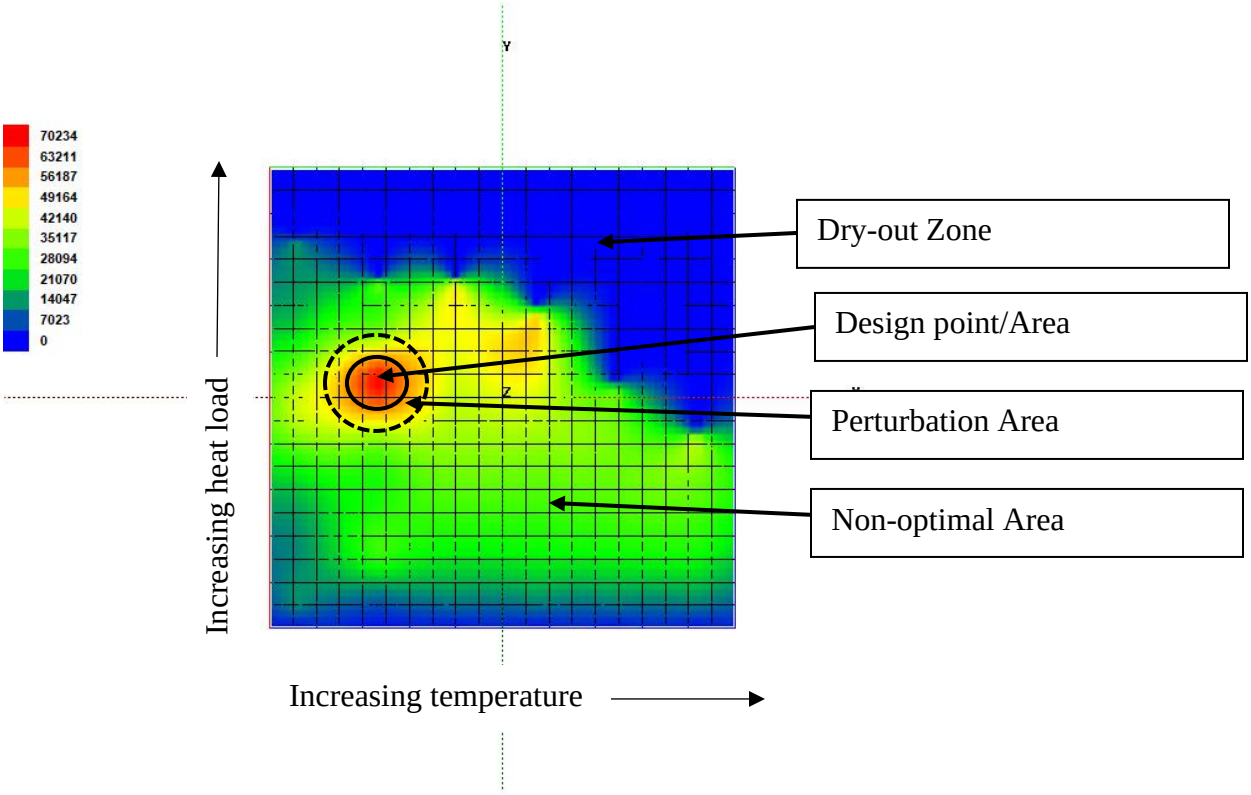

(a)

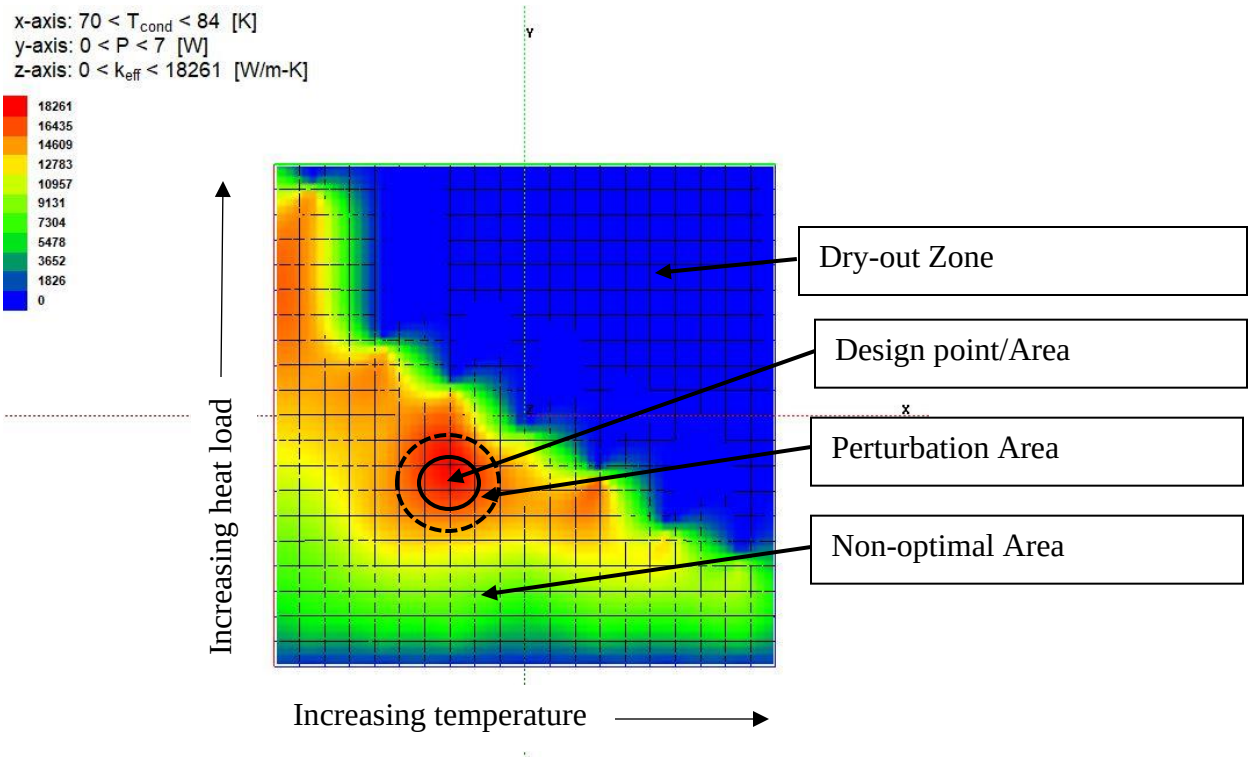

(b)

Fig 65b. Example of performance maps showing certain key areas during possible design analysis for (a) An Argon PHP (b) A Nitrogen PHP

7 Mixtures in PHPs

7.1 Background

7.1.1 Introduction to Two-Phase Mixtures

Mixtures are a combination of two or more chemical substances that do not react with one another. A two-phase mixture requires that each component of the mixture would have a liquid phase as well as a vapor phase at equilibrium. To determine the number of intensive properties needed to specify a state of a mixture, we can use the Phase Rule proposed by Gibbs:

$$F = C - \Pi + 2 \tag{7.1}$$

where F is the number of intensive properties needed to fix the state, Π is the number of phases present e.g., solid, liquid or gas, and C is the number of different chemical components in the system. For the single component fluid such as Nitrogen and Argon, the number of intensive properties needed to fix the two-phase state at equilibrium conditions is 1. The pressure or the temperature can be used as the intensive property. Along with the mass quality of the system, other properties of that state can be obtained. For a two-phase mixture, the number of intensive properties needed to fix the state is 2. Along with the temperature, the pressure in that state must be known. Then along with the molar composition of the mixture, all other properties of that state can be determined.

7.1.2 Criterion for Mixture Phase Equilibrium

At equilibrium, the chemical potential of each component of the mixture must be same in all their respective phases in the system. Since the chemical potential difference is the driving force for mass transfer from one phase to another, this ensures that mass is conserved at equilibrium. Mathematically putting,

$$\mu_{f,i} = \mu_{g,i} \quad i = 1, C \tag{7.2}$$

where $\mu_{f,i}$ is the chemical potential of species *i* in the liquid phase and $\mu_{g,i}$ is the chemical potential of species *i* in the gas phase. For an ideal solution, this conservation of chemical potential can be written as:

$$\mu_i^o + R_{univ}T \ln\left(\frac{x_i f_{sat,i}}{P_0}\right) = \mu_i^o + R_{univ}T \ln\left(\frac{y_i f_i}{P_0}\right) \quad i = 1, C \tag{7.3}$$

The only difference between the left-hand side of the equality sign and the right-hand side of the equality sign is the numerator inside both natural log brackets, therefore equation 7.3 can be reduced to:

$$x_i f_{sat,i} = y_i f_i \qquad i = 1, C \tag{7.4}$$

For a mixture where the gas phase can be modelled as an ideal gas mixture, equation 7.4 can be written as:

$$x_i P_{sat,i} = y_i P \qquad i = 1, C \tag{7.5}$$

The equation above is known as Raoult's Law.

7.2 Air as a working fluid

7.2.1. Properties of Air as a real fluid

Air is a mixture that occurs naturally in the environment. Although it is made up of multiple pure fluids, its main components are Nitrogen and Oxygen. Dry air by volume consists of approximately

79% Nitrogen and 21% Oxygen. Air has a triple point of 59.75K and a critical point of 132.63K [38]. In contrast, Nitrogen has a triple point of 63.18K and a critical point of 126.2K while Oxygen has a triple point of 54.34K and a critical point of 154.6K. To define properties of an ideal mixture such as a two-phase air mixture, two intensive properties must be specified. In addition, the molar composition of each species in the mixture must me known. Consider Air with the natural composition of 79% Nitrogen and 21% Oxygen, using Raoult's law, we can make a bubble/dew point plot of this zeotropic mixture. Fig 7-I was made using the following code below in Engineering Equation Solver (EES) for a pressure of 14.7psi

```
$UnitSystem SI J K Pa Mass Rad

P = 14.7[psi]*convert(psi,Pa)                "working pressure"
C = 2                                        "number of species in mixture"
F$[1..C] = ['Nitrogen','Oxygen']             "component of air mixture"

$ifnot parametrictable
   y[1] = 0.79[-]                            "gas mole fraction of nitrogen in dry air"
$endif
y[1] + y[2] = 1                              "gas mole fraction of the components must sum to unity"
x[1] + x[2] = 1                              "liquid mole fraction of the components must sum to unity"

Duplicate i = 1,C
   P_sat[i] = p_sat(F$[i],T=T)               "saturation pressure of each component"
   x[i]*P_sat[i] = y[i]*P                    "Raoult's law"
End
```

The vapor mole fraction of one of the species, say Nitrogen can then be varied from 0 to 1 and a plot made to show how temperature at a given pressure can change the composition of the two species. Fig 7-I is known as a boiling curve diagram and shows the typical vapor glide that occurs in mixtures

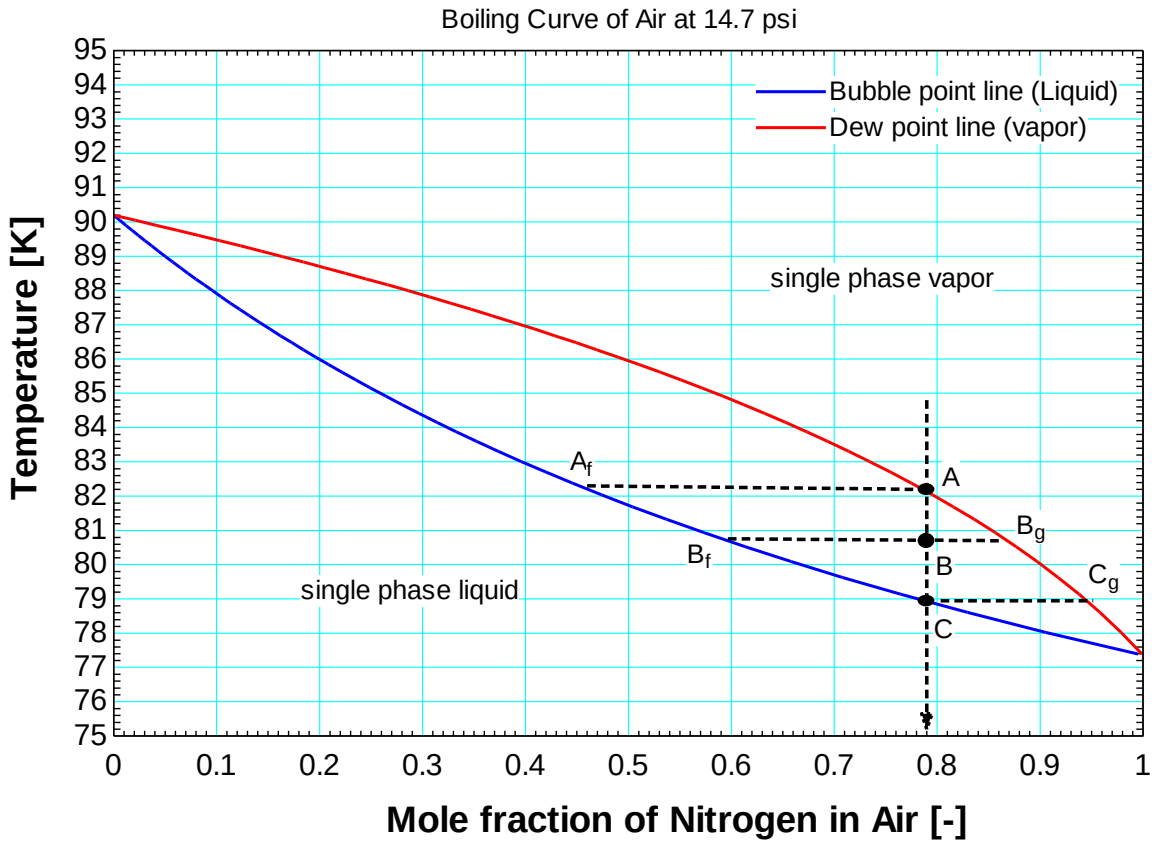

Fig 7-I. Boiling curve for Air at 1 atm

From Fig 7-I, we can see that Air mixture will be all single-phase vapor above 90K (which corresponds to the boiling point of oxygen at standard atmospheric pressure) and all liquid at 77K (which corresponds to the boiling point of Nitrogen at standard atmospheric pressure). Tracing the cool down process of Air, which has a composition 79% Nitrogen in the gaseous phase in a system, we can identify various molar compositions at different states. Above approximately 82.5K, the mixture will be in the gaseous phase. At point A, the molar fraction of gaseous Nitrogen is 79% but the first liquid that condenses at point A_f has a molar composition of 46%. That means that 54% of the liquid formed at this temperature will be Oxygen. Further reducing the temperature to point B, increases the concentration of Nitrogen in both the vapor phase B_g, and liquid phase B_f, to 86% and 60% respectively. At point C, approximately 79K, the molar composition of Nitrogen in the liquid phase becomes 79% (same as the composition of Nitrogen in the vapor phase

at 82.5K). The last vapor bubble of Nitrogen at point C_g, has a molar composition of 95%. This means that at this temperature, there will be much more Nitrogen in the vapor state. Below 79K, the mixture becomes a single-phase liquid. The temperature range of 79K to 82.5K, represents the vapor glide of the Air mixture at standard atmospheric pressure.

7.2.2. Air as an ideal solution in a system with non-uniform temperatures

The PHP is a closed device that operates using a two-phase fluid with the action of evaporation and condensation. Therefore, there are temperature gradients in the PHP. The evaporator operates at much different temperature than the condenser, even if we assume the equilibrium pressure to be constant. This means that the state, and hence the molar composition at the condenser will be different from the state and molar composition of the mixture at the evaporator. Consider Fig 7-II which shows the boiling curve of Air at 1atm.

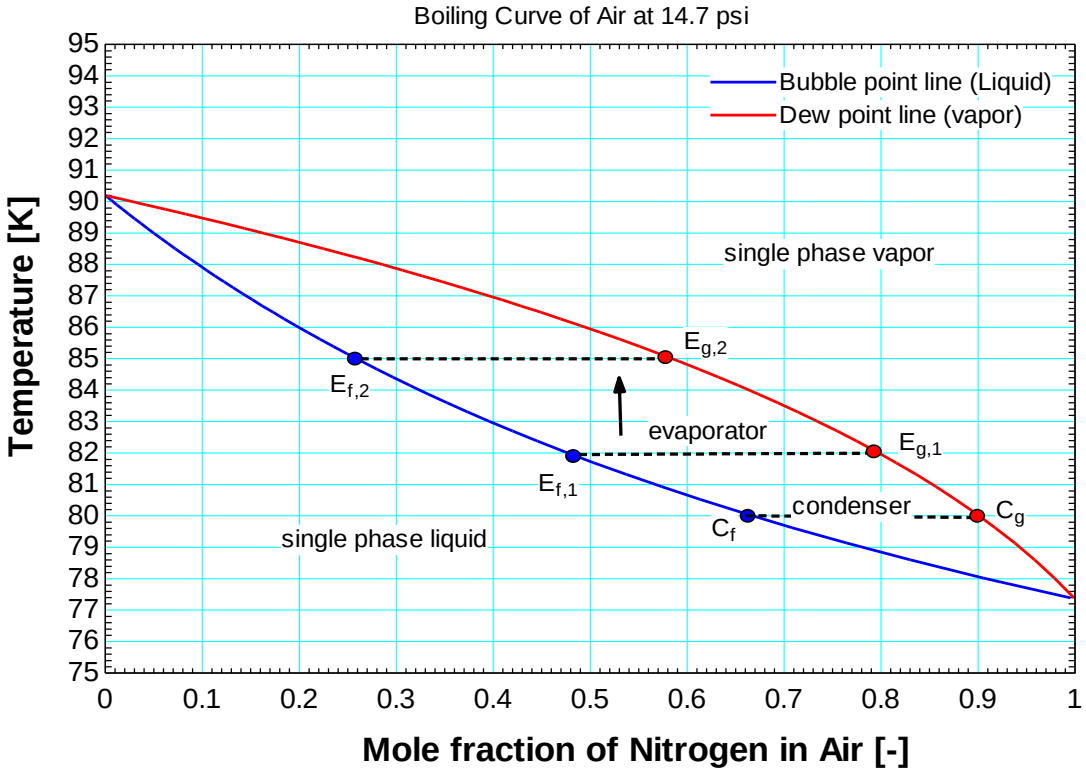

Fig 7-II. Boiling curve for Air at 1 atm during heating process

The condenser temperature is always maintained by the temperature controller. Assuming a condenser temperature of 80K is maintained with a constant pressure of 1atm, the molar composition in the condenser will always be 66% Nitrogen in the liquid phase and 90% Nitrogen in the vapor phase. Therefore, the condenser will be mostly filled with Nitrogen. Now consider the evaporator being heated from a temperature of 82K (E_1) to 85K (E_2). The Mole fraction of liquid Nitrogen reduces from 48% to 26%. Therefore, the evaporator will be filled with mostly liquid oxygen. PHPs are also designed to create flow boiling with distinct slug and plug flows. This means that vapor plugs will condense at the condenser and liquid slugs will evaporate at the evaporator. As the evaporator temperature goes up, there is less Nitrogen vapor in that region meaning that more oxygen vapor will make it to the condenser. However, the state at the condenser allows for more Oxygen in the liquid state. Since oxygen is likely to condense first, it will contribute more latent heat than sensible heat at the condenser. The same is true for the liquid slugs. There is also the fact that the pressure at high fill ratio goes up as heat is added to the system, which shifts the boiling curve upwards. Therefore, the molar composition will always be changing and will be hard to predict in this situation.

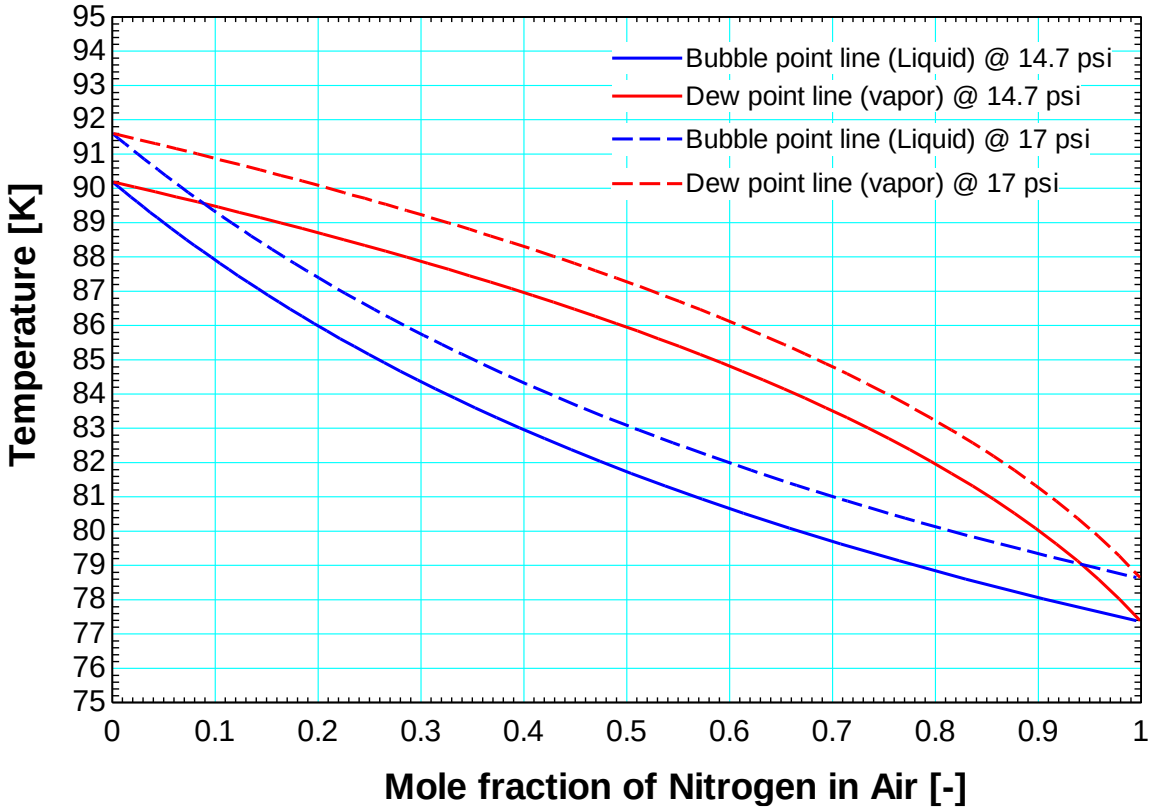

Fig 7-III. Boiling curve for Air at two different pressures

7.2.3 Initial Liquid Fill Ratio for Mixtures

Equation 5.3 is used to calculate the initial fill ratio of a mixture. The equilibrium molar quality for a given temperature and pressure is related to the molar fraction by:

$$z_i = x_i(1 - Q) + y_i Q \qquad i = 1, C \tag{7.6}$$

were x_i is the molar fraction of species *i* in the liquid phase, y_i is the molar fraction of species *i* in the gas phase, z_i is the molar fraction of species *i*, and Q is the molar quality. The molar fraction is defined as:

$$z_i = \frac{n_i}{n} \qquad i = 1, C \tag{7.7}$$

were n_i is the number of moles of species *i*, and n is the total number of moles in the system.

For Air as a real fluid, EES has a function which uses a standard Air table formulated by Eric W. Lemmon et al [44]. Given the specific volume of the system and the temperature of the condenser, the quality of the system can be calculated. i.e., Equation 5.1 to 5.4 do not have to be changed for standard Air composition.

7.3 Experimental results for Air PHP

7.3.1 Effective conductivities versus condenser temperature

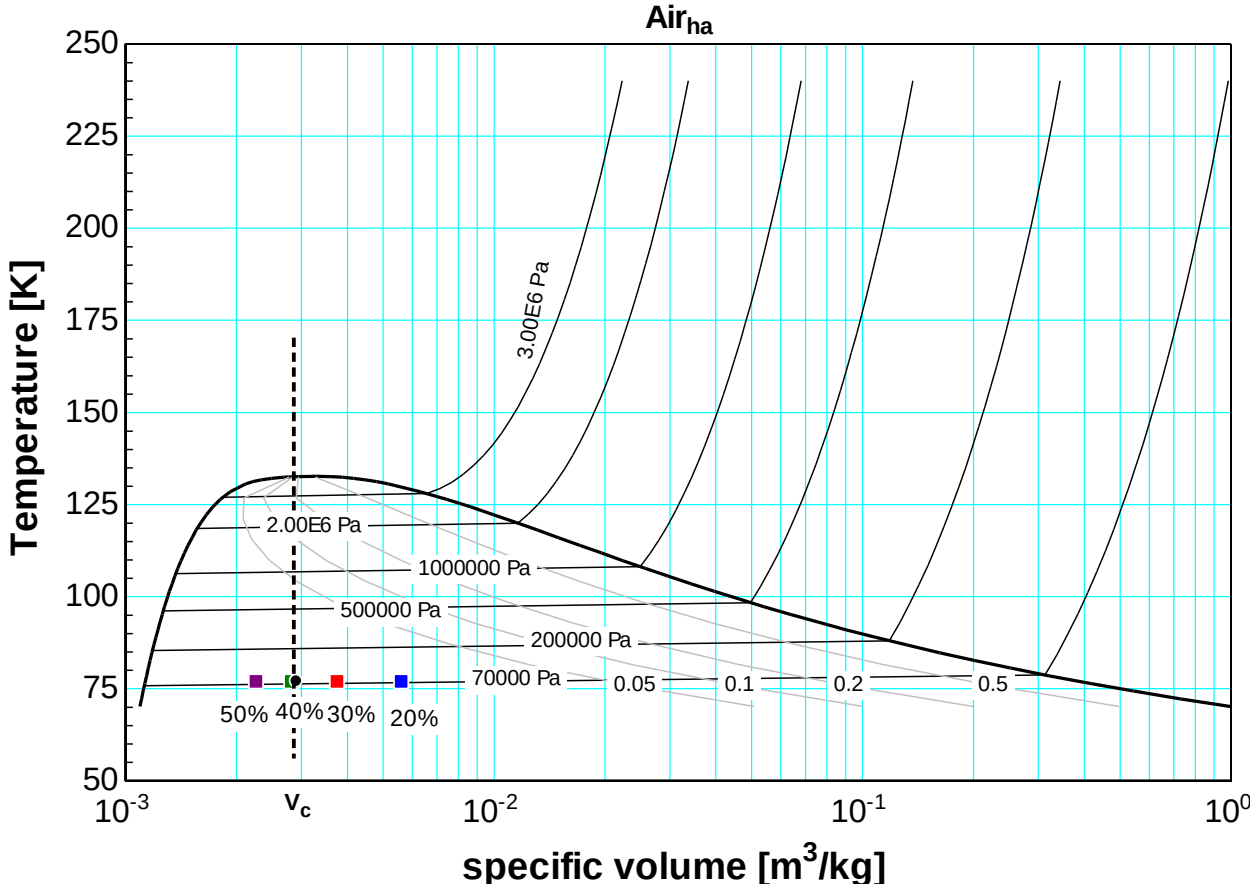

Fig 7-IV. T-v diagram for Air

Three low fill ratio runs were completed for the case of Air: 20%, 30% and 40%. These fill ratios have specific volumes to the right of the critical specific volume, V_c. One run with a high fill ratio

of 50% was also completed. These initial fill ratios were calculated at a steady state equilibrium temperature of 77K. The range of condenser temperature runs was from 63K to 86K. The results of the effective thermal conductivity as a function of head load for the various condenser temperatures at those fill ratios, are shown in Fig 7-V.

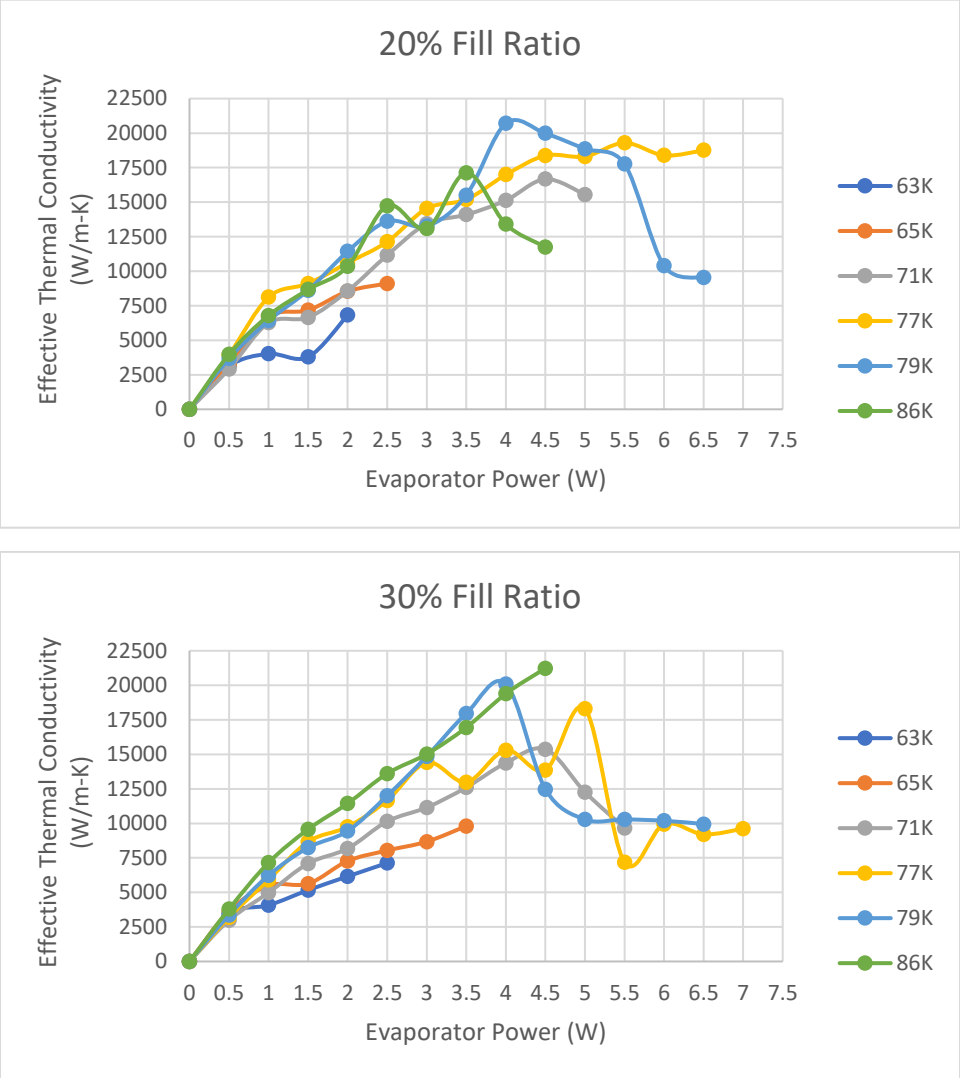

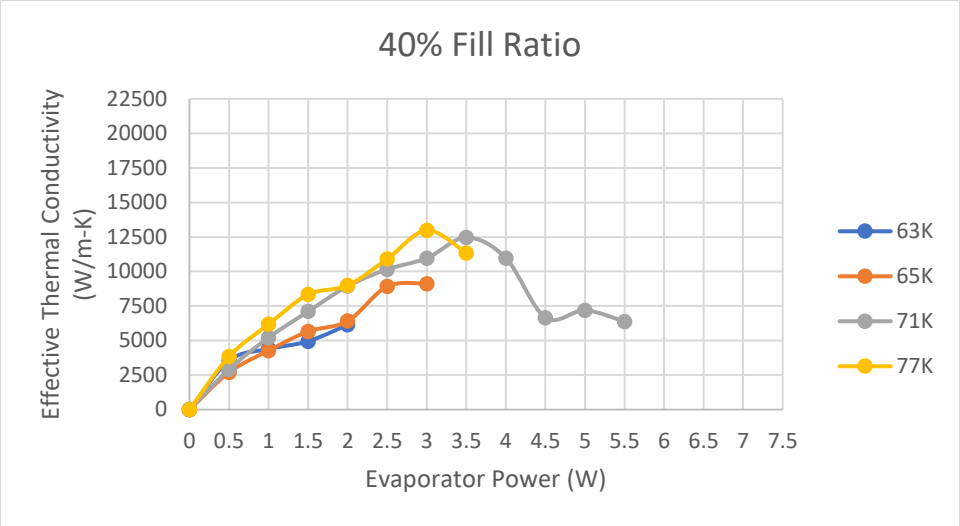

Fig 7-V. Effective thermal conductivity versus heat load for different condenser temperatures

At 40% Fill Ratio, condenser temperatures for 79K and 86K could not be recorded due to power outage in the lab that caused the pressure relief valve in the PHP to open.

The behavior of the effective thermal conductivity as a function of heat load is the same for the Air mixture as it is for the pure fluid. The fluid transport is governed mostly by slug and plug flows. This is again due to the concept of the critical diameter, where the bubble expansion is limited by the walls of the tube. Regardless of the number of species in a mixture, bubbles formed during a phase change will cause this type of flow and hence any fluid in the PHP will experience thin film convection, wall evaporation and sensible heat transfer from liquid slugs. The effective conductivity of the mixture also goes down with condenser temperature at a given fill ratio and heat load. Again, this behavior should not deviate from what was observed in a single-phase fluid as the flow formed would be slug-plug flow, as limited by the critical diameter.

7.3.3 Critical diameter for Air

Recall that the critical diameter for a fluid operating in a PHP can be calculated by:

$$D_{crit} = \sqrt[2]{\frac{4\sigma}{g(\rho_l - \rho_v)}} \tag{7.8}$$

The critical diameter of standard Air over the range of operating pressures tested for the PHP is shown in Fig 71

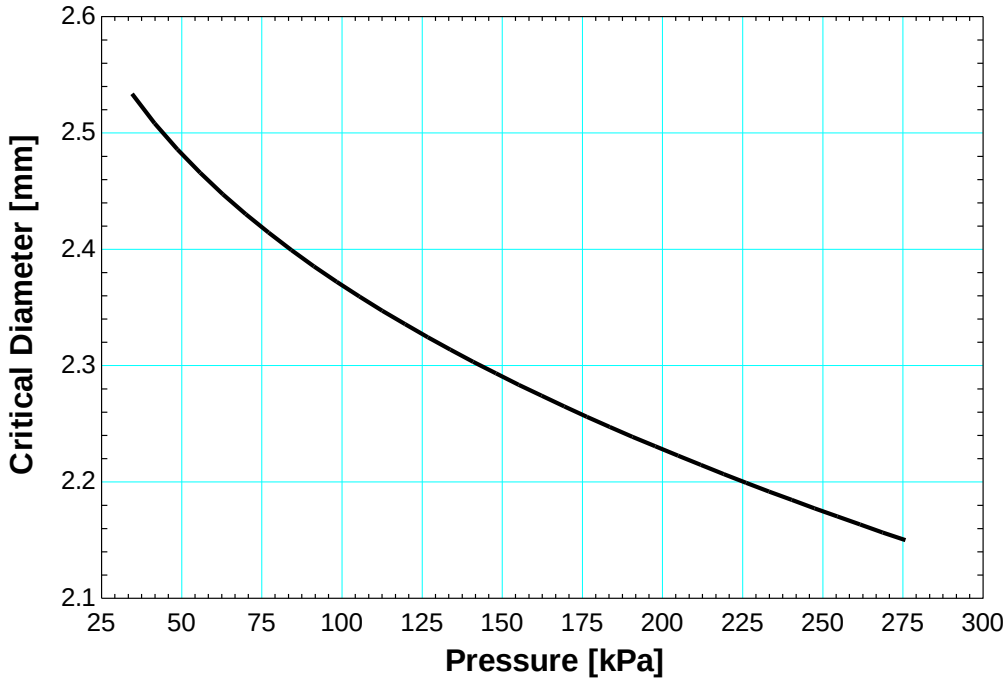

Fig 7-VI. Critical diameter for Air PHP

The critical diameter range falls above the inner diameter of the stainless tubes used in the experiment, so standard Air as a working fluid will function as a pulsating fluid in the PHP. That is, the diameter will limit the growth of nucleate bubbles and develop distinct slugs and plugs during flow boiling.

7.3.4 Boiling curves for Air

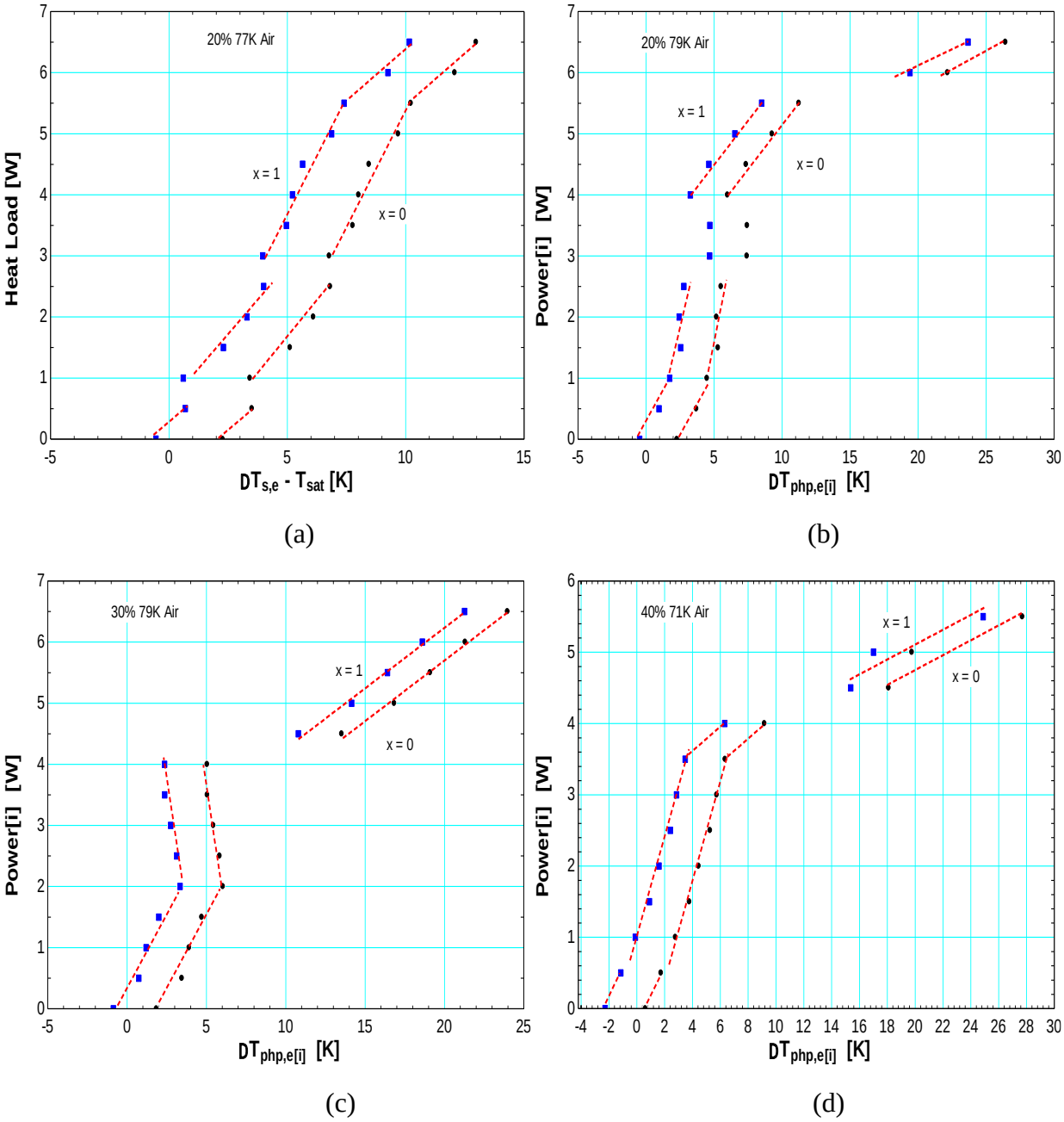

Fig 7-VII. Boiling curve for Air (a) FR 20%, T_c 77K (b) FR 20%, T_c 79K (c) FR 30%, T_c 79K(d) FR 40%, T_c 71K

The boiling curve for Air, also show distinct slope changes as you increase heat load. The actual behavior of the heat transfer coefficient will be bounded by the two lines when quality, x = 0 and x = 1. Since this is a mixture, there is no concept of a saturated temperature (unlike pure fluids)

since the temperature changes when the fluid is saturated as a liquid to when the fluid is saturated as a vapor, at any given equilibrium pressure.

7.3.5 Thermodynamic Process: Heat Addition for Air PHP

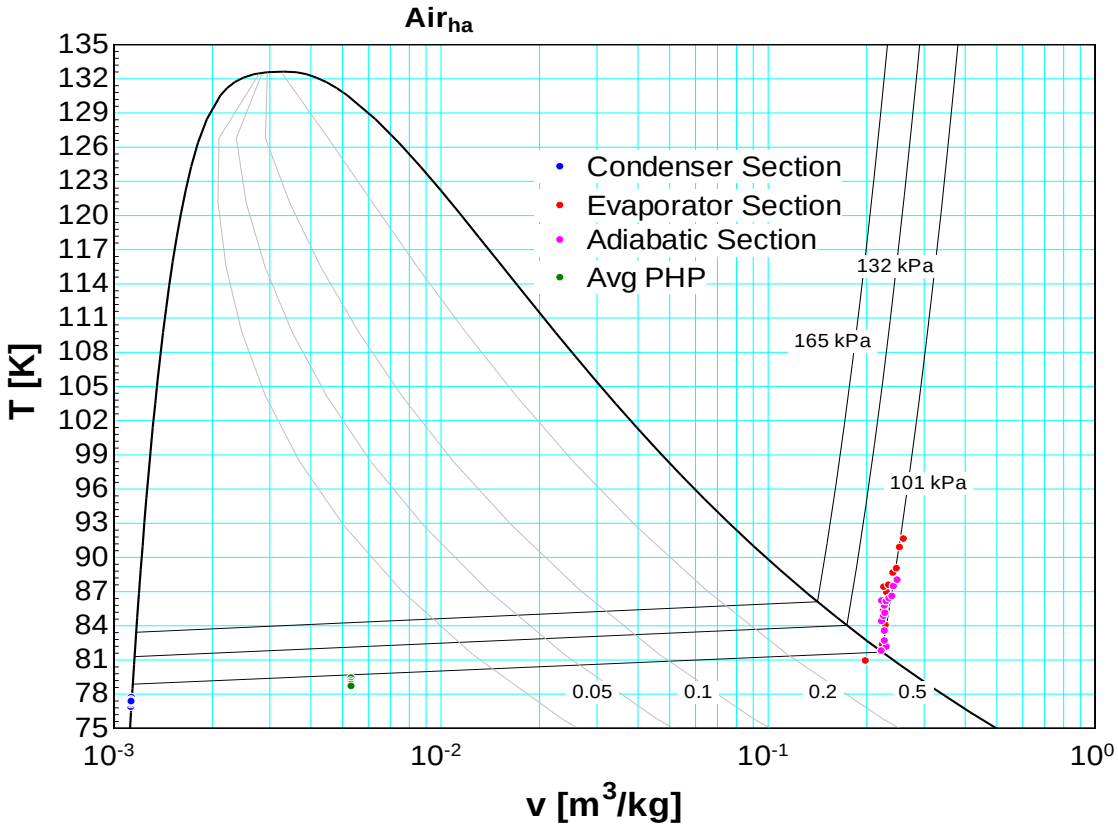

(a)

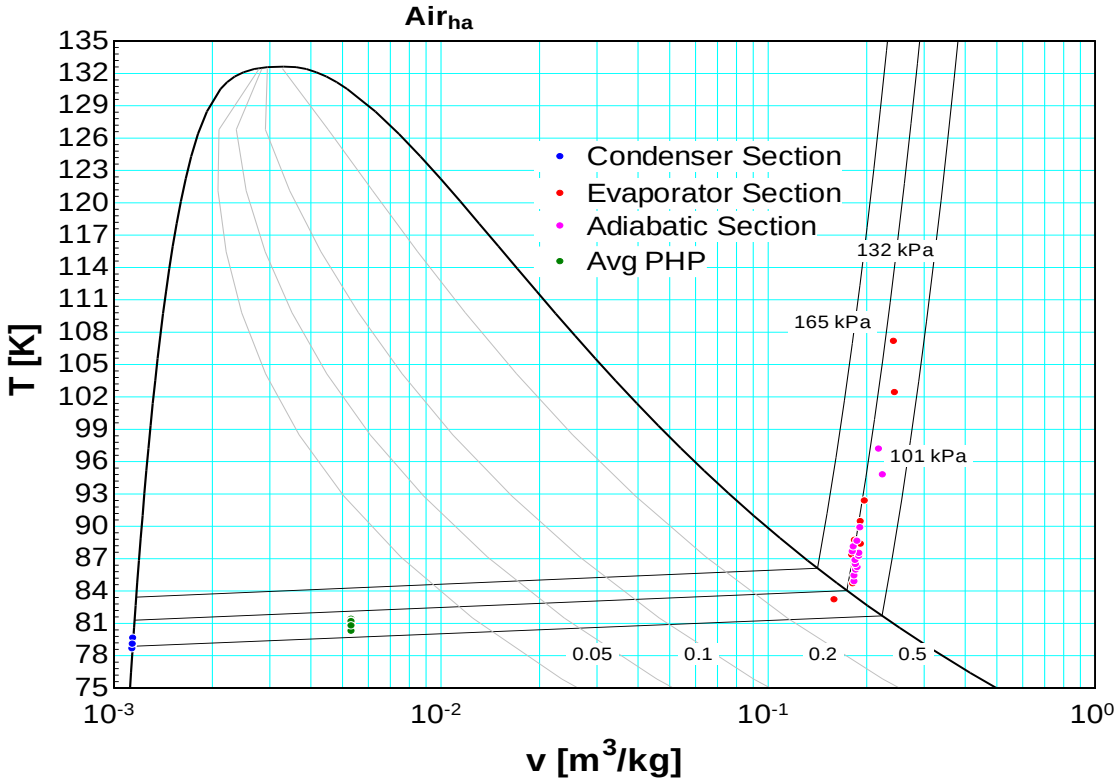
Air$_{ha}$
Condenser Section
Evaporator Section
Adiabatic Section
Avg PHP
132 kPa
165 kPa
101 kPa
0.05
0.1
0.2
0.5
T [K]
v [m^3/kg]

(b)

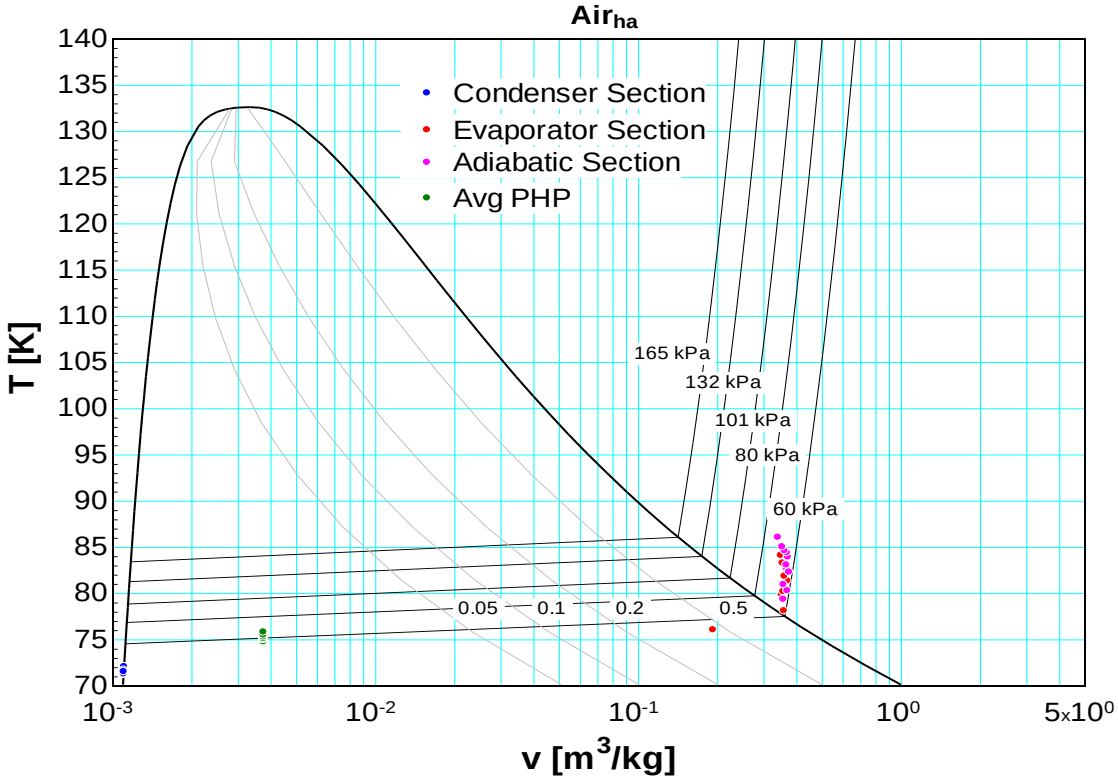
Air$_{ha}$
Condenser Section
Evaporator Section
Adiabatic Section
Avg PHP
165 kPa
132 kPa
101 kPa
80 kPa
60 kPa
0.05
0.1
0.2
0.5
T [K]
v [m^3/kg]

(c)

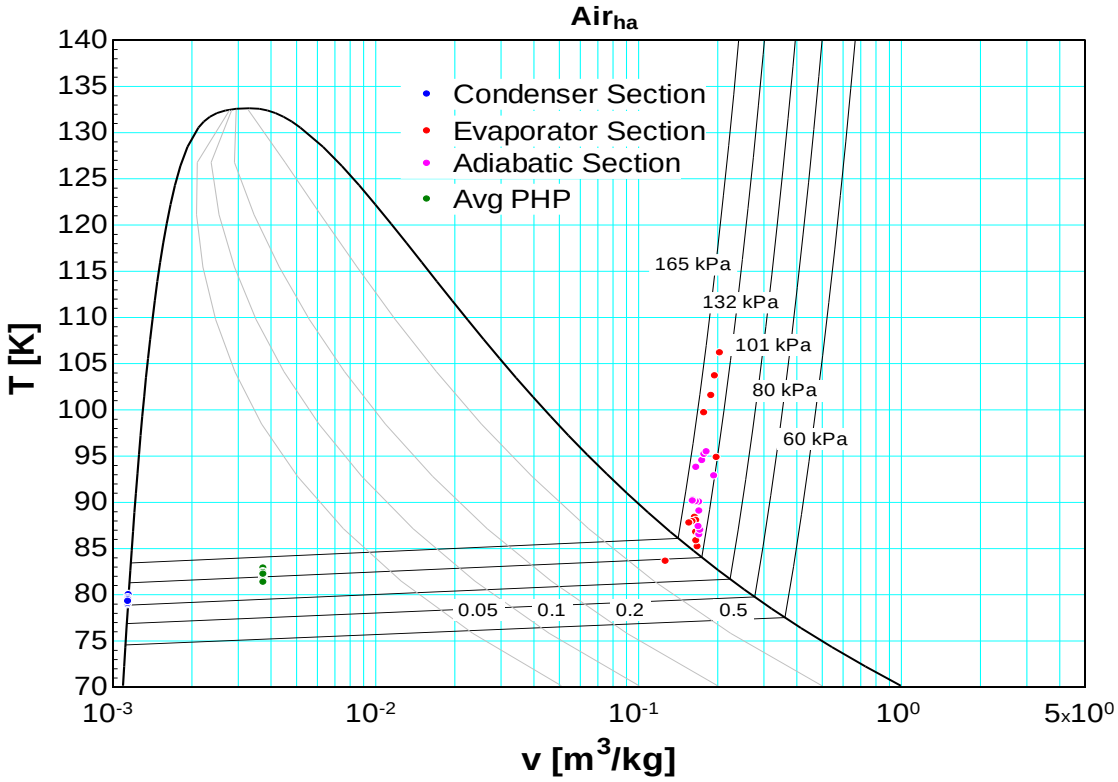
Air$_{ha}$
Condenser Section
Evaporator Section
Adiabatic Section
Avg PHP
165 kPa
132 kPa
101 kPa
80 kPa
60 kPa
0.05
0.1
0.2
0.5
T [K]
v [m^3/kg]

(d)

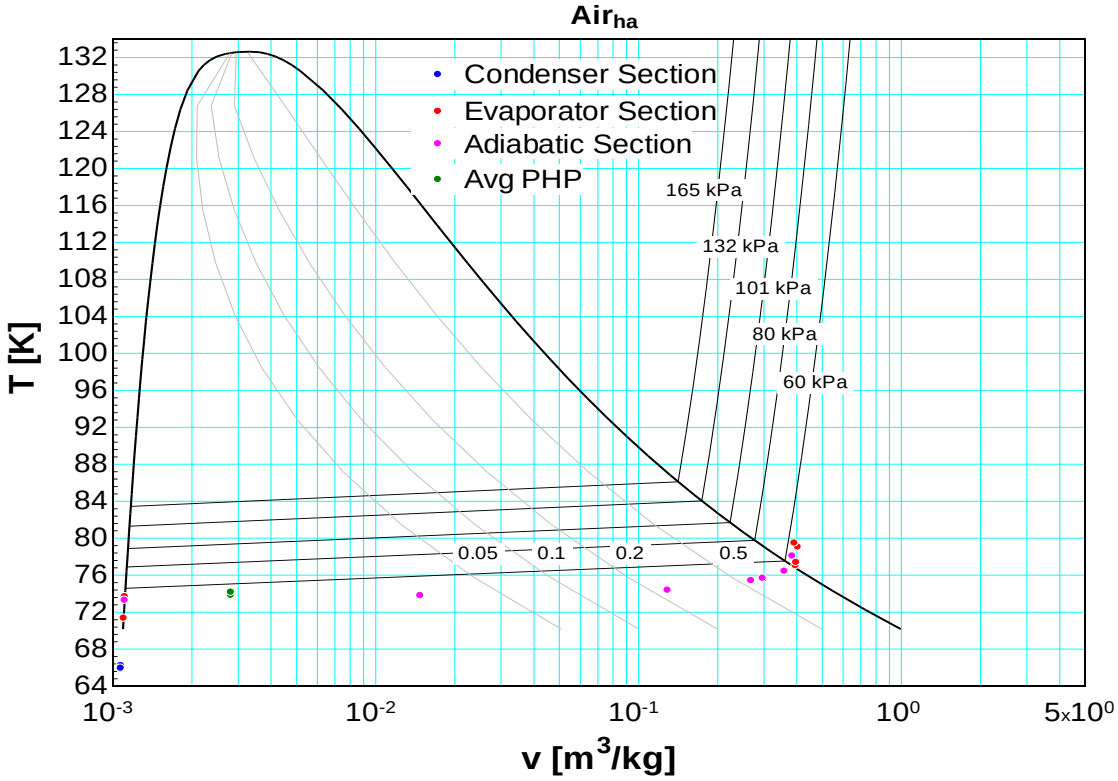
Air$_{ha}$
Condenser Section
Evaporator Section
Adiabatic Section
Avg PHP
165 kPa
132 kPa
101 kPa
80 kPa
60 kPa
0.05
0.1
0.2
0.5
T [K]
v [m^3/kg]

(e)

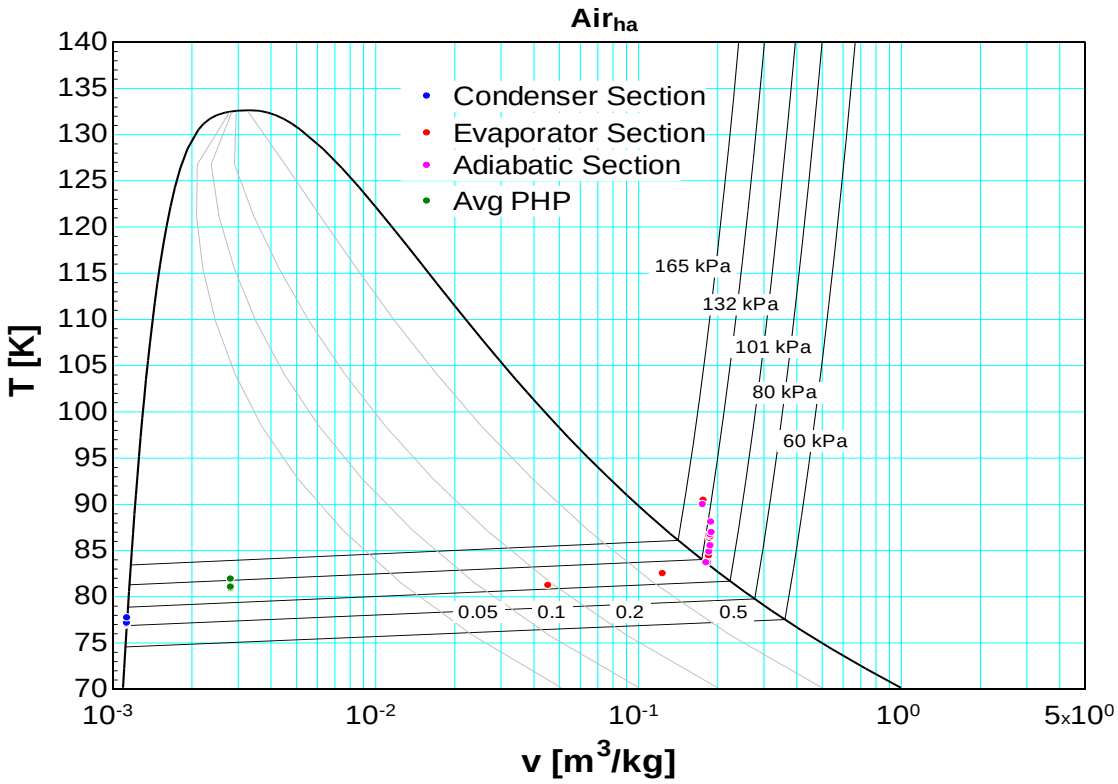

Fig 7-VIII. T-v states for (a) FR 20%, T_c 77K (b) FR 20%, T_c 79K (c) FR 30%, T_c 71K (d) FR 30%, T_c 79K (e) FR 40%, T_c 65K (f) FR 40%, T_c 77K

Fig 7-VIII show data for the thermodynamic process of the Air PHP as heat is added to the evaporator. The blue data again represents the condenser temperature which is held constant. The plots all represent initial fill ratios whose fill ratios are considered to be low fill ratios, and as such, the process follows a line of constant or near constant pressure. The state in the evaporator at no load, is mostly two-phase as different components of the mixture have a specified mole fraction of vapor and liquid. As heat is added and slug and plug flow starts to form, the evaporator becomes predominantly vapor since more single-phase vapor plugs will be found in the evaporator than liquid slugs. The density of liquid Air, $870\frac{kg}{m^3}$ is slightly higher than that of Nitrogen but lower than Argon as indicated in *section 6.2.4*, so its starting state in a two-phase region versus Argon which started in the saturated liquid state, or Nitrogen which stated in the superheated state, may

be due to density differences. The states in the PHP at the evaporator and condenser were calculated using the measured pressure of the PHP and the measured temperatures respectively. Another observation than can be seen more clearly in the mixture data is that the fluid in the evaporator experiences an increase in both quality and specific volume as it passes through the vapor dome on its way to being superheated. In addition, lower the condenser temperature, which reduces the operating pressure, leads to lower specific volume and quality in the evaporator. From Fig 7-III, we can see that decreasing the operating pressure reduces the liquid mole fraction of the less dense Nitrogen, thereby increasing the liquid mole fraction of the denser oxygen $\left(\rho = 1155\,\frac{kg}{m^3}\right)$. Oxygen also has a stronger surface tension or wettability effect than Nitrogen $\left(0.01315\,\frac{N}{m}\right)$, which would make it adhere more to the walls of the tubes.

7.3.6 Pressure responses/ Flow velocity

Fig 7-IX below shows the adiabatic section pressure oscillation of the Air PHP. As with the single component PHPs, there is an increase in the frequency and magnitude of the oscillation as heat is introduced to the evaporator. However, at dry-out, there is a reduction in both magnitude and frequency for the 20% liquid fill ratio and a reduction in only the frequency of oscillation (but not the magnitude – which increases) for 30% and 40%. This difference is due to the behavior of the fluid at dry-out, which will be discussed in a later subsection.

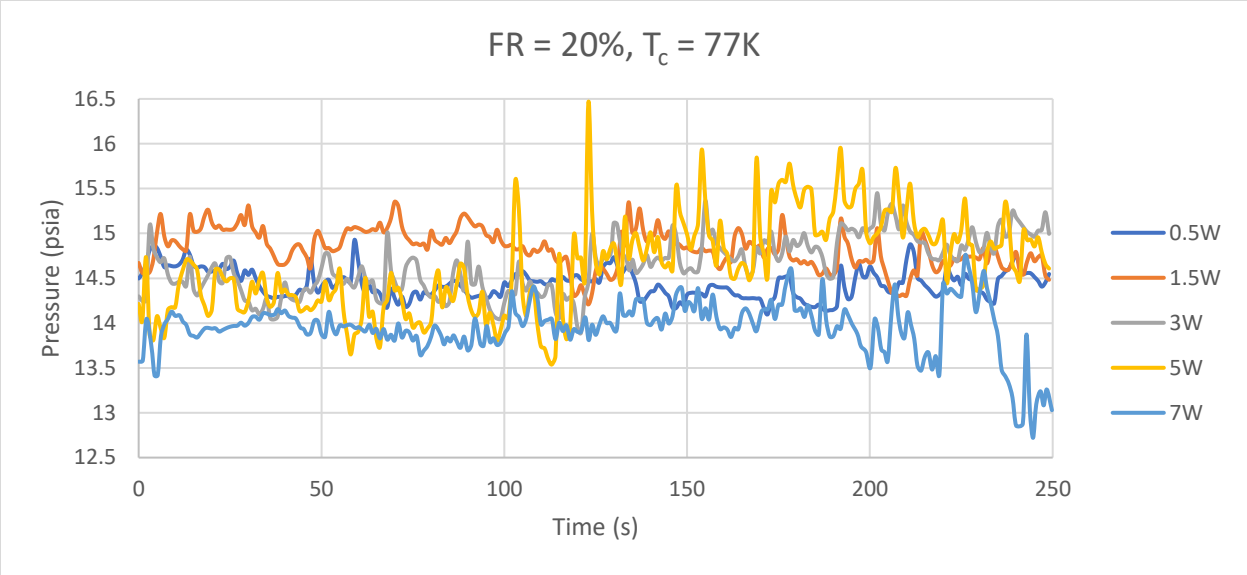
FR = 20%, T_c = 77K
Pressure (psia)
16.5
16
15.5
15
14.5
14
13.5
13
12.5
0
50
100
150
200
250
Time (s)
0.5W
1.5W
3W
5W
7W

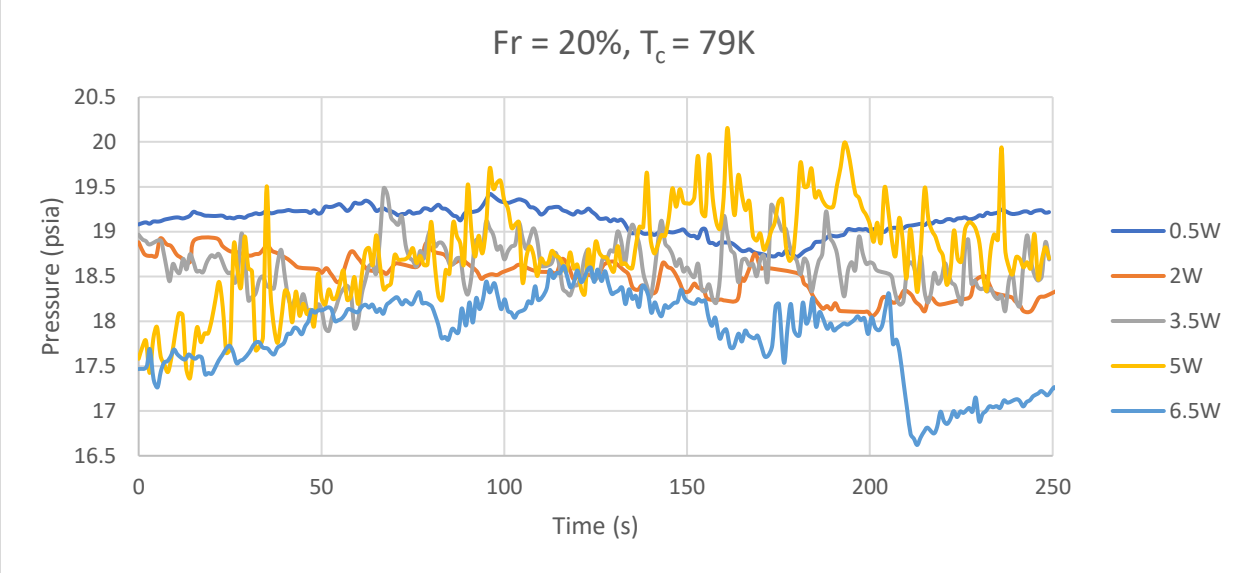
Fr = 20%, T_c = 79K
Pressure (psia)
20.5
20
19.5
19
18.5
18
17.5
17
16.5
0
50
100
150
200
250
Time (s)
0.5W
2W
3.5W
5W
6.5W

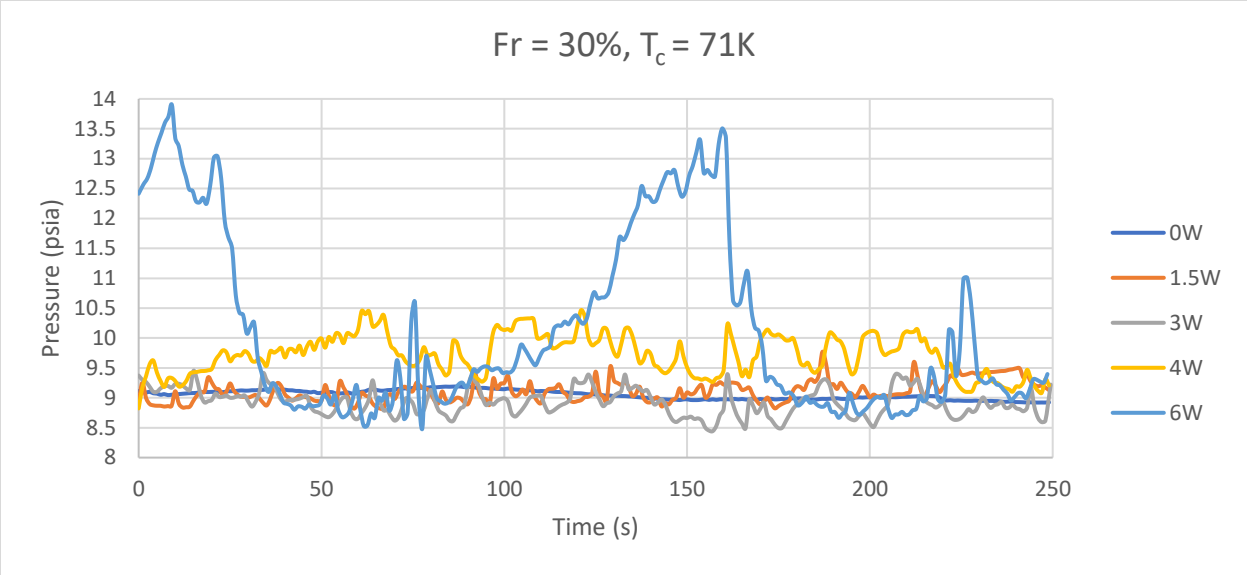
Fr = 30%, T_c = 71K
Pressure (psia)
14
13.5
13
12.5
12
11.5
11
10.5
10
9.5
9
8.5
8
0
50
100
150
200
250
Time (s)
0W
1.5W
3W
4W
6W

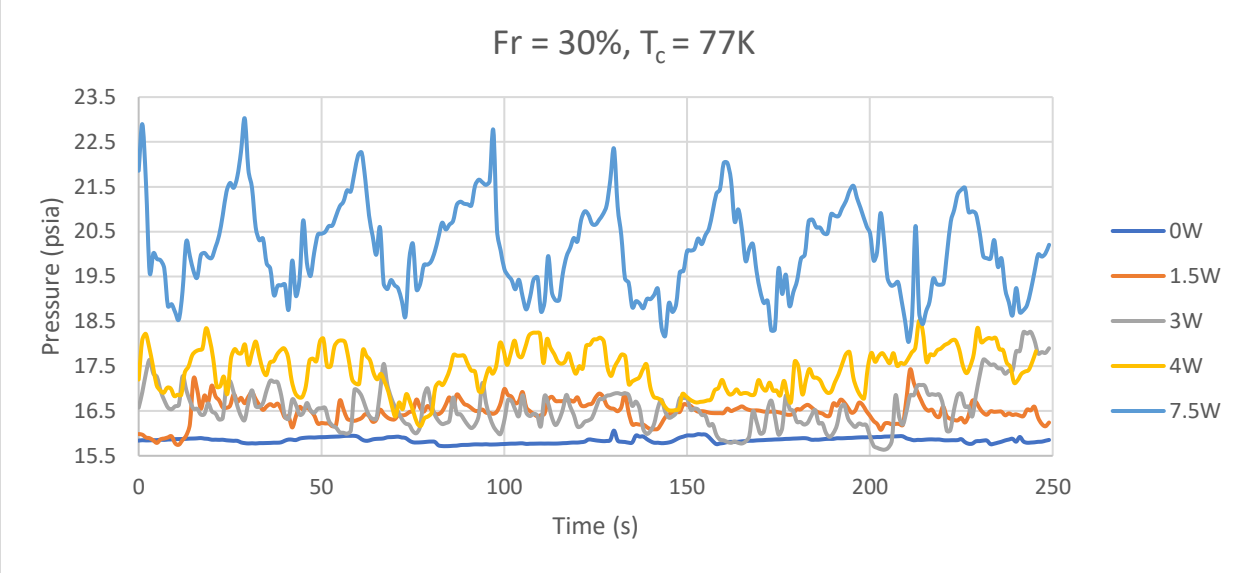
Fr = 30%, T_c = 77K
Pressure (psia)
23.5
22.5
21.5
20.5
19.5
18.5
17.5
16.5
15.5
0
50
100
150
200
250
Time (s)
0W
1.5W
3W
4W
7.5W

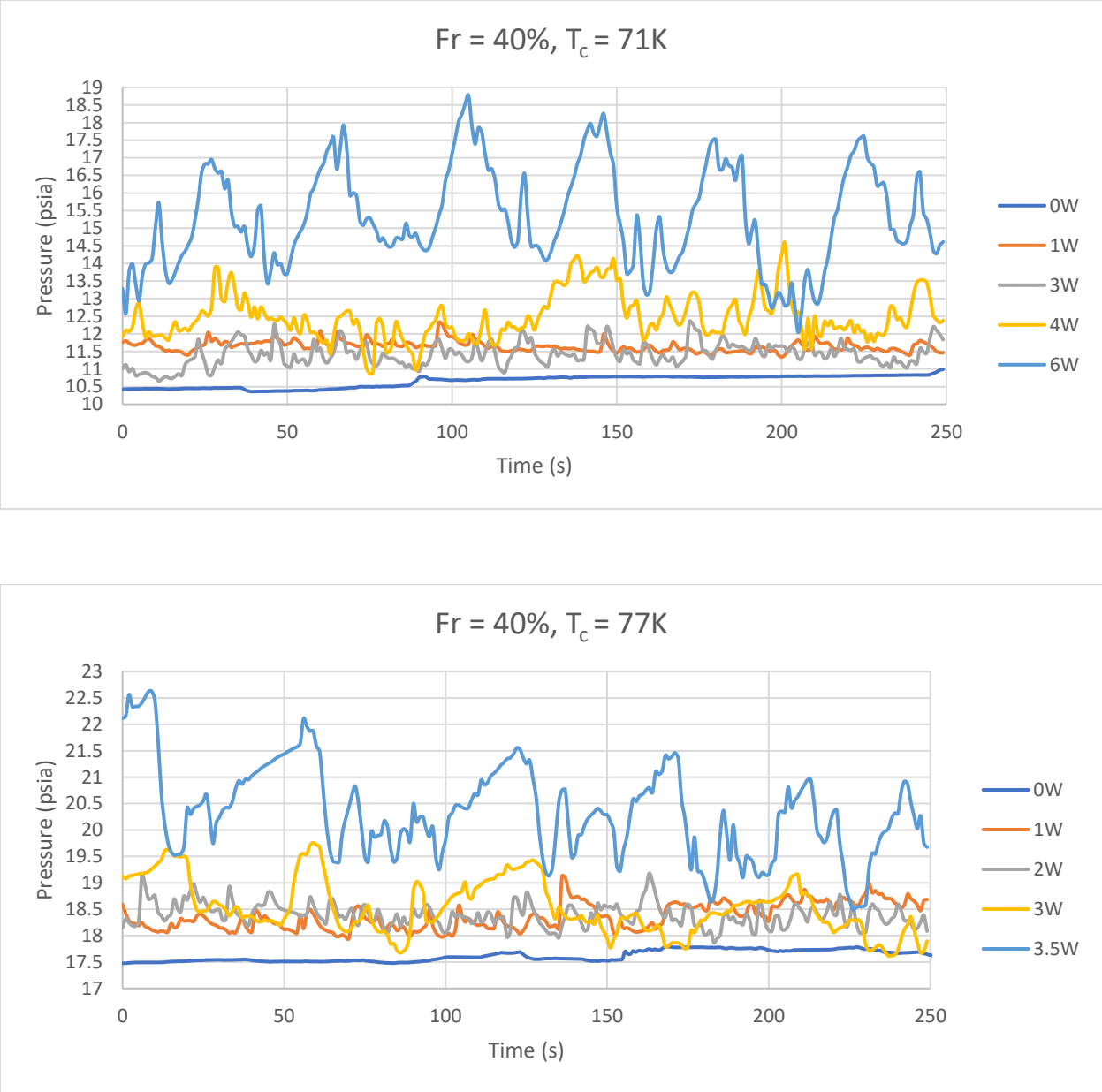

Fig 7-IX. Pressure oscillations at the adiabatic section for different Heat Loads

It might be clearer to take a closer look at the oscillation behavior in frequency plots. Fig 7-X shows the frequency plot of the Air PHP at 30% FR and 77K condenser temperature. At 0W the main frequencies lie between 0.0002Hz and 0.0024Hz. This is taken as the base frequency with little oscillation. As heat is added, the dominant frequencies increase, and more frequencies show

up on the plot. For instance, at 4W dominant frequencies with distinct peaks show up at 0.0006Hz, 0.0056Hz, 0.028Hz and 0.046Hz.

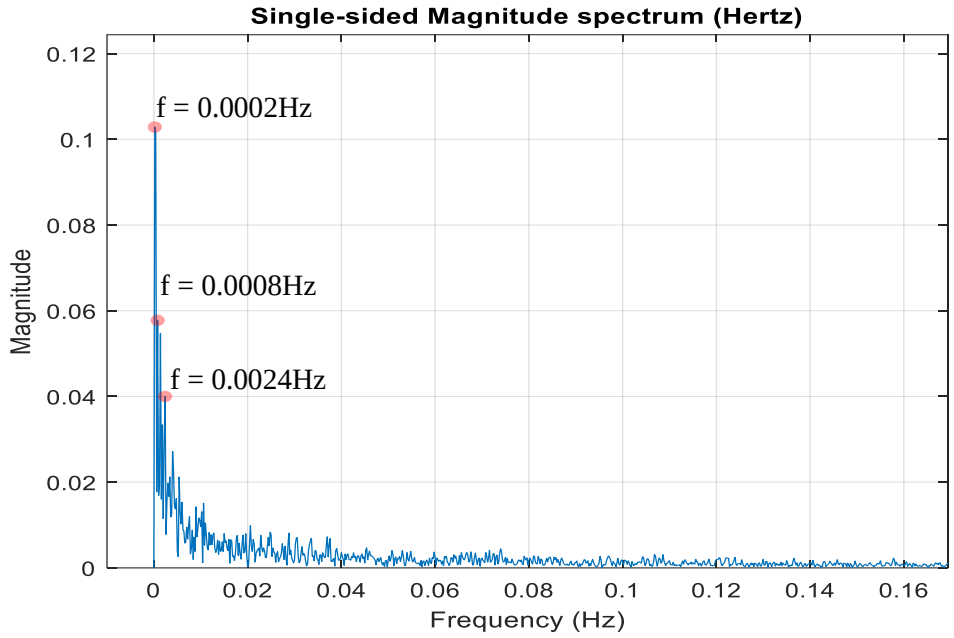

(a) 0W

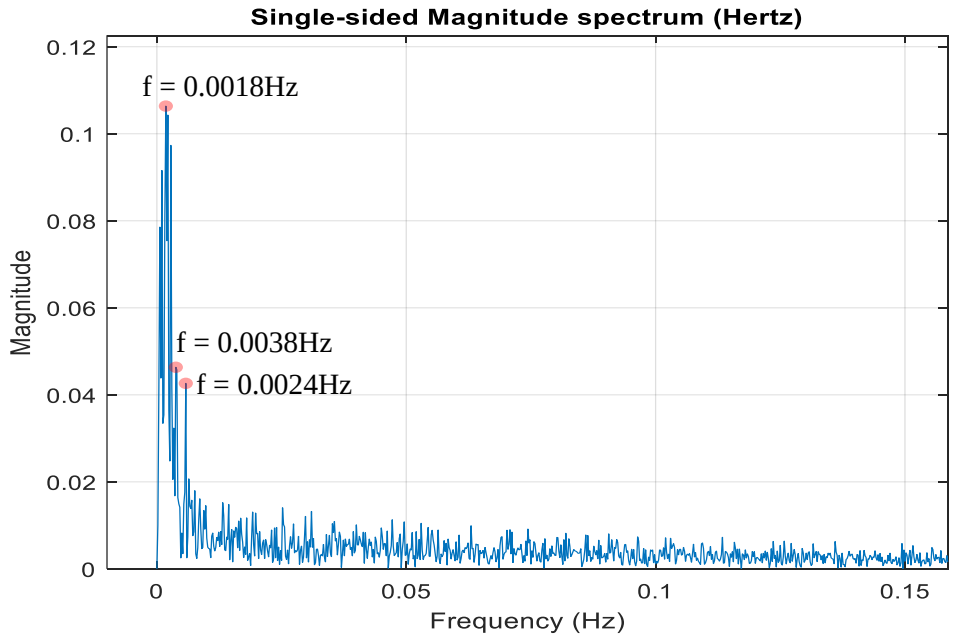

(b) 1.5W

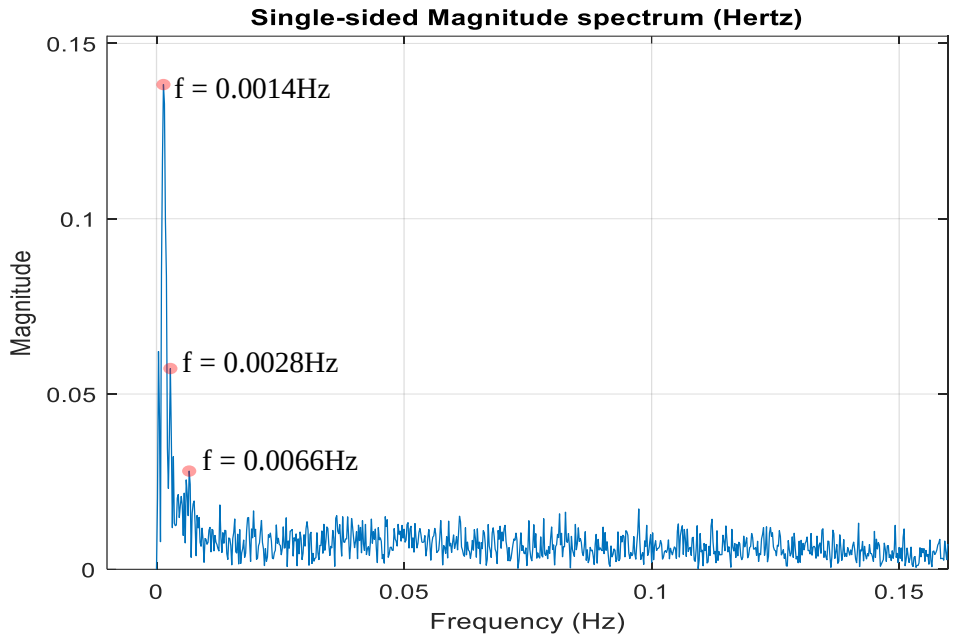
Single-sided Magnitude spectrum (Hertz)
f = 0.0014Hz
f = 0.0028Hz
f = 0.0066Hz
Magnitude
Frequency (Hz)
0.15
0.1
0.05
0
0
0.05
0.1
0.15

(c) 3W

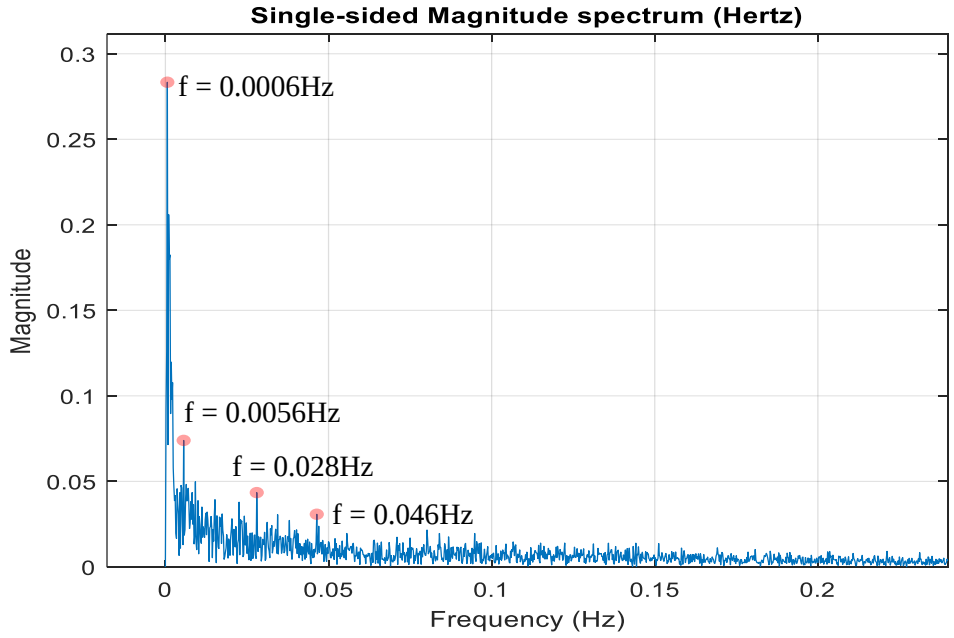
Single-sided Magnitude spectrum (Hertz)
f = 0.0006Hz
f = 0.0056Hz
f = 0.028Hz
f = 0.046Hz
Magnitude
Frequency (Hz)
0.3
0.25
0.2
0.15
0.1
0.05
0
0
0.05
0.1
0.15
0.2

(d) 4W

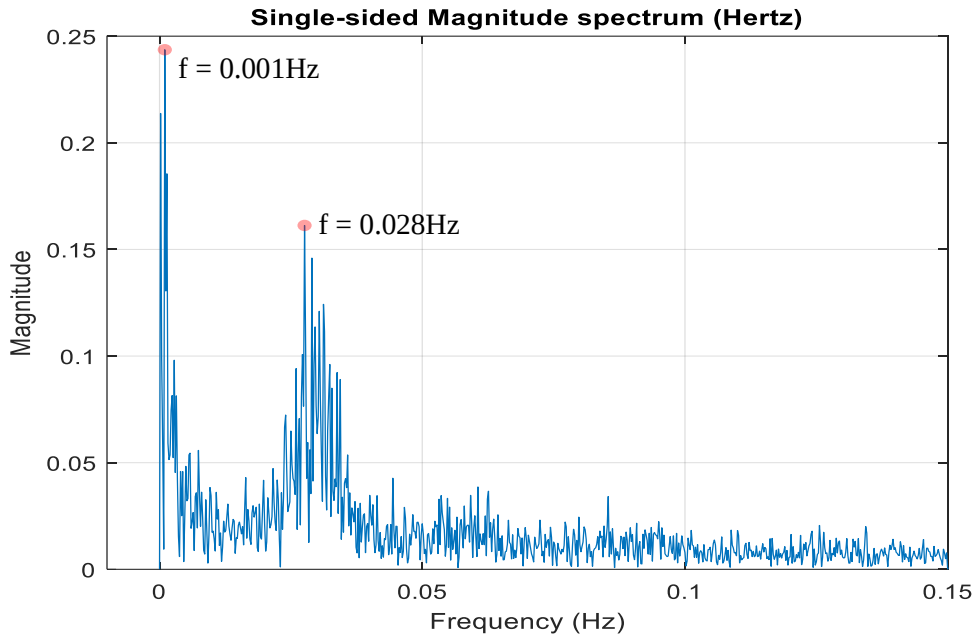

(e) 7.5W

Fig 7-X. Frequency plots of pressure oscillation for Air PHP at FR = 30% and T_c = 77K

As dry-out is reached (7.5W), the frequency reduces again with two main frequencies showing up at 0.001Hz and 0.028Hz. It should be noted that the largest dominant frequency did reduce from between 3W and 4W and there is a corresponding reduction in thermal performance between this power range. The frequency plots show that there is a correlation between the speed of the bubbles and the thermal performance of the PHP. It is also worth noting that a peak frequency of 0.0028Hz should up in three of the frequency plots and may be related to flow regime or flow direction. For comparison, Fig 7-XI shows the frequency plot at a different fill ratio and condenser temperature, as a function of heat loads.

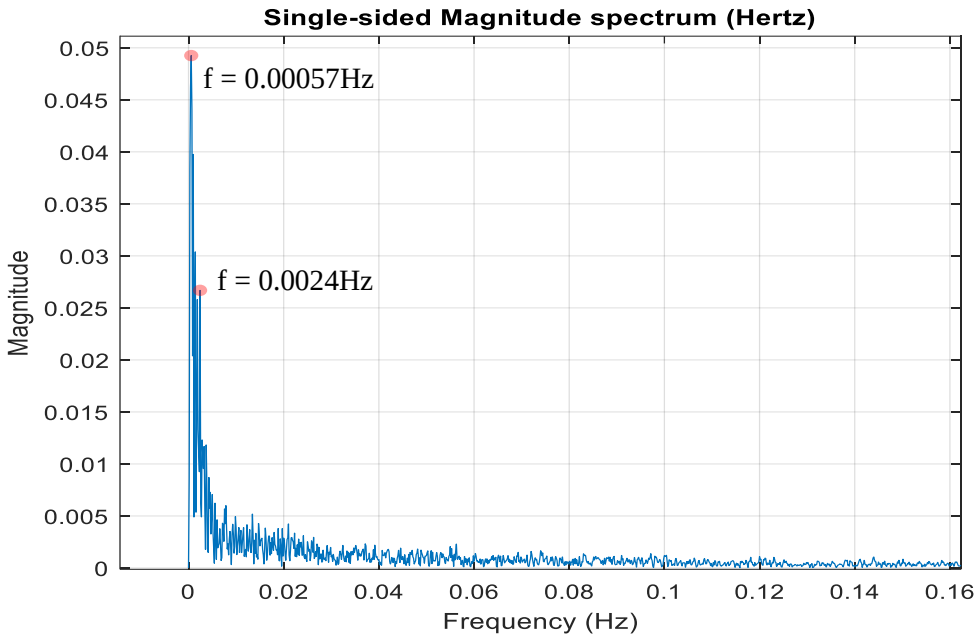
Single-sided Magnitude spectrum (Hertz)
f = 0.00057Hz
f = 0.0024Hz
Magnitude
Frequency (Hz)
0.05
0.045
0.04
0.035
0.03
0.025
0.02
0.015
0.01
0.005
0
0
0.02
0.04
0.06
0.08
0.1
0.12
0.14
0.16

(a) 0W

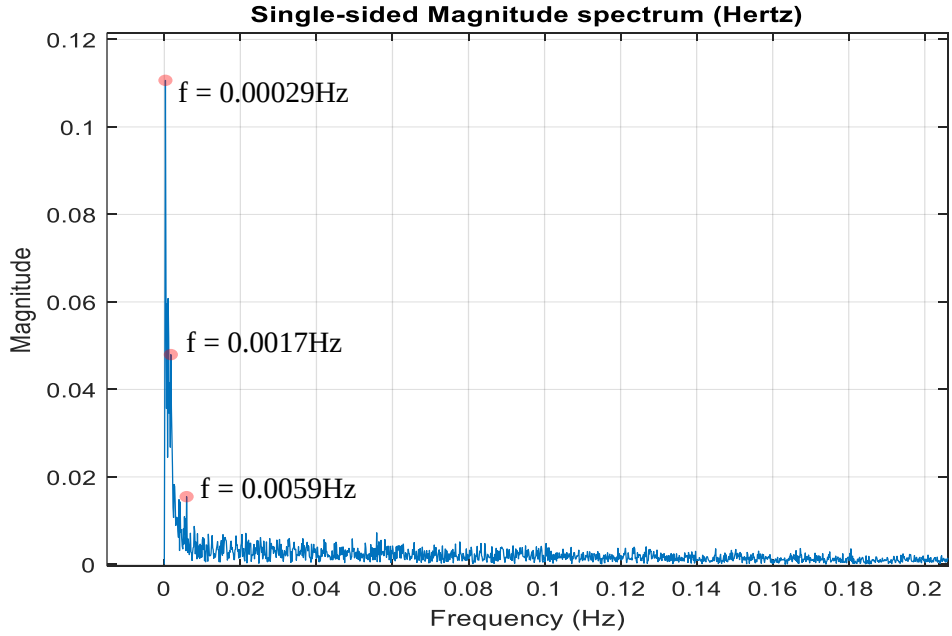
Single-sided Magnitude spectrum (Hertz)
f = 0.00029Hz
f = 0.0017Hz
f = 0.0059Hz
Magnitude
Frequency (Hz)
0.12
0.1
0.08
0.06
0.04
0.02
0
0
0.02
0.04
0.06
0.08
0.1
0.12
0.14
0.16
0.18
0.2

(b) 1W

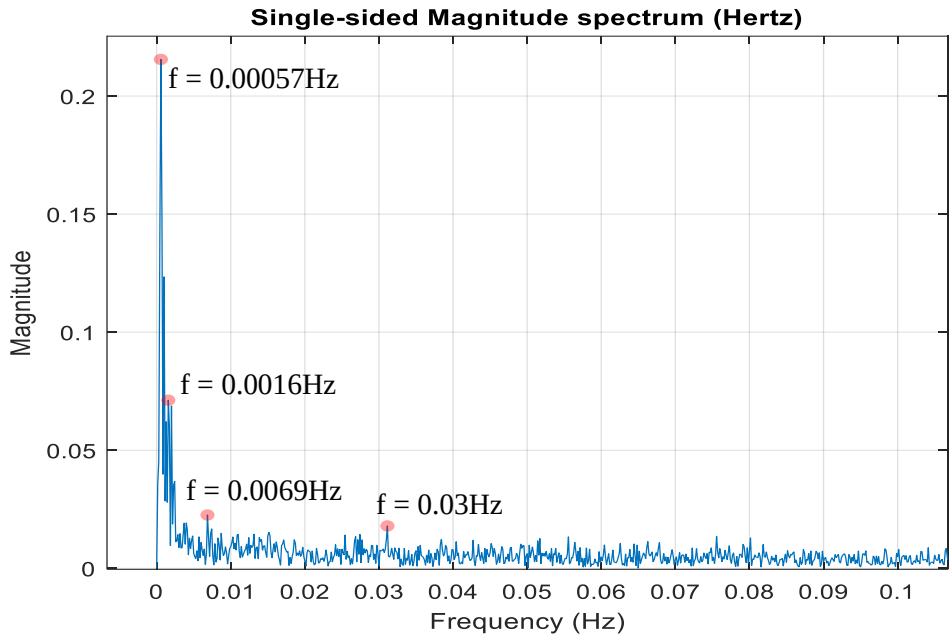
Single-sided Magnitude spectrum (Hertz)
f = 0.00057Hz
f = 0.0016Hz
f = 0.0069Hz
f = 0.03Hz
Magnitude
Frequency (Hz)
0
0.05
0.1
0.15
0.2
0.01
0.02
0.03
0.04
0.05
0.06
0.07
0.08
0.09
0.1

(c) 3W

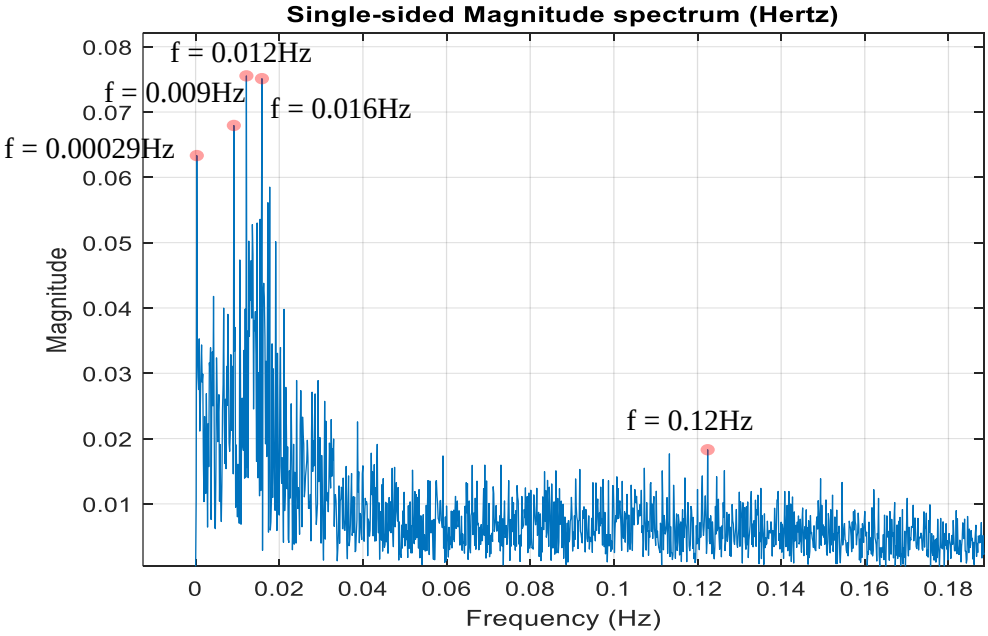
Single-sided Magnitude spectrum (Hertz)
f = 0.012Hz
f = 0.009Hz
f = 0.016Hz
f = 0.00029Hz
f = 0.12Hz
Magnitude
Frequency (Hz)
0.01
0.02
0.03
0.04
0.05
0.06
0.07
0.08
0.02
0.04
0.06
0.08
0.1
0.12
0.14
0.16
0.18

(d) 4W

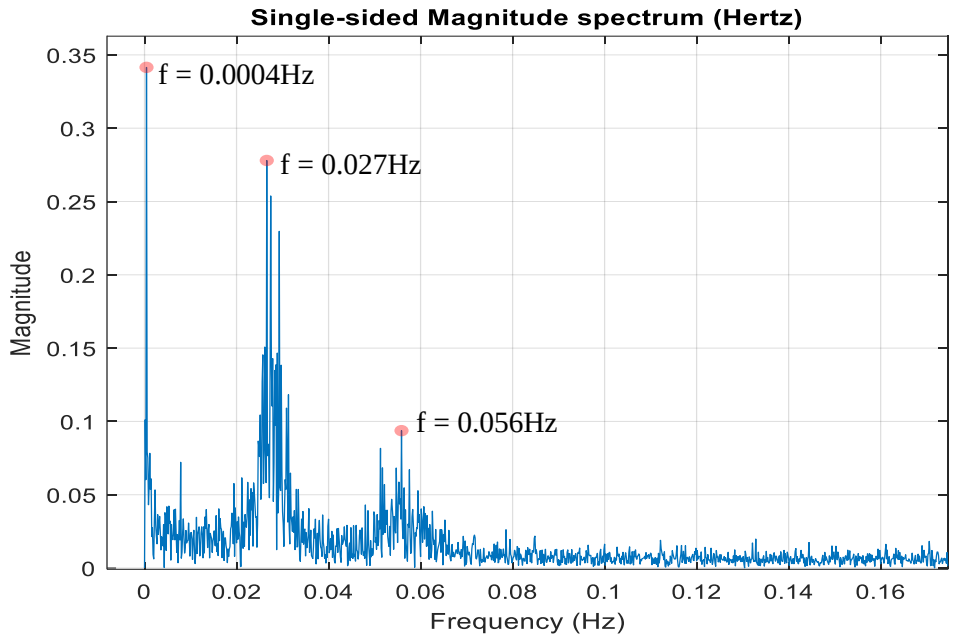

(e) 6W

Fig 7-XI. Frequency plots of pressure oscillation for Air PHP at FR = 40% and T_c = 71K

7.3.7 Dry-out versus condenser temperature

Fig 7-XII shows the dry-out power of the Air PHP as a function of condenser temperature for a few fill ratios. Just like with Nitrogen and Argon, the dry-out power exhibits a parabolic profile. This phenomenon has previously been attributed to the likely competing effects of the liquid has inventory and the enthalpy of vaporization.

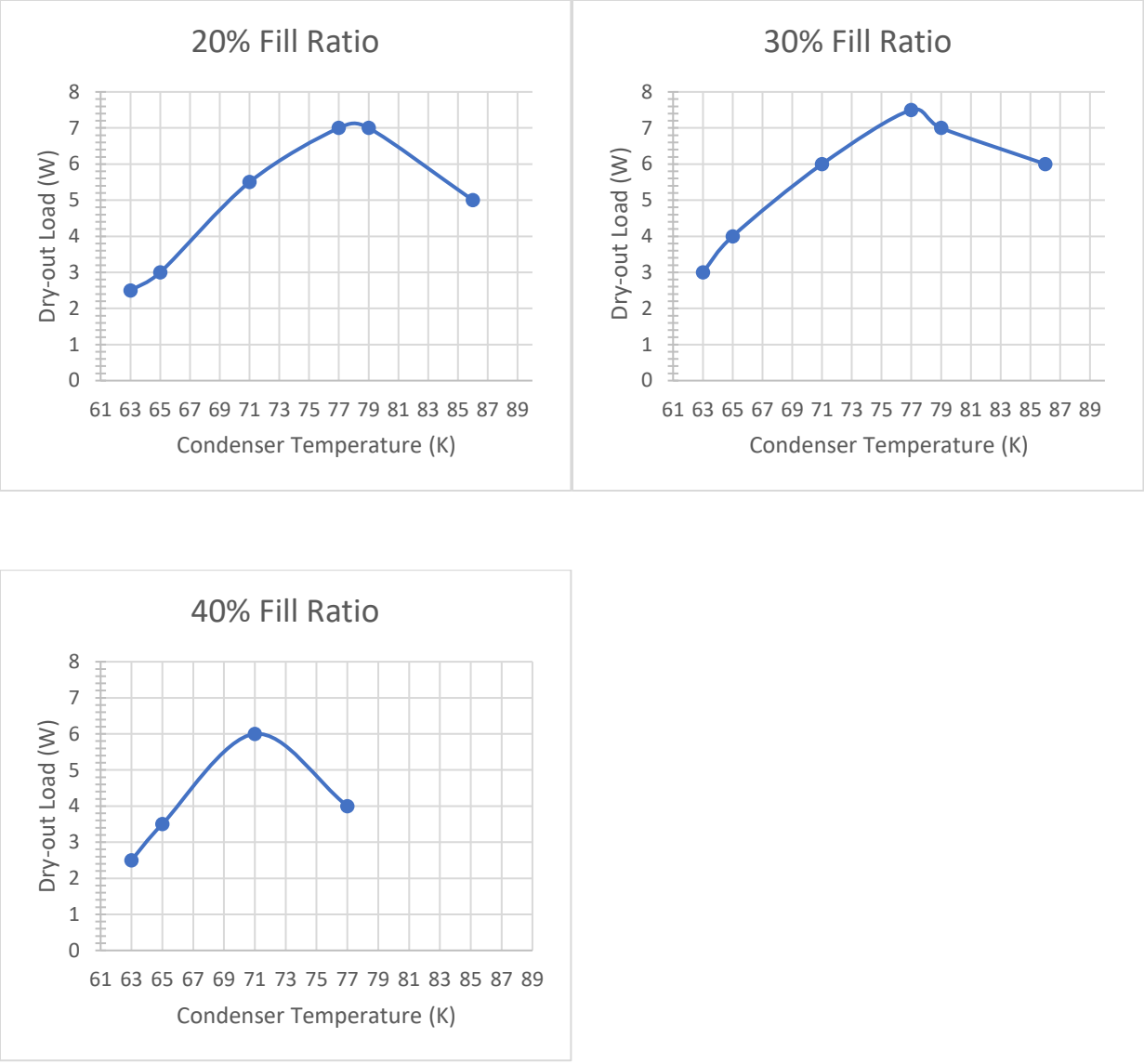

Fig 7-XII. Air PHP Dry-out load versus condenser temperature

The response of the temperature and pressure at the fill ratios shown in Fig 7-XIII are similar to the response in both the Nitrogen and Argon PHP. There are no large changes in pressure, even at the dry-out load. Also, the temperature difference between the adiabatic section and evaporator becomes largest at dry-out load. The same conclusion that was made about the other working fluids therefore can be made about the Air PHP. At dry-out load, the fluid is still in motion, albeit with

reduced oscillation and that the fluid completely dries out as it heads down to the evaporator (condensation still occurs at the condenser).

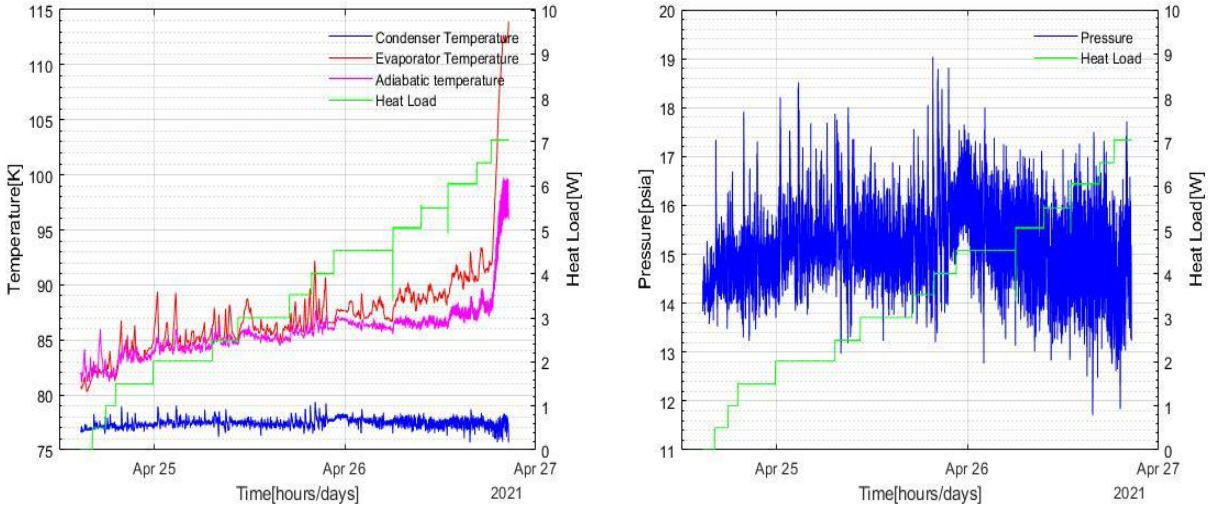

(a)

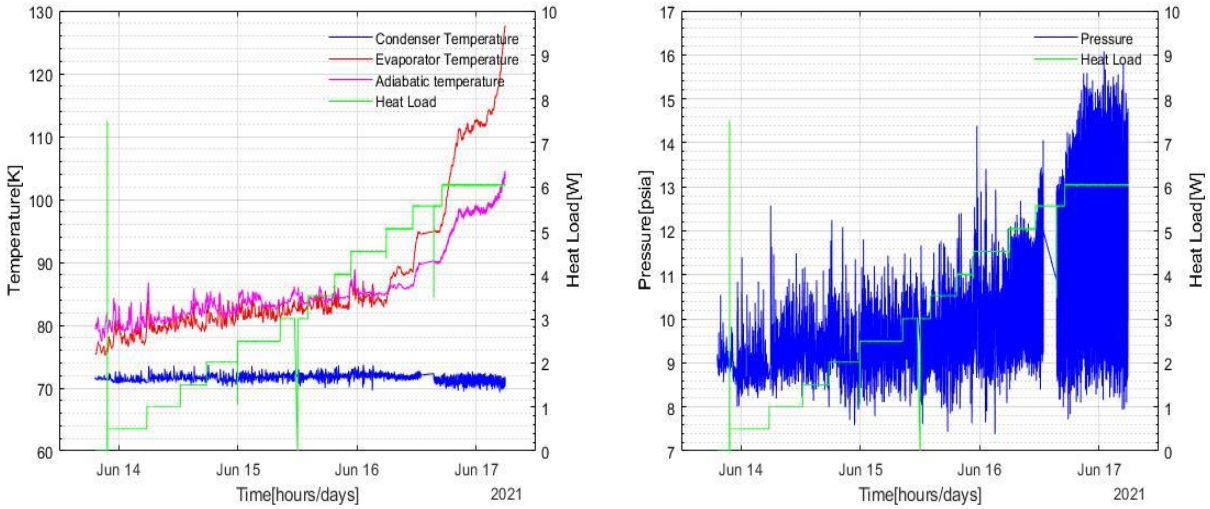

(b)

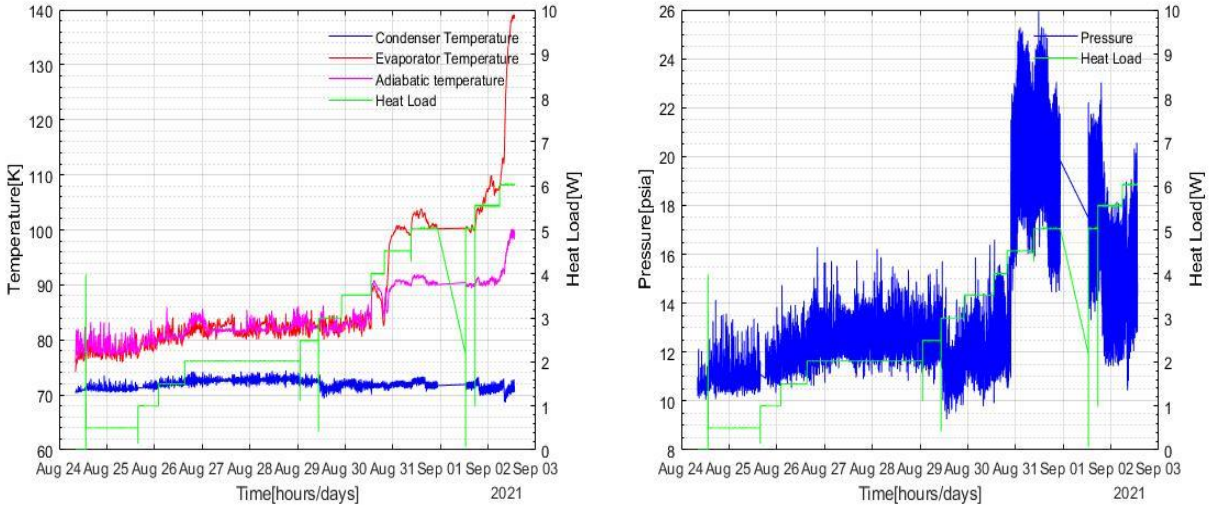

(c)

Fig 7-XIII. Temperature and Pressure data for (a) FR = 20%, Tc = 77K (b) FR = 30%, T_c = 71K (c) FR = 40%, T_c = 71K

7.4 Summary (Performance Maps)

Below are 3D plots of the Air PHP showing the relationship between effective thermal conductivity, condenser temperature and heat load. Highest order polynomial fit that does not result in unphysical behavior or does not produce multiple minimums or maximums is used. The effective conductivity is forced to zero at critical heat power. The z-axis (red) legend represents the effective conductivity K_{eff} in units of $\frac{W}{m-K}$, the x-axis (blue) is the condenser temperature T_{cond} in units of K and the y-axis (green) represents the heat load, P in units of W.

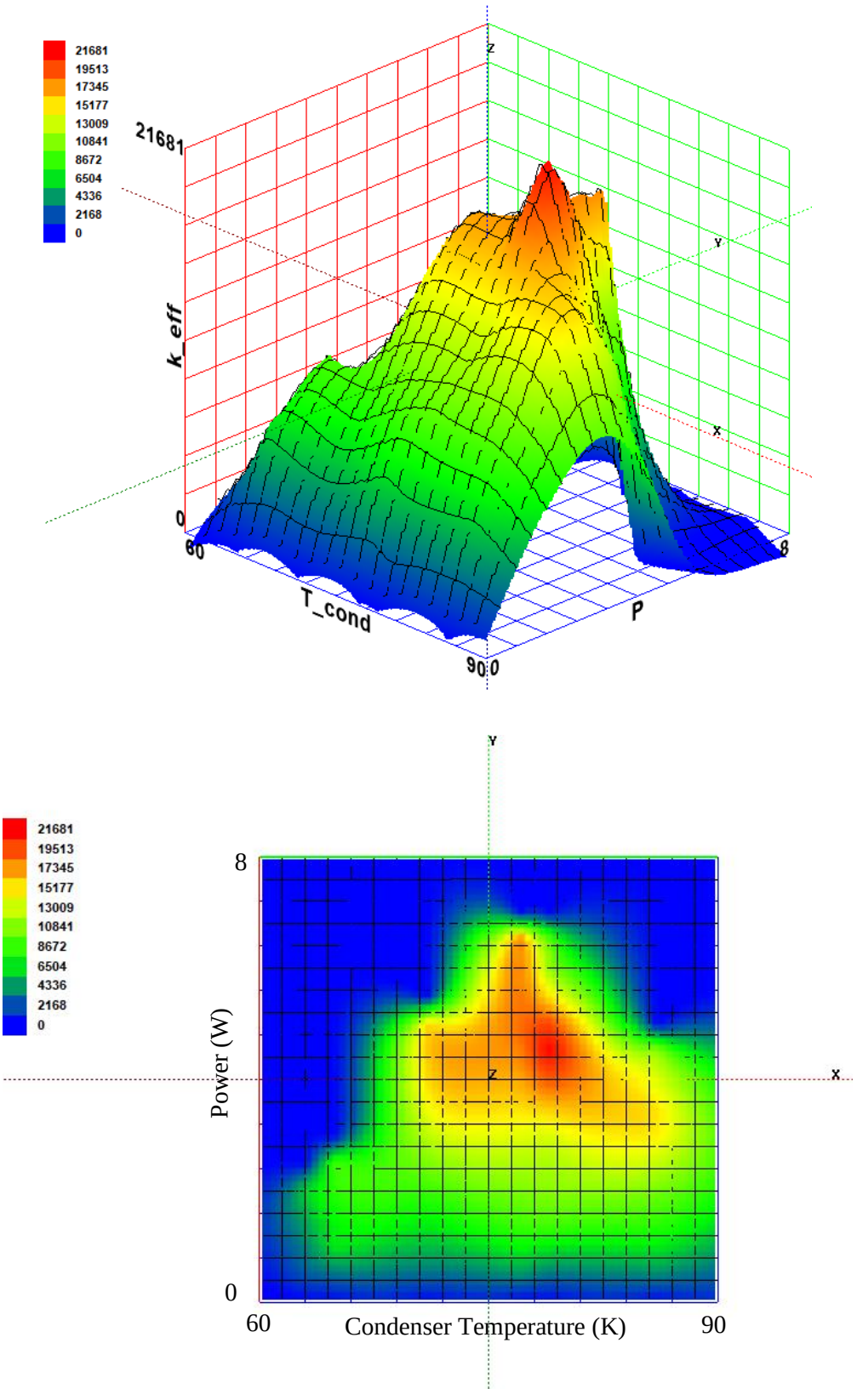
21681
19513
17345
15177
13009
10841
8672
6504
4336
2168
0
k_eff
T_cond
P
60
90
8
Power (W)
Condenser Temperature (K)

(a)

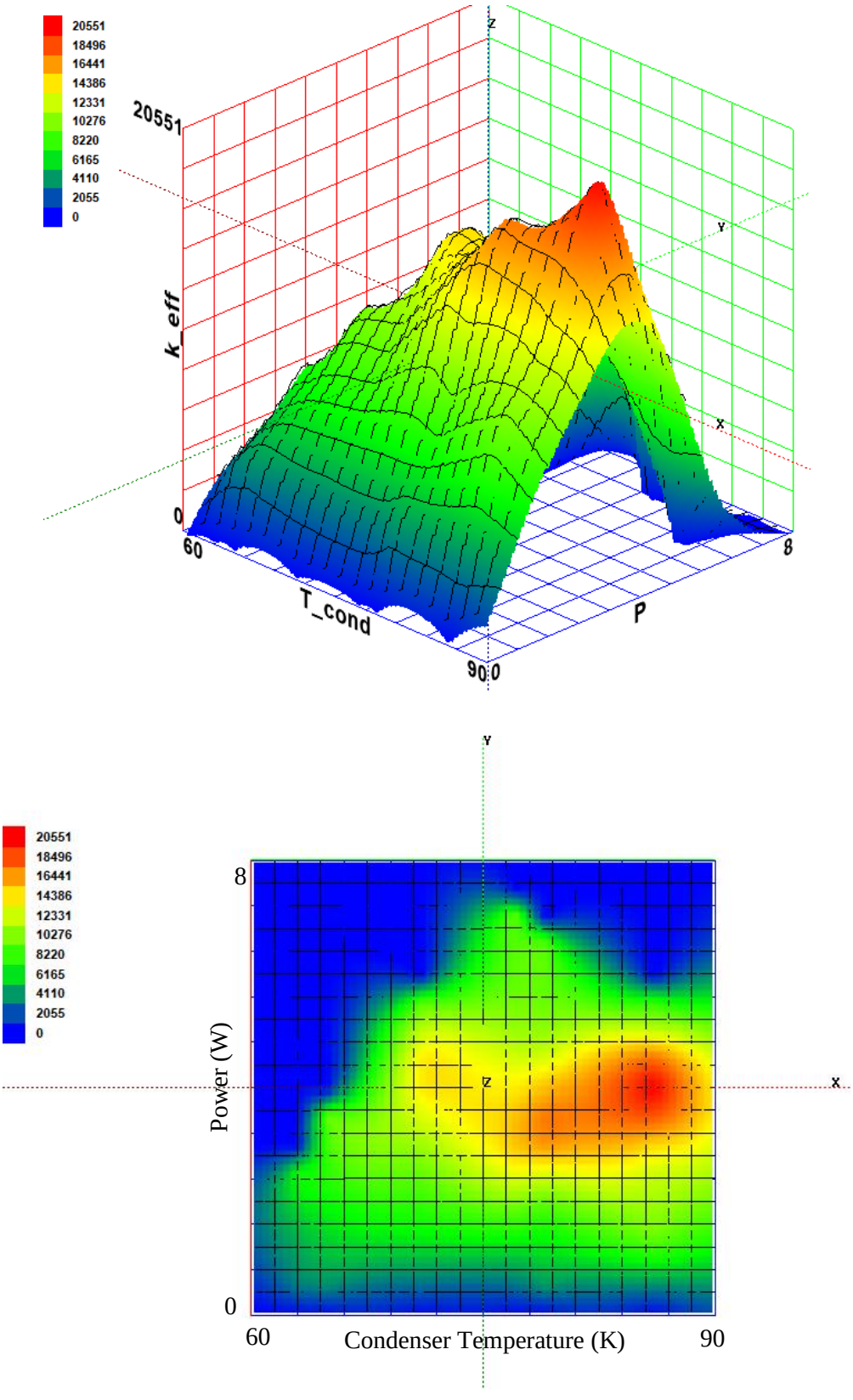
20551
18496
16441
14386
12331
10276
8220
6165
4110
2055
0
k_eff
T_cond
P
60
90
8
Power (W)
Condenser Temperature (K)

(b)

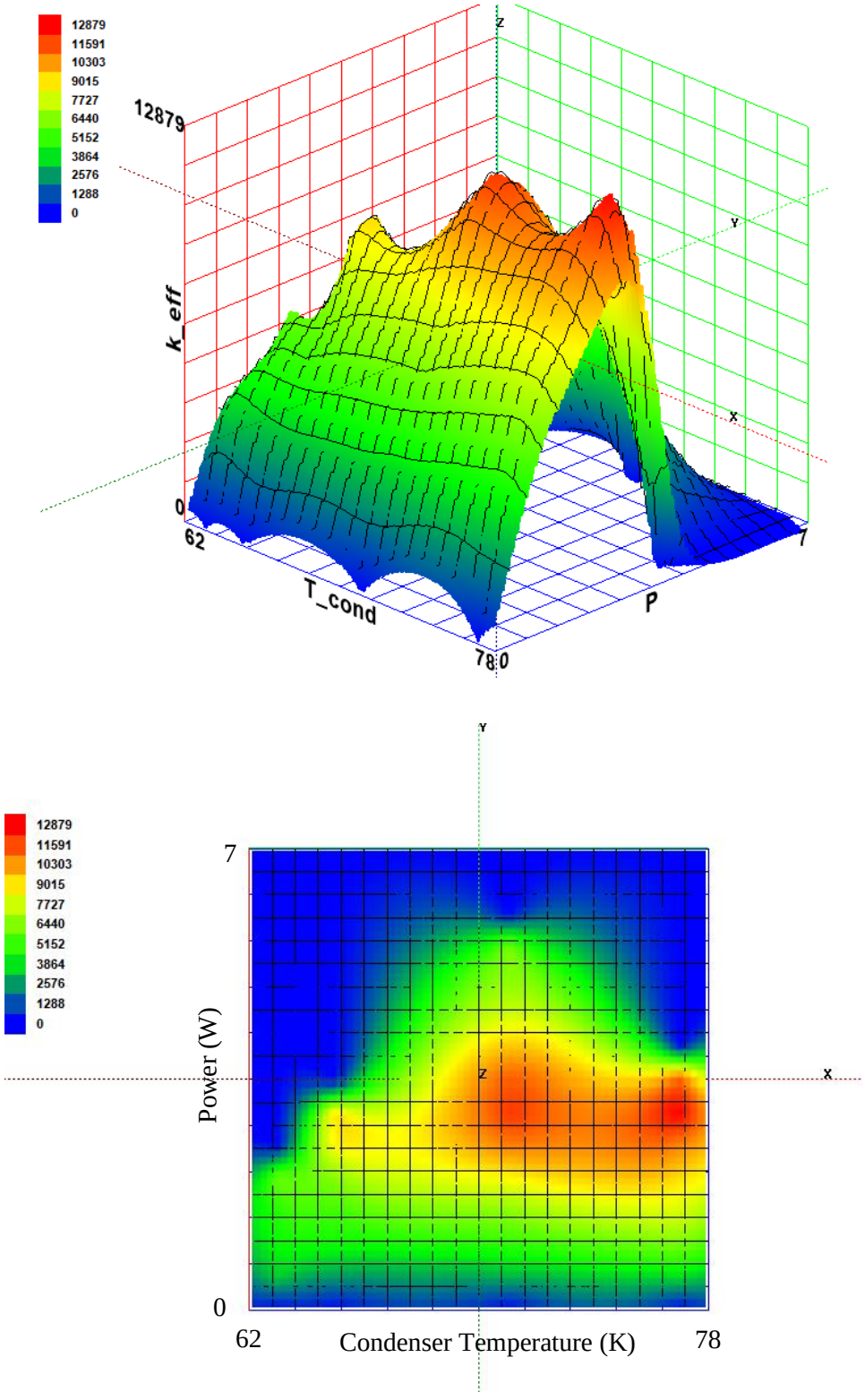

(c)

Fig 7-XIV. (a) FR 20% (b) FR 30% (c) FR 40%

The Air PHP shows an optimized area that is much larger than Argon PHP but smaller than Nitrogen PHP. Therefore, perturbations about an optimized area can still allow for comparable thermal performance of the design point. The Air PHP performance maps do not seem to increase significantly, the optimal zone/area as fill ratio is increased, like the Nitrogen PHP does. The optimized area does however move to include zones at higher temperature. Also, most of the optimized area, as fill ratio is increased, move away from the total dry-out zone and larger perturbations can drop the performance of the PHP but still allow it to operate without drying out.

8 Comparison of the Mixture PHP (Air) to the Pure Fluids PHP (Argon/Nitrogen)

8.1 Trends

8.1.1 Behavior of Effective Thermal Conductivity with increase in heat load

The effective thermal conductivity increased with increasing heat load up to the on-set of dry-out where there is an increase in wall temperature due to the intermittent disappearance of the thin film evaporative film. After this point, there is generally a reduction in the effective thermal conductivity up until complete dry-out. This phenomenon was the same for both the pure fluid PHP and mixture PHP, as seen in Fig 5-V, Fig 6-IV and Fig 7-V. It can therefore be concluded that this behavior does not depend on specific fluid properties but rather, on the fluid dynamics in the PHP. However, the value of the effective conductivity as a function of heat load is dependent on the properties of the fluid. Fig 8-I shows the comparison of the effective thermal conductivity for the three fluids tested during the experiments, as a function of heat load at a given initial fill ratio and condenser temperature

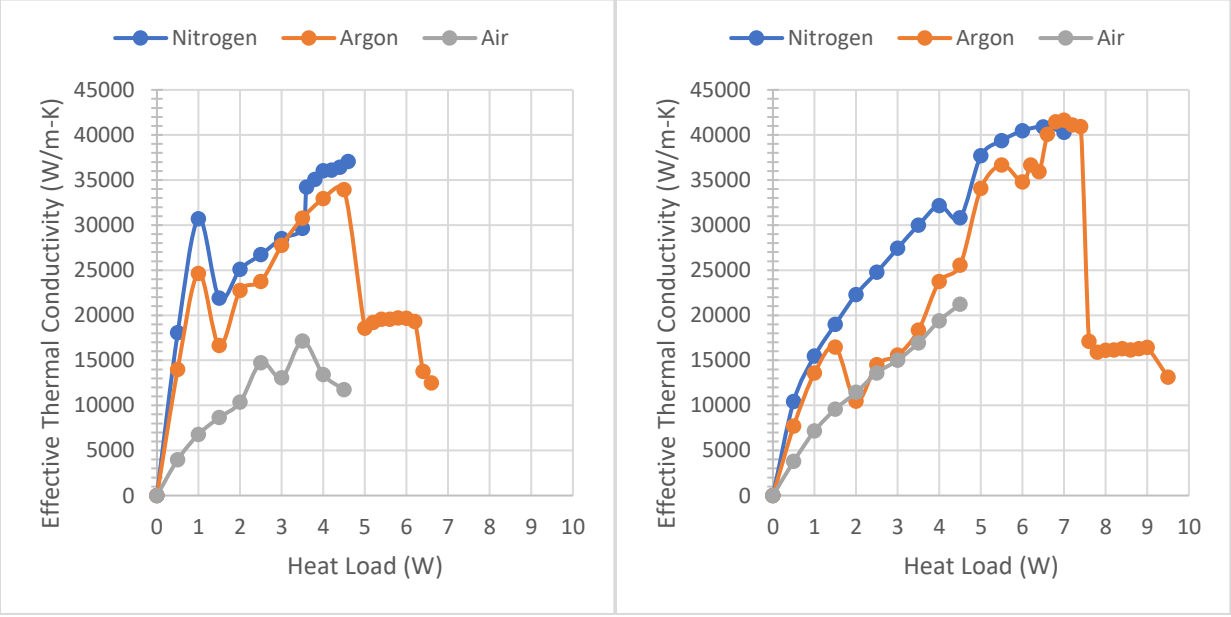

Fig 8-I. (L-R) K_{eff} versus heat load at $T_c = 86K$ for (a) 20%FR (b) 30%FR

The Nitrogen PHP had the best performance, followed by the Argon PHP and finally the Air PHP. Argon did exhibit, at lower temperature, a tendency to sustain operation at onset of dry-out, with reduced thermal performance. There are many characteristics of a fluid that affect the performance of a PHP. Some of these characteristics are:

Viscosity:

The viscosity of a fluid is a measure of the ability of the fluid to resist deformation at a given rate. Viscosity has an inverse relationship with velocity (at least in Newtonian fluids). Looking at Stoke's law for viscous drag on a spherical body (such as a bubble in a liquid):

$$F = 6\pi r\mu\bar{u} \tag{8.1}$$

where F is the drag force, μ is the viscosity of the liquid and $\bar{u}$ is the average velocity of the bubble. Then for a given force,

$$\bar{u} \propto \frac{1}{\mu} \tag{8.2}$$

Therefore, as the viscosity of a fluid goes up, the velocity of the bubble goes down. Previous chapters have shown that the performance of a PHP is affected positively by an increase in the working velocity, so a PHP using a fluid with lower viscosity (considering no other factor) would have a higher performance. For comparison the liquid viscosities of Nitrogen, Argon and Air at 86K are 117.2[μPa-s], 270.9[μPa-s] and 193.4[μPa-s] respectively. Although the viscosities are different, they are within the same order of magnitude.

Surface Tension:

The PHP is designed to have strong capillary effect to sustain oscillation. Capillary effect or wicking is the process by which a liquid rises or flows in a narrow tube without the support of external forces. The Laplace pressure gradient which governs the pressure differential that drives the liquid at the meniscus in a capillary tube is given by:

$$\Delta P_{lap} = \frac{2\sigma \cos\theta}{R} \tag{8.3}$$

where ΔP_{lap} is the Laplace pressure gradient, θ is the contact angle at the meniscus, R is the radius of the tube and σ is the surface tension of the liquid. From equation 8.3, a PHP utilizing a fluid with higher surface tension (with no other factors considered) will produce a larger driving force and hence a higher performance. However, an increase in surface tension also means a decrease in the wettability or spread of the fluid which will decrease the area exposed to heat transfer. Also, liquids with high surface tension tend to have higher contact angle which reduces the Laplace pressure gradient. This makes surface tension effect one of the most complicated effects to analyze. The surface tension of Nitrogen, Argon and Air at 86K are $0.006966\frac{N}{m}$, $0.01286\frac{N}{m}$ and $0.01002\frac{N}{m}$ respectively.

The ratio of the viscosity of the fluid to the surface tension of the fluid combines these two effects. A larger number of this ratio indicates higher performance (considering no other factors).

$$S = \frac{\mu}{\sigma} \tag{8.4}$$

This ratio looks like a capillary number with the absence of fluid velocity in the numerator. The S value for Nitrogen, Argon and Air at 86K are $0.021\frac{s}{m}$, $0.017\frac{s}{m}$ and $0.019\frac{s}{m}$ respectively.

Equation 8.4 gives an indication of the velocity or mass flow effect of the fluid. There are other properties that affect the energy potential of the fluid. Such properties as:

Specific Heat:

The specific heat capacity is the energy required to raise the temperature of a unit mass by one degree. It governs the sensible heat ability of a fluid. The higher the specific heat of a fluid for a given flow rate, the higher the sensible energy it can transport. Since the PHP is a convective device, utilizing a two-phase fluid, sensible heat is important. The sensible heat transport occurs when a liquid slug passes through the evaporator and condenser without changing phase (the temperature of the liquid slug goes up instead). From Fig 6-Ia, the specific heat of Nitrogen is much higher than the specific heat of Argon over the operating temperature range. The specific heat of liquid Nitrogen, Argon and Air at 86K are $2099\frac{J}{kg-K}$, $1116\,\frac{J}{kg-K}$ and $1970\frac{J}{kg-K}$.

Latent Heat:

The second component to heat transfer in a two-phase device is the latent heat. The latent heat is the heat required to change the phase of a substance without changing its temperature. Just like the sensible heat, the latent heat is also important in enhancing the performance of a PHP, therefore fluids with higher latent heat are desirable. Latent heat occurs when liquid slugs evaporate in the evaporator or condense in the condenser resulting in energy transport. The latent heat can change substantially over a temperature range. From Fig 6-Ib, below 107K, the specific latent heat of

Nitrogen is larger than for Argon but above 107K, Argon's specific latent heat becomes larger. The specific latent heat of liquid Nitrogen, Argon and Air at 86K are $187\frac{J}{kg-K}$, $162.1\frac{kJ}{kg}$ and $193.9\frac{kJ}{kg}$.

A combination of these four factors, along with any gravity assisted effect (denser fluid should have higher gravitational force) would result in some fluids performing better than others. On the basis of value of the properties of the fluid, Nitrogen should perform best, followed by Air and then Argon. However, Air is a mixture and the heat transfer coefficients for mixtures in macro flows have experimentally been found to be lower than those of pure fluids. One such experiment was conducted by Guilherme H.S. Olivera et al [**45**] In that study the heat transfer coefficients of pure R600a refrigerant and that of a mixture of R600a and R290 were investigated.

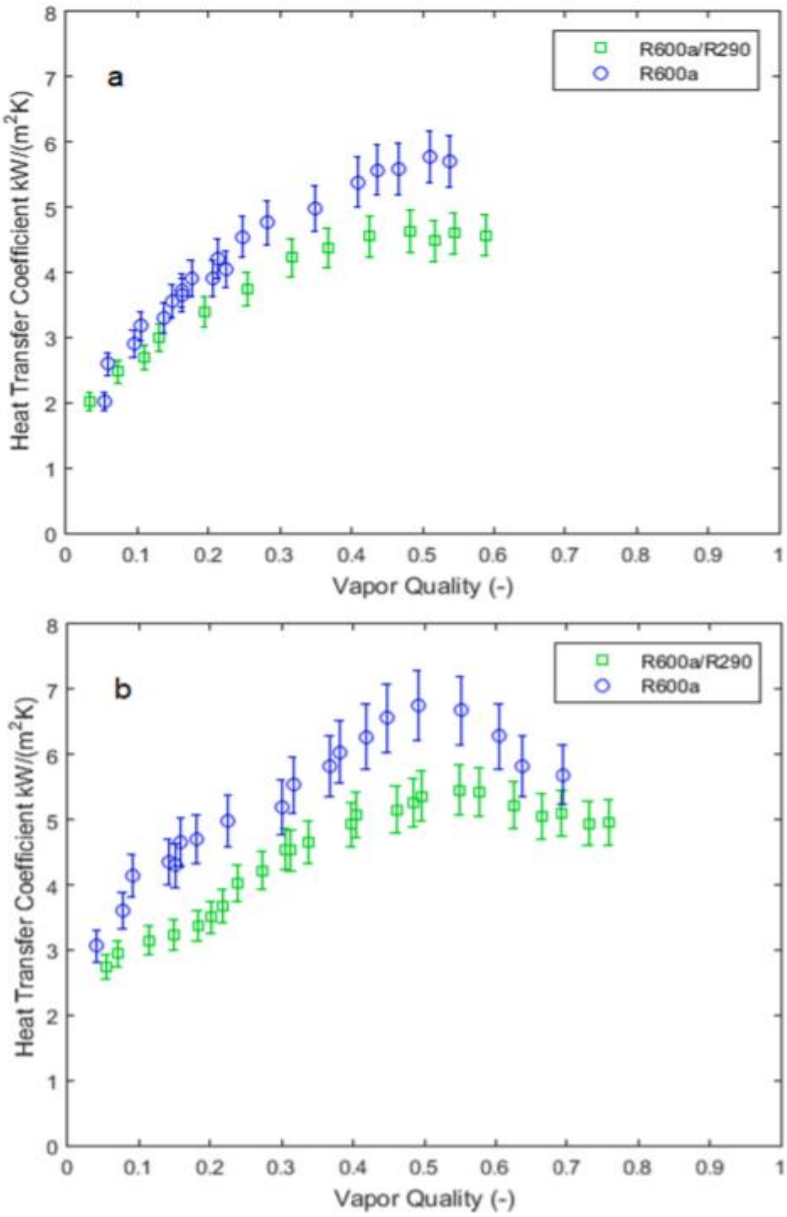

Fig 8-II. Heat transfer coefficient of R600a and mixture of R600a/R1270 at G = 300 kg/m2 s, T = 5 ◦C and, (a) q = 10 kW/m2 and (b) q = 30 kW/m2 [45]

This effect of reduced heat transfer coefficient of a fluid mixture was also seen by Rodrigo Barraza et al [46] while investigating the dilution of hydrocarbon mixture refrigerant with Nitrogen and Argon.

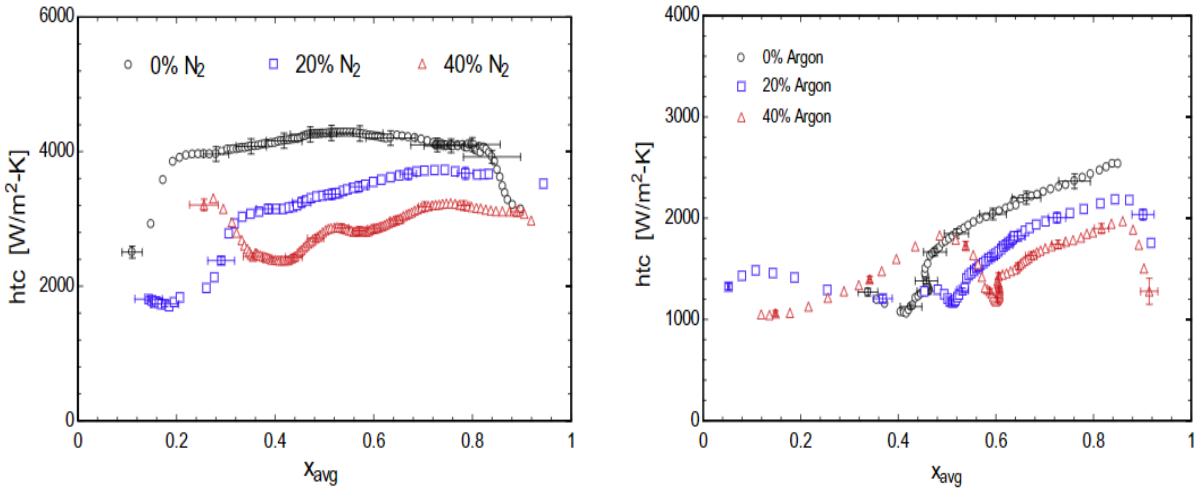

Fig 8-III. Heat transfer coefficient as a function of average quality, Composition effect, hydrocarbon mixture [46]

Mixtures with a surface-acting component or surfactant (an agent or compound that reduces the surface tension of a solution) have been observed to have improved heat transfer coefficient in pool boiling [47 & 48]. Such mixtures act to reduce surface tension and increase spread area. However, there is no research about the effects in capillary flow boiling, such as those in a PHP, where surface tension effect is desirable.

The reduction in heat transfer can be attributed to an increased mass transfer resistance in changing the phase change of the different components of the mixtures. Due to the vapor glide present in Zeotropic mixtures, there would be few degrees change in temperature to change the entire phase of the mixture from liquid to vapor. There is also the fact that there is reduced bubble formation in mixture at the nucleate site since more of the less volatile component would remain in the liquid form. There is therefore reduced heat transfer due to nucleation. In addition, there is reduced entrainment (when bubbles burst at liquid-vapor interface with the release of liquid droplets). Liquid entrainment leads to thinner film layer which improves heat transfer so a reduced entrainment will lead to thicker liquid film and reduced heat transfer coefficient. Another factor is

the reduced evaporation rate that occurs at the liquid- vapor interface because the concentration of the less volatile component of the mixture is higher there, leading to increased mass transfer resistance due to the distribution of the more volatile component within the liquid and a reduced heat transfer coefficient [45, 49 & 50].

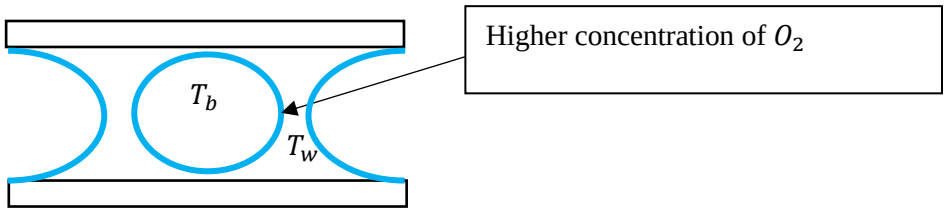

Fig 8-IV. A schematic of a bubble surrounded by liquid

8.1.2 Maximum Effective Thermal Conductivity versus Fill Ratio

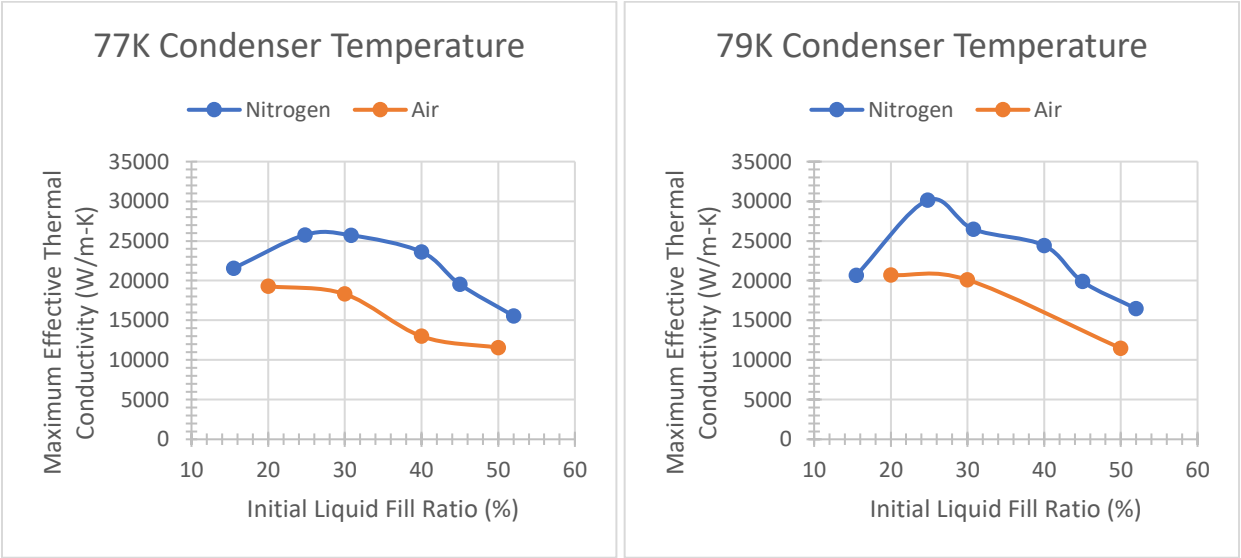

Fig 8-V. Maximum effective conductivity versus initial liquid fill ratio for Nitrogen and Air

The experimental data showed that the optimum initial fill ratio for Nitrogen was closer to 25% versus that of Air which was closer to 20%.

8.1.3 Dry-out Power versus condenser Temperature and Dry-out Behavior

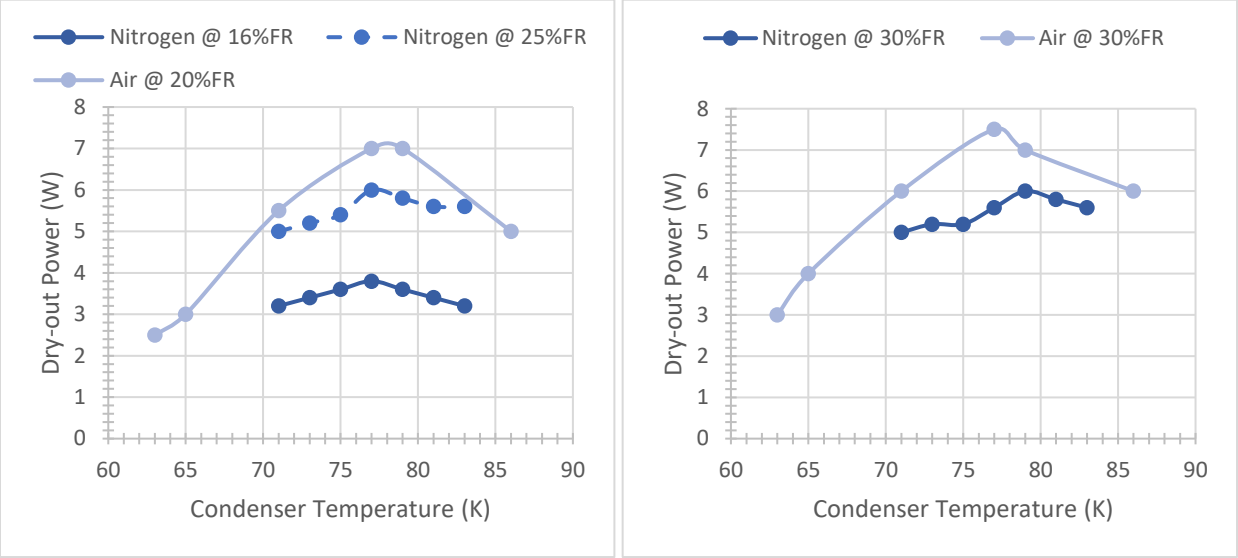

Fig 8-VI. Dry-out power versus condenser temperature for Nitrogen and Air

The mixture PHP (Air) was shown to have higher dry-out power in general. This can be attributed to the increased heat of vaporization due to the temperature glide. In pure fluids, phase change occurs at a single temperature while for mixtures, phase change of a given composition, occurs over a range of temperatures. The heat of vaporization required to change a unit mass of a pure substance from saturated liquid to saturated vapor is given as:

$$\Delta h_{vap} = h_{fg}(P) = h_v(P) - h_f(P) \tag{8.5}$$

The heat of vaporization for Nitrogen at 14.7psi is $199.2\frac{kJ}{kg}$.

The heat of vaporization required to change a unit mass of a mixture from saturated liquid to saturated vapor is given as:

$$\Delta h_{vap} = \sum_{i=1}^{c} y_i h_{v,i} - \sum_{i=1}^{c} x_i h_{f,i} \tag{8.6}$$

where c is the total number of species, y is the mole fraction in the vapor state and x is the mole fraction in the liquid state.

For standard Air (79%N_2, 21%O_2), the heat of vaporization at 14.7psi is 204.8$\frac{kJ}{kg}$.

Dry-out Behavior:

There seem to be two distinct ways that dry-out happens in the PHPs for the three fluids tested. At very low fill ratios, there are observable temperature oscillations in the adiabatic sections just before or at dry-out power, with periods that range from 5secs to 7 secs (sometimes longer). The amplitudes of these oscillation vary from 3K to 6K. This type of oscillation would suggest that the flow is in the "continuous oscillation type movement" versus the "transitional type movement" typically seen in room temperature PHPs. The oscillation will also be occurring with little velocity caused by a reduced momentum (momentum $\propto$ velocity). As fluid heads up to the condenser, the upward pressure from the liquid slug becomes greater that the pressure underneath the slug as the thin film left in the evaporator completely evaporates. This causes the slugs in the condenser to fall backwards by gravity into the evaporator and the cycle repeats. Here, the surface tension forces cannot overcome the gravitational forces. Fig 8-VII shows examples of this type of dry-out phenomenon.

As fill ratio increases, second type of dry-out behavior is observed. Here, at dry-out power or just before dry-out power, there is no observable amplitude or period of oscillation in the adiabatic section temperature. This would suggest that the flow is in "transitional type movement". The surface tension forces, and momentum can overcome gravitational pull, however there is complete evaporation of the thin film that is left behind by the liquid slug passing through the evaporator, leading to dry-out. Fig 8-VIII shows examples of this type of dry-out phenomenon.

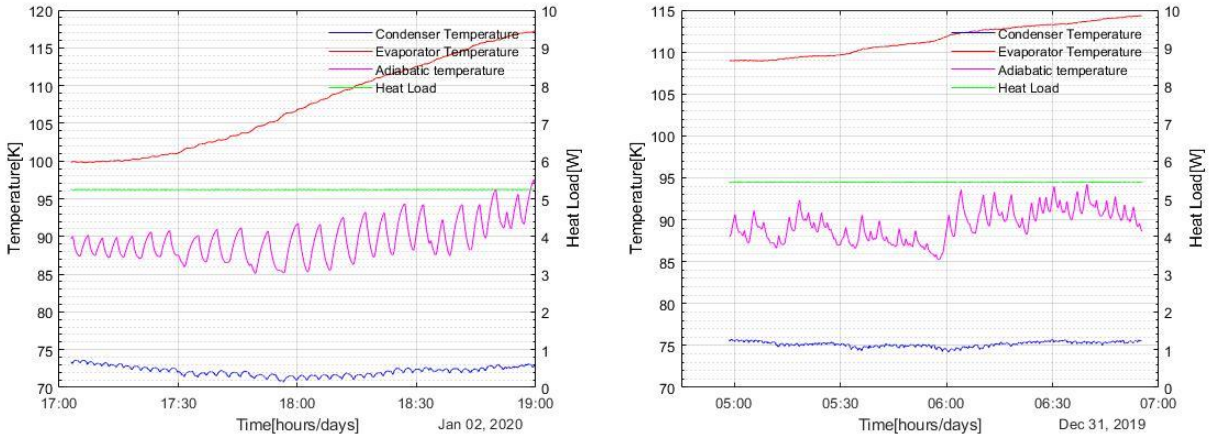

(a)

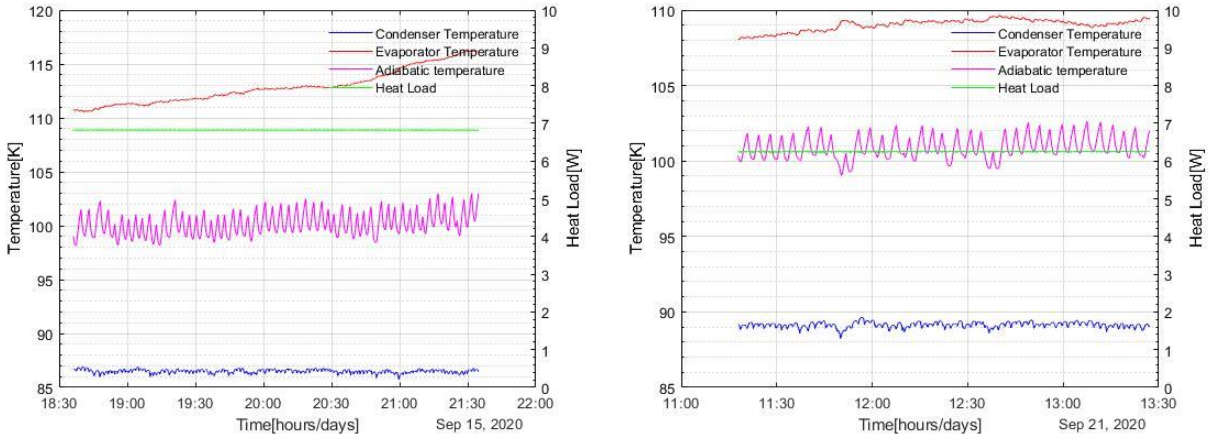

(b)

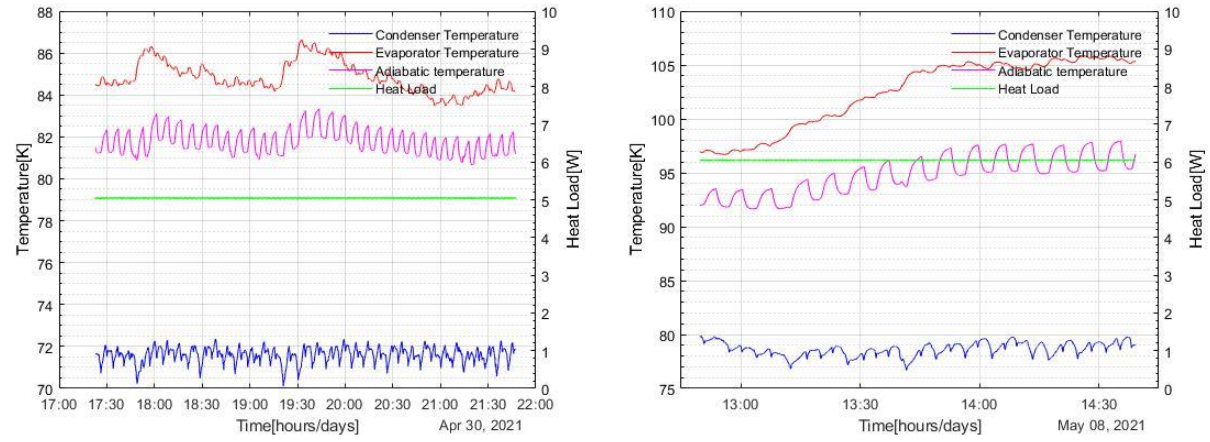

(c)

Fig 8-VII. (L-R) Temperature oscillation before/at dry-out for (a) Nitrogen 25%FR: 73K, 75K (b) Argon 20%FR: 86K, 89K (c) Air 20%FR: 71K, 79K

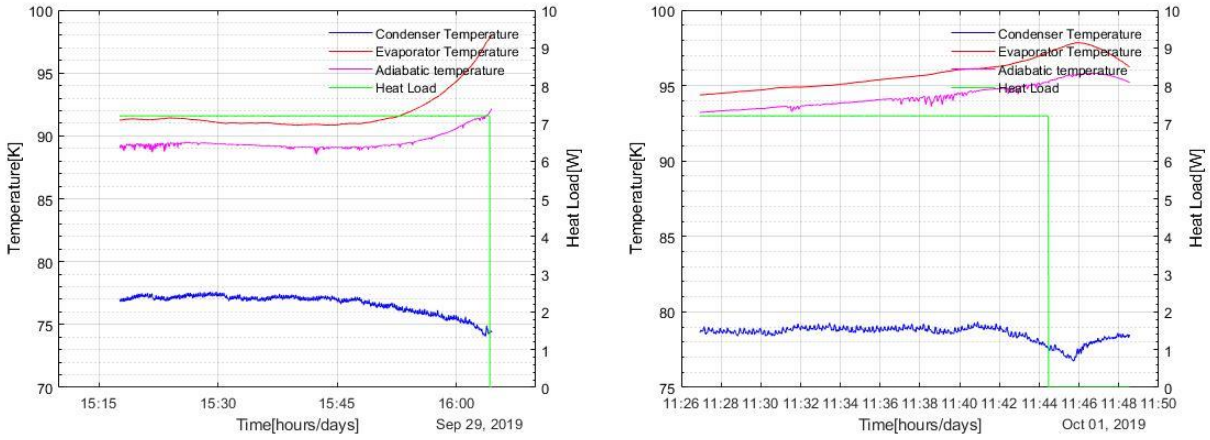

(a)

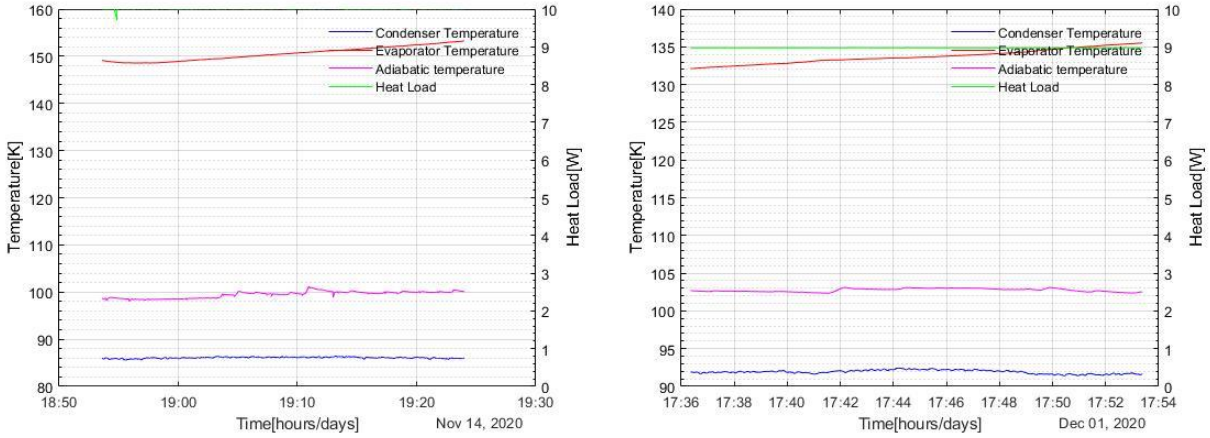

(b)

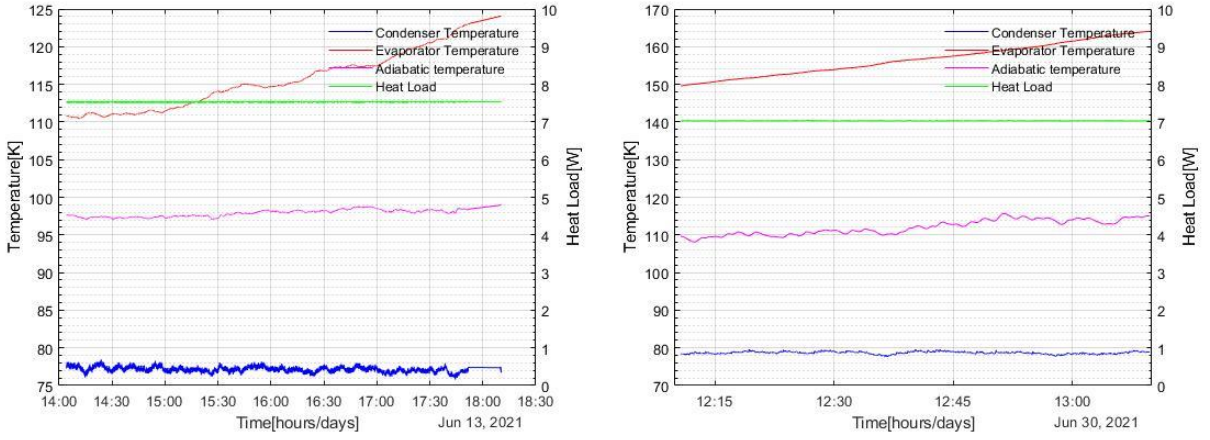

(c)

Fig 8-VIII. (L-R) Temperature oscillation before/at dry-out for (a) Nitrogen 40%FR: 77K, 79K (b) Argon 30%FR: 86K, 92K (c) Air 30%FR: 77K, 79K

The frequency plot also helps observe the behavior of the adiabatic pressure reading at dry-out. Fig 7-X and Fig 7-XI shows that as heat is increased, more equally weighted frequencies begin to show up (the dominant base frequency is always present). As dry-out is reached, most of the frequencies begin to disappear with one, two or three frequency spikes present. Fig 8-IX show some of these observations.

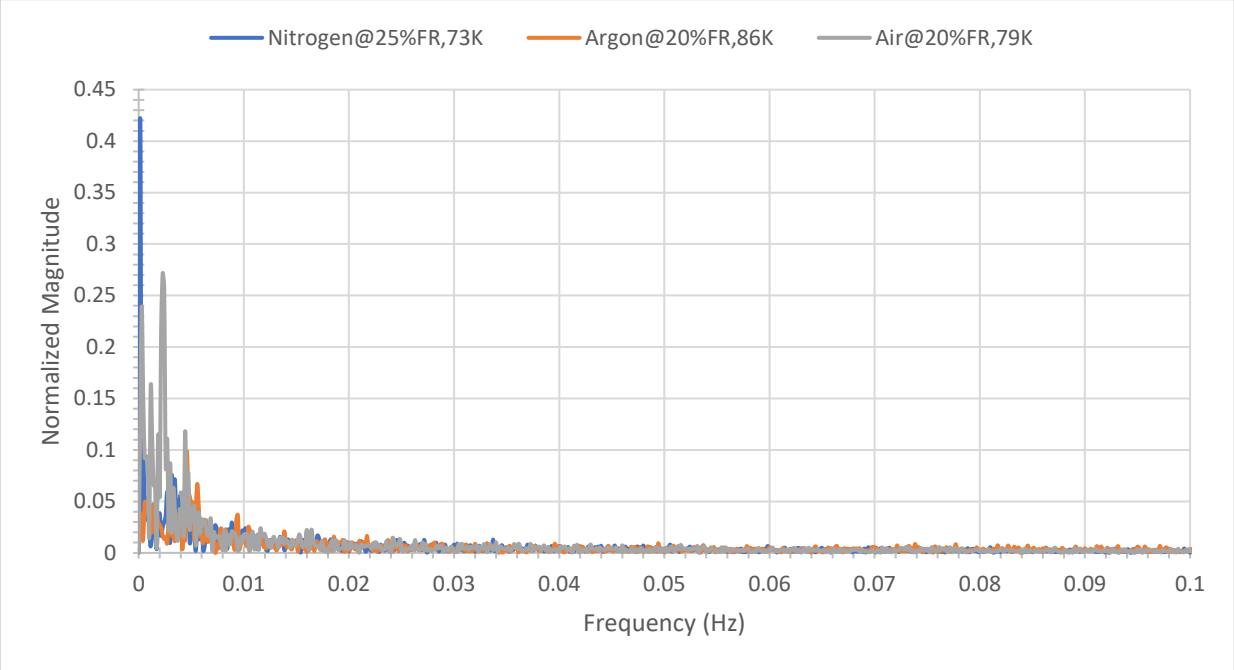

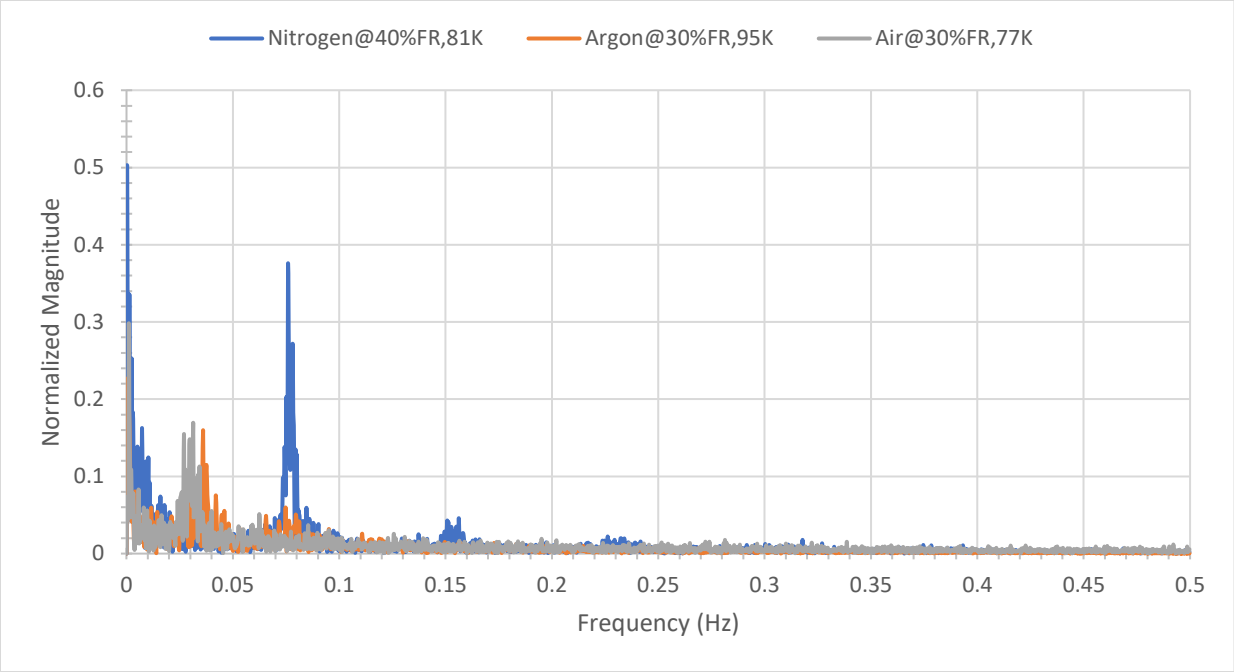

Fig 8-IX. Frequencies at dry-out for some PHP cases

In addition to improved dry-out power, the mixture PHP can allow for lower sink (condenser) temperature to be used in a device working with a pure fluid with a higher triple point. By adding one or more fluids with lower triple point than the original pure fluid, the working temperature range can be theoretically expanded. For instance, the condenser temperature limit of the Air PHP was 63K versus 69K for the Nitrogen PHP. Mixtures can also be used where operation of a single fluid with a lower triple point than the mixture might be dangerous. For example, an Oxygen PHP might be dangerous even though it might have a lower triple point, whereas a mixture such as Air can allow for operations close to the triple point of oxygen.

9 Uncertainty Analysis

Uncertainty analysis is a statistical tool needed to account for variability in predicted outcomes. It is important where measurements are involved to understand how a desired (output) variable is affected by slight variations in driving (input) variables. The desired variable in the experiment is the effective thermal conductivity. Recall the effective thermal conductivity can be calculated as:

$$k_{eff} = \frac{\dot{q}L}{NA_c(\bar{T}_e - \bar{T}_c)} \tag{9.1}$$

where $\dot{q}$ is the applied heat load, L is the effective length from the middle of the evaporator temperature sensor to the middle of the condenser temperature sensor, N is the number of capillary tubes, A_c is the inner cross-sectional area of the tubes, $\bar{T}_e$ is the average evaporator temperature and $\bar{T}_c$ is the average condenser temperature. N is a constant of known value. Assuming L and A_c are constant is very negligible error due to measurements or error due to parallax, the uncertainty in the calculated variable k_{eff} would come from the power supply that applies the head load as well as the sensors (RTDs) that measures the temperatures. The uncertainty in the calculated variable, k_{eff} can be written as:

$$dk_{eff} = \sqrt[2]{\left(\frac{\partial k_{eff}}{\partial \dot{q}}\right)^2 d\dot{q}^2 + \left(\frac{\partial k_{eff}}{\partial \bar{T}_e}\right)^2 d\bar{T}_e^2 + + \left(\frac{\partial k_{eff}}{\partial \bar{T}_c}\right)^2 d\bar{T}_c^2} \tag{9.2}$$

dk_{eff} , $d\dot{q}$, $d\bar{T}_e$ and $d\bar{T}_e$ are called uncertainties can be represented by $U_{k_{eff}}, U_{\dot{q}}, U_{\bar{T}_e}$ and $U_{\bar{T}_c}$ respectively. The uncertainty in the heat supplied $U_{\dot{q}}$ can further be broken into the components of power: current (I) and voltage (V). Therefore:

$$U_{\dot{q}} = \sqrt[2]{\left(\frac{\partial \dot{q}}{\partial I}\right)^2 U_I^2 + \left(\frac{\partial \dot{q}}{\partial V}\right)^2 U_V^2} \tag{9.3}$$

The relative uncertainty in the BK Power Supply Box which supplies and measures the voltage and current running through the heater is given as $U_I = U_V = \pm 1\%$.

$$\frac{\partial \dot{q}}{\partial I} = V \; and \; \frac{\partial \dot{q}}{\partial V} = I \tag{9.4}$$

A single point calibration was done on the temperature sensors for both the condenser and evaporator. This was done by immersing both sensors in liquid Nitrogen exposed to atmospheric pressure. The pressure recorded was 14.2psi corresponding to a saturation temperature of 77.07K. The temperature of the evaporator sensor read 76.97K and that of the condenser read 77.04K giving a temperature difference between the two sensors of $\pm$70mK. Therefore, the sensitivity on each of the sensors can be taken as $U_{\bar{T}_e} = U_{\bar{T}_c} = \pm 35$mK.

The derivatives can be evaluated as:

$$\frac{\partial k_{eff}}{\partial \dot{q}} = \frac{L}{NA_c(\bar{T}_e - \bar{T}_c)} \tag{9.5}$$

$$\frac{\partial k_{eff}}{\partial \bar{T}_e} = -\frac{IVL}{NA_c(\bar{T}_e - \bar{T}_c)^2} \tag{9.6}$$

$$\frac{\partial k_{eff}}{\partial \bar{T}_e} = \frac{IVL}{NA_c(\bar{T}_e - \bar{T}_c)^2} \tag{9.7}$$

Fig 9-I shows the error bars of the effective thermal conductivity due to uncertainty for a case run for each of the PHP.

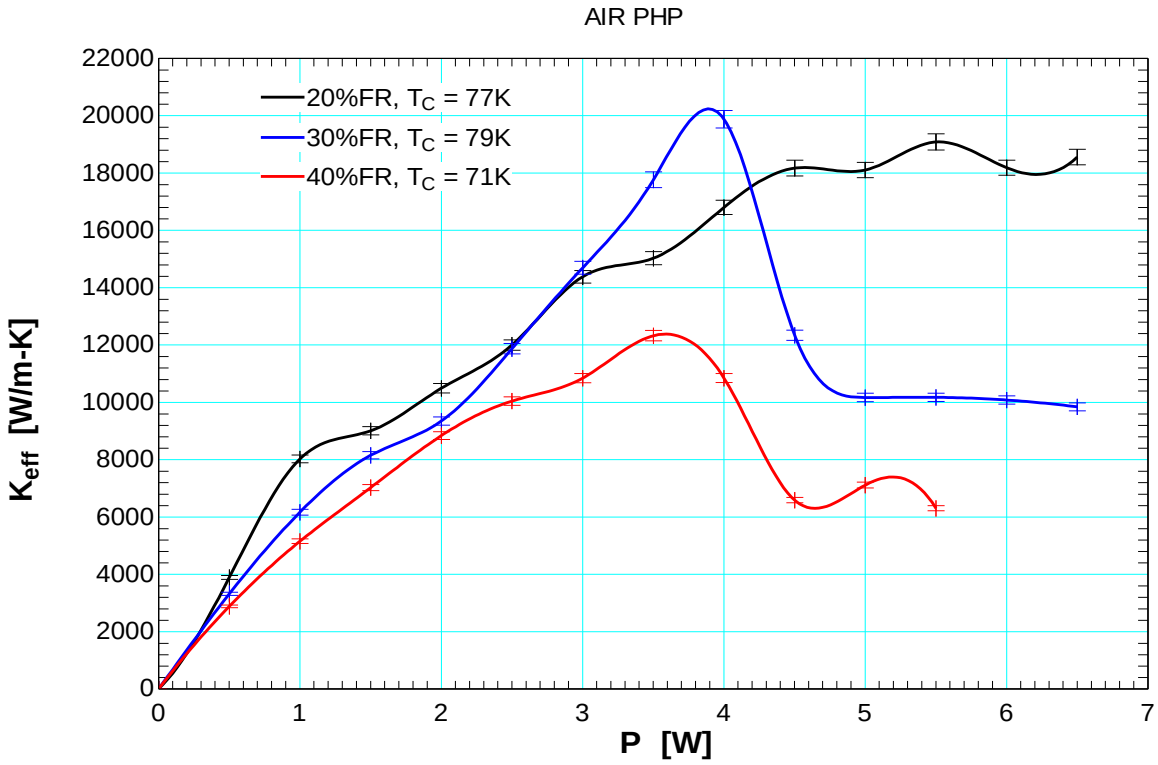
AIR PHP
20%FR, T_C = 77K
30%FR, T_C = 79K
40%FR, T_C = 71K
K_eff [W/m-K]
P [W]
0
2000
4000
6000
8000
10000
12000
14000
16000
18000
20000
22000
0
1
2
3
4
5
6
7

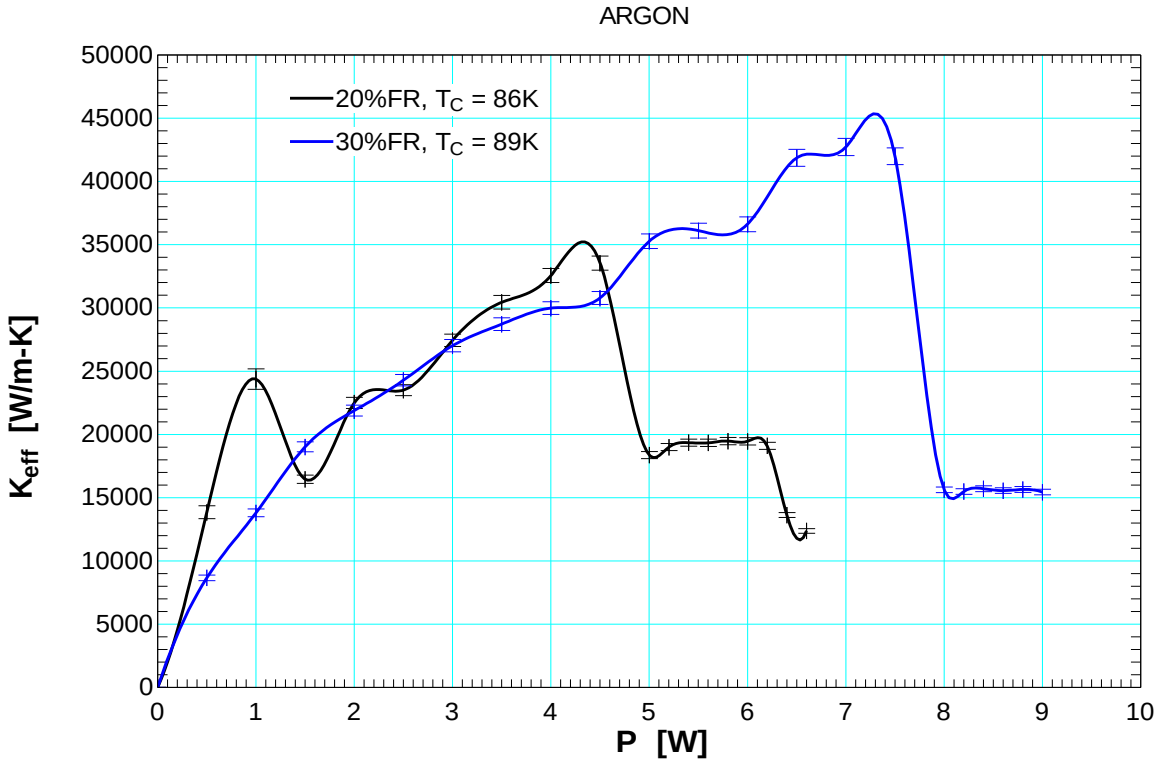
ARGON
20%FR, T_C = 86K
30%FR, T_C = 89K
K_eff [W/m-K]
P [W]
0
5000
10000
15000
20000
25000
30000
35000
40000
45000
50000
0
1
2
3
4
5
6
7
8
9
10

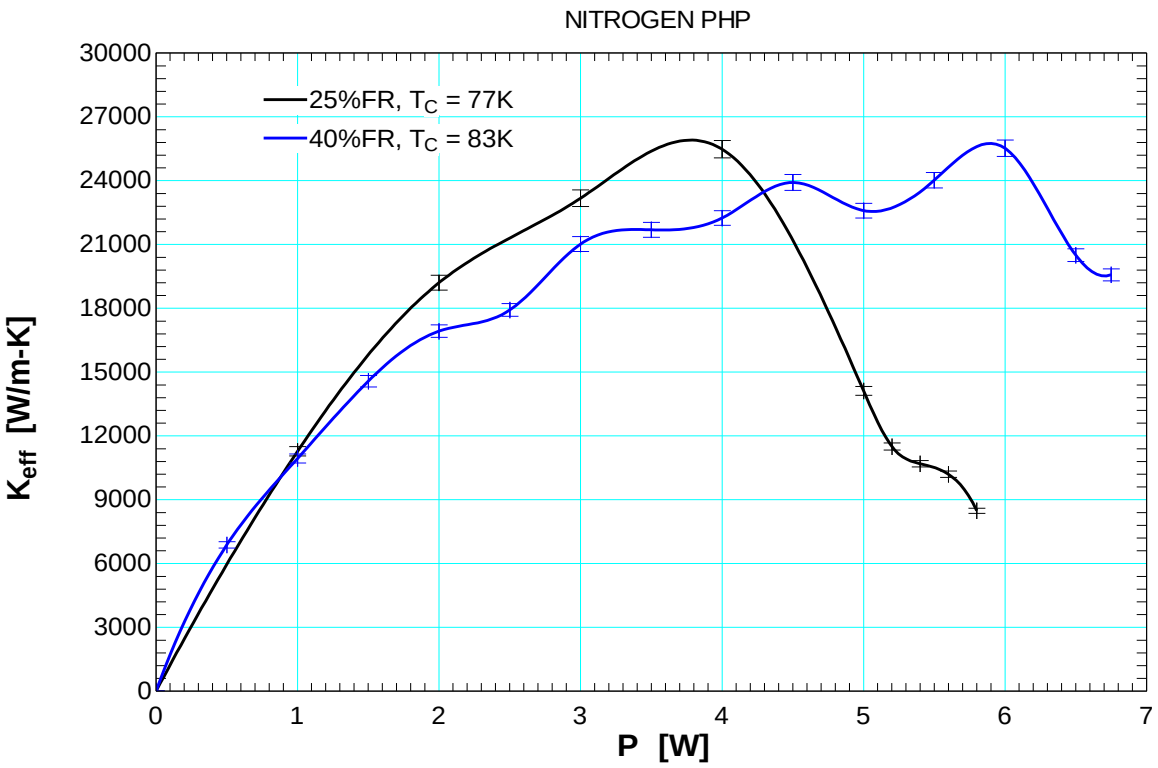

Fig 9-I. Effective conductivity versus heat load showing error bars due to uncertainties

10 Conclusion and Future Work

10.1 Conclusion

A PHP was built to test the effect of condenser temperature, heat load and fill ratios on the thermal performance of the device. The PHP was run with two pure fluids (Nitrogen and Argon) and one mixture (Air). The results and observations from the experiments can be summarized below:

i. The effective thermal conductivity at a given temperature rises as heat load is increased, generally up to a maximum point before it begins to drop due to the onset of dry-out.

ii. There is an optimum fill ratio that exists as tradeoff between lower bubble number and bubble velocities occur as fill ratio increases.

iii. The higher condenser temperature, the higher the effective thermal conductivity. This is especially true as heat load is increased. For very low heat loads (during nucleate boiling/bubble formation), the thermal performance is the same, regardless of condenser temperature.

iv. The changes in slope of the boiling curve of a PHP might give an indication of flow regimes inside a cryogenic PHP. This is important as there is no current way to visualize cryogenic PHPs.

v. Low fill ratios exhibit close to isobaric process, therefore at these fill ratios, the device would be temperature limited. High fill ratios on the other hand, causes large pressure

changes, especially at onset of dry-out/dry-out, and so, the device would be pressure limited at these fill ratios.

vi. The dry-out power at low fill ratios exhibits an optimum (positive parabolic behavior) as a function of increasing condenser temperature. This is likely due to the tradeoff between higher heat of vaporization at lower temperatures and higher liquid inventory at higher temperatures. At high fill ratios, for Nitrogen PHP, the contribution of increased liquid inventory at higher condenser temperature to extending dry-out power, is reduced. Since more influence will come from the heat of vaporization, which is higher at lower temperature, a monotonic decreasing slope is observed.

vii. There were two distinct dry-out behavior at low fill ratios, concluded to be occurring in terms of fluid flow. One in which the fluid oscillates back and forth with reduced velocity and one in which the fluid is still in translational motion with complete evaporation of the liquid film at the evaporator. In addition, at high fill ratios (Nitrogen), the PHP fluid is thought to have very little velocities to sustain any type of flow, leading to complete separation of the liquid at the condenser, from the vapor at the evaporator.

viii. Performance maps shows the 3D thermal performance of the PHP with respect to condenser temperature and heat load for different fill ratios. These maps can be used in optimization and perturbation analysis.

ix. Frequencies are dry-out exhibit distinct magnitude spikes. The number of spikes vary from one to three.

x. Mixtures in a PHP reduces the performance compared to a pure component PHP of the mixture due to reduced bubble formation and mass transfer resistances at the bubble interface of mixtures (heat transfer coefficient is reduced). On the other hand, mixtures have a higher dry-out power than its pure component. In addition, mixtures can be used as a substitute for a pure fluid with lower triple point but other safety implications.

10.2 Future Works

i. Most of the fluids tested at/around 77K have high heat capacities and so both cool down and run time takes considerably longer compared to a helium PHP. Therefore, it may be beneficial to reduce the size of the PHP to allow for faster data collection. A new PHP should be built. The new PHP should also use tube with inner diameter close to the critical diameter for a Nitrogen PHP. Much smaller tubes might not be optimal since it reduces the flow area. In addition, brazing techniques rather than soldering, should be used for the joints to eliminate/reduce possibility of leaks

ii. If possible, pressure taps should be installed at the entry and exit to the condenser or evaporator or at either ends of the condenser and evaporator. Also, investigate the addition of a cryogenic mass flow meter in the working tubes or at least investigate methods used by mass flow meters to predict mass flowrates. These will help estimate or measure the velocities in the device which is not currently done. These velocities can help with quantifying the flow or calculating capillary numbers or bubble departure.

iii. Modification to the current fill line to reduce/eliminate redundant joints will greatly reduce the uncertainty of leaks from those joints. Also looking into the possibility of installing two check valves inside the PHP assemble: one that allows flow in the filling direction (downwards) and the other in the evacuating direction (upwards). This will reduce the assumptions needed to estimate the mass of fluid in the fill line that is not part of the working flow.

iv. Standard Air was shown to improve dry-out. There might be opportunities for determining the best performance for Nitrogen-Oxygen mixtures based on varying compositions.

v. Other type of mixtures might further reduce the operating (condenser) limit on the PHP. Other mixtures, including azeotropic mixtures should be investigated as working fluids for PHPs. There have been cases of mixtures with surfactants improving heat transfer by increasing spread (reducing surface tension). Research would be needed to see the benefits of such action since surface tension is desired in PHPs.

vi. The PHP system can also be operated at different orientations to add to existing literature, the effect of inclination angle on the thermal performance.

vii. 3D data sets can be used to investigate the effects of perturbations or off-design variables on the thermal performance of the PHP. In addition, existing correlations or new

correlations can be made to include the effects of condenser temperature, as well as mixtures.

viii. Another area that might be of interest in the PHP is the pitch angle (angle of the U-bend). Research in the literature have shown that thin film is left behind at these bends when a liquid slug passes them therefore a larger pitch angle might improve the effectiveness of a PHP

ix. The current research used step loading for the heat input. It might be interesting to see the effect of ramp loading on the performance state of the PHP

11 References

1. G. R. Chandratilleke, Y. Ohtani, H. Hatakeyama, and H. Nakagome, *"Development of loop heat pipes for cryogenic applications,"* Proceedings of 16th ICEC, T. Haruyama, ed., Elsevier Science, Kitakyushu (1996) p. 501.
2. G. R. Chandratilleke, Y. Ohtani, H. Hatakeyama, M. Takahashi, and H. Nakagome, "*Development of Multi - Loop Heat Pipes for Superconducting Magnet Applications,*" Advances in Cryogenic Engineering, Vol. 43 Edited by P. Kittel, Plenum Press, New York, 1998.
3. *Pulsating Heat Pipes Phase 1*, NASA completed Technology Project (2015-2015), https://techport.nasa.gov/view/33132.
4. K. Natsume, T. Mito, N. Yanagi, H. Tamura, T. Tamada, K. Shikimachi, N. Hirano, and S. Nagaya, *"Development of Cryogenic Oscillating Heat Pipe as a New Device for Indirect/Conduction Cooled Superconducting Magnets,"* IEEE Transactions On Applied Superconductivity, Vol. 22, No. 3, June 2012.
5. Lu Qianyi, Jia Li, *"Experimental Study on Rack Cooling System based on a Pulsating Heat Pipe,"* Journal of Thermal Science Vol.25, No.1 (2016) 60–67.
6. Akachi H., "*Structure of a heat pipe*," U. S. Patent No. 4921041 (05 1990), http://www.lens.org/lens/patent/US_4921041_A.
7. Khandekar, S., Shyama Prasad Das, Frédéric Lefèvre, and Jocelyn Bonjour *"Thermally Induced Oscillatory Two-Phase Flow in a Mini-Channel: Towards Understanding Pulsating Heat Pipes,"* Proceedings of the ASME 2011 9th International Conference on Nanochannels, Microchannels, and Minichannels ICNMM2011 June 19-22, 2011 Edmonton, Alberta, Canada.
8. E.T. White and R.H. Beardmore, *"The Velocity of Rise of Single Cylindrical Air Bubbles Through Liquids Contained in Vertical Tubes,"* Chemical Engineering Science, 1962, Vol. 17, pp. 351-361. Pergamon Press Ltd., London. Printed in Great Britain.
9. Fabliha Islam, Fahima Akhter, Sifat Bin Haider, and Mohammad Ali, *"Effect of Inner Diameter on the Thermal Performance of Closed Loop Pulsating Heat Pipe,"* Proceedings of 102nd The IIER International Conference, Singapore, 2nd -3rd May 2017, ISBN: 978-93-86291-88-2.
10. Piyanun Charoensawan, Sameer Khandekar, Manfred Groll, and Pradit Terdtoon, *"Closed Loop Pulsating Heat Pipes Part A: Parametric Experimental Investigations,"* Applied Thermal Engineering 23 (2003) 2009–2020.
11. Niti Kammuang-Lue, Phrut Sakulchangsatjatai, Chansin Sriwiset, and Pradit Terdtoon, *"Investigation and Predictation of Optimum Meandering Turn Number of Vertical and Horizontal Closed-Loop Pulsating Heat Pipes,"* Thermal Science 2018 Volume 22, Issue 1 Part A, Pages: 273-284.
12. Luis Diego Fonseca, John Pfotenhauer, and Franklin Miller, *"Results of a Three Evaporator Cryogenic Helium Pulsating Heat Pipe,"* International Journal of Heat and Mass Transfer 120 (2018) 1275-1286.

13. Rahul S. Borkar and Pramod R. Pachghare, *"Effect of Working Fluid, Filling Ratio and Number of Turns on Pulsating Heat Pipe Thermal Performance,"* Frontiers in Heat Pipes (FHP), 6, 4 (2015) DOI: 10.5098/fhp.6.4.
14. Romain Bruce, Maria Barba, Antoine Bonelli and Bertrand Baudouy, *"Thermal Performance of a Meter-Scale Horizontal Nitrogen Pulsating Heat Pipe,"* Cryogenics 93 (2018) 66–74.
15. Yi Li, Qiuliang Wang, Shunzhong Chen, Baozhi Zhao and Yinming Dai, *"Experimental Investigation of the Characteristics of Cryogenic Oscillating Heat Pipe,"* International Journal of Heat and Mass Transfer 79 (2014) 713–719.
16. Luis Diego Fonseca, Franklin Miller and John Pfotenhauer, *"Design and Operation of a Cryogenic Nitrogen Pulsating Heat Pipe,"* IOP Conf. Series: Materials Science and Engineering 101 (2015) 012064 doi:10.1088/1757-899X/101/1/012064.
17. Kyohei Natsume, Toshiyuki Mito, Nagato Yanagi, Hitoshi Tamura, Tsutomu Tamada, Koji Shikimachi, Naoki Hirano, and Shigeo Nagaya, *"Heat Transfer Performance of Cryogenic Oscillating Heat Pipes for Effective Cooling of Superconducting Magnets,"* Cryogenics 51 (2011) 309–314.
18. *Cryogenic Pulsating Heat Pipes,* CEA, http://irfu.cea.fr/dap/en/Phocea/Vie_des_labos/Ast/ast_visu.php?id_ast=4679.
19. Qing Liang, Yi Lia and Qiuliang Wang, *"Effects of Filling Ratio and Condenser Temperature on the Thermal Performance of a Neon Cryogenic Oscillating Heat Pipe,"* Cryogenics 89 (2018) 102–106.
20. Monan Li, Laifeng Li and Dong Xu, *"Effect of Number of Turns and Configurations on the Heat Transfer Performance of Helium Cryogenic Pulsating Heat Pipe,"* Cryogenics 96 (2018) 159–165
21. A.J. Jiao, H.B. Ma, and J.K. Critser, *"Experimental Investigation of Cryogenic Oscillating Heat Pipes,"* International Journal of Heat and Mass Transfer 52 (2009) 3504–3509
22. https://www.lakeshore.com/products/categories/overview/temperature-products/cryogenic-accessories/varnish
23. https://www.ni.com/en-us/innovations/white-papers/06/pid-theory-explained.html
24. R. J. Corruccini, *"Gaseous Heat Conduction at Low Pressures and Temperatures,"* Vacuum, Vol. VII 6, VIII 1957-58.
25. T.S. Datta, *"Cryogenics Course Material,"* https://www.rrcat.gov.in/jas08/talk/Datta-3.pdf.
26. G. R. Cunnington, C. W. Keller, et al., *"Thermal Performance of Multilayer Insulations,"* Interim Report, LMSC-A903316/NASA CR-72605, Lockheed Missile and Space Company, Sunnyvale, CA, 1971.
27. C. W. Keller, G. R. Cunnington, et al., *"Thermal Performance of Multi-layer Insulations,"* Final Report, Contract NAS3-14377, Lockheed Missile and Space Company, Sunnyvale, CA, 1974.
28. G. E. McIntosh, *"Layer by Layer MLI Calculation using a Separated Mode Equation,"* Advances in Cryogenic Engineering, Vol 39B, Plenum Press, NY, 1993, pp. 1683-1690.

29. J. R. Feller and W. L. Johnson, *"Dependence of Multi-Layer Insulation Thermal Performance on Interstitial Gas Pressure,"* AIP Conference Proceedings **1434**, 47 (2012); https://doi.org/10.1063/1.4706904.
30. M. A. Hopcroft (2020), *"LVM file import,"* MATLAB Central File Exchange, Retrieved May 11, 2020; *https://www.mathworks.com/matlabcentral/fileexchange/19913-lvm-file-import*.
31. M. Barba, R. Bruce, F. Bouchet, A. Bonelli and B. Baudouy, *"Thermal Study of a One-Meter Long Neon Cryogenic Pulsating Heat Pipe,"* IOP Conf. Series: Materials Science and Engineering **502** (2019) 012152 IOP Publishing doi:10.1088/1757-899X/502/1/012152.
32. P. Gully, F. Bonnet, V. Nikolayev, N. Luchier and T.Q. Tran, *"Evaluation of the Vapor Thermodynamic State in PHP,"* 17th International Heat Pipe Conference, Kanpur, India, October 14-17, 2013.
33. Mauro Mameli, Marco Marengo, and Stefano Zinna, *"Thermal Simulation of a Pulsating Heat Pipe: Effects of Different Liquid Properties on a Simple Geometry,"* Heat Transfer Engineering Vol 33 no.14 2012.
34. P.Srikrishna et al, *"Experimental Investigation of a Single Closed Loop Pulsating Heat Pipe,"* Proceedings of the 24th National and 2nd International ISHMT-ASTFE Heat and Mass Transfer Conference (IHMTC-2017), December 27-30, 2017, BITS Pilani, Hyderabad, India.
35. Wei Shao and Yuwen Zhang, "*Effects of Film Evaporation and Condensation on Oscillatory Flow and Heat Transfer in an Oscillating Heat Pipe,"* Journal of Heat Transfer, DOI: 10.1115/1.4002780
36. Katpradit T, Wongratanaphisan T, Terdtoon P, Ritthidech S, Chareonsawan P, Waowaew S (2004), "*Effect of Aspect Ratios and Bond Number on Internal Flow Patterns of Closed End Oscillating Heat Pipe at Critical State*," 13th international heat pipe conference (13th IHPC), Shanghai, China, pp 298–303
37. Sung-Min Kim and Issam Mudawar, *"Theoretical Model for Local Heat Transfer Coefficient for Annular Flow Boiling in Circular Mini/Micro-Channels,"* International Journal of Heat and Mass Transfer 73 (2014) 731–742.
38. J.L. Xu, Y.X. Li and T.N. Wong, *"High Speed Flow Visualization of a Closed Loop Pulsating Heat Pipe,"* International Journal of Heat and Mass Transfer 48 (2005) 3338–3351.
39. Sameer Khandekar, Piyanun Charoensawan, Manfred Groll and Pradit Terdtoon, "*Closed Loop Pulsating Heat Pipes Part B: Visualization and Semi-empirical Modeling,"* Applied Thermal Engineering 23 (2003) 2021–2033.
40. A. Kalani and S.G. Kandlikar, "*Combining Liquid Inertia with Pressure Recovery from Bubble Expansion for Enhanced Flow Boiling,"* Applied Physics Letters 107, 181601 (2015); doi: 10.1063/1.4935211
41. L. Chen, Y.S. Tian, and T.G. Karayiannis, *"The Effect of Tube Diameter on Vertical Two-Phase Flow Regimes in Small Tubes,"* International Journal of Heat and Mass Transfer 49 (2006) 4220–4230

42. Hong Hu, Cheng Xu, Yang Zhao, Kirk J. Ziegler, and J. N. Chung, *"Boiling and Quenching Heat Transfer Advancement by Nanoscale Surface Modification,"* Scientific Reports | 7: *6117* | DOI:10.1038/s41598-017-06050-0.
43. K. Rama Narasimha, Sridhara S. N., Rajagopal M. S. and Seetharamu K. N., *"Parametric Studies on Pulsating Heat Pipe,"* International Journal of Numerical Methods for Heat and Fluid Flow; **Bradford** Vol. 20, Iss. 4, (2010): 392-415. DOI:10.1108/09615531011035802.
44. Eric W. Lemmon, Richard T Jacobsen, Steven G. Penoncello, and Daniel G. Friend, "*Thermodynamic Properties of Air and Mixtures of Nitrogen, Argon, and Oxygen From 60 to 2000 K at Pressures to 2000 MPa,"* Journal of Physical and Chemical Reference Data **29**, 331 (2000); https://doi.org/10.1063/1.1285884
45. Guilherme H.S. Oliveira, Tiago Augusto Moreira, Zahid H. Ayub, and Gherhardt *Ribatski, "Flow Boiling of Hydrocarbons and their Zeotropic Binary Mixtures under Pre- and Post-dryout Conditions,"* Applied Thermal Engineering 198 (2021) 117483
46. Rodrigo Barraza, Gregory Nellis, Sanford Klein, and Douglas Reindl, "*Measured and Predicted Heat Transfer Coefficients for Boiling Zeotropic Mixed Refrigerants in Horizontal Tubes*," International Journal of Heat and Mass Transfer 97 (2016) 683–695
47. Ali Habeeb Askar, Saif Ali Kadham, and Salah Hadi Mshehid, "*The Surfactants Effect on the Heat Transfer Enhancement and Stability of Nanofluid at Constant Wall Temperature*," Heliyon 6 (2020) e04419; https://doi.org/10.1016/j.heliyon.2020.e04419
48. Y. M. Qiao and S. Chandra, "*Experiments on Adding a Surfactant to Water Drops Boiling on a Hot Surface,"* Mathematical, Physical and Engineering Sciences, Apr. 8, 1997, Vol. 453, No. 1959 (Apr. 8, 1997), pp. 673-689
49. Stephan Karl, "*Heat Transfer in Condensation and Boiling: Multicomponent Mixtures,"* doi: 10.1615/AtoZ.m.multicomponent_mixtures_boiling_in
50. A. Rabah and S. Kabelac, "*Flow Boiling of R134a and R134a/Propane Mixtures at Low Saturation Temperatures Inside a Plain Horizontal Tube*," J. Heat Transfer. Jun 2008, 130(6): 061501, https://doi.org/10.1115/1.2897345

12 Appendix

12.1 Fill Ratio Calculation EES Code

```
Function x_php,int (x_php,int,x)
  If (x_php,int,x < 0) Then
    x_php,int := 0          Else
    If (x_php,int,x > 1) Then
      x_php,int := 1          Else
      x_php,int := x_php,int,x
    EndIf

End x_php,int

F$ = 'Air_ha'
G$ = 'Air'
        Volume Calculations
N_turn = 20 [-] number of turns
D_1 = 0.173 [in] · |0.0254 · m/in| inner diameter of (1/4)" swagelock staineless pipe
D_2 = 0.275 [in] · |0.0254 · m/in| inner diameter large top tee connected to nitrogen main tank
D_3 = 0.125 [in] · |0.0254 · m/in| inner diameter of (1/8)" swagelock staineless pipe
D_4 = 0.02 [in] · |0.0254 · m/in| inner diameter of capillary pipe
D_5 = 0.035 [in] · |0.0254 · m/in| inner diameter of copper tee
L_1 = 3 [in] · |0.0254 · m/in| length of large top tee connected to nitrogen main tank
L_2 = 27.25 [in] · |0.0254 · m/in| length from large tee to valve 3 (valve 2 closed)
L_3 = 4 [in] · |0.0254 · m/in| length of swagelock (1/4)" stainless pipe from valve 2 to Holding Tank
L_4 = 10.375 [in] · |0.0254 · m/in| length of swagelock (1/4)" stainless pipe from valve 3 to underside of Dewar cover
L_5 = 13.375 [in] · |0.0254 · m/in| length of swagelock (1/8)" stainless pipe from valve 3 to underside of Dewar cover
```

$L_6 = 11\ [in] \cdot \left| 0.0254 \cdot \frac{m}{in} \right|$ *length of swagelock (1/8)" stainless pipe inside Dewar*

$L_7 = (340.625\ [in] - 297\ [in] + 15\ [in] \cdot 38) \cdot \left| 0.0254 \cdot \frac{m}{in} \right|$ *length of capillary pipe inside dewar*

$L_8 = 68.5\ [in] \cdot \left| 0.0254 \cdot \frac{m}{in} \right|$ *length of copper tees inside dewar*

$V_{Htank} = 3.6\ [liters] \cdot \left| 0.001 \cdot \frac{m^3}{liters} \right|$ *volume of black holding tank*

$V_1 = 3.142 \cdot D_2^2 \cdot \frac{L_1}{4} + 3.142 \cdot D_1^2 \cdot \frac{L_2}{4}$ *volume from valve 1 to 3 with valve 2 closed*

$V_2 = 3.142 \cdot D_1^2 \cdot \frac{L_3}{4} + V_{Htank}$ *volume from valve 2 to end of holding tank*

$V_3 = 3.142 \cdot D_1^2 \cdot \frac{L_4}{4} + 3.142 \cdot D_3^2 \cdot \frac{L_5}{4}$ *volume from valve 3 to dewar inlet*

$V_4 = 3.142 \cdot D_3^2 \cdot \frac{L_6}{4} + 3.142 \cdot D_4^2 \cdot \frac{L_7}{4} + 3.142 \cdot D_5^2 \cdot \frac{L_8}{4}$ *volume of capillary tubes, tees and 1/8 inch inside dewar*

calculating mass that leaves holding tank

$V_{holding} = V_1 + V_2$

$P_{tank,1} = P_{start}$

$P_{tank,2} = P_{close}$

$T_{tank} = T_{amb}$

$T_{amb} = \mathbf{ConvertTemp}(C, K, 24.9\ [C])$

$R = \frac{8314\ [J/kmol\text{-}K]}{\mathbf{MolarMass}(F\$)}$

$m_{out} = (P_{tank,1} - P_{tank,2}) \cdot \frac{V_{holding}}{R \cdot T_{tank}}$

saturated vapor assumption

$T_{top} = \frac{T_{amb} + T_{sat}}{2}$ *average temperature*

$P_{top} = \mathbf{P}(F\$, T = T_{sat}, x = 1)$

$Vol_{top} = V_3$ *volume at the top*

$m_{top} = \frac{P_{top} \cdot Vol_{top}}{R \cdot T_{top}}$ *saturated mass at the top*

PHP 2 phase assumption

$m_{php} = m_{out} - m_{top} + m_{res}$ *mass left at the bottom*

$Vol_{Php} = V_4$ *volume of PHP*

$v_{php} = \frac{Vol_{Php}}{m_{php}}$ *specific volume inside PHP*

$x_{php} = \mathbf{x}(F\$, T = T_{sat}, v = v_{php})$ *quality of nitrogen inside php*

$u_{php} = \mathbf{u}(F\$, T = T_{sat}, v = v_{php})$ *quality of nitrogen inside php*

$Fill_{ratio} = \frac{(1 - x_{php}) \cdot v_f \cdot m_{php}}{Vol_{Php}}$ *$fill_{ratio}$*

$v_f = \mathbf{v}(F\$, T = T_{sat}, x = 0)$ *saturated liquid at T_{sat}*

$m_{res} = 0$

$P_{res} = 4.9\ [psi] \cdot \left| 6895 \cdot \frac{Pa}{psi} \right|$

variables

$T_{sat} = 77\ [K]$

$P_{start} = P_{start,g} + P_{std}$

$P_{close} = P_{close,g} + P_{std}$

$P_{start,g} = 47.5\ [psi] \cdot \left| 6895 \cdot \frac{Pa}{psi} \right|$

$DP = P_{start,g} - P_{close,g}$

$P_{std} = 14.5\ [psi] \cdot \left| 6895 \cdot \frac{Pa}{psi} \right|$

$Fill_{ratio} = 0.5\ [-]$

$T_{crit} = \mathbf{T}_{Crit}(F\$)$

$Nac = N_{turn} \cdot 3.142 \cdot \frac{D_4^2}{4}$

$v_1 = v_{php}$

$T_1 = T_{sat}$

$v_{c,1} = \mathbf{v}_{Crit}(F\$)$

left-over mass

Fig 12-I EES Script for fill ratio calculation

12.2 MATLAB code to read LabVIEW text file

```
clear
close all
file = lvm_import('p8pt2.lvm',2);                                   %extract lvm data
full_data = file.Segment2.data;                                     %extract DAQs dat
a
time = full_data(:,1);                                              %time logged in s
econds
real_time = file.Time;                                              %start time of da
ta acquisition
date = file.Segment2.Comment{1,1};                                  %array of date &
time in string format
cond_temp = full_data(:,2);                                         %condenser temper
atures
evap_temp = full_data(:,3);                                         %evaporator tempe
ratures
adiab_temp = full_data(:,5);                                        %adiabatic top te
mperature
%date_file =file.Date;                                               %start date of d
ata acquisition
pressure = full_data(:,9);
power = full_data(:,8);

% figure(1)
% yyaxis left
% plot(time,cond_temp)
% hold on
% plot(time,evap_temp)
% plot(time,adiab_temp)
% yyaxis right
% plot(time,power)
% grid on



%xtickformat('hh:mm:ss')
% h = hour(real_time);                                                %extract initia
l time hour
% m = minute(real_time);                                              %extract initia
l time minute
% s= second(real_time);                                               %extract initia
l time seconds
tic
%h = hour(date);                                                  %extract initial time
 hour
%m = minute(date);                                                %extract initial time
 minute
%s= second(date);                                                 %extract initial time
 seconds
% y=year(date_file);                                                %extract initia
l year of data acquisition
% month=month(date_file);                                           %extract initia
l month of data acquisition
% day=day(date_file);                                               %extract initia
l day of data acquisition
%y=year(date);                                                    %extract initial year
```

```
 of data acquisition
%month=month(date);                                          %extract initial mont
h of data acquisition
%day=day(date);                                              %extract initial day
of data acquisition
%d = datetime(y,month,day,h,m,s);                                 %compile initial
 date & time
%time_array = datetime(d+seconds(time));                          %compile running
 time (time array)
%time_array = d;

time_array = datetime(date);

%make plots
yyaxis left
plot(time_array,cond_temp,'b')
hold on
plot(time_array,evap_temp,'-r')
plot(time_array,adiab_temp,'-m')
xlabel('Time[hours/days]')
ylabel('Temperature[K]')
set(gca,'YMinorTick','on','ycolor','k')
grid('minor')
grid on
yyaxis right
plot(time_array,power,'g')
ylim([0 10]);
ylabel('Heat Load[W]')
legend('Condenser Temperature','Evaporator Temperature','Adiabatic temperature','Heat Load','
location','northeast')
legend('boxoff')
set(gca,'YMinorTick','on','ycolor','k')




figure(2)
yyaxis left
plot(time_array,pressure,'b')
hold on
xlabel('Time[hours/days]')
ylabel('Pressure[psia]')
set(gca,'YMinorTick','on','ycolor','k')
grid('minor')
grid on
grid on
yyaxis right
plot(time_array,power,'g')
ylim([0 10]);
ylabel('Heat Load[W]')
legend('Pressure','Heat Load','location','northeast')
legend('boxoff')
set(gca,'YMinorTick','on','ycolor','k')

n=1;
m = 2500;
```

```
% T_cond_avg = mean(cond_temp(n:m))
% T_evap_avg = mean(evap_temp(n:m))
% T_adiab_avg = mean(adiab_temp(n:m))
% P_avg = mean(pressure(n:m))

T_cond_avg = mean(cond_temp(n:end))
T_evap_avg = mean(evap_temp(n:end))
T_adiab_avg = mean(adiab_temp(n:end))
P_avg = mean(pressure(n:end))

% T_evap_max = max(evap_temp)
% T_evap_min = min(evap_temp)

T_cond_mean = mean(cond_temp(n:m))
T_evap_mean = mean(evap_temp(n:m))
T_adiab_mean = mean(adiab_temp(n:m))
P_mean = mean(pressure(n:m))

% Ps = polyfit(time(n:m),pressure(n:m),20);
% Psv = polyval(Ps,time(n:m));
%
%  [~,peaklocs] = findpeaks(pressure(n:m));
%  period = mean(diff(peaklocs)); % peaks may not be exactly periodic, so take mean

figure(3)
yyaxis left
plot(time_array(n:m),pressure(n:m),'b')
% hold on
% plot(time_array(n:m),Psv(n:m),'r')
% xlabel('Time[hours/days]')
% ylabel('Pressure[psia]')
set(gca,'YMinorTick','on','ycolor','k')
grid('minor')
grid on
grid on
yyaxis right
plot(time_array(n:m),power(n:m),'g')
ylim([0 10]);
ylabel('Heat Load[W]')
legend('Pressure','Heat Load','location','northeast')
legend('boxoff')
set(gca,'YMinorTick','on','ycolor','k')

figure(4)
yyaxis left
plot(time_array(n:m),cond_temp(n:m),'b')
hold on
plot(time_array(n:m),evap_temp(n:m),'-r')
plot(time_array(n:m),adiab_temp(n:m),'-m')
xlabel('Time[hours/days]')
ylabel('Temperature[K]')
set(gca,'YMinorTick','on','ycolor','k')
grid('minor')
grid on
yyaxis right
plot(time_array(n:m),power(n:m),'g')
```

```
ylim([0 10]);
ylabel('Heat Load[W]')
legend('Condenser Temperature','Evaporator Temperature','Adiabatic temperature','Heat Load','
location','northeast')
legend('boxoff')
set(gca,'YMinorTick','on','ycolor','k')

% yy =fft(pressure);
% Ts = 1;
% fs = 1/Ts;
% fs=180;
% f=(0:length(yy)-1)*fs/length(yy);
%
% figure(5)
% plot(f,abs(yy))
% xlabel('Frequency (Hz)')
% ylabel('Magnitude')
%title('Magnitude

Pt = pressure(n:m)-P_mean ;
Pf = fft(Pt);
Pf_mag = abs(Pf);
N  = length(Pt);
fs = 1;
fax_bins = 0 : N-1;
fax_Hz = fax_bins*fs/N;
N_2 = ceil(N/2);

Iv = 1:numel(fax_Hz);                    %Index vector
IV = Iv-mean(Iv);
FTsiga = double(Pf_mag(Iv)*2);    %Magnitude,Convert to double
%S_smth = sgolayfilt(FTsiga,16,249);  %Savitzky-Golay filtering of FFT

figure(5)
%plot(fax_bins, Pf_mag)
plot(fax_Hz(1:N_2),(Pf_mag(1:N_2)/N))
%semilogx(fax_Hz(1:N_2), Pf_mag(1:N_2))
xlabel('Frequency (Hz)')
ylabel('Magnitude');
title('Single-sided Magnitude spectrum (Hertz)');
axis tight
ylim([0 0.5]);
xlim([-0.1 0.5]);
grid on
% hold on
% plot(fax_Hz(1:N_2), S_smth(1:N_2))



% filename = 'pressureplot.xlsx';
% xlswrite(filename,time(n:m),1,'A1');
% xlswrite(filename,pressure(n:m),1,'B1');

 filename = 'frequencyplot.xlsx';
xlswrite(filename,fax_Hz(1:N_2)',1,'A1');
xlswrite(filename,(Pf_mag(1:N_2)/N),1,'B1');
```

Fig 12-II MATLAB script to read LabVIEW data and plot variables

12.3 LabVIEW VI Macro

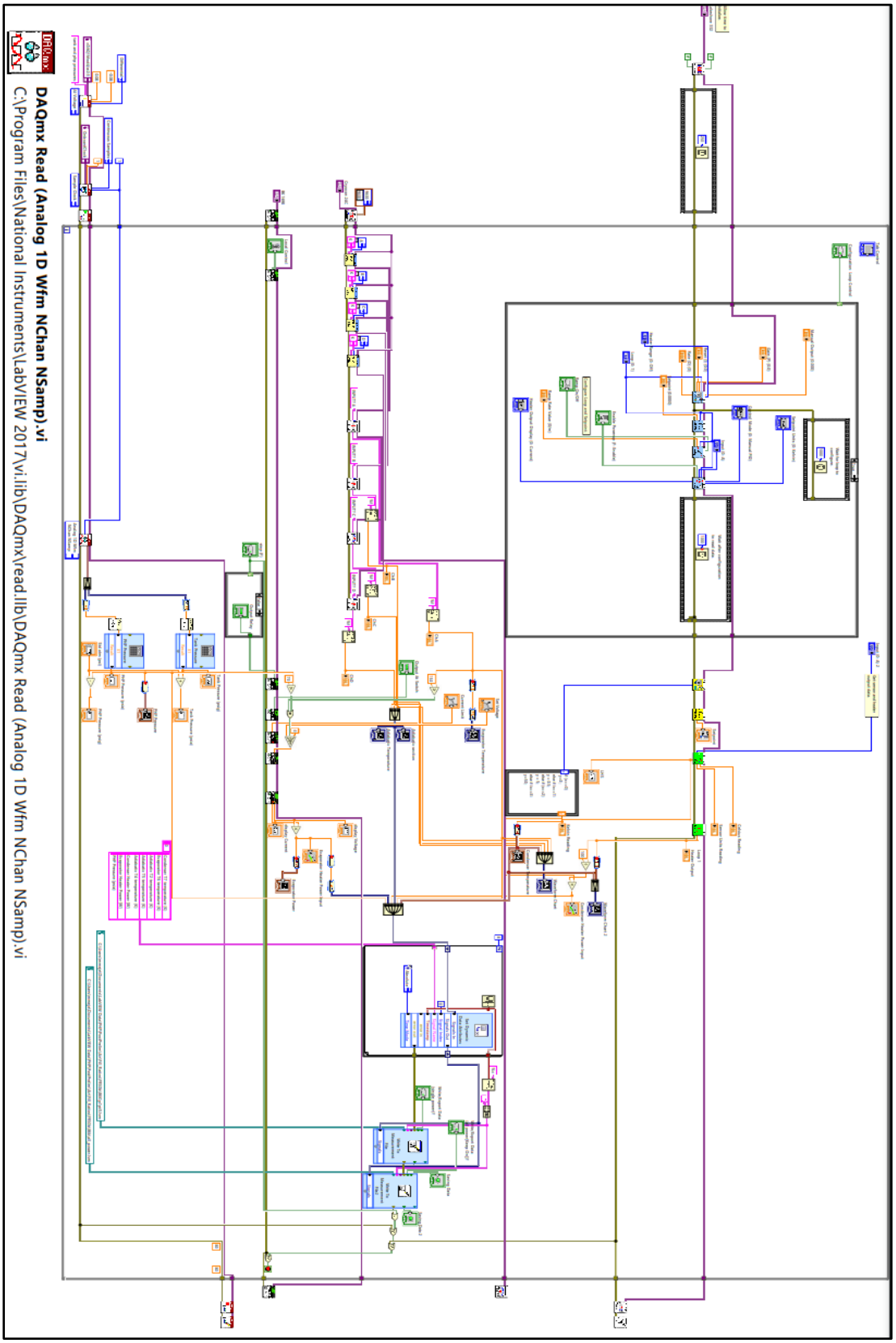

GetSetShared.lvlib:TimeType.ctl
C:\Program Files\National Instruments\LabVIEW 2017\vi.lib\express\express signal manip\GetorSetDDTAttributes\Shared VIs\TimeType.ctl

Lake Shore Cryotronics 332.lvlib:Data Heater Output.vi
C:\Program Files\National Instruments\LabVIEW 2017\instr.lib\Lake Shore Cryotronics 332\Public\Data\Data Heater Output.vi

Lake Shore Cryotronics 332.lvlib:Data Sensor.vi
C:\Program Files\National Instruments\LabVIEW 2017\instr.lib\Lake Shore Cryotronics 332\Public\Data\Data Sensor.vi

Lake Shore Cryotronics 332.lvlib:Setpoint.vi
C:\Program Files\National Instruments\LabVIEW 2017\instr.lib\Lake Shore Cryotronics 332\Public\Action-Status\Setpoint.vi

Lake Shore Cryotronics 332.lvlib:Control Parameters.vi
C:\Program Files\National Instruments\LabVIEW 2017\instr.lib\Lake Shore Cryotronics 332\Public\Action-Status\Control Parameters.vi

Lake Shore Cryotronics 332.lvlib:Config Control Mode.vi
C:\Program Files\National Instruments\LabVIEW 2017\instr.lib\Lake Shore Cryotronics 332\Public\Configure\Config Control Mode.vi

Set Voltage.vi
C:\Users\mmeje\Desktop\169x_software\LabVIEW Driver\SDP.llb\Set Voltage.vi

Lake Shore Cryotronics 332.lvlib:Config Ramp.vi
C:\Program Files\National Instruments\LabVIEW 2017\instr.lib\Lake Shore Cryotronics 332\Public\Configure\Config Ramp.vi

Lake Shore Cryotronics 332.lvlib:Config Setpoint.vi
C:\Program Files\National Instruments\LabVIEW 2017\instr.lib\Lake Shore Cryotronics 332\Public\Configure\Config Setpoint.vi

Lake Shore Cryotronics 332.lvlib:Config Control Parameters.vi
C:\Program Files\National Instruments\LabVIEW 2017\instr.lib\Lake Shore Cryotronics 332\Public\Configure\Config Control Parameters.vi

Get Voltage and Current.vi
C:\Users\mmeje\Desktop\169x_software\LabVIEW Driver\SDP.llb\Get Voltage and Current.vi

Waveform Array To Dynamic.vi
C:\Program Files\National Instruments\LabVIEW 2017\vi.lib\express\express shared\transition.llb\Waveform Array To Dynamic.vi

CC_IO.vi
C:\Program Files\National Instruments\LabVIEW 2017\instr.lib\CustomerCD12\Model24C\M24C_LV16\M24CU.llb\CC_IO.vi

Input_Units.vi
C:\Program Files\National Instruments\LabVIEW 2017\instr.lib\CustomerCD12\Model24C\M24C_LV16\M24C.llb\Input_Units.vi

ex_Modify Signal Name.vi
C:\Program Files\National Instruments\LabVIEW 2017\vi.lib\express\express shared\ex_Modify Signal Name.vi

exnFormulaBlock how many pts in the wave.vi
C:\Program Files\National Instruments\LabVIEW 2017\vi.lib\express\express arith-compare\Formula\Block\exnFormulaBlock how many pts in the wave.vi

Simple Error Handler.vi
C:\Program Files\National Instruments\LabVIEW 2017\vi.lib\Utility\error.llb\Simple Error Handler.vi

DAQmx Clear Task.vi
C:\Program Files\National Instruments\LabVIEW 2017\vi.lib\DAQmx\configure\task.llb\DAQmx Clear Task.vi

Lake Shore Cryotronics 332.lvlib:Close.vi
C:\Program Files\National Instruments\LabVIEW 2017\instr.lib\Lake Shore Cryotronics 332\Public\Close.vi

DAQmx Fill In Error Info.vi
C:\Program Files\National Instruments\LabVIEW 2017\vi.lib\DAQmx\miscellaneous.llb\DAQmx Fill In Error Info.vi

DAQmx Stop Task.vi
C:\Program Files\National Instruments\LabVIEW 2017\vi.lib\DAQmx\configure\task.llb\DAQmx Stop Task.vi

Stop Program.vi
C:\Users\mmeje\Desktop\169x_software\LabVIEW Driver\SDP.llb\Stop Program.vi

CC_Close.vi
C:\Program Files\National Instruments\LabVIEW 2017\instr.lib\CustomerCD12\Model24C\M24C_LV16\M24CU.llb\CC_Close.vi

ex_subFileWrite.vi
C:\Program Files\National Instruments\LabVIEW 2017\vi.lib\express\express output\ExFileWriteBlock.llb\ex_subFileWrite.vi

ex_propertySource.ctl
C:\Program Files\National Instruments\LabVIEW 2017\vi.lib\express\express shared\ExFile.llb\ex_propertySource.ctl

ex_userDefProperty.ctl
C:\Program Files\National Instruments\LabVIEW 2017\vi.lib\express\express shared\ExFile.llb\ex_userDefProperty.ctl

usiDataType.ctl
C:\Program Files\National Instruments\LabVIEW 2017\vi.lib\express\express shared\ex_EditUserDefinedProperties\usiDataType.ctl

NI_AALBase.lvlib:Mean.vi
C:\Program Files\National Instruments\LabVIEW 2017\vi.lib\Analysis\baseanly.llb\Mean.vi

Dynamic To Waveform Array.vi
C:\Program Files\National Instruments\LabVIEW 2017\vi.lib\express\express shared\transition.llb\Dynamic To Waveform Array.vi

ex_FileFormats.ctl
C:\Program Files\National Instruments\LabVIEW 2017\vi.lib\express\express shared\ExFile.llb\ex_FileFormats.ctl

SetT0.vi
C:\Program Files\National Instruments\LabVIEW 2017\vi.lib\express\express signal manip\GetorSetDDTAttributes\Set DDT Attributes\SetT0.vi

GetSetShared.lvlib:TimeMode Enum to Boolean.vi
C:\Program Files\National Instruments\LabVIEW 2017\vi.lib\express\express signal manip\GetorSetDDTAttributes\Shared VIs\TimeMode Enum to Boolean.vi

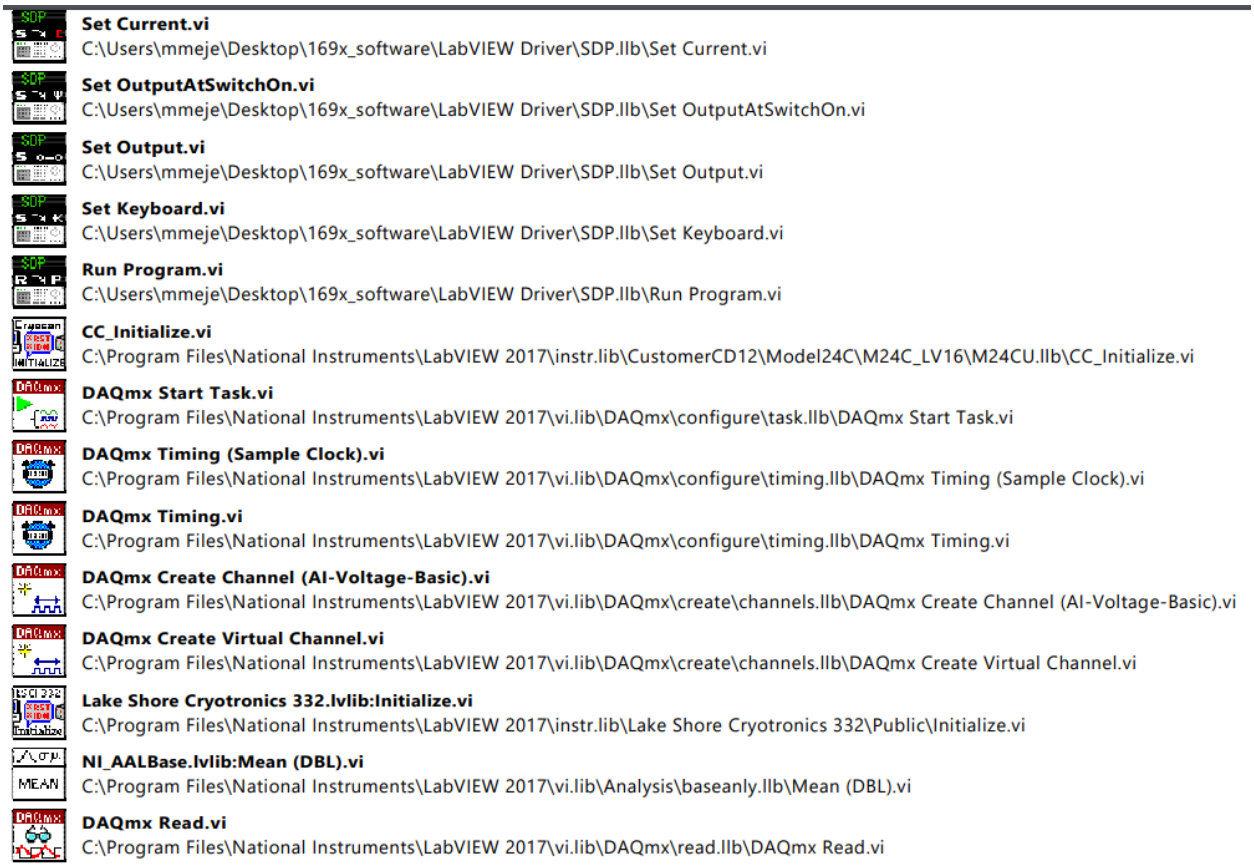

Fig 12-III LabVIEW Macro for the experiment and list of used VIs in data collection

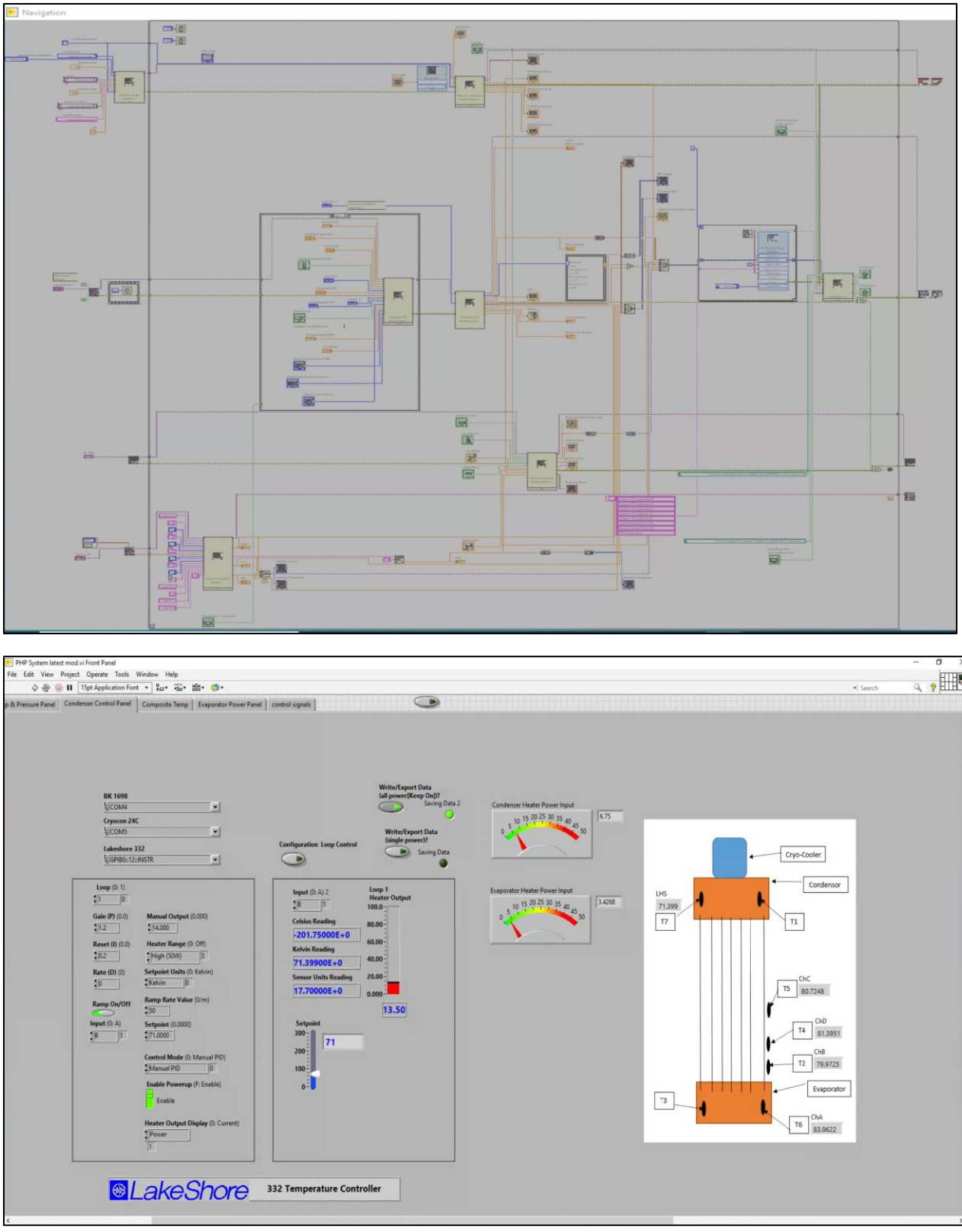

Fig 12-IV Screenshots of the PHP LabVIEW Environment (Top: Block diagram; Bottom: a section of the Front Panel)

12.4 Pressure calibration curves

Date	6/14/2020		Time	11.36am		Pressure relief Test	90 psia
std atm	14.4 psi						
Temp	23.5 C						

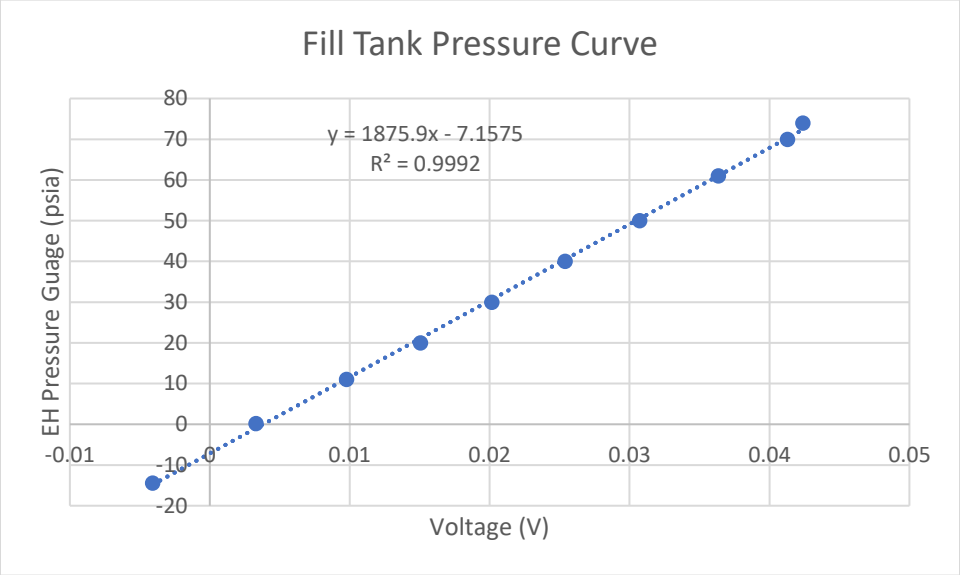

(a)

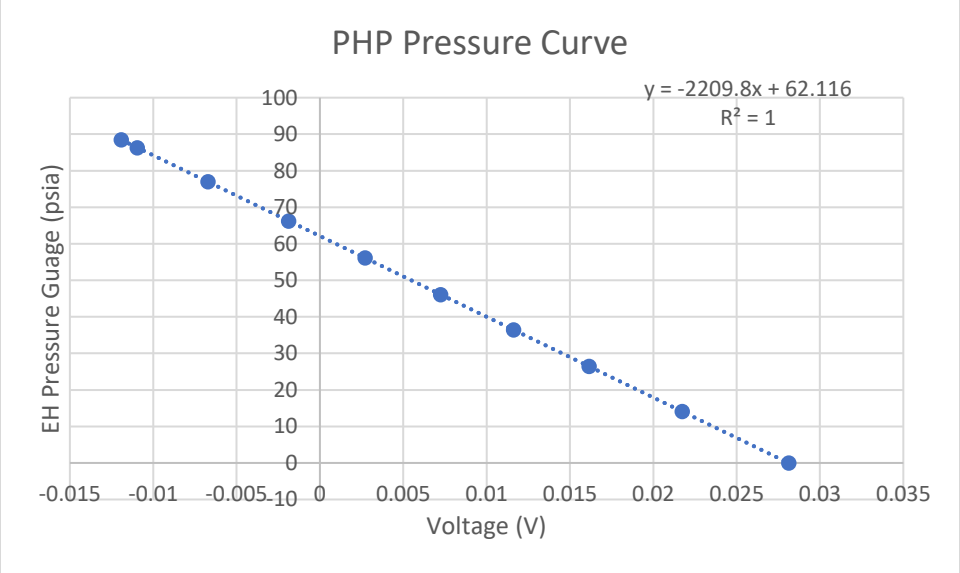

(b)

Date	3/23/2021
std atm	14.1 psi
Temp	23.5 C

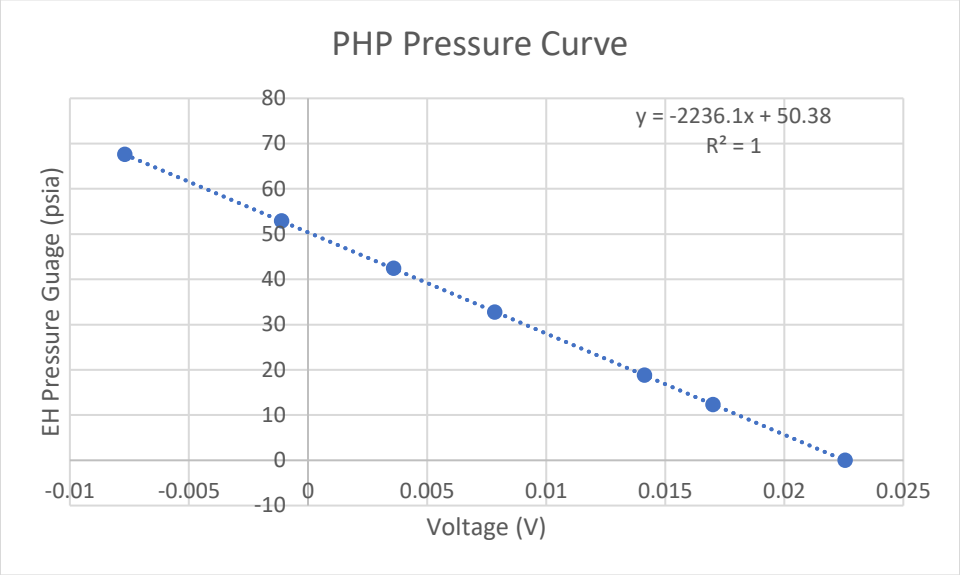

(c)

Fig 12-V Pressure calibration curve for (a) Fill tank sensor (b) PHP sensor (c) PHP sensor (previous calibration)

Accuracy Measurement

$$\varphi_0 = \frac{P_1 - P_2}{P_1} * 100\% = \frac{62.116 - 50.38}{62.116} * 100\% = 18\% \qquad (12.1)$$

φ_0 = accuracy at zero voltage

P_1 = pressure value of new calibration

P_2 = pressure value of old calibration

12.5 PHP Condenser Cooling Curve: No Fluid

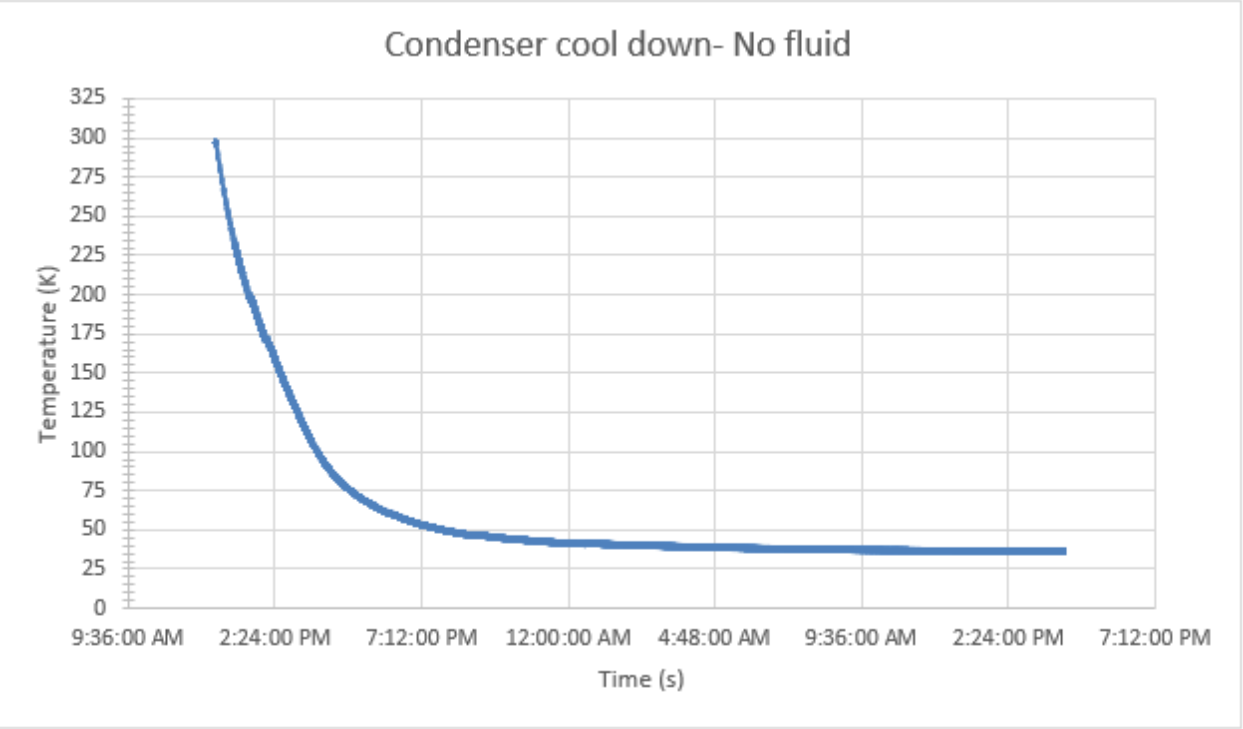

Fig 12-VI Cool down curve for the PHP when empty

12.6 Performance Maps Polyfits

12.6.1 Nitrogen

x = Power (Heat Load)

	15.5% Fill Ratio	
Condenser Temperature	Temperature Difference (T_{evap} - T_{cond}) Curve	RMS
71K	$-1.2467x^3 + 5.9x^2 - 2.9633x + 2.07$	1
73K	$-0.5816x^4 + 4.1464x^3 - 8.3379x^2 + 6.5431x + 2.01$	1
75K	$-0.6633x^3 + 3.1068x^2 - 0.0445x + 1.8262$	0.9693
77K	$-0.0094x^5 + 0.1158x^4 - 0.4581x^3 + 0.5534x^2 + 1.4981x + 1.94$	0.9999
79K	$1.0321x^3 - 4.2301x^2 + 5.3982x + 1.7664$	0.9289
81K	$1.3306x^3 - 5.399x^2 + 6.5076x + 1.5884$	0.8402
83K	$0.0633x^3 - 0.435x^2 + 2.1517x + 1.74$	1

	24.8% Fill Ratio	
Condenser Temperature	Temperature Difference (T_{evap} - T_{cond}) Curve	RMS
71K	$0.0604x^4 - 0.1675x^3 - 0.1954x^2 + 2.0325x + 2.2$	1
73K	$-0.0614x^5 + 0.7933x^4 - 3.2429x^3 + 5.0117x^2 - 0.9907x + 2.11$	1
75K	$-0.0505x^5 + 0.8013x^4 - 3.9679x^3 + 7.3539x^2 - 2.9126x + 1.9656$	0.9922
77K	$-0.0094x^5 + 0.1158x^4 - 0.4581x^3 + 0.5534x^2 + 1.4981x + 1.94$	0.9953
79K	$0.0025x^6 - 0.033x^5 + 0.1345x^4 - 0.0763x^3 - 0.6153x^2 + 1.952x + 1.9895$	0.9995
81K	$0.0005x^6 - 0.0186x^5 + 0.1803x^4 - 0.6939x^3 + 1.0448x^2 + 0.6441x + 1.8303$	0.9987
83K	$-0.0029x^6 + 0.0415x^5 - 0.2165x^4 + 0.499x^3 - 0.5586x^2 + 1.4285x + 1.7499$	0.9998

	30.8% Fill Ratio	
Condenser Temperature	Temperature Difference (T_{evap} - T_{cond}) Curve	RMS
71K	$0.1154x^4 - 0.4792x^3 - 0.2304x^2 + 3.6842x + 2.11$	1
73K	$0.1477x^5 - 1.5167x^4 + 5.5629x^3 - 9.0383x^2 + 7.7243x + 2.07$	1
75K	$0.1268x^5 - 1.3429x^4 + 5.1283x^3 - 8.6871x^2 + 7.4948x + 2.04$	1
77K	$-0.0029x^6 + 0.0584x^5 - 0.4386x^4 + 1.6279x^3 - 3.3437x^2 + 4.7594x + 1.95$	1
79K	$0.0026x^6 - 0.0431x^5 + 0.2529x^4 - 0.5043x^3 - 0.477x^2 + 3.4857x + 1.8492$	0.9996
81K	$0.0056x^6 - 0.0916x^5 + 0.5484x^4 - 1.3563x^3 + 0.7011x^2 + 2.831x + 1.789$	0.9986
83K	$0.0148x^6 - 0.2418x^5 + 1.4837x^4 - 4.0997x^3 + 4.4569x^2 + 0.9005x + 1.7895$	0.9973

	40% Fill Ratio	
Condenser Temperature	Temperature Difference (T_{evap} - T_{cond}) Curve	RMS
71K		
73K	$0.1724x^6 - 1.5067x^5 + 4.7778x^4 - 6.4567x^3 + 3.0748x^2 + 1.8683x + 2.08$	1
75K	$0.0088x^6 - 0.1154x^5 + 0.4889x^4 - 0.5383x^3 - 0.9723x^2 + 3.2193x + 2.1093$	0.9979
77K	$-0.0031x^6 + 0.0616x^5 - 0.4524x^4 + 1.5029x^3 - 2.2415x^2 + 2.734x + 2.0829$	0.9954
79K	$0.0014x^6 - 0.0199x^5 + 0.0857x^4 - 0.0317x^3 - 0.5256x^2 + 2.2398x + 1.9437$	0.9966

81K	$-0.0031x^6 + 0.0651x^5 - 0.5253x^4 + 2.0706x^3 - 4.0418x^2 + 4.5336x + 1.8638$	0.9972
83K	$0.0028x^6 - 0.0465x^5 + 0.2713x^4 - 0.6257x^3 + 0.2782x^2 + 1.8852x + 1.9434$	0.9929

	45% Fill Ratio	
Condenser Temperature	Temperature Difference (T_{evap} - T_{cond}) Curve	RMS
71K	$-0.0042x^6 + 0.0926x^5 - 0.7385x^4 + 2.5883x^3 - 3.9475x^2 + 4.3428x + 2.3435$	0.994
73K	$0.0115x^6 - 0.1845x^5 + 1.1154x^4 - 3.0761x^3 + 3.4706x^2 + 1.049x + 2.5257$	0.9838
75K	$-0.0276x^6 + 0.4774x^5 - 3.0732x^4 + 9.188x^3 - 12.773x^2 + 8.2776x + 2.0865$	0.9969
77K	$0.0251x^5 - 0.2132x^4 + 0.6893x^3 - 1.3018x^2 + 2.937x + 2.3192$	0.9967
79K	$-0.0099x^5 + 0.1394x^4 - 0.4935x^3 + 0.2317x^2 + 2.2105x + 1.8629$	0.9967
81K	$-0.0217x^4 + 0.3043x^3 - 1.0978x^2 + 2.7181x + 1.8911$	1
83K	$0.0468x^5 - 0.4909x^4 + 1.907x^3 - 3.246x^2 + 3.4373x + 1.8795$	0.9966

	52% Fill Ratio	
Condenser Temperature	Temperature Difference (T_{evap} - T_{cond}) Curve	RMS
71K	$0.001x^6 - 0.0297x^5 + 0.2912x^4 - 1.1388x^3 + 1.4114x^2 + 2.7915x + 2.2771$	0.9763
73K	$0.0744x^6 - 0.9401x^5 + 4.3723x^4 - 8.9868x^3 + 7.5866x^2 + 0.2459x + 2.3298$	0.9492
75K	$-0.0756x^5 + 0.8813x^4 - 3.0924x^3 + 3.52x^2 + 1.1383x + 2.1809$	0.9799
77K	$1.0387x^3 - 4.458x^2 + 6.6264x + 2.2409$	0.892
79K	$-0.0108x^4 + 0.198x^3 - 0.9235x^2 + 2.9541x + 2.0502$	0.9979
81K	$-0.2467x^4 + 1.8678x^3 - 4.0119x^2 + 4.5229x + 2.1501$	0.9997
83K	$0.2229x^2 + 1.9672x + 2.0318$	0.9044

12.6.2 Argon

x = Power (Heat Load)

	20% Fill Ratio	
Condenser Temperature	Temperature Difference (T_{evap} - T_{cond}) Curve	RMS
86K	$0.0122x^5 - 0.1732x^4 + 0.9462x^3 - 2.195x^2 + 2.8951x + 1.0246$	0.9541

89K	$0.0829x^5 - 1.133x^4 + 5.3969x^3 - 10.537x^2 + 8.1589x + 1.1802$	0.938
92K	$0.0015x^6 - 0.0285x^5 + 0.2147x^4 - 0.7694x^3 + 1.1536x^2 + 0.4711x + 1.6807$	0.9999
95K	$-0.0034x^6 + 0.0516x^5 - 0.283x^4 + 0.6728x^3 - 0.7615x^2 + 1.3666x + 1.6323$	0.9973
98K	$-0.0116x^6 + 0.0959x^5 - 0.2397x^4 + 0.1184x^3 + 0.0894x^2 + 1.0156x + 1.6709$	0.9996
101K	$0.5147x^5 - 3.1673x^4 + 6.6136x^3 - 5.387x^2 + 2.5699x + 1.5867$	0.9937

	30% Fill Ratio	
Condenser Temperature	Temperature Difference (T_{evap} - T_{cond}) Curve	RMS
86K	$-0.0002x^6 - 0.0058x^5 + 0.2103x^4 - 1.775x^3 + 5.1349x^2 - 2.5584x + 2.0955$	0.9235
89K	$-0.006x^6 + 0.1533x^5 - 1.4443x^4 + 6.1597x^3 - 11.717x^2 + 8.9276x + 1.1751$	0.9624
92K	$0.0002x^6 - 0.0041x^5 + 0.0411x^4 - 0.1816x^3 + 0.2738x^2 + 0.8374x + 1.7784$	0.9929
95K	$-4E\text{-}05x^6 + 0.0014x^5 - 0.014x^4 + 0.0399x^3 - 0.0259x^2 + 0.8526x + 1.7124$	0.9945
98K	$0.0011x^6 - 0.0183x^5 + 0.1151x^4 - 0.3184x^3 + 0.3329x^2 + 0.769x + 1.7102$	0.9985
101K	$0.0037x^6 - 0.0517x^5 + 0.2571x^4 - 0.5497x^3 + 0.448x^2 + 0.7513x + 1.6862$	0.9994

12.6.3 Air

x = Power (Heat Load)

	20% Fill Ratio	
Condenser Temperature	Temperature Difference (T_{evap} - T_{cond}) Curve	RMS
63K	$-8.94x^4 + 27.78x^3 - 22.665x^2 + 9.445x + 4.63$	1
65K	$4.2133x^5 - 27.493x^4 + 63.547x^3 - 60.887x^2 + 23.11x + 3.65$	1
71K	$0.0104x^6 - 0.1697x^5 + 1.0874x^4 - 3.2487x^3 + 3.9428x^2 + 0.6861x + 5.4104$	0.944
77K	$-0.0024x^6 + 0.0383x^5 - 0.192x^4 + 0.2631x^3 + 0.2373x^2 + 1.1702x + 4.1519$	0.9916
79K	$-0.0265x^6 + 0.505x^5 - 3.5251x^4 + 11.188x^3 - 16.166x^2 + 10.225x + 3.9819$	0.981
86K	$-0.0332x^6 + 0.4167x^5 - 1.798x^4 + 3.2506x^3 - 2.5757x^2 + 2.6862x + 4.1659$	0.9683

	30% Fill Ratio	

Condenser Temperature	Temperature Difference (T_{evap} - T_{cond}) Curve	RMS
63K	$2.1767x^4 - 12.131x^3 + 20.996x^2 - 7.2598x + 5.9202$	0.994
65K	$-0.2813x^5 + 2.6479x^4 - 8.938x^3 + 12.245x^2 - 1.6394x + 4.08$	0.9905
71K	$-0.0156x^6 + 0.2989x^5 - 2.0374x^4 + 6.347x^3 - 9.6029x^2 + 8.4329x + 4.592$	0.9958
77K	$-0.0345x^5 + 0.5001x^4 - 2.2272x^3 + 3.3483x^2 + 0.6034x + 4.8004$	0.8934
79K	$0.0197x^6 - 0.4189x^5 + 3.269x^4 - 11.211x^3 + 16.059x^2 - 5.6107x + 5.0348$	0.9827
86K	$-0.0435x^6 + 0.7481x^5 - 4.6437x^4 + 12.902x^3 - 15.874x^2 + 8.2029x + 4.2731$	0.9877

	40% Fill Ratio	
Condenser Temperature	Temperature Difference (T_{evap} - T_{cond}) Curve	RMS
63K	$0.5x^4 - 4.7933x^3 + 10.335x^2 - 0.9117x + 4.24$	1
65K	$1.152x^5 - 7.9982x^4 + 18.942x^3 - 18.457x^2 + 10.246x + 5.3753$	0.9889
71K	$-0.0036x^6 - 0.0504x^5 + 1.0118x^4 - 4.4709x^3 + 6.9181x^2 - 1.509x + 6.177$	0.9732
77K	$0.2107x^6 - 1.8389x^5 + 5.8551x^4 - 8.4563x^3 + 5.526x^2 + 0.9168x + 4.3032$	0.9968
79K		
86K		

Table 12.1 Polynomial fit tables for performance maps

12.7 Velocity estimate for fluid inside PHP

$$u_l = \frac{(1-x)v_l G}{1-\alpha} \tag{12.2}$$

$$\alpha = \left(1 + \left[\frac{1-x}{x}\right]\left[\frac{\rho_v}{\rho_l}\right]\right)^{-1} \tag{12.3}$$

$$G = \frac{\dot{m}}{A_c} \tag{12.4}$$

$$\dot{m} = \frac{\dot{Q}}{h_e - h_c} \tag{12.5}$$

x = quality (v = volume of PHP, P = pressure of PHP)

v_l = volume (x = 0, P = pressure of PHP)

ρ_v = density (x = 1, P = pressure of PHP)

ρ_l = density (x = 0, P = pressure of PHP)

$\dot{m}$ = estimated mass flowrate of fluid in PHP

A_c = inner cross-sectional area of capillary tubes

h_c = enthalpy (T = T_{cond}, P = pressure of PHP)

h_e = enthalpy (T = T_{evap}, P = pressure of PHP)